# DESIGN AND DEVELOPMENT OF NOVEL PHOSPHORESCENT IRIDIUM(III) COMPLEXES FOR LIGHTING AND SENSING APPLICATIONS

**Thesis Submitted to AcSIR for the Award of the Degree of**
**DOCTOR OF PHILOSOPHY**
**in Chemical Sciences**

By

**K. S. BEJOY MOHAN DAS**

**Registration No: 10CC12A39008**

**Under the guidance of**

**Dr. M. L. P. REDDY**

**CSIR-NATIONAL INSTITUTE FOR INTERDISCIPLINARY**
**SCIENCE AND TECHNOLOGY (CSIR-NIIST)**
**THIRUVANANTHAPURAM-695 019, KERALA, INDIA**

**2016**

*…Dedicated to*

*My Beloved Parents ….*

# DECLARATION

I hereby declare that the matter embodied in the thesis entitled: "**Design and development of novel phosphorescent iridium(III) complexes for lighting and sensing applications**" is the result of the investigations carried out by me at the Materials Science and Technology Division, CSIR-National Institute for Interdisciplinary Science and Technology (CSIR-NIIST), Trivandrum, under the supervision of Dr. M. L. P. Reddy and the same has not been submitted elsewhere for any other degree.

In keeping with the general practice of reporting scientific observations, due acknowledgement has been made wherever the work described is based on the findings of other investigators.

**K. S. BEJOY MOHAN DAS**

COUNCIL OF SCIENTIFIC & INDUSTRIAL RESEARCH
NATIONAL INSTITUTE FOR INTERDISCIPLINARY SCIENCE AND TECHNOLOGY (CSIR-NIIST)
Industrial Estate P.O., Trivandrum - 695 019, India

**Dr. M. L. P. Reddy, FAPSc**
Chief Scientist

Tel: 91-471-2515 360
Fax: +91-471-2491 712
E-mail: mlpreddy55@gmail.com

# CERTIFICATE

This is to certify that the work incorporated in this Ph.D. thesis entitled "**Design and development of novel phosphorescent iridium(III) complexes for lighting and sensing applications**" submitted by **Mr. K. S. BEJOY MOHAN DAS** to Academy of Scientific and Innovative Research (AcSIR), in partial fulfilment of the requirements for the award of the **Degree of Doctor of Philosophy in Chemical Sciences**, embodies original research work under my supervision and guidance at the Materials Science and Technology Division of the CSIR-National Institute for Interdisciplinary Science and Technology (CSIR-NIIST), Trivandrum. I further certify that this work has not been submitted to any other University or Institution in part or full for the award of any degree or diploma. Research material obtained from other sources has been duly acknowledged in the thesis. Any text, illustration, table etc., used in the thesis from other sources, have been duly cited and acknowledged.

**K. S. BEJOY MOHAN DAS**

**Dr. M. L. P. REDDY**
(Thesis Supervisor)

Thiruvananthapuram
October, 2016

# ACKNOWLEDGEMENTS

*It is with great pleasure that I extend my deep sense of gratitude and indebtedness to Dr. M. L. P. Reddy, my research supervisor, for suggesting the research problem and his valuable guidance leading to the successful completion of this research work.*

*I sincerely thank Dr. A. Ajayaghosh, Director, NIIST, and former Directors Dr. Suresh Das and Dr. Gangan Pratap, for providing the necessary facilities and infrastructure to carry out this investigation.*

*My sincere thanks are also due to:*

- ✓ *Dr. R. Luxmi Varma and Dr. Mangalam S. Nair, present and former AcSIR co-ordinators.*
- ✓ *Dr. E. Bhoje Gowd, Dr. C. Vijayakumar and Dr. C. H. Suresh, my DAC members.*
- ✓ *Dr. S. Natarajan and Mr. S. Bhattacharya from Indian Institute of Science (Bangalore) and Dr. Sunil Varughese of Chemical Sciences and Technology Division, NIIST for X-ray single crystal measurements.*
- ✓ *Dr. V. Subramanian and Mr. E. Varathan from CSIR-Central Leather Research Institute (Chennai) for Theoretical calculations.*
- ✓ *Dr. Arunandan Kumar from Universite ´de Bourgogne (France), Dr. K. N. Narayanan Unni, Ms. Anjali Soman and Mr. V. R. Rajeev of Chemical Sciences and Technology Division, NIIST for Electroluminescence measurements.*
- ✓ *Dr. V. Divya, Dr. S. Sarika, Dr. A. R. Ramya, Dr. Biju Francis, Dr. Sheethu Jose, Ms. P. Aiswaria, Mr. T. M. George, Ms. T. V. Usha Gangan, Mrs. J. Anaswara, Mr. K. R. Ajay, Mr. S. Sreenadh, Mrs. M. V. Lucky, Mr. P. K. Thejus, Mr. Alikunhi, Mrs. S. Surya, Ms. S. Anila, Ms. Syamasrit Dash, my roommates and all other friends at NIIST family for their help and cooperation.*
- ✓ *All technical supportive staff of CSIR-NIIST for their timely help in the utilization of sophisticated analytical instruments.*
- ✓ *All my teachers for their encouragement at different stages of my academic career.*
- ✓ *Council of Scientific and Industrial Research (CSIR) and Department of Science and Technology (DST), Government of India for financial assistance.*

*I am deeply and forever indebted to my parents for their constant source of love, inspiration and blessings. Finally I would like to thank, my beloved sisters, my brothers in law, friends and relatives for their excellent support and encouragement.*

*Above all, I thank Almighty for giving me all these people to help and encourage me, and for the skills and opportunity for the successful completion of this thesis.*

***K. S. BEJOY MOHAN DAS***

# CONTENTS

## CHAPTER 4: AIPE-Active Green Phosphorescent Iridium(III) Complex Impregnated Test Strips for the Vapor-Phase Detection of 2,4,6-Trinitrotoluene (TNT) 177-210

# List of Schemes

# List of Figures

**Page**

# List of Tables

# List of Abbreviations

| | |
|---|---|
| MLCT | metal–to–ligand charge transfer |
| LC | ligand centered |
| MC | metal centered |
| ILET | intramolecular inter–ligand energy transfer |
| SOC | spin−orbit coupling |
| $\xi_{Ir}$ | spin−orbit coupling constant |
| ISC | intersystem crossing |
| LEECs | light emitting electrochemical cells |
| OLEDs | organic light emitting diodes |
| PhOLEDs | phosphorescent organic light emitting diodes |
| PDT | photodynamic therapy |
| DNA | deoxyribonucleic acid |
| C^N | cyclometalating ligand |
| L^X | ancillary ligand |
| DFT | density functional theory |
| HOMO | highest occupied molecular orbital |
| LUMO | lowest unoccupied molecular orbital |
| LFSE | ligand field stabilization energy |
| MOs | molecular orbitals |
| CIE | Commission Internationale de L′Eclairage |
| EL | Electroluminescence |
| PL | Photoluminescence |
| $\lambda_{max}$ | wavelength at emission maximum |
| $\Phi_{PL}$ | photoluminescence quantum yield |
| $\tau$ | phosphorescence lifetime |
| $k_{isc}$ | intersystem crossing rate constant |
| $k_{nr}$ | non–radiative decay rate constant |
| $\eta_p$ | power efficiency |
| $\eta_c$ | current efficiency |

| | |
|---|---|
| $L_{max}$ | maximum brightness |
| EQE | external quantum efficiency |
| ppy | 2–phenylpyridine |
| dfpypy | 2′,6′–difluoro–2,3′–bipyridine |
| dfppy | 2–(4,6–difluorophenyl)pyridine |
| dpm | Dipivaloylmethanate |
| dtBubpy | 4,4′−di−tert−butyl−2,2′−bipyridine |
| NHC | N–heterocyclic carbenes |
| $Ph_2P=O$ | diphenyl phosphoryl |
| Htpip | tetraphenylimidodiphosphinic acid |
| dipcca | 9H–(carbazol–9–yl)(diisopropyl)amidate |
| mppy | 5−methyl−2−phenylpyridine |
| CBP | 4,4′–bis(N–carbazolyl)–1,10–biphenyl |
| ITO | indium–tin oxide |
| PEDOT:PSS | poly(3,4–ethylenedioxythiophene):poly(styrenesulfonate) |
| TAPC | 4,4′–cyclohexylidenebis[N,N–bis(4–methylphenyl)aniline] |
| mCP | 1,3–bis(N–carbazolyl)benzene |
| TSPO1 | diphenylphosphine oxide–4–(triphenylsilyl)phenyl |
| B3PyPB | 1,3–bis(3,5–dipyrid–3–ylphenyl)benzene |
| PPO21 | 3–diphenylphosphinyl–9–(4′–diphenylphosphinylphenyl)carbazole |
| TmPyPB | 1,3,5–tri(m–pyridin–3–ylphenyl)benzene |
| mCPPO1 | 9–(3–(9H–carbazol–9–yl)phenyl)–9Hcarbazol–3–yl)diphenylphosphine oxide |
| *fac* | facial |
| *mer* | meridional |
| BTPBA | bis(2–(2–benzothiazolyl–N3)phenyl–C) iridium(III) (phenyl)( N,N′–diisopropylbenzimidamidate) |
| BTIPG | bis(2–(2–benzothiazolyl–N3)phenyl–C) iridium(III) (9H–carbazol–9–yl)(1,1,2,3–tetraisopropylguanidinate) |

# PREFACE

Cyclometalated iridium(III) complexes have unique photophysical properties as phosphorescence materials, since they possess high luminescent quantum yields and have relatively longer phosphorescent lifetimes ($\tau \sim \mu s$) than the fluorescence analogue. The highly efficient spin−orbit coupling (SOC) of iridium(III) metal ion in the complexes promote intersystem crossing (ISC) from the singlet state to the triplet state. As a result, the complexes exhibit strong phosphorescence even at room temperature. Because of these excellent photochemical properties, iridium(III) complexes are utilized as phosphorescent emitters in organic light-emitting diodes (OLEDs), chemosensors, photoredox catalysis, and as luminescent probes for biological systems etc. The performance of these materials in such roles depends heavily on their excited-state properties, which can be tuned through ligand and substituent effects. Therefore the main objective of the current thesis is to design and develop novel phosphorescent iridium compounds and investigate their photophysical properties for use in potential applications.

The thesis comprises of four Chapters. The first Chapter begins with a brief introduction to the structural aspect on the photophysical properties of cyclometalated iridium(III) complexes and its applications, particularly on electroluminescence. Further, this chapter focuses on the recent developments and state of the art knowledge on phosphorescent iridium(III) compounds, especially on heteroleptic complexes derived from 2,3′−bipyridine class of cyclometalating ligands, highlighting the excited state phenomenon behind their emission behaviour.

Chapter-II deals with the synthesis and characterization of a series of 2',6'-difluoro-2,3'-bipyridine cyclometalating ligands by substituting electron-withdrawing (–CHO, –$CF_3$, –CN) and electron-donating (–OMe, –$NMe_2$) groups at the 4′ position of the pyridyl moiety. The designed ligands have been employed for the construction of five new iridium(III) complexes (**Ir1-Ir5**) in the presence of picolinate as an ancillary ligand. The photophysical and electrochemical properties of the developed iridium(III) compounds were investigated with a view to understand the substituent effects. Excited-state properties of these complexes are also found to be sensitive to the microenvironments around the complex (i.e., rigidity, temperature) because of their charge-transfer character and asymmetric structure, which has been evaluated from the emission characteristics observed from 77K freeze matrix and doped PMMA films. Comprehensive density functional theory (DFT) and time-dependent DFT (TD-DFT) approaches have been performed on the ground and excited states of the synthesized iridium(III) complexes, in order to obtain information about the absorption and emission processes and to gain deeper insight into photophysical properties. Multi-layered Phosphorescent Organic Light Emitting Diodes (PhOLEDs) were designed using the phosphorescent dopants **Ir2**, **Ir3** and **Ir4** and their electroluminescence properties were evaluated.

A new phosphorescent iridium(III) compound, bis[2′,6′-difluorophenyl-4-formylpyridinato-N,C4′]iridium(III)(picolinate) (**IrC**), was synthesized, fully characterized by various spectroscopic techniques, and utilized for the detection of cyanide ion on the basis of the widely known hypothesis of the formation of cyanohydrins. These results have been described in Chapter-III. A unique colorimetric and ratiometric phosphorescence response to the cyanide is realized through interaction of the electron-deficient formyl moiety of the cyclometalated iridium(III) complex with $CN^-$ through the formation of cyanohydrin. In addition, phosphorescent test strips have been fabricated and utilized for the detection of nanogram levels of cyanide in drinking water.

The detection of explosives, especially, trinitrotoluene (TNT), is of utmost importance due to its highly explosive nature and environmental hazard. In chapter-IV, a new aggregation-induced phosphorescent emission (AIPE)-active iridium(III) bis(2-(2,4-difluorophenyl)pyridinato-*N*,*C*2′) (2-(2-pyridyl)benzimidazolato-*N*,*N*′) complex [**FIrPyBiz**] has been developed and utilized for the detection of TNT in the vapour phase, solid phase, and aqueous media. In addition, phosphorescent test strips have been constructed by impregnating Whatman filter paper with aggregates of **FIrPyBiz** for trace detection of TNT in contact mode, with detection limits in nanograms, by taking advantage of the excited state interaction of AIPE active phosphorescent iridium(III) complex with that of TNT and the associated photophysical properties.

# Chapter 1

## Introduction: Phosphorescent Iridium(III) Complexes

There has been an upsurge of interest in phosphorescent iridium(III) compounds due to their fascinating photophysical properties such as promising phosphorescence quantum yields, relatively shorter excited−state lifetimes, large cross−section for the exciton formation and facile tuning of emission colors through molecular engineering.[1] The efficient phosphorescent emission is essentially ascribed to the strong SOC−induced by the 5*d* orbitals of $Ir^{3+}$ ion ($\xi_{Ir} = 4430\ cm^{-1}$),[2] which facilitates efficient ISC of the singlet excited state to the triplet manifold ($k_{isc} < 1$ ps).[3] Thus, mixing of the singlet and triplet excited states allows the radiative relaxation of the triplet state, which is known as spin−forbidden.[1n, 4] The emission from phosphorescent iridium(III) complexes mainly arises from triplet metal−to−ligand charge transfer ($^3$MLCT) or the mixture of $^3$MLCT and ligand−centered ($^3$LC) transitions.[3a] Further, in some of the iridium(III) complexes, intramolecular inter−ligand energy transfer (ILET), ligand−to−ligand charge transfer (LLCT) and other processes[5] are also known (Figure 1.1).

The lowest excited state energy can be controlled in a more desirable way by tuning the energy of the ligand orbitals *via* substituent effects in the cyclometalating or ancillary ligand systems, which can generate a diverse range of emission colors from iridium(III) complexes. Consequently, phosphorescent iridium(III) compounds have been extensively explored for many potential applications (Figure 1.2) including OLEDs,[6] light−emitting electrochemical cells (LEECs),[7] biological labelling,[8] photodynamic therapy (PDT),[9] photosensitizers for photo−driven water splitting,[10] nonlinear optics,[11] chemosensors,[8e, 12] metallo−pharmaceuticals,[13] photocatalyst for organic synthesis and $CO_2$ reduction,[14] luminescent sensitizers for charge−transfer reactions in DNA,[15] singlet oxygen sensitizers,[16] dye−sensitized solar cells[17] and electro−generated chemiluminescence.[18]

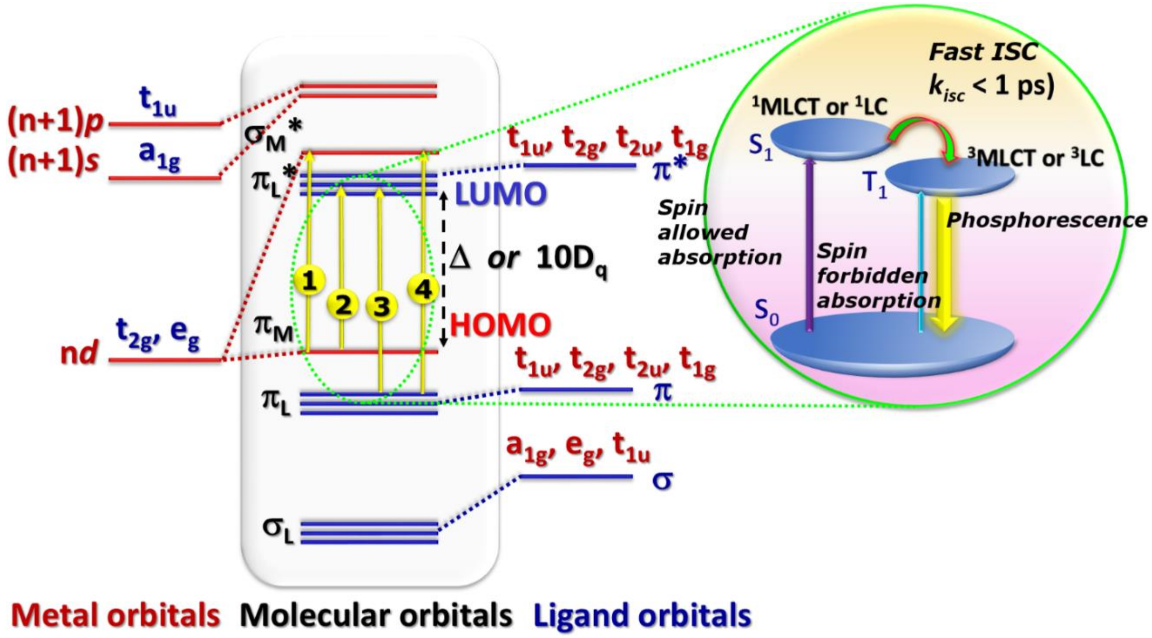

**Figure 1.1.** Schematic and simplified molecular orbital diagram for iridium(III) complex in octahedral coordination geometry. The labelled arrows represent, (1) metal centered ligand field transition $(d_{\pi}\rightarrow d_{\sigma}^{*})$, (2) metal−to−ligand charge transfer (MLCT), (3) intraligand charge transfer (ILCT) or ligand−to−ligand charge transfer (LLCT) (4) ligand−to−metal charge transfer (LMCT) transitions. Radiative phosphorescence at room temperature followed by the fast intersystem crossing can be seen from the inset.

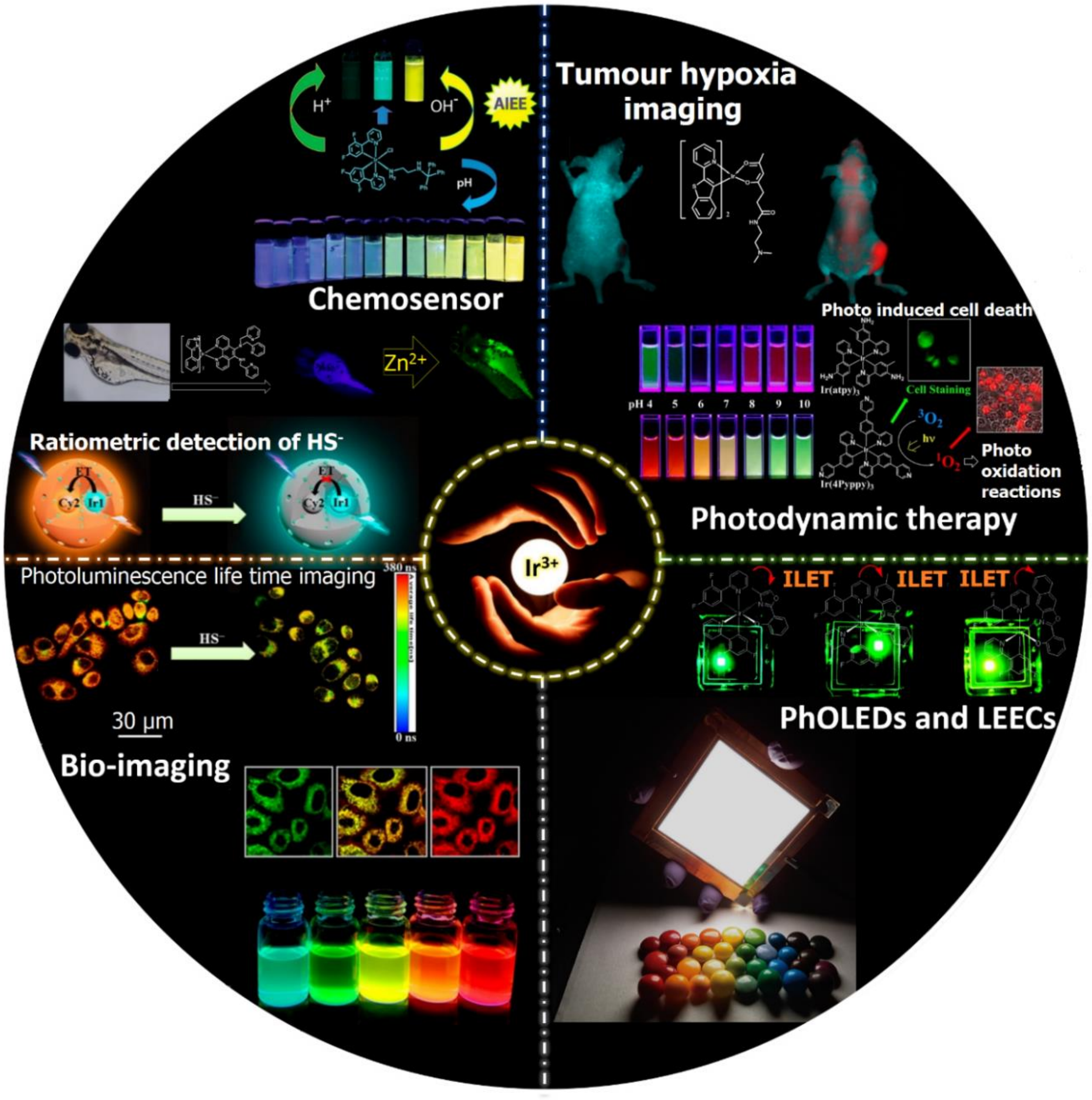

**Figure 1.2.** Applications of cyclometalated iridium(III) complexes inspired from the attractive photophysical properties.

The cyclometalated iridium(III) complexes are recognized as excellent phosphorescent emitters and have been widely investigated because of their ability to achieve maximum internal quantum efficiency, nearly 100%, as well as high external quantum efficiencies in OLEDs.[6c] A simplified working principle of an OLED motif can be seen from Figure 1.3.

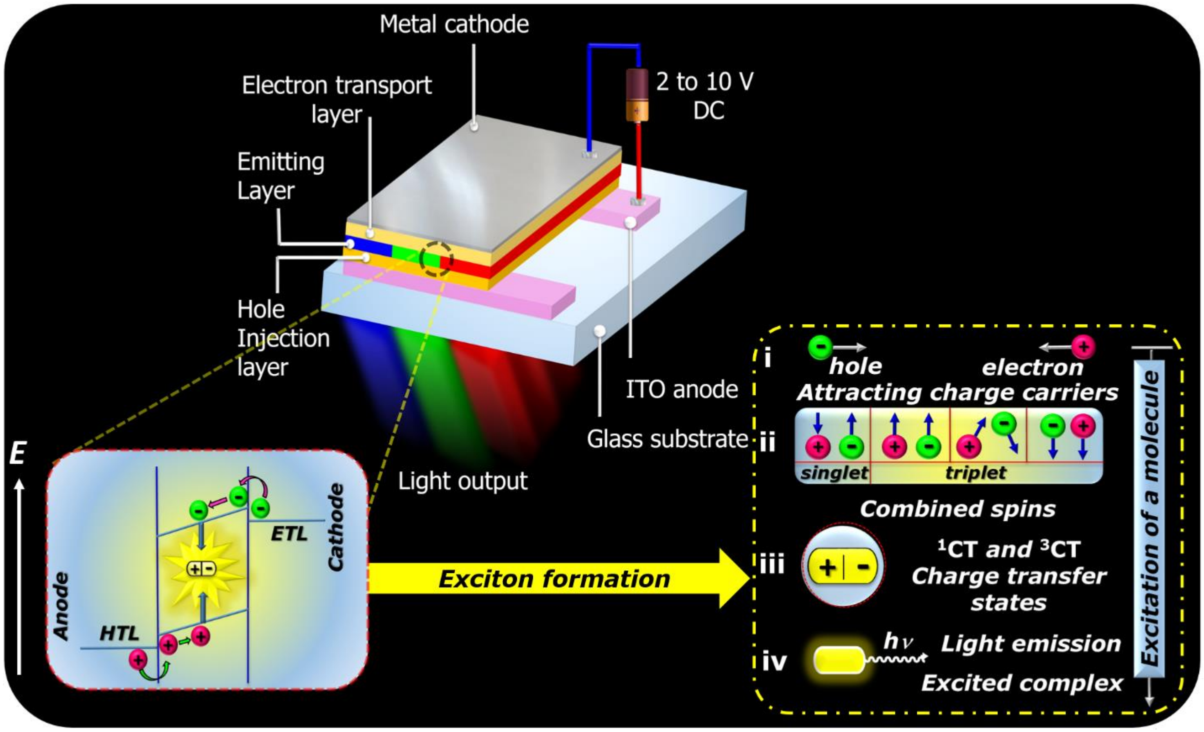

**Figure 1.3.** Basic structure and working principle of a typical OLED with an illustrated exciton formation mechanism. Schematic representation of (i) recombination of charge carriers such as electron – hole, (ii) possible combined spin states, (iii) formation of singlet and triplet charge transfer (CT) states (includes the emitter and the neighbouring host molecules) leading to the population of lowest excited states, (iv) relaxations from CT states populate the emissive excited states of the electroluminescent molecule.

In quest of developing novel iridium(III) compounds with high quantum yields for use in organic light emitting diodes, many heteroleptic complexes having the general formula $[Ir(C^{\wedge}N)_2(L^{\wedge}X)]$ were designed during the last decade, where $C^{\wedge}N$ is a monoanionic cyclometalating chelate and $L^{\wedge}X$ is an ancillary ligand.[1b, 1c, 3b, 7c, 19] It is well documented that the phosphorescence from $[Ir(C^{\wedge}N)_2(L^{\wedge}X)]$ compounds originates from $^3$LC and $^3$MLCT transitions.[20] In such iridium(III) complexes, DFT predictions indicate that the HOMO is primarily metal–centered, while the LUMO is localized on the heterocyclic rings of the cyclometalated chelates (Figure 1.4).[21] On the other hand, the ancillary ligand can also influence the energy of the excited state by altering the electron−density at the metal center.[22]

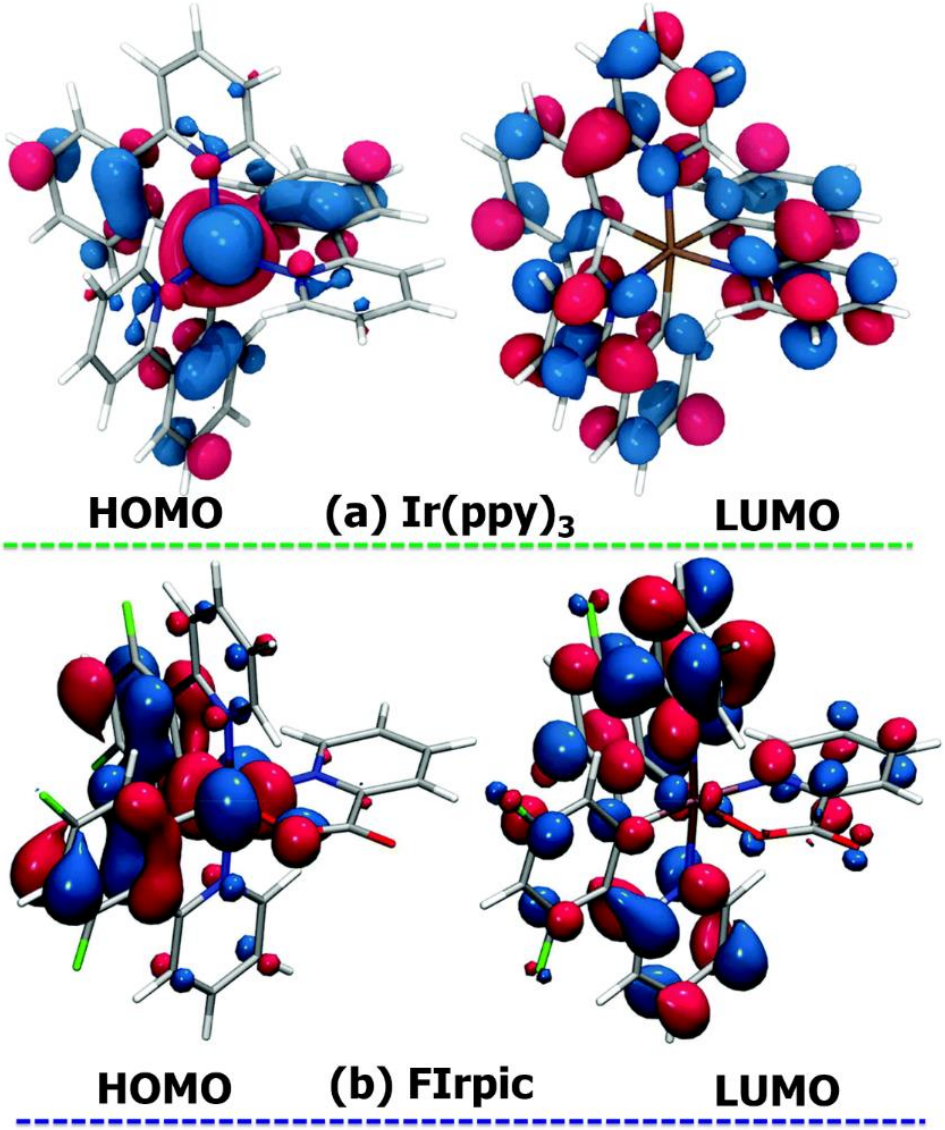

**Figure 1.4.** Kohn–Sham HOMO (left) and LUMO (right) orbital localization of (a) *fac*−tris homoleptic $Ir(ppy)_3$ and (b) FIrpic obtained using the DFT (M06)/IEF−PCM (ACN) level of theory.

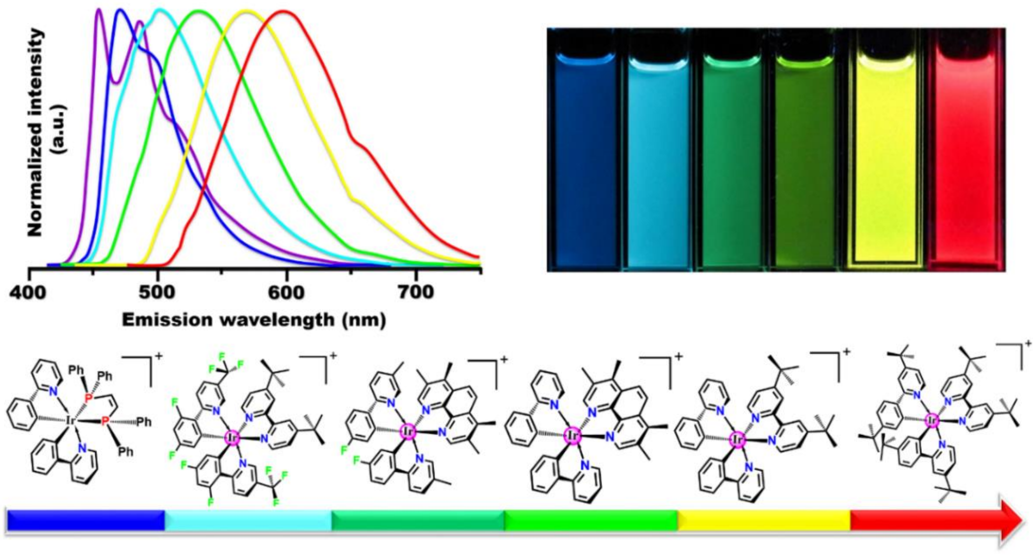

**Figure 1.5.** Color versatility explicated by a series of six cationic luminescent iridium(III) complexes. Their structures are placed in the order of increasing emission wavelength (blue to red).

One of the most effective methods for controlling the excited state properties of iridium(III) compounds involves prudent functionalization of the cyclometalated chelates *via* substituent groups, which essentially induce electronic effects and the symmetry around the metal center. Thus, it is possible to control metal−ligand bonding as well as ligand orbital energies and, which ultimately control the nature of the lowest excited state. Fabulous colour versatility has been accomplished with iridium(III) luminophores involving 2−phenylpyridine as a cyclometalated ligand (Fig. 5), with a wide range of excited−state lifetimes (µs), as well as excellent emission quantum yields (~100%).[1n, 21, 23] Among the various 2−phenylpyridine class of iridium(III) complexes, FIrpic has been widely studied bis-cyclometallated iridium complex, especially in OLED applications because of its attractive sky-blue emission, high emission efficiency, and suitable energy levels.[24] However, FIrpic has specific issues that preclude it from being a fully satisfying phosphorescent emitter for OLEDs.[25] The shortcomings of FIrpic as an emitter for OLEDs are its unattractive CIE colour point for display, significant roll-off efficiency impacting the device architecture, and low stability due to chemical degradation in devices.[26] Because of these limitations of phenyl pyridine class of ligands for use in OLEDs, there is a continuous effort to design and develop an alternative cyclometalates, especially for blue phosphorescent emitters.[27]

## 1.1. Evolution of 2, 3′−Bipyridine Class of Cyclometalating Ligands as Efficient Phosphorescent Iridium(III) Emitters

In 2009, Kang and coworkers[28] have proposed a novel strategy, especially to stabilize HOMO *via* increasing the electronegativity of the Ir−C coordinating aryl ring by incorporating a hetero atoms such as nitrogen into the ring system. The reactivity and the photophysical properties of an aryl ring is strongly influenced by the irregular distribution of electron density ensued from the insertion nitrogen (Figure 1.6). Therefore, an unequal electron density distribution creates a partial positive charge at carbon atoms positioned *ortho* and *para* to the nitrogen atom in the pyridine ring and can be described as electron−poor or π electron−deficient.[29] Thus, the fundamental characteristics such as electron−donating or electron−withdrawing ability of the aryl ring strongly depends on the nature of the heteroatom.[30]

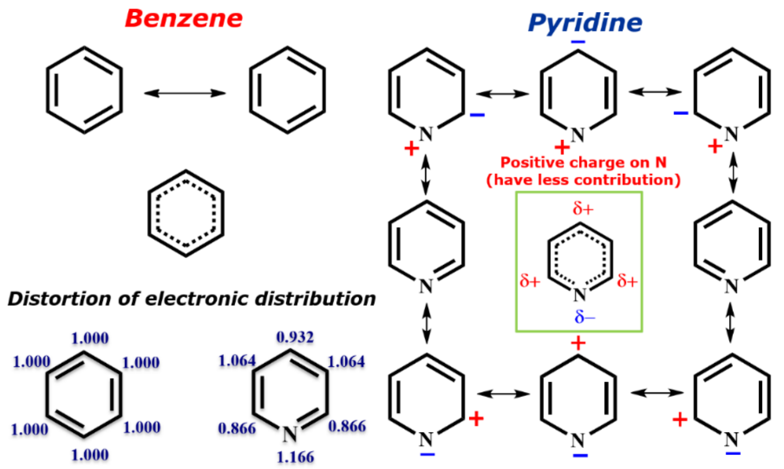

**Figure 1.6.** Resonance structures of benzene and pyridine along with difference in electronic distribution.

In 1996, Tamao et al.[31] utilized this π−electron deficient character of the pyridyl rings for the development of efficient electron transporting materials by lowering the HOMO energy. Thus the phenyl ring of the well−known 2−phenylpyridine can be replaced with pyridine for the development of 2,3′−bipyrine class of cyclometalating ligands. In addition to the N atom, the introduction of −F substituents into the pyridine ring significantly lowered the HOMO energy level and experienced a highly efficient true−blue emission in the solution and film states. Thus, 2,3′−bipyridine class of compounds emerged as a potential alternative ligands for 2−phenylpyridine derivatives for achieving true−blue emission colors from iridium(III) complexes and largely attracted by the global scientific community. Decent device performance (power efficiency > 30 lm $W^{-1}$) using a blue emitter with bipyridyl ligands has also been well recognized.[32] In recent years, some of the iridium(III) blue emitters from the 2,3′−bipyridine family were made available in the market, which indicates its growing commercial interest over 2−phenylpyridine based iridium(III) emitters (http://www.lumtec.com.tw). Further, less has been known about a collective structure–property relationships for obtaining better phosphorescence quantum efficiency in this class of cyclometalates. Thus this chapter evokes the story behind the evolution of this new type of iridium(III) complexes and its importance over traditional 2−phenylpyridine class of ligands for use in PhOLEDs (Chart 1).

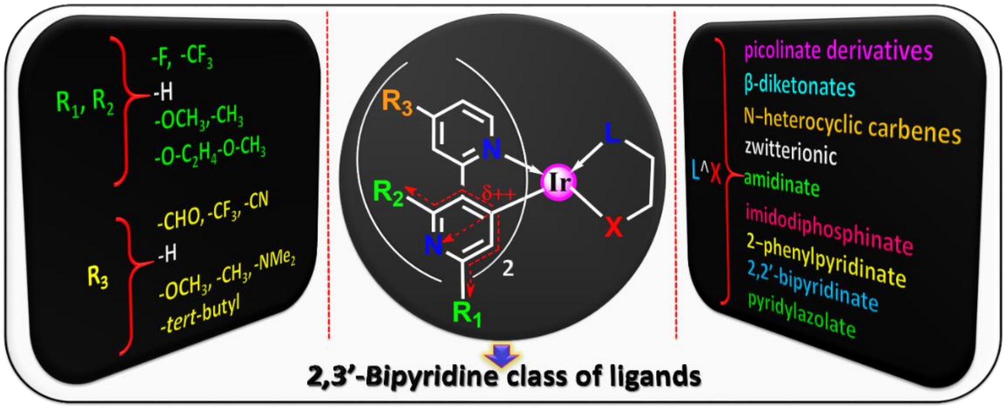

**Chart 1.1.** State of the art structural modifications carried out on the phosphorescent iridium(III) complexes derived from 2,3'-bipyridine class of cyclometalating ligands.

## 1.2. Homoleptic Iridium(III) Complexes Based on 2,3′−Bipyridine Ligands

Kang et al.[28] have first time introduced a new cyclometalated ligand, namely, 2′,6′−difluoro−2,3′−bipyridine (dfpypy) as a viable alternative to the 2−phenylpyridine for the development of an intense blue−emitting phosphorescent iridium(III) complex. The design of the cyclometalated ligand is essentially based on the concept of inducing more electron−deficiency at iridium(III) bonded carbon atom by introducing an electronegative N atom at C5′ position and more electron−withdrawing F atoms at C2′, C6′ –positions of the 2,3′–bipyridine ligand (Figure 1.7), which may exert significant influence on the HOMO energy levels. The synthesized cyclometalated ligand has been successfully employed for the development of a *fac*–tris(2′,6′–difluoro–2,3′–bipyridinato–N,C4′)iridium(III) complex (**Ir1**) [Chart 1.2]. The **Ir1** displayed a true–blue (CIE$_{x,y}$ = 0.14, 0.12) phosphorescence emission at room–temperature in degassed dichloromethane solution with vibronic peaks at 438 and 463 nm (Figure 1.8). Interestingly, **Ir1** exhibited a remarkable quantum yield of 0.77, which is moderately higher than that of the well–known sky–blue emitter FIrpic ($\Phi_{PL}$ = 0.61).[25]

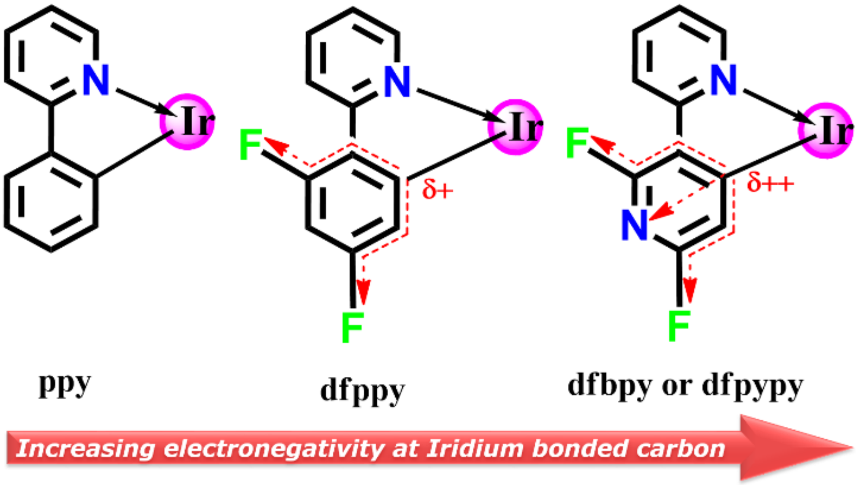

**Figure 1.7.** Comparison of electronegativity difference at iridium(III) bonded carbon atom in the 2–phenylpyridine (ppy), 2,6–diflurophenyl pyridine (dfppy) and 2',6'–difluoro–2,3'–bipyridine (dfpypy) cyclometalating ligands.

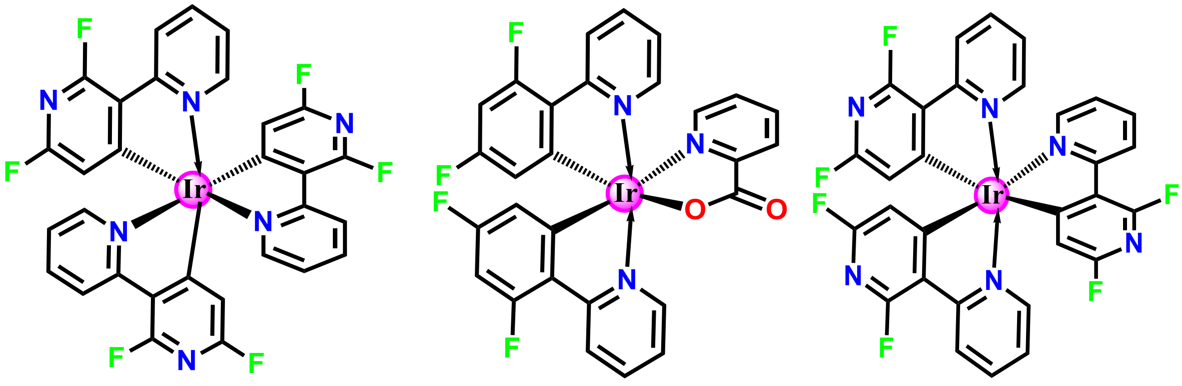

***fac*-Ir(dfpypy)$_3$ (Ir1)** **FIrpic** ***mer*-Ir(dfpypy)$_3$ (Ir2)**

**Chart 1.2.** Chemical Structures of *fac*−tris(2',6'−difluoro−2,3'−bipyridinato−N,C4')iridium(III) (**Ir1**), bis[2–(4,6–difluorophenyl)pyridinato– N, C2]iridium(III) (picolinate) (**FIrpic**) and *mer*−tris (2',6'−difluoro−2,3'−bipyridinato−N,C4')iridium(III) complex (**Ir2**).

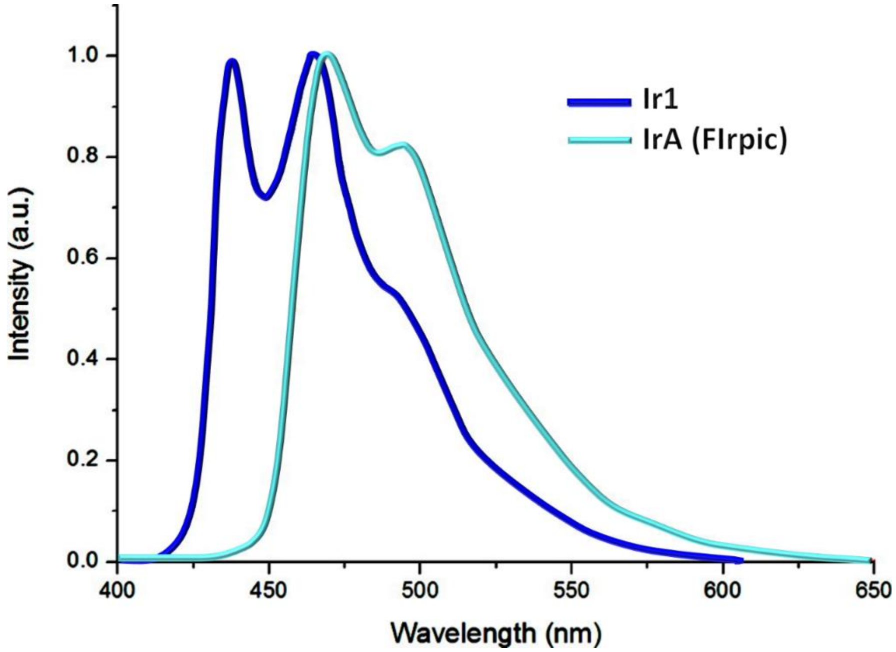

**Figure 1.8.** Comparison of emission profiles of Ir(dfpypy)$_3$ (**Ir1**) and FIrpic (**IrA**) at room temperature under identical conditions (concentration, 2.5 × $10^{-5}$ M; solvent, $CH_2Cl_2$).

The higher luminescent efficiency can be attributed to (i) the facial arrangement of dfpypy chelates that improves the overall orbital degeneracy, and (ii) the inhibition of a thermally activated, nonradiative decay channel, which involves temporal formation of a five−coordinate species by rupturing one of the Ir–N bonds at the excited state. Further, the substitution of phenyl ring in ppy with pyridine and incorporation of −F substituents into the pyridine ring dramatically enhances the thermal stability and molecular rigidity due to the strong intermolecular interactions in the solid state, which is evident from the crystal structure. Molecular rigidity reduces the possibility of non-radiative transitions by decreasing molecular vibrations, minimizing thereby the collision heat loss.[7b, 33] Based on the DFT calculations, the authors have concluded that the substituents have significant influence on the frontier molecular orbital energy levels, where the decrease of the HOMO energy (1.60 eV) is larger than the LUMO (1.04 eV) as compared to that of Ir(ppy)$_3$. The decrease of the HOMO level is a little remarkable, indicating that the fluorine substituents and the replacement of pyridine have significant influence on the HOMO energy levels. Although, **Ir1** exhibits excellent photophysical features such as true−blue emission, high quantum efficiency with good colour purity and high thermal stability, it has a very low−lying HOMO energy (~6.4−6.5 eV) and hence it is hard to find a desirable host material for use in OLED applications. In the later studies, Kang and coworkers have isolated a blue phosphorescent meridional isomer *mer*−Ir(dfpypy)$_3$ (**Ir2**) of **Ir1** and evaluated its photoluminescence properties [Chart 1.2].[34] Surprisingly, the HOMO of *mer*−Ir(dfpypy)$_3$ (−5.97 eV) is higher than that of facial isomer (−6.20 eV). This has been attributed to the lengthening of the transoid Ir−C bonds in the *mer*−isomer. The absorption and emission profiles are found to be identical in both the isomers, while MLCT and emission bands in meridional isomer are bathochromically shifted. However, the photoluminescence quantum efficiency of **Ir2** in degassed dichloromethane solution is found to be inferior, which may be due to the dissociation of Ir−C bond in the excited state.

## 1.3. Modifications on 2,3′−Bipyridine Cyclometalating Ligand

The beauty of iridium(III) complex relies on the possibility of facile tuning of the photophysical and electrochemical properties *via* altering the electron density at the cyclometalated ligand system. This section details the important efforts carried out on the cyclometalating dfpypy ligands to develop promising iridium(III) based phosphorescent emitters.

### 1.3.1 Substitutions on Ir−N Coordinating Pyridyl Ring

#### 1.3.1.1 Tuning of Emission Colors by Various Substituents on Ir−N Coordinating Pyridyl ring

A series of dfpypy cyclometalating ligand derivatives have designed by the incorporation of electron−withdrawing (–CHO, $-CF_3$, and –CN) and electron−donating (–OMe and $-NMe_2$) substituents at the 4′ position of the Ir−N coordinated pyridyl moiety with a view to understand the electronic effects on the photophysical and electroluminescent properties of the corresponding iridium(III) phosphorescent complexes (**Ir3**–**Ir7)** as compared to the unsubstituted **Ir8** in presence of picolinate as an ancillary ligand [Chart 1.2].[35] PhOLEDs have been fabricated using **Ir4** and **Ir5** as the emissive material and the corresponding EL spectra display blue and green emissions in the visible region, respectively.

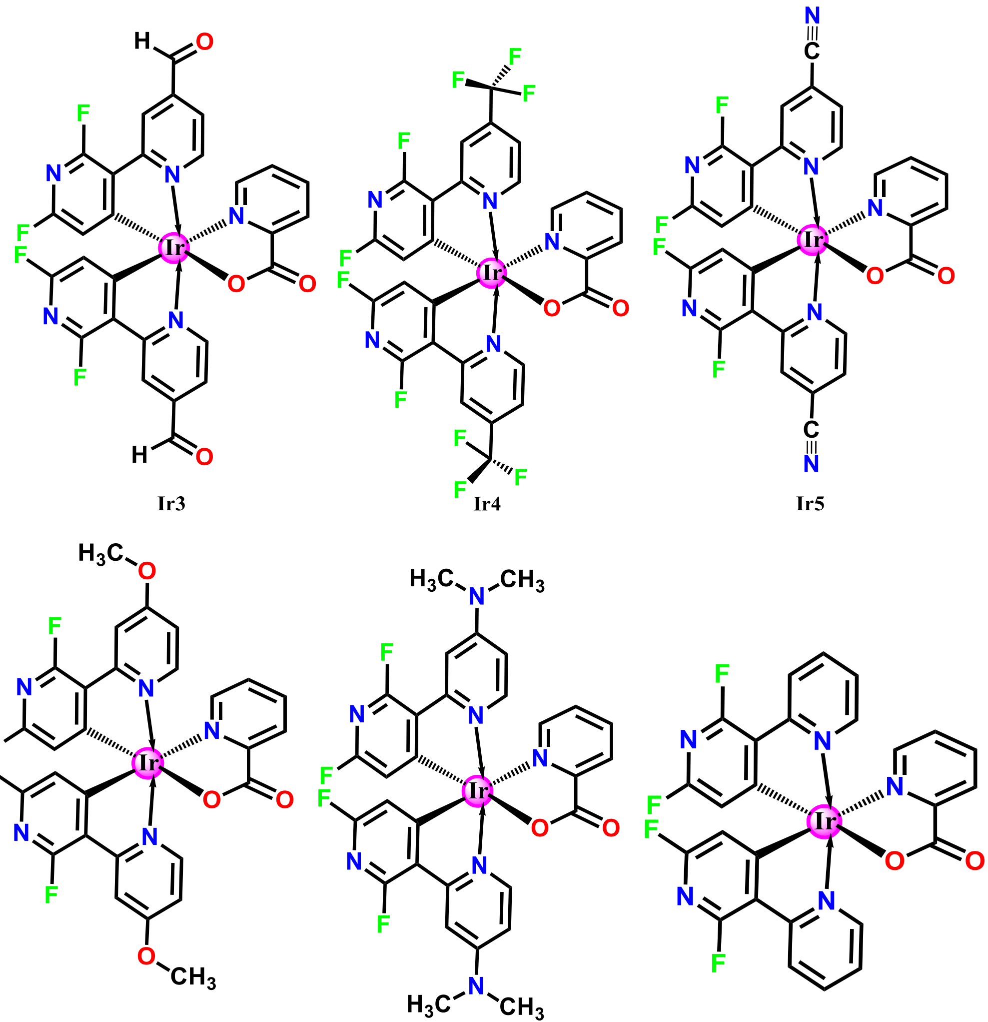

**Ir3** **Ir4** **Ir5**

**Ir6** **Ir7** **Ir8**

**Chart 1.2.** Chemical Structures of bis(2',6'–difluoro–4–formyl–2,3'–bipyridinato–N,C4')iridium(III) (picolinate) (**Ir3**), bis(2',6'–difluoro–4–trifluoromethyl–2,3'–bipyridinato–N,C4')iridium(III) (picolinate) (**Ir4**), bis(2',6'–difluoro–4–cyano–2,3'–bipyridinato–N,C4')iridium(III) (picolinate) (**Ir5**), bis(2',6'–difluoro–4–methoxy–2,3'–bipyridinato–N,C4')iridium(III) (picolinate) (**Ir6**), bis(2',6'–difluoro–4–N,N–dimethylamine–2,3'–bipyridinato–N,C4')iridium(III) (picolinate) (**Ir7**) and bis(2',6'–difluoro–2,3'–bipyridinato–N,C4')iridium(III) (picolinate) (**Ir8**).

The device consisting of **Ir4** in CBP as an emissive layer exhibits bright electroluminescence of about 15000 cd m$^{-2}$ with a peak current and a power efficiency of 12.6 cd A$^{-1}$ and 5.3 lm W$^{-1}$, respectively. In the meantime, the current as well as power efficiencies for similarly structured OLED with **Ir5** was found to be 14.5 cd A$^{-1}$, 7.6 lm W$^{-1}$, respectively. The non−optimized electroluminescence device results demonstrated that the developed series of phosphorescent emitters have the potential for use in PhOLEDs. A detailed scientific discussion regarding the substituent effects on these complexes can be seen from Chapter 2.

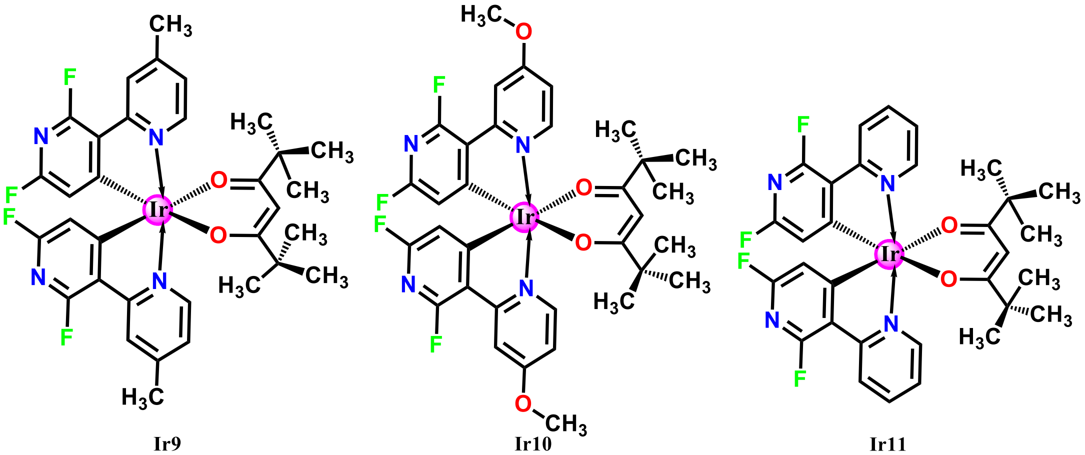

**Ir9** **Ir10** **Ir11**

**Chart 1.4.** Chemical Structures of bis(2',6'–difluoro–4–methyl–2,3'–bipyridinato–N,C4')iridium(III) (dipivaloylmethanoate) (**Ir9**), bis(2',6'–difluoro–4–methoxy–2,3'–bipyridinato–N,C4')iridium(III) (dipivaloyl-methanoate) (**Ir10**) and bis(2',6'–difluoro–2,3'–bipyridinato–N,C4')iridium(III) (dipivaloyl-methanoate) (**Ir11**).

Kang's group have also investigated the effect of electron−donating (–OCH$_3$ or –CH$_3$) substituent effects on the 4′ position of the N−coordinating pyridyl moiety of cyclometalated ligand in iridium(III) complexes in the presence of dipivaloylmethanate (dpm) as an ancillary ligand [Chart 1.4].[36] The compounds **Ir9** and **Ir10** showed moderate blue−shifted emissions (5 nm) in the fluid−state as compared with their non−substituted counterpart (**Ir11**, $\Phi_{PL}$ = 0.58) with low to modest quantum efficiencies (0.25 for **Ir9** and 0.50 for **Ir10**).[37] The low quantum efficiency noted, especially in the case of **Ir9** is probably due to the destabilization of the LUMO level, that decreases the energy gap between $^3$MC *d–d** and $^3$MLCT or $^3$LC based emissive states, and creates more deactivation channels. This observation implies that the electron−donating substituents have negligible effect on the emission profiles of these systems as indicated earlier by Reddy and coworkers.[35] Further, these authors fabricated a multi−layer electroluminescent device [(ITO, 50 nm)/ (PEDOT: PSS, 60 nm)/ (TAPC, 20 nm)/mCP (10 nm)/host: dopant **Ir9** (25 nm)/TSPO1 (35 nm)/LiF (1 nm)/Al (200 nm)] using mCP as a host and **Ir9** as the dopant material and investigated the electroluminescence behavior. The EL device at a 5 wt% doping level of **Ir9** exhibited an external quantum efficiency of 14.6%, current efficiency of 18.3 cd $A^{-1}$ with $CIE_{(x, y)}$ coordinates of 0.14 and 0.17.

#### 1.3.1.2. Bulky Substituents on Ir−N Coordinating Pyridyl Ring for Minimizing the Aggregation Caused Quenching

To prevent detrimental aggregation phenomena, De Cola and coworkers have introduced a bulky *tert*−butyl substituent on the cyclometalated or azolated chelates at various positions and prepared a series of iridium complexes (**Ir12**−**Ir15**) and investigated their photoluminescence properties [Chart 1.5].[38] All the developed compounds exhibit highly efficient true blue emissions ($\lambda_{max}$ = 440 nm) at room temperature in solution as well as in thin film with promising quantum yield in the range 0.77−0.87 and 0.62−0.93, respectively.

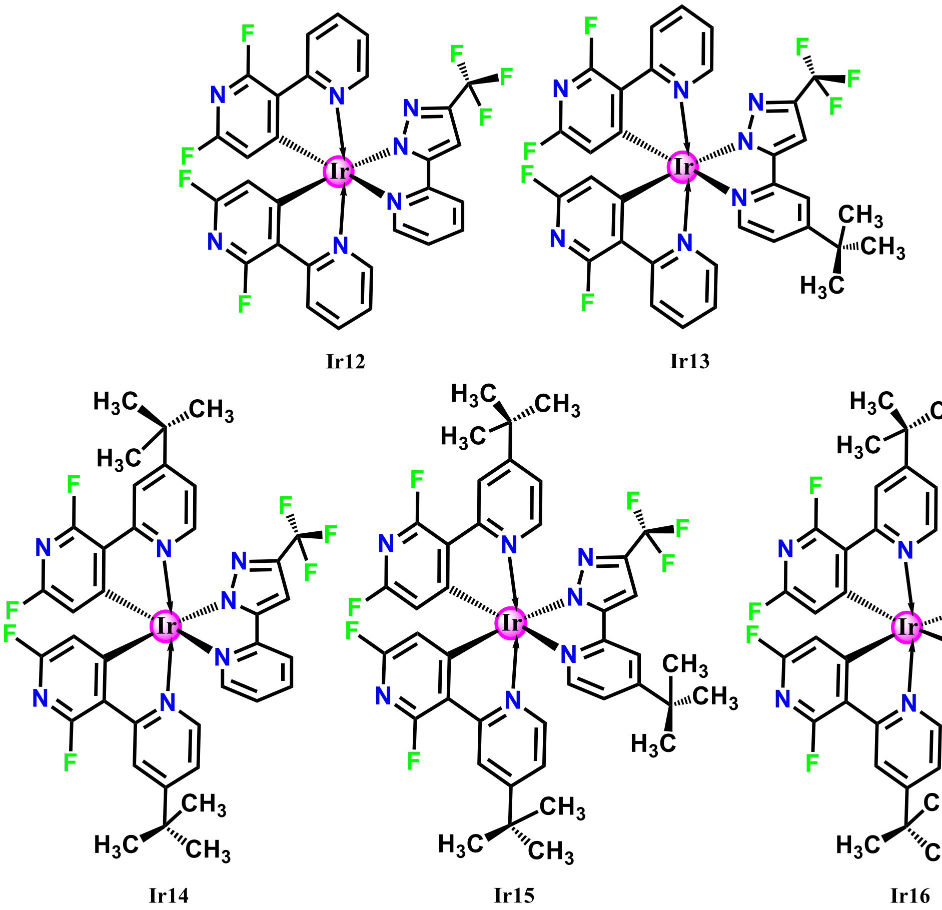

**Chart 1.5.** Chemical Structures of bis(2',6'–difluoro–2,3'–bipyridinato–N,C4')iridium(III) (3–trifluoromethyl–5–(2–pyridyl) pyrazolate) (**Ir12**), bis(2',6'–difluoro–2,3'–bipyridinato–N,C4')iridium(III) (3–(trifluoromethyl)–5–(4–t–butylpyridyl)pyrazolate) (**Ir13**), bis(2',6'–difluoro–4–tert–butyl–2,3'–bipyridinato–N,C4')iridium(III) (3–trifluoromethyl–5–(2–pyridyl) pyrazolate) (**Ir14**), bis(2',6'–difluoro–4–tert–butyl –2,3'–bipyridinato–N,C4')iridium(III) (3–(trifluoromethyl)–5–(4–t–butylpyridyl)pyrazolate) (**Ir15**) and bis(2',6'–difluoro–4– tert–butyl–2,3'–bipyridinato–N,C4')iridium(III) (1,10–Dimethyl–3,3'–methylenediimidazolate) (**Ir16**).

The introduction of *tert*−butyl groups lead to a larger distance between the iridium centers (Ir···Ir* = 9.5222(6) Å) in **Ir15** as compared to non−substituted **Ir12** (Ir···Ir* = 7.3564(3) Å). Indeed, the presence of bulky groups in the cyclometalated iridium(III) complexes play a significant role in preventing the stacking of the complexes, and thus reducing the quenching effect especially in the film state and consequently results in high quantum yields. The constructed device based on the bulkiest **Ir15** displays remarkable external quantum efficiency as high as 7.0 % in non−optimized device and power efficiency of 4.14 lm $W^{-1}$, with a true−blue chromaticity coordinates ($CIE_{x,y}$ = 0.159, 0.185) recorded at 300 cd $m^{-2}$.

A charged bis−cyclometalated iridium(III) complex (**Ir16**) with deep−blue emission at 440 nm has been developed by Baranoff and coworkers[39] based on dfpypy skeleton with the bulky *tert*−butyl groups at 4−position with a view to limit the inter−molecular interactions and bis−imidazolium carbene was used as an ancillary ligand [Chart 1.5]. The photoluminescence profile of **Ir16** in the solid−state is found to be similar to that of solution pattern. This can be attributed to the bulky *tert*−butyl substituents attached to the emitting ligand which prevents intermolecular stacking. The emission quantum yields of 0.59 and 0.17 are observed for **Ir16** in a 5% doped PMMA film and in a more concentrated film, respectively. The decrease in photoluminescence quantum yield when increasing the concentration of **Ir16** in a solid film indicates that significant exciton hopping occurs in a more concentrated film. The performance of the light emitting electrochemical cells are found to be significantly improved while employing **Ir16** as the emissive dopant. A greenish–blue electroluminescence with the maximum emission intensity at 500 nm is observed with a fast response time of 17s, brightness of over 100 cdm$^{-2}$ with current and power efficiencies of 5 cd A$^{-1}$ and 2 lm W$^{-1}$, respectively.

A high–performance blue phosphorescent OLED has been disclosed by Kessler and co–workers[32] employing a novel bis–heteroleptic iridium(III) complex (**Ir17**) with bulky *tert*–butyl group substituted at 4′–position in fluorinated 2,3′–bipyridine cyclometalated ligand and acetylacetonate as an ancillary ligand [Chart 1.6]. The **Ir17** doped mCP film (11 wt%) showed a emission peak at 454 nm with high quantum yield (0.78) and phosphorescence lifetime of 1.51µs at room temperature. The radiative decay rate of **Ir17** in mCP was found to be $5.1 \times 10^5$ s$^{-1}$, which is similar to that of FIrpic. The transient PL decay curve of the Ir17 doped mCP film exhibited almost single exponential decay (98%) with a short phosphorescence lifetime of 1.51µs at room temperature, indicating the effective suppression of the **Ir17** exciton quenching in the host and the expected small efficiency roll–off. The blue device with a structure of [ITO (130 nm)/TAPC (40 nm)/**Ir17** 11–20 wt% doped mCP (10 nm)/B3PyPB (50 nm)/LiF (0.5 nm)/Al (100 nm)] exhibited a high power efficiency of over 30 lm W$^{-1}$ and an external quantum efficiency of 17% with the CIE$_{x,y}$ coordinates of 0.16, 0.25. This is the highest performance OLED device so far has been reported based on blue emitting iridium(III) complex, derived from 2,3′–bipyridine class of ligands. Although the y value of the CIE color coordinate is relatively high.

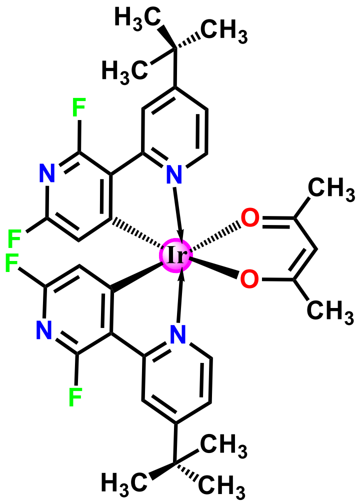

**Ir17**

**Chart 1.6.** Chemical Structure of bis(2',6'–difluoro–4– tert–butyl–2,3'–bipyridinato–N,C4')iridium(III) (acetylacetonate) (**Ir17**).

### 1.3.2. Substitutions on Ir−C Bonded Pyridyl Ring

The insights provided by the DFT calculations on tris−2,6−difluro−2,3′−bipyrine cyclometalated iridium(III) complex (**Ir1**) clearly indicates that the HOMO energy levels are mostly contributed from the π−orbitals of the Ir−C bonded pyridyl moiety as well as iridium(III) *d* orbitals. Hence any change of substitution on the corresponding pyridyl ring will have major implications on the highest occupied molecular orbitals, which ultimately reflect on the electrochemical as well as emission properties. Based on this concept, several substitution strategies were carried out on the Ir−C bonded pyridyl ring to develop efficient phosphorescent emitters from 2,6−difluro−2,3′−bipyrine class of compounds.

#### 1.3.2.1 Replacing of −F with More Electron−Withdrawing –$CF_3$

It is well documented that the fluorination in phosphorescent molecules can heighten the electron mobility and consequently balances the better charge injection and transport properties. The presence of C–F bond in a molecule can diminish the rate of radiationless deactivation. Further, the bulky –$CF_3$ substituents can influence the molecular packing and the steric protection around the metal, which can inhibit the self−quenching phenomenon. Based on the above facts, Zheng and coworkers have derived an iridium(III) complex (**Ir18**) from –$CF_3$ substitution on the Ir−C bonded pyridyl ring of 2,3′−bipyridine as the cyclometalated ligand and tetraphenylimidodiphosphinate as an ancillary ligand and evaluated the photoluminescence and electrochemical properties [Chart 1.7].[40] The **Ir18** displays green emission at 500 nm with a quantum efficiency of 0.63. Moreover, it is interesting to note that the presence of more electron−withdrawing –$CF_3$ substituent has dramatically shifted the emission profile of **Ir18** towards the red region ($\lambda_{max}$ = 500 nm) as compared to its fluorinated compound **Ir19** ($\lambda_{max}$ = 457 nm), which is contrary to the expected trend.[41] The noted red shift may be due to the large electron−withdrawing ability of the –$CF_3$ in the Ir−C bonded pyridyl ring placed at the *ortho*/*para* positions to the N−coordinated pyridyl ring, which stabilizes the LUMO levels rather than HOMO. This is in consistent with the observed experimental HOMO/LUMO levels (−6.00/−3.20 eV for **Ir18** and −5.93/−3.05 eV for **Ir19**). In addition, **Ir18** exhibits superior electron mobility (7.00–7.20 × $10^6$ $cm^2$ $V^{-1}$ $s^{-1}$) than that of $Alq_3$ (4.74–4.86 × $10^6$ $cm^2$ $V^{-1}$ $s^{-1}$). The OLED device prepared based on **Ir18** as the emitter with a device structure of ITO/TAPC (40 nm)/ mCP (10 nm)/**Ir18** (8 wt %): PPO21 (25 nm)/TmPyPB (50 nm)/LiF (1 nm)/Al (100 nm) show excellent current efficiency ($\eta_c$) of 101.96 cd $A^{-1}$ (at 7.8 V) at a brightness of 10000 cd $m^{-2}$ with a maximum EQE of 31.6 %. The exceptional device performance has been attributed to the high quantum efficiency as well as high electron mobility associated with **Ir18**.

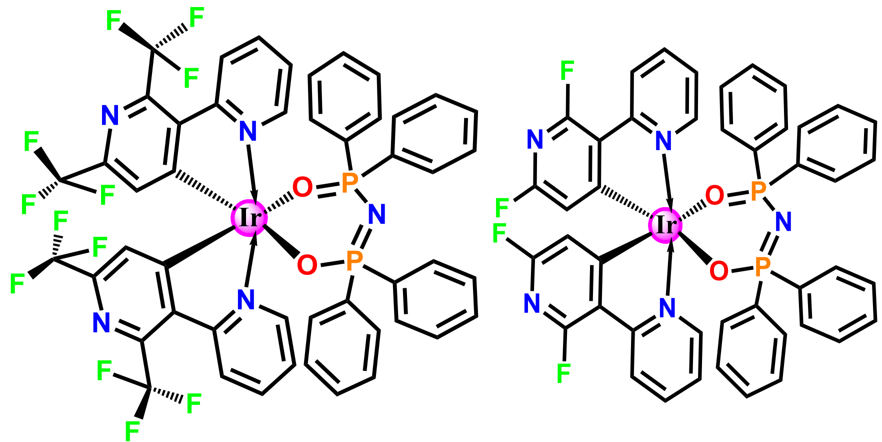

**Ir18** **Ir19**

**Chart 1.7.** Chemical Structures of bis(2',6'–trifluoromethyl–2,3'–bipyridinato–N,C4')iridium(III) (tetraphenylimidodiphosphinate) (**Ir18**) and bis(2',6'–difluoro–2,3'–bipyridinato–N,C4')iridium(III) (tetraphenylimidodiphosphinate) (**Ir19**).

### 1.3.2.2. Replacing of −F with Alkoxy− or Alkyl− Substituents (Fluorine−Free 2,3′−Bipyridine Ligands)

One of the popular approaches to design and develop novel blue emitters based on iridium(III) compounds is to functionalize C^N with electron−withdrawing groups (−F or $-CF_3$) or substitute electron−donor moieties on N^N. However, the use of fluorine groups is not desirable in cyclometalated ligand systems for use in OLED applications, which breaks the –C–F bonds during the operation of the device,[42] and from an environmental point of view. In view of these inherent limitations, several efforts have been made over the years to prepare fluorine−free blue phosphorescent iridium complexes, with a view to improving the long−term stability of the emitters in PhOLEDs.[43] Kang and coworkers accidentally noted the formation of fluorine−free blue emitting heteroleptic iridium(III) complex **Ir20** in the process of preparation of a heteroleptic iridium(III) complex using 2,6−difluoro−2,3′−bipyridine (dfpypy) cyclometalating ligand [Chart 1.8].[44]

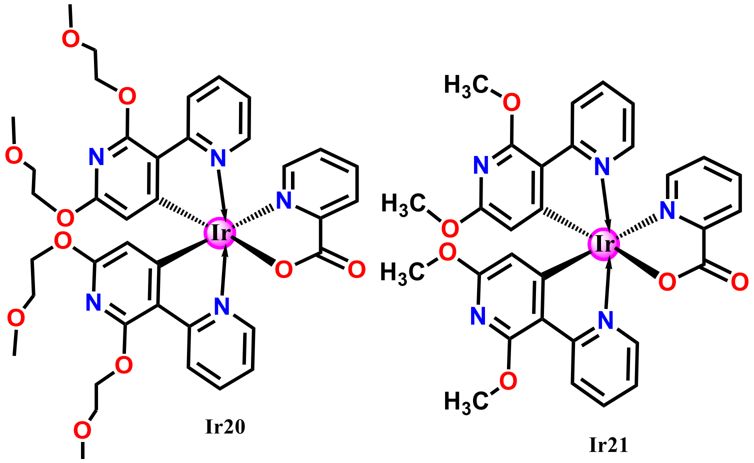

**Ir20**

**Ir21**

**Chart 1.8.** Chemical Structures of bis(2',6'–bis(2–methoxyethoxy)–2,3'–bipyridinato–N,C4')iridium(III) (picolinate) (**Ir20**) and bis(2',6'–dimethoxy–2,3'–bipyridinato–N,C4')iridium(III) (picolinate) (**Ir21**).

During the synthesis process, the nucleophilic substitution of fluorine atoms in dimer complex $[(\text{dfpypy})_2\text{Ir}(\mu{-}\text{Cl})]_2$ by a methoxy-ethanol in the presence of ancillary ligand picolinate led to the formation of new alkoxy−functionalized heteroleptic iridium(III) compound $\text{Ir}[(\text{RO})_2\text{pypy}]_2(\text{N}^\wedge\text{O})$. Interestingly, the alkoxy−substituted complex **Ir20** shows identical emission behaviour as that of the fluorine−substituted counterpart (**Ir8**) with excellent quantum efficiencies ($\Phi_{PL}$ = 0.76 in solution and 0.96

in the solid state). Thus, the above strategy gives a pathway to isolate fluorine−free bright blue phosphorescent iridium(III) compounds (**Ir21**) based on 2,3′− bipyridine ligands with methoxy substituents in the presence picolinic acid as an ancillary ligand. These authors have pointed out that, although the compounds **Ir20** and **Ir21** are having very similar structural features, except for the alkoxy groups (methoxyethoxy *versus* methoxy), the emission energy of **Ir20** is about 10 nm blue−shifted relative to that of **Ir21**, indicating the possibility of tuning the emission colour by alkoxy−substituent. These results clearly suggest that the substitution of a fluorine atom with an alkoxy−group has significantly improved the solubility of these compounds in usual organic solvents without altering the emission colour and efficiencies, leading to their potential use in solution−processable PhOLEDs.

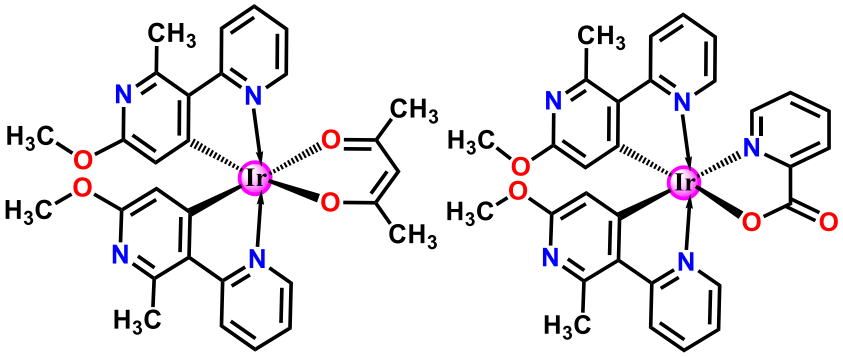

**Ir22** **Ir23**

**Chart 1.9.** Chemical Structures of bis(6'–methoxy–2'–methyl–2,3'–bipyridinato–N,C4')iridium(III) (acetylacetonate) (**Ir22**) and bis(6'–methoxy–2'–methyl–2,3'–bipyridinato–N,C4')iridium(III) (picolinate) (**Ir23**).

With the aid of Hammet parameter model, fluorine−free iridium complexes **Ir22** and **Ir23** have been developed by replacing fluorine acceptor groups with methyl and methoxy donor groups at 2′ and 6′ positions of Ir−C bonded pyridyl ring of 2,3′−bipyridine ligands and compared their emission properties with the commercially available sky−blue emitter FIrpic [Chart 1.9].[27] The designed fluorine−free iridium(III) complex (**Ir23**) displays a broader sky−blue emission with a slight blue shift in degassed acetonitrile solution at ambient−temperature, which is similar to that of FIrpic ($\Phi_{PL}$= 0.61, τ = 1.69 μs ) with a quantum yield of 0.54 and excited state lifetime of 1.29 μs. The blue shift induced by methoxy can be mainly attributed to the strong donor character towards the *para* position, leading to a more robust destabilization of the LUMO than the HOMO. Also, a virtually identical redox potentials were noticed for this fluorine−free **Ir23** as that of FIrpic.

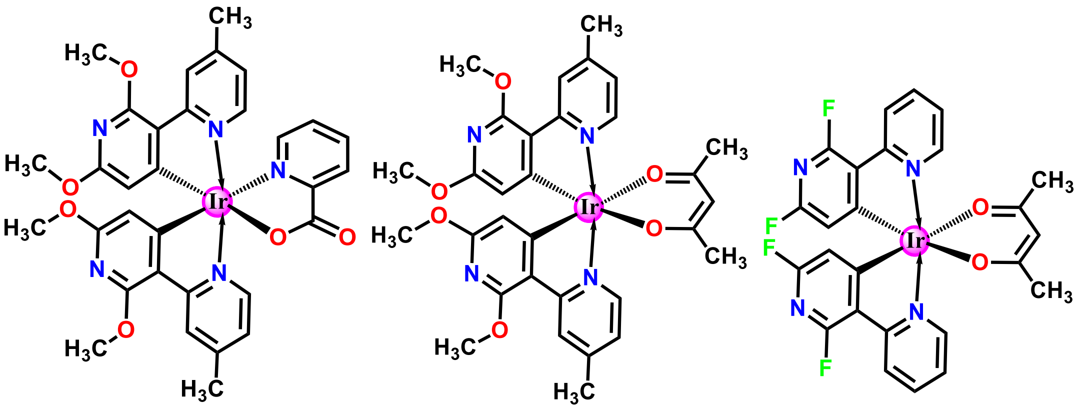

**Ir24** **Ir25** **Ir26**

**Chart 1.10.** Chemical Structures of bis(2',6'–dimethoxy–4–methyl–2,3'–bipyridinato–N,C4')iridium(III) (picolinate) (**Ir24**), bis(2',6'–dimethoxy–4–methyl–2,3'–bipyridinato–N,C4')iridium(III) (acetylacetonate) (**Ir25**) and bis(2',6'–difluoro–2,3'–bipyridinato–N,C4')iridium(III) (acetylacetonate) (**Ir26**).

Kang and coworkers have designed a fluorine−free cyclometalated ligand, namely, 2′,6′−dimethoxy−4−methyl−2,3′−bipyridine and utilized for the development of heteroleptic iridium(III) compounds **Ir24** or **Ir25** with blue phosphorescence in the presence of acetylacetonate or picolinate as the ancillary ligand [Chart 1.10].[45] An increased molar extinction coefficient ($\varepsilon > 5000$ $M^{-1}$ $cm^{-1}$) of the $^1$MLCT transitions observed for **Ir24** and **Ir25** in comparison with the corresponding fluorinated congeners (**Ir26**, and **Ir8,** $\varepsilon \sim 4300$ $M^{-1}$ $cm^{-1}$**)** reveals the existence of strong spin–orbit coupling. A Multi−layer PhOLED was fabricated using **Ir24** and **Ir25** as the dopant and mCPPO1 as a host material with a device configuration of (ITO, 50 nm)/ (PEDOT: PSS, 60 nm)/ TAPC (20 nm)/mCP (10 nm)/ mCPPO1–dopant **Ir24** or **Ir25** (25 nm)/TSPO1 (35 nm)/LiF (1 nm)/Al (200 nm). EL device based on **Ir25** at a doping level of 5% shows the best performance with a high external quantum efficiency of 15.3%. This result is found to be one of the best device performances using a blue phosphorescent iridium(III) emitter with a fluorine−free 2,3′−bipyridine ligand.

A new class of charged cyclometalated iridium(III) compounds (**Ir27**−**Ir30**) have been developed using methoxy− and methyl− substituted 2,3′−bipyridine as the primary ligands and 4,4′−di−tert−butyl−2,2′−bipyridine (dtBubpy), as the ancillary ligand [Chart 1.11].[22] The charged complexes exhibit bluish−green emission with moderate quantum yields of about 40% in degassed solution and emission lifetimes of the excited state are about 1.4 μs. The solid−state emission spectra of these cationic

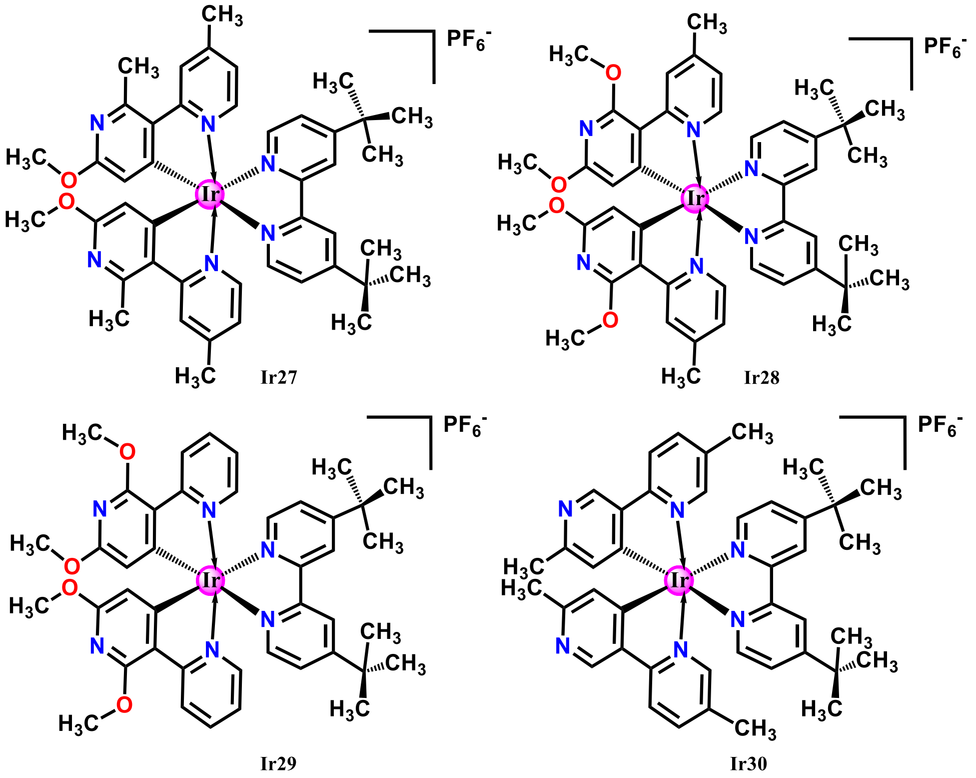

**Chart 1.11.** Chemical Structures of bis(6'–methoxy–2'–methyl–4–methyl–2,3'–bipyridinato–N,C4') iridium(III) (4,4'–di–tert–butyl–2,2'–bipyridine) hexafluorophosphate (**Ir27**), bis(2',6'–dimethoxy–4–methyl–2,3'–bipyridinato–N,C4')iridium(III) (4,4'–di–tert–butyl–2,2'–bipyridine) hexafluorophosphate (**Ir28**), bis(2',6'–dimethoxy–2,3'–bipyridinato–N,C4')iridium(III) (4,4'–di–tert–butyl–2,2'–bipyridine) hexafluorophosphate (**Ir29**) and bis(5,6'–Dimethyl–2,3'–bipyridinato–N,C4')iridium(III) (4,4'–di–tert–butyl–2,2'–bipyridine) hexafluorophosphate (**Ir30**).

complexes are red−shifted (< 10 nm) compared to the solution− state spectra. However, a large red−shift of about 32 nm has been noted in **Ir30**, due to aggregation, where the bulky tertiary butyl substituents are present in the ancillary ligand are not sufficient to prevent such red−shifts. The $\Phi_{PL}$ values in thin films of the cationic complexes are found to be somewhat lower than that observed in solution, ranging from 19−32% for **Ir27**−**Ir29**. Conversely, poor $\Phi_{PL}$ value of about 2% noted in the case of **Ir30**. Thus it can be concluded that larger methoxy groups in the cyclometalated ligands are required to prevent the quenching. In order to evaluate the potential of these complexes for electroluminescence, LEECs were fabricated. Compared to an earlier device with fluorine−containing emitters, the present devices exhibits a slightly red−shifted electroluminescence due to methyl substituents on the ancillary and cyclometalated ligands, while the overall device performances, including stability, are similar. **Ir28** leads to the best LEEC figures among the series with a maximum luminance of 1000 cd $m^{-2}$ and efficacy of 9.47 cd $A^{-1}$, which is promising in view of replacing fluorine substituents with methoxy groups in the blue phosphorescent emitters.

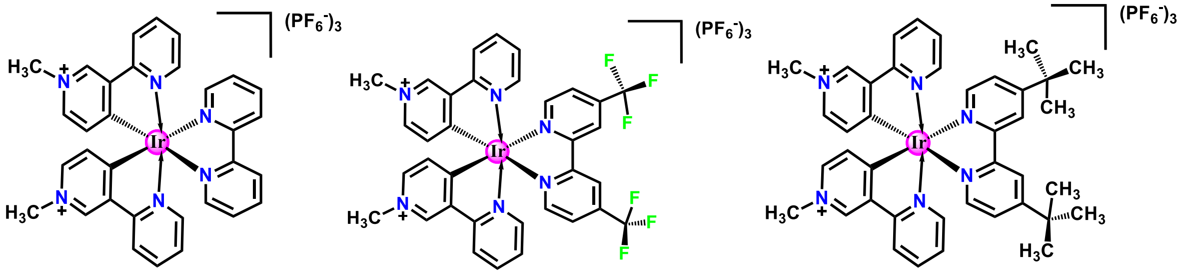

Ir31 Ir32 Ir33

**Chart 1.12.** Chemical Structures of bis(1–methyl–3–(2'–pyridyl)pyridinium –N,C4')iridium(III) (2,2'–bipyridine) tris–hexafluorophosphate (**Ir31**), bis(1–methyl–3–(2'–pyridyl)pyridinium –N,C4')iridium(III) (4,4'–di–methyl–2,2'–bipyridine) tris–hexafluorophosphate (**Ir32**) and bis(1–methyl–3–(2'–pyridyl)pyridinium –N,C4')iridium(III) (4,4'–di–tert–butyl–2,2'–bipyridine) tris–hexafluorophosphate (**Ir33**).

Coe and coworkers have developed an alternative approach for creating a series of fluorine−free iridium(III) luminophores using 1−methyl−3−(2′−pyridyl) −pyridinium as the cyclometalated ligand and *tert*−butyl or $-CF_3$ substituted (at 4,4′ positions) 2,2′−bipyridine as ancillary ligands [Chart 1.12].[46] The placing of quaternized nitrogen opposite to the Ir−C bonded carbon in the cyclometalated ligand is crucial in blue−shifting the emission. The developed water soluble complexes **Ir31** , **Ir32** and **Ir33** displays efficient luminescence in acetonitrile or aqueous solutions with a large range of lifetimes (≈ 1–12 μs) and relatively high quantum yields ($\Phi_{PL}$ ≈ 42–45%). The emission profiles are found to be similar for unsubstituted **Ir31** and *tert*−butyl substituted **Ir33** ($\lambda_{em}$ = 468–474 nm). On the other hand, replacing –H with –$CF_3$ group significantly red−shifted the emission to 494 nm in **Ir32**. The almost identical spectra of **Ir31** and **Ir33** disclose that mainly $^3$LC emission involving C^N with little $^3$MLCT contribution. However, the red−shift for **Ir32** indicates that emission is associated with N^N. Thus the presence of electron−withdrawing –$CF_3$ groups stabilizes the π* orbitals of N^N ligand, lowering the energy of $^3$LC state. The bright blue emission in acetonitrile or water for the fluorine−free complexes **Ir31** and **Ir33** suggest potential applications in highly efficient OLEDs or bio−imaging.

## 1.4. Modifications on Ancillary Ligand

### 1.4.1. Enhancing Emission Properties Using Ancillary Ligand without Any Spectral Change

The influence of ancillary ligand affecting the phosphorescence emission in heteroleptic iridium(III) complexes is somewhat different from that of cyclometalated ligands. The ancillary ligand chelates (L^X) which possess higher triplet excited states than that of the cyclometalated C^N ligands are capable of modulating the photophysical properties of heteroleptic iridium(III) complexes due to their intrinsic ligand field strength and electronic influences towards the central iridium atom.[11, 47] With the above concept in mind, Kang et al. have replaced one of the cyclometalated dfpypy ligand with an appropriate ancillary ligand in Ir(dfpypy)$_3$ in order to elevate the HOMO energy level without altering the emissive energy gap, and also to match well with those of the common host materials for OLED applications.[37] A series of heteroleptic iridium(III) compounds Ir(dfpypy)$_2$(L^X) [where L^X is either picolinate, acetylacetonate or dipivaloylmethanoate as can be seen from Figure 1.9] has been synthesized and their photophysical properties were investigated. All the iridium(III) compounds exhibit bright blue phosphorescence ($\lambda_{max}$ = 440−460 nm) with quantum efficiencies in the range 0.60−0.95 in both solution and solid state. The results demonstrated that the ancillary ligand has been found to significantly change the energy of both HOMO and LUMO orbitals, without altering the phosphorescence energy. This can be well understood from the single crystal X−ray structure of these compounds, where C^N chelates forms stronger bonds with iridium(III) centers compared to that of Ir(dfpypy)$_3$, due to the weak trans directing effect of the ancillary ligands. In the subsequent studies, Kang and co−workers have developed efficient deep−blue PhOLEDs utilizing the heteroleptic compounds **Ir11** and **Ir26** as dopants and mCPPO1 as the host material.[48] The EL device of **Ir11** at a doping level of 3.0 wt % shows the best performance with EQE of 18.5 – 20.4 % at the brightness of 100−1000 cdm$^{-2}$ and the CIE$_{(x, y)}$ colour coordinates of (0.14, 0.18) at 1000 cdm$^{-2}$.

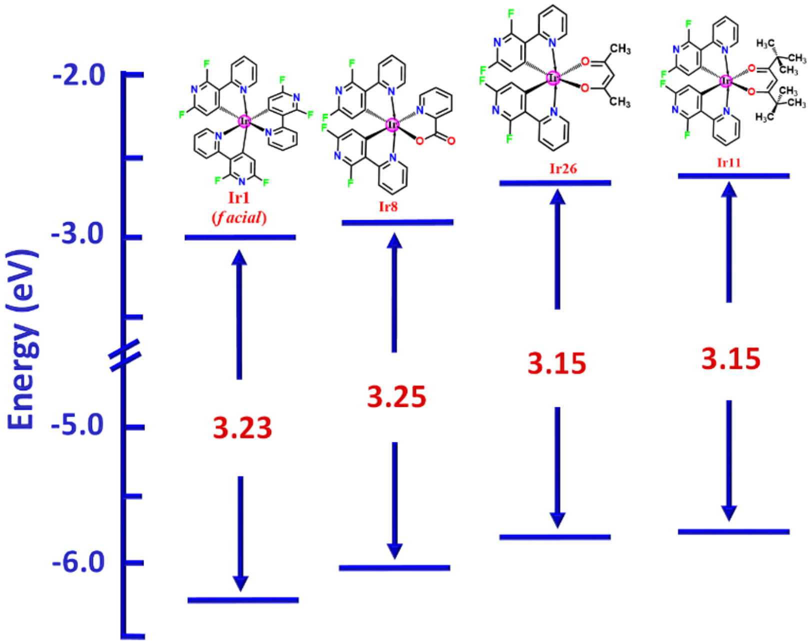

**Figure 1.9.** Comparison of experimental HOMO–LUMO energy levels of **Ir1**, **Ir8**, **Ir11** and **Ir26**.

Hung and co-workers have synthesized two chemically stable iridium(III) metal complexes (**Ir34** and **Ir35**) containing a cyclometalated ligand, 2’,6’-dimethoxy-4-t-butyl-2,3’-bipyridine in the presence of 5-pyridin-2-yl-pyrazolate or 5-pyridin-2-yl-pyrrolide as ancillary ligands (Chart 1. 13) and investigated their photophysical and electroluminescence properties with a view to construct a longer lifespan OLED devices.[49] The isolated iridium(III) complexes showed essentially identical spectral features, with two peak maxima at 458 and 489 nm and a less intense shoulder in the longer wavelength region. The occurrence of these vibronic envelopes reflected the strong influence of the $^3\pi$-$\pi$* excited states along with a minor contribution from the $^3$MLCT excited states. The photophysical studies demonstrated that the existence of intense, structured blue phosphorescence with a $E_{0\text{-}0}$ peak (≤ 458 nm) with a high quantum yield ($\Phi_{PL} \geq 0.79$) in $CH_2Cl_2$. High quantum yields have been observed in the present system when compared to similarly structured complex **Ir24** ($\Phi_{PL} = 0.44$) having picolinate as an ancillary ligand. This can be attributed to the more rigidity of the pyridyl azolate or pyrrolide ancillary ligand, which supresses the nonradiatative decay pathways. As for the OLED applications, **Ir35** exhibited highest efficiency characteristics i.e. maximum external quantum ($\eta_{ext}$), current ($\eta_c$), and power efficiencies ($\eta_p$) of 14.3%, 23.8 cd $A^{-1}$, and 18.2 lm $W^{-1}$, respectively with a blue $CIE_{(x,y)}$ coordinates of 0.16 and 0.24.

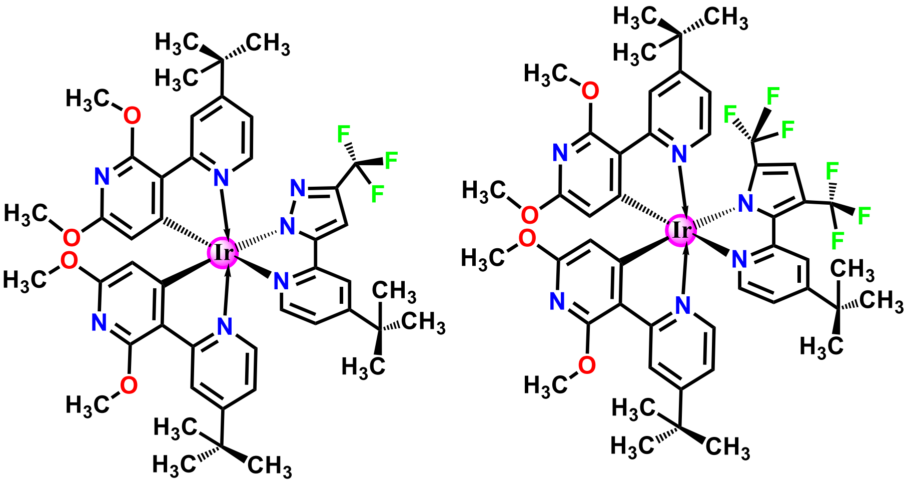

**Ir34** **Ir35**

**Chart 1.13.** Chemical Structures of bis(2',6'–dimethoxy–4–tert–butyl–2,3'–bipyridinato–N,C4') iridium(III) (3–(trifluoromethyl)–5–(4–t–butylpyridyl)pyrazolate) (**Ir36**) and bis(2',6'–dimethoxy–4–tert–butyl–2,3'–bipyridinato–N,C4') iridium(III) (2,4–(bistrifluoromethyl)–5–(4–t–butylpyridyl)pyrrolate) (**Ir37**).

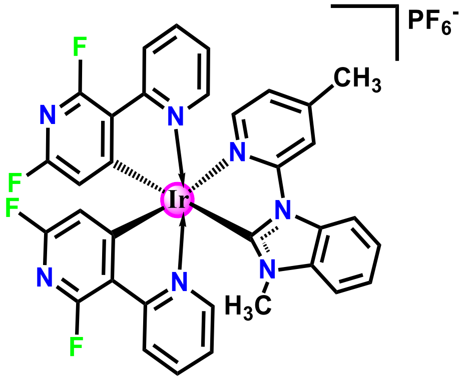

**Ir36**

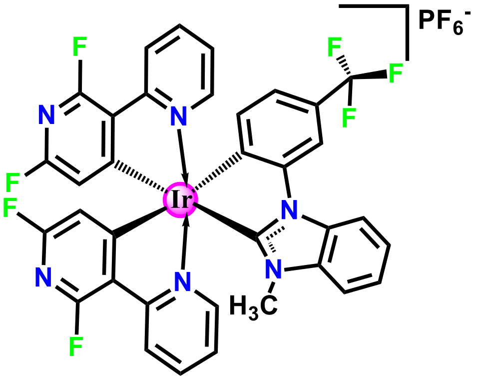

**Ir37**

**Chart 1.14.** Chemical Structures of bis(2',6'–difluoro–2,3'–bipyridinato–N,C4')iridium(III) 3–methyl–1–(4–methyl–2–pyridyl)benzimidazolium hexafluorophosphate (**Ir36**) and bis(2',6'–difluoro–2,3'–bipyridinato–N,C4')iridium(III) 3–methyl–1–(4–trifluoromethyl–2–pyridyl)benzimidazoliumhexafluoro phosphate (**Ir37**).

N−heterocyclic carbenes (NHC) have been evolved as a new class of cyclometalating as well as ancillary ligands for the transition metal complexes.[50] The shorter distance usually seen between the metal and coordinating carbon of a carbene ligand, which is primarily responsible for the strong dative interaction in these complexes. As a result of this, the experienced large ligand field strength upon the metal center could destabilize the thermally accessible *d*−*d** excited states away from the emissive triplet excited states, which helps in exhibiting efficient phosphorescence emission.[19a, 43d] Baranoff et al., first time utilized a neutral pyridine−carbene ((1−methyl−3−(3−(methyl)pyridyl) −benzimidazolin−2−ylidene−N,C2′)) ancillary ligand for the development of a charged biscyclometalated complex (**Ir36**) using 2′,6′−difluoro−2,3′−bipyridine as cyclometalating ligand [Chart 1.14].[51] Upon excitation, **Ir36** shows blue emission with a quantum yield of 0.20 in degassed acetonitrile at room temperature. Meanwhile, Zheng et al. utilized a new type of N−heterocyclic carbene, namely, 1−methyl−3−(3−(trifluoromethyl)phenyl)−benzimidazolin−2−ylidene−C,C2′ as an ancillary ligand for the development of blue emitting iridium(III) complex (**Ir37**) using dfpypy as the main cyclometalated ligand.[52] **Ir37** exhibits an identical emission profile as well as less quantum efficiency ($\Phi_{PL}$ = 0.09) compared to the analogue complexes such as **Ir8** and **Ir26** containing picolinate or acetylacetonate as ancillary ligands.

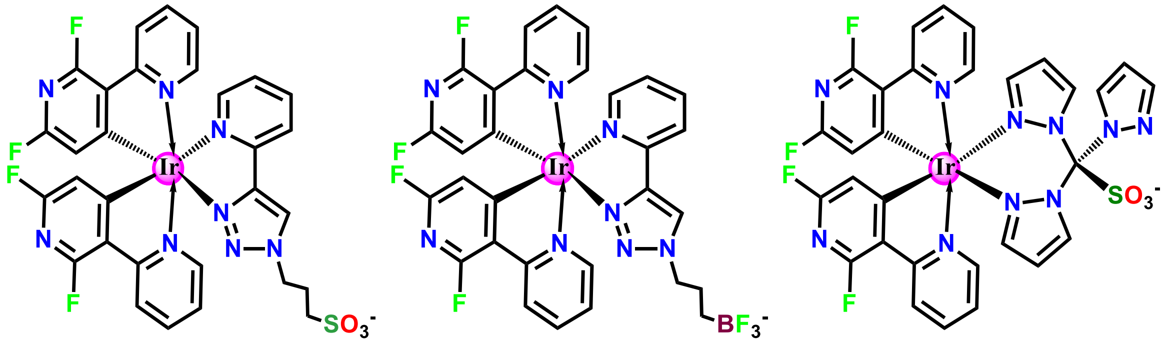

**Ir38** **Ir39** **Ir40**

**Chart 1.15.** Chemical Structures of bis(2',6'–difluoro–2,3'–bipyridinato–N,C4')iridium(III) 3–(4–(pyridin–2–yl)–1H–1,2,3–triazol–1–yl)propane–1–sulfonate (**Ir38**), bis(2',6'–difluoro–2,3'–bipyridinato–N,C4') iridium(III) trifluoro((4–(pyridin–2–yl)–1H–1,2,3–triazol–1–yl)methyl)–borate (**Ir39**) and bis(2',6'–difluoro–2,3'–bipyridinato–N,C4')iridium(III) tris(pyrazolyl)–methanesulfonates (**Ir40**).

In addition to the neutral, cationic and anionic iridium(III) complexes, zwitterionic compounds of iridium(III) complexes constitutes an alternate and an attracting emitting systems for OLED applications.[53] Due to the higher dielectric constant in the soft−salt lattice, the charge mobility is expected to be superior to that of neutral molecules.[54] Luisa De Cola and co−workers have reported a series of highly efficient blue and deep−blue emitting zwitterionic iridium(III) compounds

(**Ir38**−**Ir40**), containing a cationic iridium(III) center and a N,N′−heteroaromatic (N^N) ancillary ligand having negatively charged side groups, such as sulfonate and borate [Chart 1.15].[55] These zwitterionic compounds display intense−blue ($\lambda_{max}$ at 450 nm) and deep−blue ($\lambda_{max}$ at 435 nm) emissions in deaerated solution similar to that of cationic complexes reported elsewhere.[1c] The photoluminescent quantum yields and excited state lifetimes of dfpypy based zwitterionic complexes are found to be higher ($\Phi_{PL}$= 0.50−0.72) than the values of dfppy analogues ($\Phi_{PL}$= 0.20).

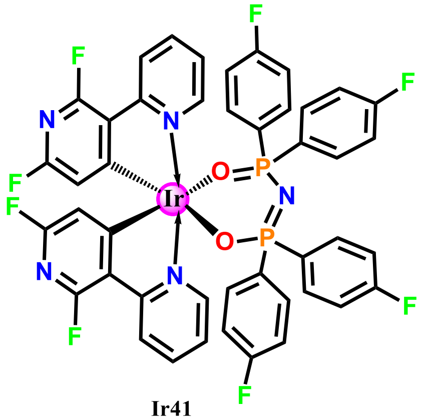

**Ir41**

**Chart 1.16.** Chemical Structure of bis(2',6'–difluoro–2,3'–bipyridinato–N,C4')iridium(III) (4–fluorophenyl)imidodiphosphinate) (**Ir41**).

Diphenyl phosphoryl ($Ph_2P=O$) units have been widely employed in OLEDs with an aim to develop electron−transport and ambipolar host materials because of its electron−deficient nature with enhanced electron injecting and transporting abilities.[56] Zheng et al. have first time introduced $Ph_2P=O$ units in the ancillary ligand,[40, 57] namely, tetraphenylimidodiphosphinate acid (Htpip) and isolated two iridium(III) complexes (**Ir19** and **Ir41**) using dfpypy as a cyclometalated ligand and investigated their photoluminescence and device performances [Chart 1.7 and 1. 14].[41] The iridium compounds **Ir19** and **Ir41** exhibit sky–blue emission in $CH_2Cl_2$ when excited at 370 nm. These compounds almost display identical emission behaviour with a maximum at 475 nm, indicating that the introduction of fluorine in tpip ancillary ligand have no obvious effect on absorption as well as emission properties. The $(dfpypy)_2Ir(tpip)$ and $(dfpypy)_2Ir(Ftpip)$ compounds exhibited blue emission at 457 nm with quantum yields of 7.0 % and 7.1%, respectively. OLED devices with the structure of ITO/TAPC (40 nm)/mCP (10 nm)/**Ir19** or **Ir41** (8 wt %): PPO21 (25 nm)/TmPyPB (50 nm)/LiF (1 nm)/Al (100 nm) showed performances with the maximum current efficiency ($\eta_c$) values of 22.83 and 20.79 cd $A^{-1}$, respectively, with low–efficiency roll–off. The presence of four bulky phenyl groups lead to a significant spatial separation of the neighboring molecules of the iridium(III) complexes and as a result, suppress the triplet–triplet annihilation and triplet–polaron annihilation effects and hence excellent current efficiency and low–efficiency roll–off was observed in these devices.

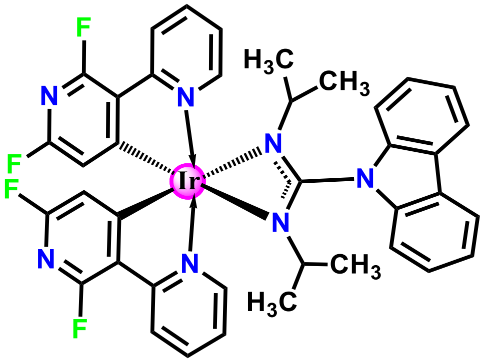

**Ir42**

**Chart 1.17.** Chemical Structure of bis (2',6'–difluoro–2,3'–bipyridinato–N,C4')iridium(III) (9H–carbazol–9–yl)(diisopropyl)amidate (**Ir42**).

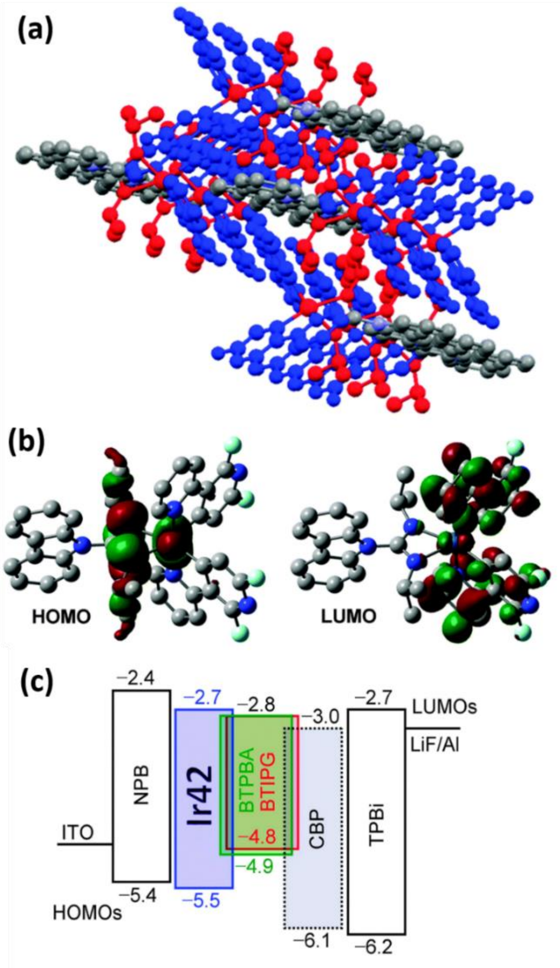

**Figure 1.10.** (a) Molecular packing diagram indicates holes (red) and electrons (blue) transporting channels for of **Ir42**. (b) Contour plots of HOMO and LUMO in **Ir42** from DFT calculations. (c) Energy level diagram of the materials used in OLEDs where **Ir42** acts as a host as well as hole− transporting material. BTPBA and BTIPG serve as red and green phosphorescent dopants, respectively.

Liu et al. have demonstrated an effective molecular design strategy for the development of a bipolar phosphorescent iridium(III) complex host (**Ir42**) based on amidinate (N^N) as an ancillary ligand (dipcca) and dfpypy as a cyclometalating ligand [Chart 1.17].[58] Based on the DFT calculations the authors have concluded that the

HOMO of the synthesized iridium(III) complex is primarily distributed on the d−orbitals of the Ir atoms an N atoms of the ancillary ligand while the LUMO is located in the cyclometalated ligands. Such large spatial distribution of HOMO and LUMO can provide hole− and electron−transporting channels, respectively, where both type of charges can realize intermolecular hopping smoothly along their respective pathways (Figure 1.10). The derived bipolar phosphorescent complex has been used as a host material for realizing efficient red PhOLEDs. The constructed PhOLED showed stable deep−red emitting colour and high external quantum efficiency (EQE > 23%) under wide luminance range of 1000−10000 cd/$m^2$.

### 1.4.2. Facile Color Tuning Using Ancillary Chelate in Heteroleptic Iridium(III) Complexes

It is also known in the literature that when the ligand−centered energy gap of C^N chelate is greater than that of the L^X ancillary ligand, longer wavelength emissions have been realized in some heteroleptic iridium(III) complexes.[5c, 5d, 5f, 5g] One of the best known example was successfully demonstrated by Park et al.[5e] regarding the phosphorescence colour tuning by virtue of intramolecular interligand energy transfer (ILET) in a series heteroleptic iridium(III) complexes Ir(dfppy)$_2$(L^X) [where dfppy =2,6′−difluorophenylpyridine and L^X = quinaldinate, isoquinolinate and pyrazinate]. Subsequently, Kang and coworkers[44] have observed similar kind of phenomenon in a series of heteroleptic Ir(dfpypy)$_2$(L^X) complexes **Ir43**−**Ir45** [where L^X = pyrazinate, isoquinolinate and quinolinate] involving 2,6′−difluoro−2,3′−bipyridine cyclometated ligand and various picolinate derivatives as ancillary ligands [Chart 1.18]. These compounds exhibit intense−blue to yellow phosphorescence ($\lambda_{max}$ = 453 to 558 nm) with moderate to high quantum efficiencies (0.20−0.96).

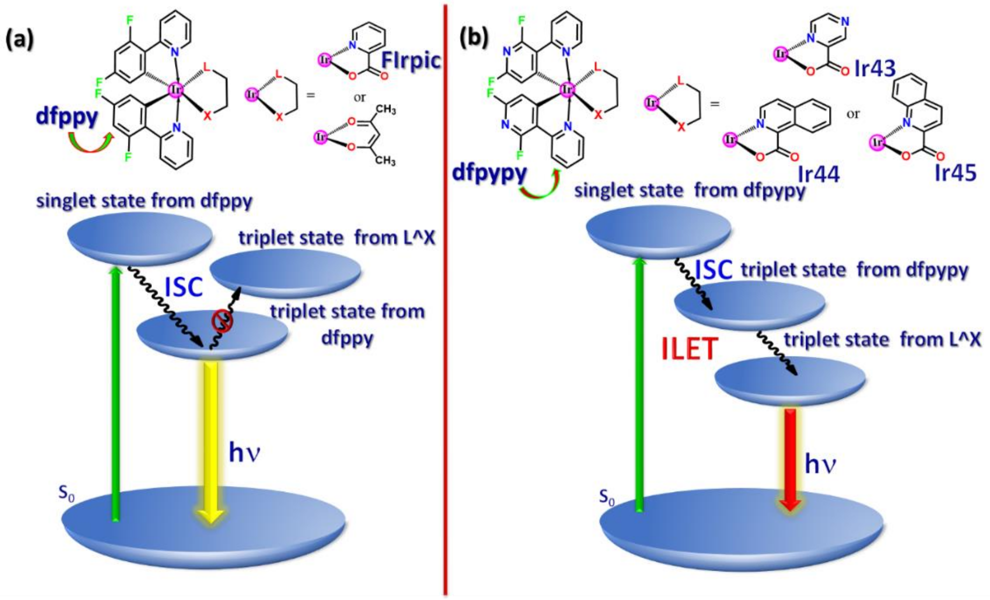

**Figure 1.11.** (a) Schematic representation of a typical $^3$MLCT/$^3$LC based emission process in a heteroleptic iridium(III) complex involving a low lying triplet state from a cyclometalating ligand rather than from a high energy ancillary L^X ligand. (b) Intramolecular inter−ligand energy transfer (ILET) process involving the low lying triplet state of an ancillary L^X ligand.

These results demonstrated that cyclometalated ligand is preferentially excited, then the low energy ancillary ligand accepts the excited state energy through ILET mechanism, eventually giving rise to the ancillary ligand−centered phosphorescence (Figure 1.11). These authors also noted similar kind of energy transfer mechanism in a series of heteroleptic Ir[(RO)$_2$pypy]$_2$(L^X) complexes **Ir46**−**Ir48** [where L^X =

pyrazinate, isoquinolinate and quinolinate; and RO stands for 2,6′–bis(2–methoxyethoxy)–2,3′–bipyridine] complexes [Chart 1.18].

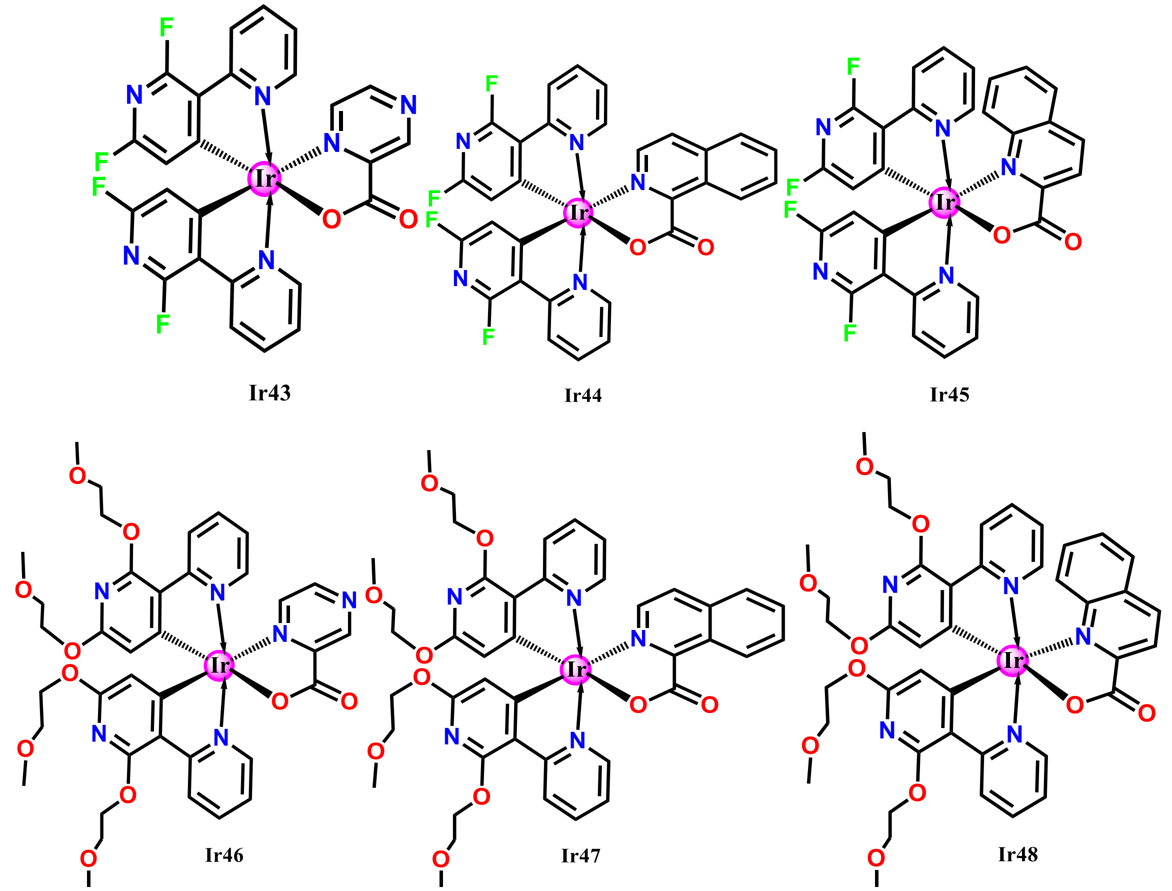

**Ir43** **Ir44** **Ir45**

**Ir46** **Ir47** **Ir48**

**Chart 1.18.** Chemical Structures of bis(2',6'–difluoro–2,3'–bipyridinato–N,C4')iridium(III) (pyrazinate) (**Ir43**) bis(2',6'–difluoro–2,3'–bipyridinato–N,C4')iridium(III) (isoquinolinate) (**Ir44**), bis(2',6'–difluoro–2,3'–bipyridinato–N,C4')iridium(III) (quinaldinate) (**Ir45**), bis(2',6'–bis(2–methoxyethoxy)–2,3'–bipyridinato–N,C4')iridium(III) (pyrazinate) (**Ir46**), bis(2',6'–bis(2–methoxyethoxy)–2,3'–bipyridinato–N,C4')iridium(III) (isoquinolinate) (**Ir47**) and bis(2',6'–bis(2–methoxyethoxy)–2,3'–bipyridinato–N,C4') iridium(III) (quinaldinate) (**Ir48**).

In the later studies, these authors have isolated a heteroleptic cyclometalated iridium(III) compound **Ir49**, possessing 2,6′–difluoro–2,3′–bipyridine as main ligand and 5–methyl–2–phenylpyridine as an ancillary ligand and investigated the photophysical properties [Chart 1.19].[59] A remarkable 30 nm red shifted emission in the fluid and solid states has been observed in the derived heteroleptic iridium(III) compound as compared to its homoleptic iridium counterpart **Ir1**. This behaviour indicates that mppy ancillary ligand plays an important role in the red shifted emission. The triplet energy level of mppy was found to be lower than that of dfpypy cyclometalating ligand and hence the excited state energy can be easily transferred from primary to the ancillary ligand through intramolecular interligand energy transfer process.

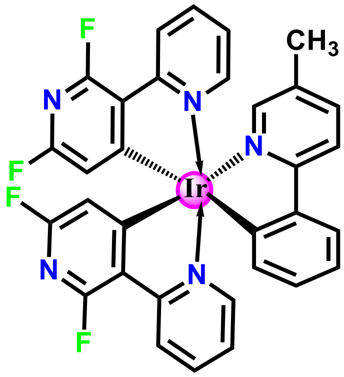

**Ir49**

**Chart 1.19.** Chemical Structure of bis(2',6'–difluoro–2,3'–bipyridinato–N,C4')iridium(III) 5–methyl–2–phenylpyridinate (**Ir49**).

Based on these literature reports, it can be summed up that cyclometalating chelates based on 2,3′−bipyridine class of ligands are highly appropriate for constructing the novel phosphorescent emitters required for building efficient OLED devices, mainly due to their stronger metal−chelate bonding character and greater versatility in tuning the emission wavelengths with high quantum efficiencies.

## 1.5. Objectives of the Present Investigation

Nowadays, the design and development of novel phosphorescent iridium(III) complexes for various optoelectronic applications is a well−recognized area of research. The fascinating photophysical properties of iridium(III) compounds are strongly influenced by the spin−orbit coupling exerted by the iridium(III) core, usually resulting in intense emissions with short excited−state lifetimes, which can be precisely controlled with the aid of molecular engineering of the chelating ligand. These attractive properties make them promising and prominent candidates, not only for use in organic light emitting diodes (OLEDs) as phosphorescent emitters but also for biological applications such as chemosensors and cellular imaging probes.

The evolution of 2, 3′−bipyridine class of cyclometalating ligands for developing novel phosphorescent iridium(III) compounds offers tremendous opportunities for its potential application in the fields of OLEDs and LEECs. The nature and energy of the excited state properties in heteroleptic $[Ir(C^{\wedge}N)_2(L^{\wedge}X)]$ complexes can be manipulated by simple modification of the 2′,6′−difluoro− 2,3′−bipyridine cyclometalated or ancillary ligands by deliberate incorporation of electron−withdrawing and electron−donating substituents at an appropriate position. Therefore the primary objective of the current thesis work is to design and develop efficient iridium(III) emitters based on 2,3-bipyridine ligands by substituting electron-withdrawing (–CHO, $–CF_3$, and –CN) and electron-donating (–OMe and $–NMe_2$) groups at the 4′ position of the N-coordinating pyridyl moiety and evaluate their photophysical and electroluminescence properties for use in OLED applications.

The recognition and quantitative estimation of cyanide ion in an aqueous environment is an important task for chemists and biologists. Consequently, a lot of efforts have been made for the construction of suitable sensors based on readily synthesizable fluorescent molecules. However, the detection of cyanide ions using chemosensors based on well-known strategies such as chemidosimetric strategy, wherein cyanide ions are coordinated to carbonyl group containing chromophores interacting with phosphorescent iridium metal complexes is scarce. Thus, another objective of the present investigation is to design and develop a new phosphorescent iridium(III) complex, functionalized with electron-deficient carbonyl units with a view to develop a chemosensor for the detection of $CN^-$ ions.

Aggregation-induced emission (AIE) refers to a photophysical phenomenon shown by a group of luminogenic materials that are non-emissive when they are dissolved in good solvents as molecules but become highly luminescent when they are clustered in poor solvents or solid states as aggregates. However, phosphorescent AIE (AIPE) materials based on iridium(III) complexes are comparatively less known as compared to fluorescent organic molecules. Thus, yet an another objective of the present work is to develop AIPE active iridium(III) complexes and utilizes for the detection of explosives such as 2, 4, 6-trinitrotoluene (TNT).

## 1.6. References

(1) (a) Chou, P.-T.; Chi, Y., *Chem.–Eur. J.* **2007,** *13*, 380-395. (b) Lowry, M. S.; Bernhard, S., *Chem.–Eur. J.* **2006,** *12*, 7970-7977. (c) You, Y.; Park, S. Y., *Dalton Trans.* **2009**, 1267-1282. (d) Djurovich, P. I.; Thompson, M. E., Cyclometallated Organoiridium Complexes as Emitters in Electrophosphorescent Devices. In *Highly Efficient OLEDs with Phosphorescent Materials*, Wiley-VCH Verlag GmbH & Co. KGaA: 2008; pp 131-161. (e) Mak, C. S. K.; Chan, W. K., Electroluminescence from Metal-Containing Polymers and Metal Complexes with Functional Ligands. In *Highly Efficient OLEDs with Phosphorescent Materials*, Wiley-VCH Verlag GmbH & Co. KGaA: 2008; pp 329-362. (f) Tsuboyama, A.; Okada, S.; Ueno, K., Highly Efficient Red-Phosphorescent Iridium Complexes. In *Highly Efficient OLEDs with Phosphorescent Materials*, Wiley-VCH Verlag GmbH & Co. KGaA: 2008; pp 163-183. (g) Yersin, H.; Finkenzeller, W. J., Triplet Emitters for Organic Light-Emitting Diodes: Basic Properties. In *Highly Efficient OLEDs with Phosphorescent Materials*, Wiley-VCH Verlag GmbH & Co. KGaA: 2008; pp 1-97. (h) Carlson, G. A.; Djurovich, P. I.; Watts, R. J., *Inorg. Chem.* **1993,** *32*, 4483-4484. (i) Colombo, M. G.; Brunold, T. C.; Riedener, T.; Guedel, H. U.; Fortsch, M.; Buergi, H.-B., *Inorg. Chem.* **1994,** *33*, 545-550. (j) Colombo, M. G.; Hauser, A.; Guedel, H. U., *Inorg. Chem.* **1993,** *32*, 3088-3092. (k) Garces, F. O.; King, K. A.; Watts, R. J., *Inorg. Chem.* **1988,** *27*, 3464-3471. (l) Lamansky, S.; Djurovich, P.; Murphy, D.; Abdel-Razzaq, F.; Kwong, R.; Tsyba, I.; Bortz, M.; Mui, B.; Bau, R.; Thompson, M. E., *Inorg. Chem.* **2001,** *40*, 1704-1711. (m) Schmid, B.; Garces, F. O.; Watts, R. J., *Inorg. Chem.* **1994,** *33*, 9-14. (n) Baranoff, E.; Yum, J.-H.; Graetzel, M.; Nazeeruddin, M. K., *J. Organomet. Chem.* **2009,** *694*, 2661-2670. (o) Ohsawa, Y.; Sprouse, S.; King, K. A.; DeArmond, M. K.; Hanck, K. W.; Watts, R. J., *J. Phys. Chem.* **1987,** *91*, 1047-1054. (p) Wilde, A. P.; King, K. A.; Watts, R. J., *J. Phys. Chem.* **1991,** *95*, 629-634. (q) Wilde, A. P.; Watts, R. J., *J. Phys. Chem.* **1991,** *95*, 622-629. (r) King, K. A.; Spellane, P. J.; Watts, R. J., *J. Am. Chem. Soc.* **1985,** *107*, 1431-1432. (s) King, K. A.; Watts, R. J., *J. Am. Chem. Soc.* **1987,** *109*, 1589-1590. (t) Tamayo, A. B.; Alleyne, B. D.; Djurovich, P. I.; Lamansky, S.; Tsyba, I.; Ho,

N. N.; Bau, R.; Thompson, M. E., *J. Am. Chem. Soc.* **2003,** *125*, 7377-7387. (u) Colombo, M. G.; Hauser, A.; Gudel, H. U., *Top. Curr. Chem.* **1994,** *171*, 143-171.

(2) (a) Smith, A. R. G.; Burn, P. L.; Powell, B. J., *ChemPhysChem* **2011,** *12*, 2429-2438. (b) Moore, S. A.; Davies, D. L.; Karim, M. M.; Nagle, J. K.; Wolf, M. O.; Patrick, B. O., *Dalton Trans.* **2013,** *42*, 12354-12363. (c) Zanoni, K. P. S.; Kariyazaki, B. K.; Ito, A.; Brennaman, M. K.; Meyer, T. J.; Murakami Iha, N. Y., *Inorg. Chem.* **2014,** *53*, 4089-4099.

(3) (a) Chou, P.-T.; Chi, Y.; Chung, M.-W.; Lin, C.-C., *Coord. Chem. Rev.* **2011,** *255*, 2653-2665. (b) Flamigni, L.; Barbieri, A.; Sabatini, C.; Ventura, B.; Barigelletti, F., *Top. Curr. Chem.* **2007,** *281*, 143-203.

(4) You, Y.; Nam, W., *Chem. Soc. Rev.* **2012,** *41*, 7061-7084.

(5) (a) Huang, K.; Wu, H.; Shi, M.; Li, F.; Yi, T.; Huang, C., *Chem. Commun.* **2009**, 1243-1245. (b) Zhao, Q.; Li, L.; Li, F.; Yu, M.; Liu, Z.; Yi, T.; Huang, C., *Chem. Commun.* **2008**, 685-687. (c) You, Y.; Seo, J.; Kim, S. H.; Kim, K. S.; Ahn, T. K.; Kim, D.; Park, S. Y., *Inorg. Chem.* **2008,** *47*, 1476-1487. (d) You, Y.; Kim, K. S.; Ahn, T. K.; Kim, D.; Park, S. Y., *J. Phys. Chem. C* **2007,** *111*, 4052-4060. (e) You, Y.; Park, S. Y., *J. Am. Chem. Soc.* **2005,** *127*, 12438-12439. (f) Chang, C.-J.; Yang, C.-H.; Chen, K.; Chi, Y.; Shu, C.-F.; Ho, M.-L.; Yeh, Y.-S.; Chou, P.-T., *Dalton Trans.* **2007**, 1881-1890. (g) Duan, H.-S.; Chou, P.-T.; Hsu, C.-C.; Hung, J.-Y.; Chi, Y., *Inorg. Chem.* **2009,** *48*, 6501-6508.

(6) (a) Fan, C.; Yang, C., *Chem. Soc. Rev.* **2014,** *43*, 6439-6469. (b) Omae, I., *Coord. Chem. Rev.* **2016,** *310*, 154-169. (c) Yersin, H.; Rausch, A. F.; Czerwieniec, R.; Hofbeck, T.; Fischer, T., *Coord. Chem. Rev.* **2011,** *255*, 2622-2652. (d) Adachi, C.; Baldo, M. A.; Thompson, M. E.; Forrest, S. R., *J. Appl. Phys.* **2001,** *90*, 5048-5051. (e) Jurow, M. J.; Mayr, C.; Schmidt, T. D.; Lampe, T.; Djurovich, P. I.; Brutting, W.; Thompson, M. E., *Nat. Mater.* **2016,** *15*, 85-91. (f) Lee, J.; Chen, H.-F.; Batagoda, T.; Coburn, C.; Djurovich, P. I.; Thompson, M. E.; Forrest, S. R., *Nat. Mater.* **2016,** *15*, 92-98. (g)

Baldo, M. A.; O'Brien, D. F.; You, Y.; Shoustikov, A.; Sibley, S.; Thompson, M. E.; Forrest, S. R., *Nature* **1998,** *395*, 151-154. (h) Reineke, S.; Lindner, F.; Schwartz, G.; Seidler, N.; Walzer, K.; Lussem, B.; Leo, K., *Nature* **2009,** *459*, 234-238. (i) Minaev, B.; Baryshnikov, G.; Agren, H., *Phys. Chem. Chem. Phys.* **2014,** *16*, 1719-1758.

(7) (a) Meier, S. B.; van Reenen, S.; Lefevre, B.; Hartmann, D.; Bolink, H. J.; Winnacker, A.; Sarfert, W.; Kemerink, M., *Adv. Funct. Mater.* **2013,** *23*, 3531-3538. (b) Xu, H.; Chen, R.; Sun, Q.; Lai, W.; Su, Q.; Huang, W.; Liu, X., *Chem. Soc. Rev.* **2014,** *43*, 3259-3302. (c) Zanoni, K. P. S.; Coppo, R. L.; Amaral, R. C.; Murakami Iha, N. Y., *Dalton Trans.* **2015,** *44*, 14559-14573.

(8) (a) Lv, W.; Yang, T.; Yu, Q.; Zhao, Q.; Zhang, K. Y.; Liang, H.; Liu, S.; Li, F.; Huang, W., *Adv. Sci.* **2015,** *2*, 1500107. (b) Zhao, Q.; Huang, C.; Li, F., *Chem. Soc. Rev.* **2011,** *40*, 2508-2524. (c) Zhao, Q.; Li, F.; Huang, C., *Chem. Soc. Rev.* **2010,** *39*, 3007-3030. (d) Baggaley, E.; Weinstein, J. A.; Williams, J. A. G., *Coord. Chem. Rev.* **2012,** *256*, 1762-1785. (e) Guerchais, V.; Fillaut, J.-L., *Coord. Chem. Rev.* **2011,** *255*, 2448-2457. (f) Lo, K. K.-W.; Louie, M.-W.; Zhang, K. Y., *Coord. Chem. Rev.* **2010,** *254*, 2603-2622.

(9) (a) Abrahamse, H.; Hamblin, Michael R., *Biochem. J.* **2016,** *473*, 347-364. (b) Ashen-Garry, D.; Selke, M., *Photochem. Photobiol.* **2014,** *90*, 257-274. (c) Lai, C.-W.; Wang, Y.-H.; Lai, C.-H.; Yang, M.-J.; Chen, C.-Y.; Chou, P.-T.; Chan, C.-S.; Chi, Y.; Chen, Y.-C.; Hsiao, J.-K., *Small* **2008,** *4*, 218-224. (d) Li, Y.; Tan, C.-P.; Zhang, W.; He, L.; Ji, L.-N.; Mao, Z.-W., *Biomaterials* **2015,** *39*, 95-104.

(10) (a) Whang, D. R.; Sakai, K.; Park, S. Y., *Angew. Chem., Int. Ed.* **2013,** *52*, 11612-11615. (b) Thomsen, J. M.; Huang, D. L.; Crabtree, R. H.; Brudvig, G. W., *Dalton Trans.* **2015,** *44*, 12452-12472. (c) DiSalle, B. F.; Bernhard, S., *J. Am. Chem. Soc.* **2011,** *133*, 11819-11821.

(11) (a) He, L.; Tan, C.-P.; Ye, R.-R.; Zhao, Y.-Z.; Liu, Y.-H.; Zhao, Q.; Ji, L.-N.; Mao, Z.-W., *Angew. Chem., Int. Ed.* **2014,** *53*, 12137-12141. (b) Zhou, J.; Liu, Q.; Feng, W.;

Sun, Y.; Li, F., *Chem. Rev.* **2015,** *115*, 395-465. (c) Aubert, V.; Ordronneau, L.; Escadeillas, M.; Williams, J. A. G.; Boucekkine, A.; Coulaud, E.; Dragonetti, C.; Righetto, S.; Roberto, D.; Ugo, R.; Valore, A.; Singh, A.; Zyss, J.; Ledoux-Rak, I.; Le Bozec, H.; Guerchais, V., *Inorg. Chem.* **2011,** *50*, 5027-5038.

(12) (a) Liu, Z.; He, W.; Guo, Z., *Chem. Soc. Rev.* **2013,** *42*, 1568-1600. (b) Bejoymohandas, K. S.; Kumar, A.; Sreenadh, S.; Varathan, E.; Varughese, S.; Subramanian, V.; Reddy, M. L. P., *Inorg. Chem.* **2016,** *55*, 3448-3461. (c) Bejoymohandas, K. S.; George, T. M.; Bhattacharya, S.; Natarajan, S.; Reddy, M. L. P., *J. Mater. Chem. C* **2014,** *2*, 515-523. (d) Lu, L.; Zhong, H.-J.; He, B.; Leung, C.-H.; Ma, D.-L., *Scientific Reports* **2016,** *6*, 19368.

(13) (a) Liu, Z.; Sadler, P. J., *Acc. Chem. Res.* **2014,** *47*, 1174-1185. (b) Ma, D.-L.; Chan, D. S.-H.; Leung, C.-H., *Acc. Chem. Res.* **2014,** *47*, 3614-3631.

(14) (a) Nagib, D. A.; MacMillan, D. W. C., *Nature* **2011,** *480*, 224-228. (b) McNally, A.; Prier, C. K.; MacMillan, D. W. C., *Science* **2011,** *334*, 1114-1117.

(15) (a) Shao, F.; Elias, B.; Lu, W.; Barton, J. K., *Inorg. Chem.* **2007,** *46*, 10187-10199. (b) Shao, F.; Barton, J. K., *J. Am. Chem. Soc.* **2007,** *129*, 14733-14738.

(16) (a) Sun, J.; Zhao, J.; Guo, H.; Wu, W., *Chem. Commun.* **2012,** *48*, 4169-4171. (b) Ruggi, A.; van Leeuwen, F. W. B.; Velders, A. H., *Coord. Chem. Rev.* **2011,** *255*, 2542-2554.

(17) (a) Schulz, G. L.; Holdcroft, S., *Chem. Mater.* **2008,** *20*, 5351-5355. (b) Yang, C.-M.; Wu, C.-H.; Liao, H.-H.; Lai, K.-Y.; Cheng, H.-P.; Horng, S.-F.; Meng, H.-F.; Shy, J.-T., *Appl. Phys. Lett.* **2007,** *90*, 133509.

(18) Liu, Z.; Qi, W.; Xu, G., *Chem. Soc. Rev.* **2015,** *44*, 3117-3142.

(19) (a) Chi, Y.; Chou, P.-T., *Chem. Soc. Rev.* **2010,** *39*, 638-655. (b) Chen, Z. Q.; Bian, Z. Q.; Huang, C. H., *Adv. Mater.* **2010,** *22*, 1534-1539.

(20) Lamansky, S.; Djurovich, P.; Murphy, D.; Abdel-Razzaq, F.; Lee, H.-E.; Adachi, C.; Burrows, P. E.; Forrest, S. R.; Thompson, M. E., *J. Am. Chem. Soc.* **2001,** *123*, 4304-4312.

(21) Hay, P. J., *J. Phys. Chem. A* **2002,** *106*, 1634-1641.

(22) Evariste, S.; Sandroni, M.; Rees, T. W.; Roldan-Carmona, C.; Gil-Escrig, L.; Bolink, H. J.; Baranoff, E.; Zysman-Colman, E., *J. Mater. Chem. C* **2014,** *2*, 5793-5804.

(23) King, K. A.; Watts, R. J., *J. Am. Chem. Soc.* **1987,** *109*, 1589-1590.

(24) (a) Yook, K. S.; Lee, J. Y., *Adv Mater* **2012,** *24*, 3169-3190. (b) Ho, C.-L.; Wong, W.-Y., *New J. Chem.* **2013,** *37*, 1665. (c) Jou, J.-H.; Kumar, S.; Agrawal, A.; Li, T.-H.; Sahoo, S., *J. Mater. Chem. C* **2015,** *3*, 2974-3002.

(25) Baranoff, E.; Curchod, B. F. E., *Dalton Trans.* **2015,** *44*, 8318-8329.

(26) Scholz, S.; Kondakov, D.; Lussem, B.; Leo, K., *Chem. Rev.* **2015,** *115*, 8449-8503.

(27) Frey, J.; Curchod, B. F. E.; Scopelliti, R.; Tavernelli, I.; Rothlisberger, U.; Nazeeruddin, M. K.; Baranoff, E., *Dalton Trans.* **2014,** *43*, 5667-5679.

(28) Lee, S. J.; Park, K.-M.; Yang, K.; Kang, Y., *Inorg. Chem.* **2009,** *48*, 1030-1037.

(29) (a) Chen, Z.; Sun, P.; Fan, B.; Liu, Q.; Zhang, Z.; Fang, X., *Appl. Catal., B* **2015,** *170–171*, 10-16. (b) Zhang, X. X.; Bordunov, A. V.; Kou, X.; Dalley, N. K.; Izatt, R. M.; Mangum, J. H.; Li, D.; Bradshaw, J. S.; Hellier, P. C., *Inorg. Chem.* **1997,** *36*, 2586-2593. (c) Hill, M. P.; Carroll, E. C.; Toney, M. D.; Larsen, D. S., *J. Phys. Chem. B* **2008,** *112*, 5867-5873.

(30) (a) Katritzky, A. R.; Ramsden, C. A.; Joule, J. A.; Zhdankin, V. V., 2.2 - Structure of Six-membered Rings. In *Handbook of Heterocyclic Chemistry (Third Edition)*, Elsevier: Amsterdam, 2010; pp 37-86. (b) Katritzky, A. R.; Ramsden, C. A.; Joule, J. A.; Zhdankin, V. V., 2.3 - Structure of Five-Membered Rings with One Heteroatom.

In *Handbook of Heterocyclic Chemistry (Third Edition)*, Elsevier: Amsterdam, 2010; pp 87-138.

(31) Tamao, K.; Uchida, M.; Izumizawa, T.; Furukawa, K.; Yamaguchi, S., *J. Am. Chem. Soc.* **1996,** *118*, 11974-11975.

(32) Kessler, F.; Watanabe, Y.; Sasabe, H.; Katagiri, H.; Nazeeruddin, M. K.; Gratzel, M.; Kido, J., *J. Mater. Chem. C* **2013,** *1*, 1070-1075.

(33) Yang, X.; Zhou, G.; Wong, W.-Y., *Chem. Soc. Rev.* **2015,** *44*, 8484-8575.

(34) Jung, N.; Lee, E.; Kim, J.; Park, H.; Park, K. M.; Kang, Y., *Bull. Korean Chem. Soc.* **2012,** *33*, 183-188.

(35) Bejoymohandas, K. S.; Kumar, A.; Varughese, S.; Varathan, E.; Subramanian, V.; Reddy, M. L. P., *J. Mater. Chem. C* **2015,** *3*, 7405-7420.

(36) Lee, J.; Park, H.; Park, K.-M.; Kim, J.; Lee, J.-Y.; Kang, Y., *Dyes Pigm.* **2015,** *123*, 235-241.

(37) Kang, Y.; Chang, Y.-L.; Lu, J.-S.; Ko, S.-B.; Rao, Y.; Varlan, M.; Lu, Z.-H.; Wang, S., *J. Mater. Chem. C* **2013,** *1*, 441-450.

(38) Yang, C.-H.; Mauro, M.; Polo, F.; Watanabe, S.; Muenster, I.; Fröhlich, R.; De Cola, L., *Chem. Mater.* **2012,** *24*, 3684-3695.

(39) Meier, S. B.; Sarfert, W.; Junquera-Hernandez, J. M.; Delgado, M.; Tordera, D.; Orti, E.; Bolink, H. J.; Kessler, F.; Scopelliti, R.; Gratzel, M.; Nazeeruddin, M. K.; Baranoff, E., *J. Mater. Chem. C* **2013,** *1*, 58-68.

(40) Xu, Q.-L.; Liang, X.; Zhang, S.; Jing, Y.-M.; Liu, X.; Lu, G.-Z.; Zheng, Y.-X.; Zuo, J.-L., *J. Mater. Chem. C* **2015,** *3*, 3694-3701.

(41) Xu, Q.-L.; Liang, X.; Jiang, L.; Zhao, Y.; Zheng, Y.-X., *RSC Adv.* **2015,** *5*, 89218-89225.

(42) (a) Sivasubramaniam, V.; Brodkorb, F.; Hanning, S.; Loebl, H. P.; van Elsbergen, V.; Boerner, H.; Scherf, U.; Kreyenschmidt, M., *J. Fluorine Chem.* **2009,** *130*, 640-649. (b) Chang, C.-H.; Wu, Z.-J.; Chiu, C.-H.; Liang, Y.-H.; Tsai, Y.-S.; Liao, J.-L.; Chi, Y.; Hsieh, H.-Y.; Kuo, T.-Y.; Lee, G.-H.; Pan, H.-A.; Chou, P.-T.; Lin, J.-S.; Tseng, M.-R., *ACS Appl. Mater. Interfaces* **2013,** *5*, 7341-7351. (c) Kozhevnikov, V. N.; Dahms, K.; Bryce, M. R., *J. Org. Chem.* **2011,** *76*, 5143-5148. (d) Zheng, Y.; Batsanov, A. S.; Edkins, R. M.; Beeby, A.; Bryce, M. R., *Inorg. Chem.* **2012,** *51*, 290-297.

(43) (a) Fu, H.; Cheng, Y.-M.; Chou, P.-T.; Chi, Y., *Materials Today* **2011,** *14*, 472-479. (b) Lin, C.-H.; Chang, Y.-Y.; Hung, J.-Y.; Lin, C.-Y.; Chi, Y.; Chung, M.-W.; Lin, C.-L.; Chou, P.-T.; Lee, G.-H.; Chang, C.-H.; Lin, W.-C., *Angew. Chem., Int. Ed.* **2011,** *50*, 3182-3186. (c) Xiao, L.; Chen, Z.; Qu, B.; Luo, J.; Kong, S.; Gong, Q.; Kido, J., *Adv. Mater.* **2011,** *23*, 926-952. (d) Holmes, R. J.; Forrest, S. R.; Sajoto, T.; Tamayo, A.; Djurovich, P. I.; Thompson, M. E.; Brooks, J.; Tung, Y.-J.; D’Andrade, B. W.; Weaver, M. S.; Kwong, R. C.; Brown, J. J., *Appl. Phys. Lett.* **2005,** *87*, 243507.

(44) Oh, H.; Park, K.-M.; Hwang, H.; Oh, S.; Lee, J. H.; Lu, J.-S.; Wang, S.; Kang, Y., *Organometallics* **2013,** *32*, 6427-6436.

(45) Lee, J.; Oh, H.; Kim, J.; Park, K.-M.; Yook, K. S.; Lee, J. Y.; Kang, Y., *J. Mater. Chem. C* **2014,** *2*, 6040-6047.

(46) Coe, B. J.; Helliwell, M.; Sanchez, S.; Peers, M. K.; Scrutton, N. S., *Dalton Trans.* **2015,** *44*, 15420-15423.

(47) (a) Song, Y. H.; Yeh, S. J.; Chen, C. T.; Chi, Y.; Liu, C. S.; Yu, J. K.; Hu, Y. H.; Chou, P. T.; Peng, S. M.; Lee, G. H., *Adv. Funct. Mater.* **2004,** *14*, 1221-1226. (b) Hwang, F.-M.; Chen, H.-Y.; Chen, P.-S.; Liu, C.-S.; Chi, Y.; Shu, C.-F.; Wu, F.-I.; Chou, P.-T.; Peng, S.-M.; Lee, G.-H., *Inorg. Chem.* **2005,** *44*, 1344-1353. (c) Zhou, G.; Ho, C.-L.; Wong, W.-Y.; Wang, Q.; Ma, D.; Wang, L.; Lin, Z.; Marder, T. B.; Beeby, A., *Adv. Funct. Mater.* **2008,** *18*, 499-511. (d) Zhou, G.; Wang, Q.; Ho, C.-L.; Wong, W.-Y.; Ma, D.; Wang, L.; Lin, Z., *Chem.–Asian J.* **2008,** *3*, 1830-1841.

(48) Park, J.; Oh, H.; Oh, S.; Kim, J.; Park, H. J.; Kim, O. Y.; Lee, J. Y.; Kang, Y., *Org. Electron* **2013,** *14*, 3228-3233.

(49) Duan, T.; Chang, T. K.; Chi, Y.; Wang, J. Y.; Chen, Z. N.; Hung, W. Y.; Chen, C. H.; Lee, G. H., *Dalton Trans.* **2015,** *44*, 14613-14624.

(50) (a) Sajoto, T.; Djurovich, P. I.; Tamayo, A.; Yousufuddin, M.; Bau, R.; Thompson, M. E.; Holmes, R. J.; Forrest, S. R., *Inorg. Chem.* **2005,** *44*, 7992-8003. (b) Chien, C.-H.; Fujita, S.; Yamoto, S.; Hara, T.; Yamagata, T.; Watanabe, M.; Mashima, K., *Dalton Trans.* **2008**, 916-923.

(51) Kessler, F.; Costa, R. D.; Di Censo, D.; Scopelliti, R.; Orti, E.; Bolink, H. J.; Meier, S.; Sarfert, W.; Gratzel, M.; Nazeeruddin, M. K.; Baranoff, E., *Dalton Trans.* **2012,** *41*, 180-191.

(52) Li, T.-Y.; Liang, X.; Zhou, L.; Wu, C.; Zhang, S.; Liu, X.; Lu, G.-Z.; Xue, L.-S.; Zheng, Y.-X.; Zuo, J.-L., *Inorg. Chem.* **2015,** *54*, 161-173.

(53) (a) Mauro, M.; Schuermann, K. C.; Prétôt, R.; Hafner, A.; Mercandelli, P.; Sironi, A.; De Cola, L., *Angew. Chem., Int. Ed.* **2010,** *49*, 1222-1226. (b) Wu, C.; Chen, H.-F.; Wong, K.-T.; Thompson, M. E., *J. Am. Chem. Soc.* **2010,** *132*, 3133-3139.

(54) (a) D'Andrade, B. W.; Forrest, S. R., *Adv. Mater.* **2004,** *16*, 1585-1595. (b) Jiang, W.; Gao, Y.; Sun, Y.; Ding, F.; Xu, Y.; Bian, Z.; Li, F.; Bian, J.; Huang, C., *Inorg. Chem.* **2010,** *49*, 3252-3260.

(55) Darmawan, N.; Yang, C.-H.; Mauro, M.; Frohlich, R.; De Cola, L.; Chang, C.-H.; Wu, Z.-J.; Tai, C.-W., *J. Mater. Chem. C* **2014,** *2*, 2569-2582.

(56) (a) Jeon, S. O.; Jang, S. E.; Son, H. S.; Lee, J. Y., *Adv. Mater.* **2011,** *23*, 1436-1441. (b) Chou, H.-H.; Cheng, C.-H., *Adv. Mater.* **2010,** *22*, 2468-2471.

(57) (a) Teng, M.-Y.; Zhang, S.; Jin, Y.-M.; Li, T.-Y.; Liu, X.; Xu, Q.-L.; Lin, C.; Zheng, Y.-X.; Wang, L.; Zuo, J.-L., *Dyes Pigm.* **2014,** *105*, 105-113. (b) Teng, M.-Y.; Zhang,

S.; Jiang, S.-W.; Yang, X.; Lin, C.; Zheng, Y.-X.; Wang, L.; Wu, D.; Zuo, J.-L.; You, X.-Z., *Appl. Phys. Lett.* **2012,** *100*, 073303. (c) Wang, J.; Liu, J.; Huang, S.; Wu, X.; Shi, X.; Chen, C.; Ye, Z.; Lu, J.; Su, Y.; He, G.; Zheng, Y., *Org. Electron* **2013,** *14*, 2854-2858. (d) Zhu, Y.-C.; Zhou, L.; Li, H.-Y.; Xu, Q.-L.; Teng, M.-Y.; Zheng, Y.-X.; Zuo, J.-L.; Zhang, H.-J.; You, X.-Z., *Adv. Mater.* **2011,** *23*, 4041-4046. (e) Li, H.-Y.; Zhou, L.; Teng, M.-Y.; Xu, Q.-L.; Lin, C.; Zheng, Y.-X.; Zuo, J.-L.; Zhang, H.-J.; You, X.-Z., *J. Mater. Chem. C* **2013,** *1*, 560-565. (f) Zhang, F.; Li, W.; Yu, Y.; Jing, Y.; Ma, D.; Zhang, F.; Li, S.; Cao, G.; Li, Z.; Guo, G.; Wei, B.; Zhang, D.; Duan, L.; Li, C.; Feng, Y.; Zhai, B., *J. Mater. Chem. C* **2016**, DOI: 10.1039/c1036tc01041e. (g) Wang, J.; Liu, J.; Huang, S.; Wu, X.; Shi, X.; He, G.; Zheng, Y., *Org. Electron* **2013,** *14*, 2682-2686. (h) Xu, Q.-L.; Wang, C.-C.; Li, T.-Y.; Teng, M.-Y.; Zhang, S.; Jing, Y.-M.; Yang, X.; Li, W.-N.; Lin, C.; Zheng, Y.-X.; Zuo, J.-L.; You, X.-Z., *Inorg. Chem.* **2013,** *52*, 4916-4925. (i) Wang, C.-C.; Jing, Y.-M.; Li, T.-Y.; Xu, Q.-L.; Zhang, S.; Li, W.-N.; Zheng, Y.-X.; Zuo, J.-L.; You, X.-Z.; Wang, X.-Q., *Eur. J. Inorg. Chem.* **2013,** *2013*, 5683-5693.

(58) Feng, Y.; Li, P.; Zhuang, X.; Ye, K.; Peng, T.; Liu, Y.; Wang, Y., *Chem. Commun.* **2015,** *51*, 12544-12547.

(59) Oh, S.; Jung, N.; Lee, J.; Kim, J.; Park, K.-M.; Kang, Y., *Bull. Korean Chem. Soc.* **2014,** *35*, 3590-3594.

# Chapter 2

## Photophysical and Electroluminescence Properties of Bis-(2′,6′-difluoro-2,3′-bipyridinato-N,C4′)iridium(picolinate) Complexes: Effect of Electron-Withdrawing and Electron-Donating Group Substituents at the 4′ Position of the Pyridyl Moiety of the Cyclometalated Ligand

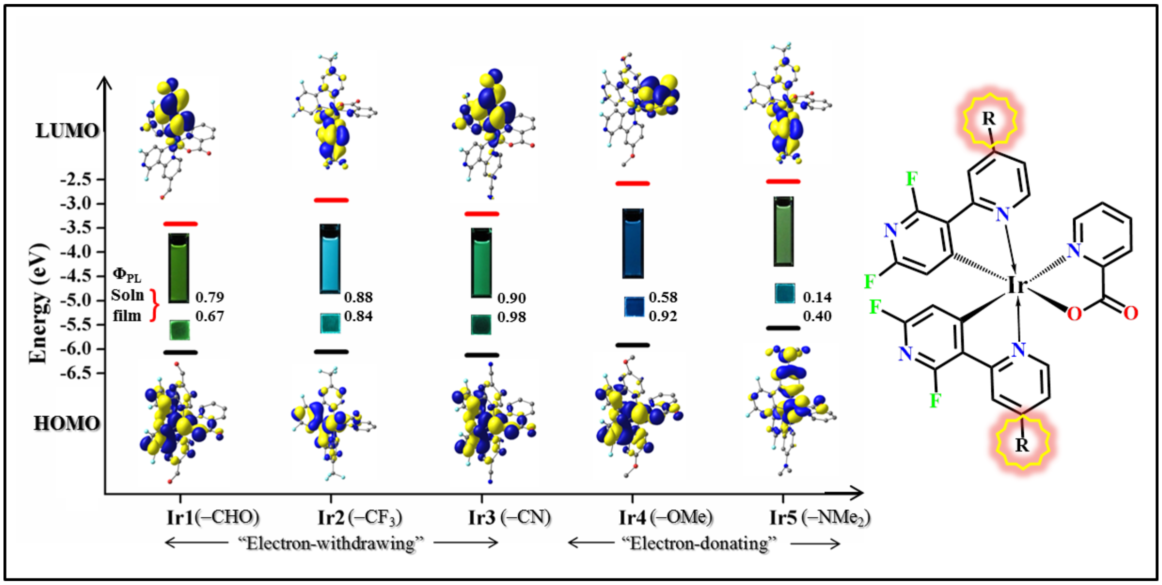

## 2.1. Abstract

*A series of 2′,6′-difluoro-2,3′-bipyridine cyclometalating ligands were synthesized by substituting electron-withdrawing (–CHO, –CF$_3$, and –CN) and electron-donating (–OMe and –NMe$_2$) groups at the 4′ position of the pyridyl moiety and utilized them for the construction of five new iridium(III) complexes (**Ir1–Ir5**) in the presence of picolinate as an ancillary ligand. The photophysical properties of the developed iridium(III) compounds were investigated with a view to understand the substituent*

*effects. The strong electron-withdrawing (–CN) group containing the iridium(III) compound (**Ir3**) exhibits highly efficient genuine green phosphorescence ($\lambda_{max}$ = 508 nm) at room temperature in solution and in thin film, with an excellent quantum efficiency ($\Phi_{PL}$) of 0.90 and 0.98, respectively. On the other hand, the $–CF_3$ group substituted iridium(III) compound (**Ir2**) displays a sky-blue emission ($\lambda_{max}$ = 468 nm) with a promising quantum efficiency ($\Phi_{PL}$ = 0.88 and 0.84 in solution and in thin film, respectively). The –CHO substituted iridium(III) complex (**Ir1**) showed greenish-yellow emission ($\lambda_{max}$ = 542 nm). Most importantly, the strong electron-donating $–NMe_2$ substituted iridium(III) complex (**Ir5**) gives a structureless and a broad emission profile in the wavelength region 450 to 700 nm ($\lambda_{max}$ = 520 nm) with a poor quantum efficiency. An intense blue phosphorescence with impressive quantum efficiency, especially in thin-film noted in the case of the –OMe substituted iridium(III) complex (**Ir4**). Comprehensive density functional theory (DFT) and time-dependent DFT (TD-DFT) approaches have been performed on the ground and excited states of the synthesized iridium(III) complexes, in order to obtain information about the absorption and emission processes and to gain deeper insights into the photophysical properties. The combinations of a smaller $\Delta E_{S_1–T_1}$ and higher contribution of $^3$MLCT in the emission process result in the higher quantum yields and lifetime values for complexes **Ir1**–**Ir3**. Multi-layered Phosphorescent Organic Light Emitting Diodes (PhOLEDs) were designed using the phosphorescent dopants **Ir2**, **Ir3** and **Ir4** and their elecroluminescence properties were evaluated. Compound **Ir4** at a doping level of 5 wt% shows the best performance with an external quantum efficiency of 4.7%, in the nonoptimized device, and a power efficiency of 5.8 lm $W^{-1}$, together with a true-blue chromacity $CIE_{x,y}$ = 0.15, 0.17 recorded at the maximum brightness of 33180 cd $m^{-2}$.*

**K. S. Bejoymohandas**; Arunandan Kumar; S. Varughese; E. Varathan; V. Subramanian; and M. L. P. Reddy, *Journal of Materials Chemistry C*, 3, **2015**, 7405–7420.

## 2.2. Introduction

Cyclometalated iridium(III) complexes are frequently considered as the most promising family of triplet emitters due to their potential applications in phosphorescent organic light emitting diodes (PhOLEDs).[1] This is essentially due to their excellent phosphorescence quantum efficiencies, short lifetimes of triplet excited states, flexibility in colour tuning and thermal and electrochemical stability.[2] In particular, phosphorescence emitting compounds based on iridium(III) phenylpyridine derivatives have drawn attention and have been successfully applied in PhOLED fabrication because they are efficient phosphorescent materials emitting light in the regions of blue, green and red.[2c, 3] Accordingly, several groups have demonstrated that phosphorescence emission wavelengths can be tuned in the blue to red region by functionalization on the phenyl moiety of 2-phenylpyridine of iridium(III) complexes with electron-withdrawing and electron-donating substituents.[4] However, there are some genuine difficulties in the development of blue phosphorescent complexes with respect to chromaticity, emission efficiency and stability of the material, as compared with green and red phosphorescent complexes.[1w, 5]

In order to overcome some of the difficulties in developing a robust blue emitter, Lee et al.[6] have introduced a new type of fac-iridium(III) complex containing fluorinated bipyridine as a cyclometalated ligand and investigated the photophysical properties. The emission maximum of the *fac*-tris(2′,6′-difluoro-2,3′-bipyridinato-

N,*C*4′)iridium(III) complex at room temperature has been reported to be 438 nm with a high quantum efficiency ($\Phi_{PL}$ = 0.71). However, it has a very low-lying HOMO energy (*ca*. 6.4–6.5 eV), making it difficult to find a suitable host in the PhOLED applications. In the subsequent studies, Kang and co-workers[7] have addressed these limitations by replacing one of the dfpypy ligands with an appropriate ancillary ligand such as 2-picolinate, acetylacetonate or dipivolylmethonate to elevate the HOMO energy of the $Ir(dfpypy)_3$ compound, so that it matches well with that of the common host molecule such as 4,4′-N,N′-dicarbazolebiphenyl (CBP). To prevent detrimental aggregation phenomena, Yang et al.[8] have introduced a bulky *tert*-Butyl group in the 4′ position of the pyridyl moiety of 2′,6′-difluoro-2,3′-bipyridine and constructed a series of heteroleptic iridium(III) complexes in the presence of pyridyl-azole as an ancillary ligand and investigated their photophysical properties. These complexes displayed intense phosphorescence blue emission ($\lambda_{ems}$ = 440 nm) at room temperature in solution and in thin film with a high quantum yield in the range 0.77–0.87 and 0.60–0.93, respectively. Park et al.[9] developed iridium(III) complexes with 2′,6′-difluoro-4-methyl-2,3′-bipyridine as a cyclometalated ligand and introduced a variety of ancillary ligands such as acetylacetonate, 2-picolinate or 2-(5-methyl-2H-1,2,4-triazol-3-yl)pyridinate to the iridium center to compare the effect of the ancillary ligands on the emission properties. These complexes exhibited blue emission at 447, 440 and 425 nm in $CH_2Cl_2$ solutions. However, the emission intensities of these complexes have not been quantified. More recently, Kessler and coworkers[10] have developed a novel bis-heteroleptic iridium(III) complex based on 4-(tert-butyl)-2′,6′-difluoro-2,3′-bipyridine and acetylacetonate as an ancillary ligand and investigated the photophysical as well as electroluminescence properties. The developed blue PhOLED showed superior performance compared to the published results on similar complexes with the maximum power efficiency of over 30 lm $W^{-1}$, indicating the great interest in this class of compounds throughout the scientific community. A preliminary report on the electroluminescence of tris-(2′,6′-difluoro-4-*N*,*N*-dimethylamine-2,3′-bipyridinato-N,*C*4)iridium(III) and (2′,6′-difluoro-4-O-alkyl-2,3′-bipyridinato-N,*C*4)iridium(III) picolinate has been disclosed by Lee and coworkers.[11]

It is clear from the literature review that no systematic correlations are reported on the photophysical properties of iridium(III) complexes involving the 2′,6′-difluoro-2,3′-bipyridine ligand with electron-withdrawing and electron-donating group substitutions on the 4′ position of the pyridyl moiety. This has inspired us to design and develop a series of cyclometalated ligands by substituting electron-withdrawing (–CHO, $–CF_3$ and –CN) and electron-donating groups (–OMe and $–NMe_2$) at the 4′ position on the pyridyl moiety of the cyclometalated ligand, 2′,6′-difluoro-2,3′-bipyridine and utilized for the construction of a series of iridium(III) compounds in the presence of picolinate as an ancillary ligand (Chart 2.1). The designed new iridium(III) compounds have been well characterized by various spectroscopic techniques and their electrochemical and photophysical properties have been investigated. Density functional theory calculations are used to rationalize the differences in the photophysical behaviour observed upon changes of the ligands. Finally, the developed compounds have been successfully used as dopants in 4,4′-bis(N-carbazolyl)-1,1′-biphenyl (CBP) as a host material and multilayer PhOLED devices have been fabricated and investigated the electroluminescence properties.

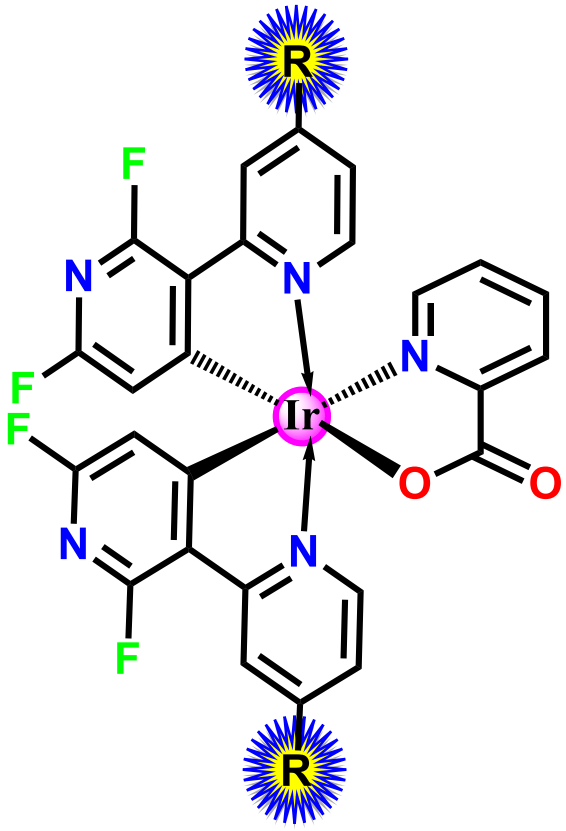

**Ir1 : R = -CHO**
**Ir2 : R = -$CF_3$**
**Ir3 : R = -CN**
**Ir4 : R = -OMe**
**Ir5 : R = -$NMe_2$**

**Chart 2.1.** Chemical Structures of the Iridium(III) Complexes **Ir1-Ir5**.

## 2.3. Experimental Section

### 2.3.1. General Information and Materials

A Bruker 500 MHz NMR spectrometer was used to record the $^{1}H$, $^{19}F$ and $^{13}C$ NMR spectra of the complexes in $CDCl_3$ solution. The chemical shifts ($\delta$) of the signals are given in ppm and referenced to the internal standard tetramethylsilane (TMS). The signal splitting is abbreviated as follows: s = singlet; d = doublet; t = triplet; q = quartet; and m = multiplet. All coupling constants ($J$) are given in Hertz (Hz). The electrospray ionization (ESI) mass spectrum was recorded on a thermo scientific exactive benchtop LC/MS orbitrap mass spectrometer. The matrix assisted laser desorption ionization time-of-flight (MALDI-TOF) mass spectrum was recorded on a KRATOS analytical spectrometer (Shimadzu Inc.). Elemental analyses for C, H, and N were performed on an Elementar-vario MICRO cube elemental analyzer. The complex doped PMMA films were prepared by spin coating onto a 2 cm × 2 cm glass plate for 60 s at a spin speed of 1000 rpm. Sodium hydride, iodomethane, sodium carbonate, tetrakis(triphenyl phosphine) palladium(0), 2,6-difluoropyridine-3-boronic acid, 2-bromo-4-aminopyridine, 2-bromo-4-(trifluoromethyl) pyridine, 2-bromo-4-formylpyridine, 2-bromo-4-cyanopyridine, 2-bromo-4-methoxypyridine, picolinic acid and $IrCl_3 \cdot x(H_2O)$ were purchased from Alfa Aesar and were used without any further purification. The cyclometalated ligands, namely 2′,6′-difluoro-4-(formyl)-2,3′-bipyridine [CHOdfpypy] (**L1**), 2′,6′-difluoro-4-(trifluoromethyl)-2,3′-bipyridine

[$CF_3$dfpypy] (**L2**) and 2′,6′-difluoro-4-(cyano)-2,3′-bipyridine [CNdfpypy] (**L3**), were synthesized and fully characterized for the first time. Other cyclometalating ligands such as 2′,6′-difluoro-4-(methoxy)-2,3′-bipyridine [OMedfpypy] (**L4**), 2′,6′-difluoro-4-(*N*,*N*-dimethylamine)-2,3′-bipyridine [$NMe_2$dfpypy] (**L5**), and the precursor for **L5** namely 2-bromo-4-*N*,*N*-dimethylaminopyridine (**L5a**) were synthesized according to previously reported procedures.[11]

The iridium dimer complexes $[(C\text{^}N)_2Ir(\mu\text{-}Cl)]_2$ (C^N = CHOdfpypy or $CF_3$dfpypy or CNdfpypy or OMedfpypy or $NMe_2$dfpypy) were synthesized using $IrCl_3{\cdot}x(H_2O)$ and CHOdfpypy or $CF_3$dfpypy or CNdfpypy or OMedfpypy or $NMe_2$dfpypy in a mixture of 2-ethoxyethanol and water according to the literature method.[12] Reactions were monitored by thin layer chromatography (TLC). Commercial TLC plates (silica gel 60 F254, Merck Co.) were used and the spots were observed under UV light at 254 and 365 nm. Silica column chromatography was performed using silica gel (230–400 mesh, Merck Co.) The dry solvents were used as received from Merck Millipore. All other reagents of analytical grade were used as received from Alfa Aesar, unless otherwise stated.

### 2.3.2. Synthesis of Cyclometalating Ligand Precursor

Synthesis of 2-bromo-4-*N*,*N*-dimethylaminopyridine (**L5a**): to a suspension of sodium hydride (1.38 g, 34.6 mmol, 60% dispersion in mineral oil) in THF (20 mL) at 0 °C, 2-bromo-4-aminopyridine (2.00 g, 11.56 mmol) was added. The reaction mixture was stirred for 30 min under an argon atmosphere at the same temperature. After methyl iodide (4.10 g, 28.90 mmol) was added, the resultant mixture was stirred at room temperature for 3 h. The reaction was quenched with water and organic materials were extracted with ethyl acetate. The combined extracts were washed with brine and dried over $Na_2SO_4$. After removal of solvents under reduced pressure, the residue was recrystallized from ethanol (1.30 g, 6.46 mmol, 55.8%). $^1$H NMR ($CDCl_3$, 500 MHz): $\delta$ 7.94 (d, $J$ = 5 Hz, 1H), 6.64 (d, $J$= 2 Hz, 1H), 6.44–6.43 (m,1H), 2.99 (s, 6H). $^{13}$C NMR ($CDCl_3$, 126 MHz): $\delta$ 155.79, 149.30, 143.11, 109.27, 106.20, 39.24. MS (ESI): *m*/*z* 203.00 [M+2].

### 2.3.3. General Synthesis of Cyclometalating Ligands

To a suspension of one equivalent of substituted bromopyridine [2-bromo-4-formylpyridine or 2-bromo-4-(trifluoromethyl) pyridine or 2-bromo-4-(cyano)pyridine or 2-bromo-4-methoxypyridine or 2-bromo-4-(*N*,*N*-dimethylamino)pyridine] with 1.2 equivalents of 2,6-difluropyridyl-3-boronic and 0.06 equivalents of tetrakis(triphenylphosphine)palladium(0) were dissolved in 25 mL of dry THF. A solution of 5% $Na_2CO_3$ (10 mL) was added and the mixture was refluxed with stirring for 24 h, under a nitrogen atmosphere. After being cooled, the mixture was poured into water, and extracted with ethyl acetate. The organic layer was dried over $Na_2SO_4$. The solvent was removed under reduced pressure to give a crude residue. The crude product was then purified by silica column chromatography with ethyl acetate : *n*-hexane (1 : 9) as the eluent to give the final product.

**2′,6′-Difluoro-4-(formyl)-2,3′-bipyridine [CHOdfpypy] (L1).** Yield: 69%.$^1$H NMR ($CDCl_3$, 500 MHz): $\delta$ 10.16 (s, 1H); 8.98 (d, $J$ = 5 Hz, 1H); 8.79–8.74 (m, 1H); 8.29 (s, 1H); 7.74 (t, $J$ = 5 Hz, 1H); 7.04–7.02 (m, 1H). $^{13}$C NMR ($CDCl_3$, 126 MHz): $\delta$ 191.07, 162.60, 160.60, 159.68, 152.19, 151.23, 146.14, 142.56, 122.84, 121.17, 107.37. $^{19}$F NMR ($CDCl_3$, 470 MHz): $\delta$ −68.51, −66.49. MS (ESI): *m*/*z* 221.05 [M$^+$].

**2′,6′-Difluoro-4-(trifluoromethyl)-2,3′-bipyridine [$CF_3$dfpypy] (L2).** Yield: 65%.$^1$H NMR ($CDCl_3$, 500 MHz): $\delta$ 8.90 (d, $J$ = 5 Hz, 1H), 8.77–8.72 (m, 1H), 8.09 (s, 1H), 7.54 (d, $J$ = 5 Hz, 1H), 7.03–7.01 (m, 1H). $^{13}$C NMR ($CDCl_3$, 126 MHz): $\delta$ 162.59, 160.59, 157.52, 151.74, 150.79, 146.18, 123.73, 121.55, 119.29, 118.65, 107.37. $^{19}$F NMR ($CDCl_3$, 470 MHz): $\delta$ −68.56, −66.29, −64.93. MS (ESI): *m*/*z* 261.04 [M$^+$].

**2′,6′-Difluoro-4-(cyano)-2,3′-bipyridine [CNdfpypy] (L3).** Yield: 62%.$^1$H NMR ($CDCl_3$, 500 MHz): $\delta$ 8.90 (t, $J$ = 5 Hz, 1H); 8.78–8.73 (m, 1H); 7.66 (s, 1H); 8.12 (s, 1H); 7.54–7.45 (m, 1H); 7.04–7.01 (m, 1H). $^{13}$C NMR ($CDCl_3$, 126 MHz): $\delta$ 162.81, 160.93, 157.68, 151.76, 150.80, 146.10, 125.30, 124.38, 121.61, 116.24, 107.60. $^{19}$F NMR ($CDCl_3$, 470 MHz): $\delta$ −68.10, −65.45. MS (ESI): *m*/*z* 218.05 [M$^+$].

**2′,6′-Difluoro-4-(methoxy)-2,3′-bipyridine [OMedfpypy] (L4).** Yield: 64%. $^1$H NMR ($CDCl_3$, 500 MHz): $\delta$ 8.69–8.64 (m, 1H); 8.53 (d, 5.5 Hz, 1H); 7.38 (s, 1H); 6.97–6.95 (m, 1H); 6.84–6.83 (m, 1H); 3.91 (s, 3H). $^{13}$C NMR ($CDCl_3$, 126 MHz): $\delta$ 162.11, 160.14, 157.29, 151.80, 150.90, 146.18, 119.05, 110.39, 109.08, 106.90, 55.29. $^{19}$F NMR ($CDCl_3$, 470 MHz): $\delta$ −69.22, −68.04. MS (ESI): *m*/*z* 223.06 [M+1].

**2′,6′-Difluoro-4-(*N*,*N*-dimethylamine)-2,3′-bipyridine [$NMe_2$dfpypy] (L5).** Yield: 60%. $^1$H NMR ($CDCl_3$, 500 MHz): $\delta$ 8.63–8.58 (m, 1H), 8.31 (d, $J$ = 6 Hz, 1H), 7.03 (s, 1H), 6.94–6.92 (m, 1H), 6.52–6.50 (m, 1H), 3.07 (s, 6H).$^{13}$CNMR ($CDCl_3$, 126 MHz): $\delta$ 161.66, 159.81, 154.82, 150.55, 149.73, 146.25, 120.29, 106.95, 106.45, 105.97, 39.24. $^{19}$F NMR ($CDCl_3$, 470 MHz): $\delta$ −69.07, −69.60. MS (ESI): *m*/*z* 236.09 [$M^+$].

### 2.3.4. Synthesis of the Iridium(III) Dimer Complex

**Synthesis of [(CHOdfpypy)$_2$Ir(μ-Cl)]$_2$.** $IrCl_3 \cdot xH_2O$ (224.36 mg, 0.75 mmol) and CHOdfpypy (**L1**) (350 mg, 1.58 mmol) were dissolved in 20 mL of 2-ethoxyethanol and water (8 : 2) mixture and refluxed at 140 °C for 24 h. After the solution was cooled, the addition of 40 mL of $H_2O$ gave a pale yellow precipitate that was filtered and washed with diethyl ether. The crude product was used for the next reaction without further purification (yield: 55%).

**Synthesis of [(CF$_3$dfpypy)$_2$Ir(μ-Cl)]$_2$.** IrCl$_3$·$x$H$_2$O (191.36 mg, 0.64 mmol) and CF$_3$dfpypy (**L2**) (350 mg, 1.34 mmol) were dissolved in 20 mL 2-ethoxyethanol and water (8 : 2) mixture and refluxed at 140 °C for 24 h. After the solution was cooled, the addition of 40 mL of H$_2$O gave a yellow precipitate that was filtered and washed with diethyl ether. The crude product was used for the next reaction without further purification (yield: 60%).

**Synthesis of [(CNdfpypy)$_2$Ir(μ-Cl)]$_2$.** IrCl$_3$·$x$H$_2$O (227.47 mg, 0.76 mmol) and CNdfpypy (**L3**) (350 mg, 1.61 mmol) were dissolved in 20 mL 2-ethoxyethanol and water (8 : 2) mixture and refluxed at 140 °C for 24 h under dry and inert conditions. After the solution was cooled, the addition of 40 mL of H$_2$O gave an orange precipitate that was filtered and washed with diethyl ether. The crude product was used for the next reaction without further purification (yield: 40%).

**Synthesis of [(OMedfpypy)$_2$Ir(μ-Cl)]$_2$.** IrCl$_3$·$x$H$_2$O (222.38 mg, 0.74 mmol) and OMedfpypy (**L4**) (350 mg, 1.57 mmol) were dissolved in 20 mL 2-ethoxyethanol and water (8 : 2) mixture and refluxed at 140 °C for 24 h. After the solution was cooled, the addition of 40 mL of H$_2$O gave a pale yellow precipitate that was filtered and washed with diethyl ether. The crude product was used for the next reaction without further purification (yield: 67%).

**Synthesis of [(NMe$_2$dfpypy)$_2$Ir(μ-Cl)]$_2$.** IrCl$_3$·$x$H$_2$O (211.36 mg, 0.70 mmol) and NMe$_2$dfpypy (**L5**) (350 mg, 1.48 mmol) were dissolved in 20 mL 2-ethoxyethanol and water (8 : 2) mixture and refluxed at 140 °C for 24 h. After the solution was cooled, the addition of 40 mL of $H_2O$ gave a pale yellow precipitate that was filtered and washed with diethyl ether. The crude product was used for the next reaction without further purification (yield: 60%).

### 2.3.5. General Synthesis Procedure for Complexes Ir1–Ir5

A mixture of one equivalent of the corresponding dimer, 2.6 equivalents of picolinic acid and 11.0 equivalents of sodium carbonate were stirred overnight in a mixture (3 : 1) of dichloromethane and ethanol (40 mL) at 60 °C under an argon atmosphere. The solvent was removed by evaporation under reduced pressure. The crude product obtained was poured into water and extracted with ethyl acetate (3 × 50 mL). The combined organic layer was dried over $Na_2SO_4$. The solvent was removed under reduced pressure to give a crude residue. The crude product was purified by using silica gel column chromatography with $CH_2Cl_2$: methanol in 9 : 1 ratio as the eluent, giving the desired complex as light yellow powder with the following yields: **Ir1** (65%), **Ir2** (80%), **Ir3** (36%), **Ir4** (90%) and **Ir5** (76%). All purified samples were recrystallized and vacuum dried before conducting all analysis.

**Spectral data of (CHOdfpypy)$_2$Ir(pic), Bis[2′,6′-difluoro-4-(formyl)-2,3′-bipyridinato-*N*,*C*4′]iridium(III) (Picolinate) (Ir1).** $^1$H NMR ($CDCl_3$, 500 MHz): $\delta$ 10.23 (s, 2H); 9.08 (d, $J = 6$ Hz, 1H); 8.73–8.68 (m, 2H); 8.42–8.41 (m, 1H); 8.12–8.07 (m, 1H); 7.79–7.68 (m, 3H); 7.60–7.52 (m, 2H); 5.84 (s, 1H); 5.55 (s, 1H). $^{19}$F NMR (CDCl$_3$, 470 MHz): $\delta$ −67.63, −67.01, −66.66, −65.96. MALDI-TOF calcd for $C_{28}H_{14}F_4IrN_5O_4$ 754.49 ([M + H]$^+$); found 755.49. Elem. anal. calcd (%) for $C_{28}H_{14}F_4IrN_5O_4$: C, 44.68; H, 1.89; N, 9.30. Found: C, 44.36; H, 2.10; N, 9.21.

**Spectral data of (CF$_3$dfpypy)$_2$Ir(pic), Bis[2′,6′-difluoro-4-(trifluoromethyl)-2,3′-bipyridinato-*N*,*C*4′]iridium(III) (Picolinate) (Ir2).** $^1$H NMR (CDCl$_3$, 500 MHz): $\delta$ 9.00 (d, *J* = 6 Hz, 1H), 8.47 (s, 1H), 8.53 (s, 1H), 5.54 (s, 1H), 8.41 (d, *J* = 7.5 Hz, 1H), 8.12 (t, *J* = 15.5 Hz, 1H), 7.77 (d, *J* = 5 Hz, 1H), 7.58 (s, 1H), 7.55 (d, *J* = 5.5 Hz, 1H), 7.34 (d, *J* = 6 Hz, 1H), 5.86 (s, 1H). $^{19}$F NMR (CDCl$_3$, 470 MHz): $\delta$ −67.22, −66.57, −66.27, −65.66, −65.04, −64.84. MALDI-TOF calcd for $C_{28}H_{12}F_{10}IrN_5O_2$ 833.05 ([M + H]$^+$); found 832.99. Elem. anal. calcd (%) for $C_{28}H_{12}F_{10}IrN_5O_2$: C, 40.39; H, 1.45; N, 8.41. Found: C, 40.51; H, 1.61; N, 8.21.

**Spectral data of (CNdfpypy)$_2$Ir(pic), Bis[2′,6′-difluoro-4-(cyano)-2,3′-bipyridinato-*N*,*C*4′]iridium(III) (Picolinate) (Ir3).** $^1$H NMR (CDCl$_3$, 500 MHz): $\delta$ 9.01(d, 1H, *J* = 6 Hz); 8.57 (s, 1H); 8.51 (s, 1H); 8.43 (d, *J* = 7.5 Hz, 1H); 8.15–8.11 (m, 1H); 7.75 (d, 1H, *J* = 5 Hz); 7.63–7.60 (m, 2H); 7.56–7.54 (m, 1H); 7.33–7.32 (m, 1H); 5.84 (s, 1H); 5.54 (s, 1H). $^{19}$F NMR (CDCl$_3$, 470 MHz): $\delta$ −66.13, −65.51, −65.39, −64.80. MALDI-TOF calcd for $C_{28}H_{12}F_4IrN_7O_2$ 747.70 ([M + H]$^+$); found 748.90. Elem. anal. calcd (%) for $C_{28}H_{12}F_4IrN_7O_2$: C, 45.04; H, 1.62; N, 13.13. Found: C, 44.84; H, 1.79; N, 12.93.

**Spectral data of (OMedfpypy)$_2$Ir(pic), Bis[2′,6′-difluoro-4-methoxy-2,3′-bipyridinato-*N*,*C*4′]iridium(III) (Picolinate) (Ir4).** $^1$H NMR (CDCl$_3$, 500 MHz): $\delta$ 8.52 (d, 1H, $J$ = 5 Hz); 8.37 (d, 8 Hz, 1H); 8.03–8.00 (m, 1H); 7.81–7.75 (m, 3H); 7.51−7.48 (m, 1H); 7.20 (d, 1H, $J$ = 6.5 Hz); 6.86–6.84 (m, 1H); 6.66–6.64 (m, 1H); 4.02 (d, $J$ = 3 Hz, 6H); 5.89 (s, 1H); 5.64 (s, 1H). $^{19}$F NMR (CDCl$_3$, 470 MHz): $\delta$ −70.85, −70.21, −69.40, −68.78. MALDI-TOF calcd for $C_{28}H_{18}F_4IrN_5O_4$ 757.94 ([M + H]$^+$); found 758.94. Elem. anal. calcd (%) for $C_{28}H_{18}F_4IrN_5O_4$: C, 44.44; H, 2.40; N, 9.26. Found: C, 44.62; H, 2.48; N, 9.08.

**Spectral data of (NMe$_2$dfpypy)$_2$Ir(pic), Bis[2′,6′-difluoro-4-(*N*,*N*-dimethylamine)-2,3′-bipyridinato-*N*,*C*4′]iridium(III) (Picolinate) (Ir5).** $^1$H NMR (CDCl$_3$, 500 MHz): $\delta$ 8.33 (d, $J$ = 3 Hz, 1H), 8.19 (d, $J$ = 7 Hz, 1H), 7.97–7.94 (m, 1H), 7.78 (d, $J$ = 5 Hz, 1H), 7.45–7.39 (m, 3H) 6.93 (d, $J$ = 7 Hz, 1H), 6.46–6.44 (m, 1H), 6.26–6.24 (m, 1H), 5.95 (s, 1H), 5.74 (s, 1H) 3.18 (d, $J$ = 5 Hz, 12H). $^{19}$F NMR (CDCl$_3$, 470 MHz): $\delta$ −73.15, −72.48, −71.08, −70.57. MALDI-TOF calcd for $C_{30}H_{24}F_4IrN_7O_2$ 785.16 ([M + H]$^+$); found 785.52. Elem. anal. calcd (%) for $C_{30}H_{24}F_4IrN_7O_2$: C, 46.03; H, 3.09; N, 12.53. Found: C, 45.81; H, 3.26; N, 12.44.

### 2.3.6. X-ray Crystallographic Analysis

The diffraction data of the single crystal were collected on a Rigaku Saturn 724+ diffractometer using graphite monochromated Mo-Kα radiation. The data were processed using the Rigaku Crystal Clear software.[13] The structure solution was carried out by direct methods, and the refinements were performed by full-matrix least-squares on $F^2$ using the SHELXTL suite of programs.[14] All of the hydrogen atoms were placed in geometrically ideal positions (using the corresponding HFIX) and refined in the riding mode. Final refinements included the atomic positions of all the atoms, anisotropic thermal parameters for all of the non-hydrogen atoms, and isotropic thermal parameters for all of the hydrogen atoms. The disordered solvent molecules could not be adequately modeled. The bypass procedure in Platon (Spek, 1990) was used to remove the electronic contribution from these solvents. For complex **Ir2**, the total potential solvent (dichloromethane and water) accessible void volume was 2519 Å (which is 34% of the unit cell volume) and the electron count/cell = 606.

### 2.3.7. Thermal Analysis

Thermo-gravimetric analyses were performed on an EXSTAR TG-DTA 6200 instrument (SII Nanotechnology Inc.) heated from 30 to 1000 °C in flowing nitrogen at the heating rate of 10 °C min$^{-1}$. The temperature at which a 5% weight loss occurred has been considered as the decomposition temperature ($T_d$). Differential scanning calorimetry was performed using a TA Q20 general-purpose DSC instrument in sealed aluminum pans under nitrogen flow at a heating/cooling rate of 5 °C min$^{-1}$. The endothermic peak observed in the second heating cycle has been considered as the glass transition temperature ($T_g$).

### 2.3.8. Photophysical Characterization

The electronic absorption spectrum of the complex was measured on a Shimadzu, UV-2450 UV-vis-NIR spectrophotometer. The photoluminescence (PL) spectrum of the iridium(III) complex was recorded on a Spex-Fluorolog FL22 spectrofluorimeter equipped with a double grating 0.22 m Spex 1680 monochromator and a 450 W Xe lamp as the excitation source and a Hamamatsu R928P photomultiplier tube detector. Emission and excitation spectra were corrected for source intensity (lamp and grating) by standard correction curves. Phosphorescence lifetimes were measured using the IBH (Fluoro Cube) time-correlated pico second single photon counting (TCSPC) system. A pulsed diode laser (<100 ps pulse duration) at a wavelength of 375 nm (Nano LED-10) were used to excite at the MLCT states of the complexes with a repetition rate of 50 KHz. The detection system consists of a microchannel plate photomultiplier (5000 U-09B, Hamamatsu) with a 38.6 ps response time coupled to a monochromator (5000 M) and TCSPC electronics (Data Station Hub including Hub-NL, Nano LED controller and preinstalled Fluorescence Measurement and Analysis Studio (FMAS) software). The phosphorescence lifetime values were determined by deconvoluting the instrument response function with mono-exponential decay using DAS6 decay analysis software. The quality of the fit has been judged by the fitting parameters such as $\chi^2$ (<1.2) as well as the visual inspection of the residuals. The luminescence quantum efficiencies in the solution state were calculated by a comparison of the emission intensities (integrated areas) of a standard sample and the unknown sample according to eqn (1).

$$\Phi_{\mathrm{unk}} = \Phi_{\mathrm{std}}(I_{\mathrm{unk}}/I_{\mathrm{std}})(A_{\mathrm{std}}/A_{\mathrm{unk}})(\eta_{\mathrm{unk}}/\eta_{\mathrm{std}})^2 \qquad (1)$$

Where $\Phi_{\mathrm{unk}}$ and $\Phi_{\mathrm{std}}$ are the luminescence quantum yields of the unknown sample and the standard sample, respectively. $I_{\mathrm{unk}}$ and $I_{\mathrm{std}}$ are the integrated emission intensities of the unknown sample and standard sample solution, respectively. $A_{\mathrm{unk}}$ and $A_{\mathrm{std}}$ are the absorbances of the unknown sample and standard sample solution at their excitation wavelengths, respectively. The $\eta_{\mathrm{unk}}$ and $\eta_{\mathrm{std}}$ terms represent the refractive indices of the corresponding solvents (pure solvents were assumed). Quinine sulphate monohydrate ($\Phi_{\mathrm{PL}} = 0.54$) in 0.05 M $H_2SO_4$ has been used as a standard for the blue emitting complex **Ir4**.[15] Ir(ppy)$_3$ has been used as a standard for green emitting complexes **Ir1–Ir3** and **Ir5**.[16] All solutions for the photophysical studies were deaerated with pre-purified Argon gas prior to the measurements. Solid state photoluminescence quantum yields of the PMMA films were measured by an absolute method using a calibrated integrating sphere in a SPEX Fluorolog Spectrofluorimeter on the basis of the de Mello method.[17]

### 2.3.9. Cyclic Voltammetry

Cyclic voltammetry experiments were carried out using a BAS 50 W voltammetric analyzer using three electrode cell assemblies. Platinum wires were used as counter electrodes, a silver wire was used as an $Ag/Ag^+$ quasi reference electrode and a platinum electrode was used as a working electrode. Measurements were carried out in acetonitrile solution with tetrabutylammonium hexafluorophosphate as the supporting electrolyte at a scan rate of 100 mV $s^{-1}$. Concentrations of the iridium(III) complex and the supporting electrolyte were $5 \times 10^{-3}$ and 0.1 M, respectively. The ferrocenium/ferrocene couple ($FeCp_2^+/FeCp_2^0$) was used as an internal reference. The energy level of $FeCp_2^+/FeCp_2^0$ was assumed at −4.8 eV to vacuum.[18] All solutions for the electrochemical studies were deaerated with pre-purified argon gas prior to the measurements.

### 2.3.10. Computational Methods

The geometrical structures of the singlet ground state ($S_0$) and the lowest lying triplet excited state ($T_1$) were optimized by using density functional theory (DFT) based on a method using the Becke's three-parameter functional and the Lee–Yang–Parr functional (B3LYP)[19] with LANL2DZ basis set for the Iridium (Ir) atom and 6-31G* for the rest of the atoms. Frequency calculations were also executed at the same level of theory. The optimizations and the vibrational data confirmed that the structures were true minima on the potential energy surface because there were no imaginary frequencies. On the basis of the optimized ground and excited state geometry structures, the absorption spectral properties in dichloromethane media were calculated by time-dependent density functional theory (TD-DFT) approach with

(B3LYP/6-31G*). As solvent effects are known to play a crucial role in predicting the absorption and emission spectra, the same was incorporated in the TD-DFT calculations within the PCM framework. The Swizard program has been employed to evaluate the contribution of singly excited state configurations to each electronic transition.[20] All calculations were carried out using Gaussian 09 package.[21]

### 2.3.11. PhOLED Device Fabrication

PhOLEDs were fabricated on indium-tin oxide (ITO) coated glass substrates (a sheet resistance of 20 ohm sq$^{-1}$) by first cleaning them using trichloroethylene, acetone, and isopropyl alcohol and deionized water sequentially for 20 min using an ultrasonic bath and dried under flowing nitrogen. Prior to film deposition, the ITO substrates were treated with UV-ozone for 5 min. Organic materials and cathodes were sequentially deposited under high vacuum ($4 \times 10^{-7}$ torr). The deposition rate of organic materials was kept at 6 nm min$^{-1}$, whereas the deposition rates of LiF and Al were 0.6 nm min$^{-1}$ and 30 nm min$^{-1}$, respectively. The thickness of the deposited layers was monitored using an *in situ* quartz crystal monitor. The cathode was deposited on the top of the structure through a shadow mask. The used device structure was ITO (120 nm)/$F_4$-TCNQ (2.5 nm)/α-NPD (45 nm)/emissive layer (30 nm)/BCP (6 nm)/$Alq_3$ (30 nm)/LiF (1 nm)/Al (150 nm). *N*,*N*-Diphenyl-*N*′,*N*′-bis(1-naphthyl)-1,1′-biphenyl-4,4′-diamine (α-NPD) (Sigma Aldrich) was used as a hole transport layer, 4,4′-bis(*N*-carbazolyl)-1,1′-biphenyl (CBP) as a host layer with 5 wt%

doped iridium complex **Ir2–Ir4** was used as an emissive layer, 2,9-dimethyl-4,7-diphenyl-1,10-phenanthroline (BCP) as a hole blocking layer, tris(8-hydroxyquinoline)-aluminium ($Alq_3$, Sigma Aldrich) as an electron transport layer, LiF (Merck, Germany) as an electron injection layer and Al as the cathode. 2,3,5,6-Tetrafluoro-7,7′,8,8′-tetracyanoquinodimethane ($F_4$-TCNQ) is utilized due to efficient hole injection from ITO to α-NPD and its thickness is used as optimized by Tyagi *et al.*[22] for the enhanced efficiency and life time of PhOLEDs. Synthesized materials **Ir2**, **Ir3** and **Ir4** were mixed in CBP with 5 wt% concentration for using them as the emissive layer. The size of each pixel was 3 × 4 mm$^2$. EL spectra were measured using an Ocean Optics high resolution spectrometer (HR-2000CG UV-NIR). The *J–V–L* characteristics were measured with a luminance meter (LMT 1-1009) and a Keithley 2400 programmable voltage–current digital source meter. All the measurements were carried out at room temperature under ambient conditions.

## 2.4. Results and Discussion

### 2.4.1. Synthesis and Characterization

The C^N chelating ligands used in the current study were synthesized by conventional Suzuki coupling reaction of the corresponding 2-bromopyridine with 2,6-difluropyridinyl-3-boronic acid in the presence of sodium carbonate and tetrakis(triphenylphosphine) palladium(0) as a catalyst as shown in Scheme 2.1.

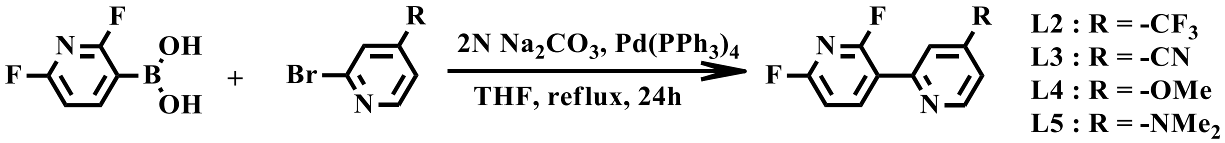

L1 : R = -CHO
L2 : R = $-CF_3$
L3 : R = -CN
L4 : R = -OMe
L5 : R = $-NMe_2$

**Scheme 2.1.** Synthetic Route of Cyclometalating Ligands **L1–L5**

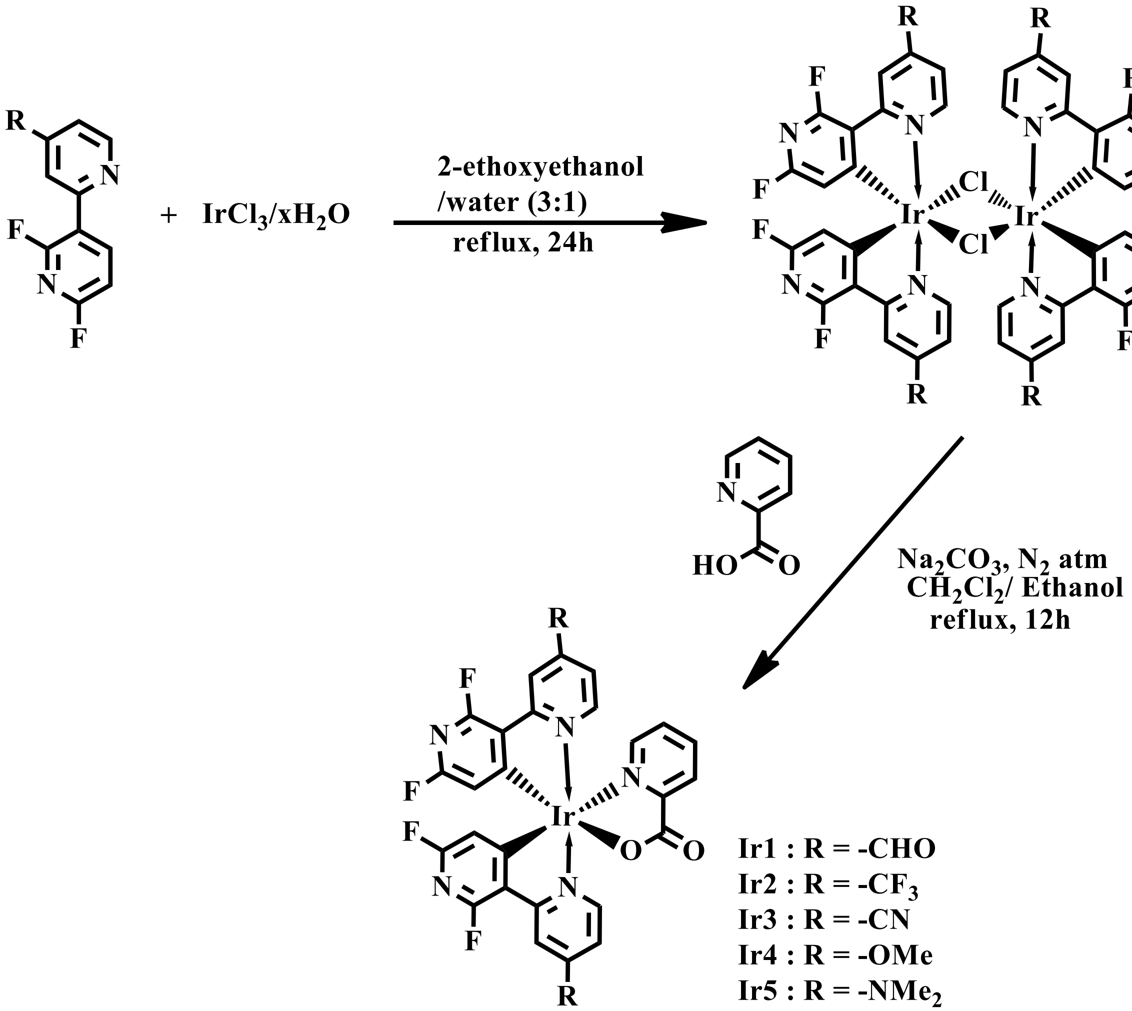

Ir1 : R = -CHO
Ir2 : R = $-CF_3$
Ir3 : R = -CN
Ir4 : R = -OMe
Ir5 : R = $-NMe_2$

**Scheme 2.2.** Synthetic Routes of Heteroleptic $Ir^{3+}$ Complexes **Ir1–Ir5**

It is important to mention that pure ligands could only be obtained after column chromatographic separations. The dimer precursors to obtain iridium(III) complexes **Ir1–Ir5** were prepared by a standard procedure proposed by Watts and co-workers.[12b] The μ-chloro bridged dimer was formed through the reaction of the cyclometalated ligand precursor with $IrCl_3 \cdot H_2O$ in a mixture of 2-ethoxyethanol and water. The new iridium complexes **Ir1–Ir5** were obtained in the presence of $Na_2CO_3$ *via* the reaction of the μ-chloro bridged dimer and the ancillary ligand picolinic acid.[10, 23] A pictorial synthetic pathways leading to the designed iridium(III) compounds is depicted in Scheme 2.2. After purification and recrystallization of the compounds detailed characterizations were carried out by $^1$H, $^{19}$F and $^{13}$C NMR, MALDI-TOF mass spectrometry and elemental analyses.

### 2.4.2. X-ray Single Crystal Structures

Single crystals of **Ir2** and **Ir4** have been grown by slow diffusion of hexane into a dichloromethane solution of the complexes. The compounds **Ir2** and **Ir4** were structurally authenticated by X-ray single-crystal diffraction and the corresponding molecular structures are depicted in Figures 2.1 and 2.2, respectively. Selected crystallographic data and structure refinement parameters are given in Table 2.1. Both the iridium(III) complexes adopt a distorted octahedral geometry around the Ir$^{3+}$ center with N-binding pyridines in *trans* positions in relative to each other. These results are in good agreement with that of the earlier disclosed X-ray single crystal structure of $(dfpypy)_2Irpic$.[7] Overall the geometry around the metal is not significantly influenced by the various substituted cyclometalated ligands.

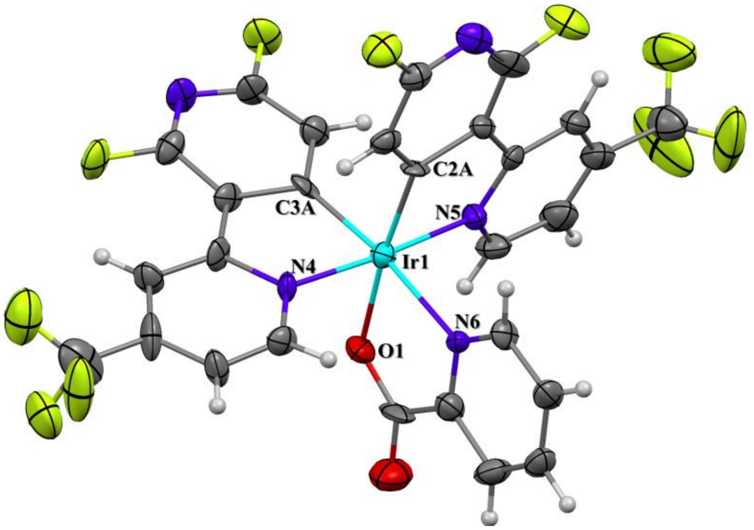

**Figure 2.1.** Crystal structure of complex **Ir2** with atom numbering scheme. Selected bond lengths (Å) and angles (˚): Ir(1)−C(3A) 1.966(16), Ir(1)−C(2A) 1.987(10), Ir(1)−O(1) 2.115(11), Ir(1)−N(6) 2.150(11), Ir(1)−N(5) 2.045(11), Ir(1)−N(4) 2.026(10); N(4)−Ir(1)−N(6) 175.2(5), C(3A)−Ir(1)−N(6) 172.5(5), C(2A)−Ir(1)−O(1) 174.5(5).

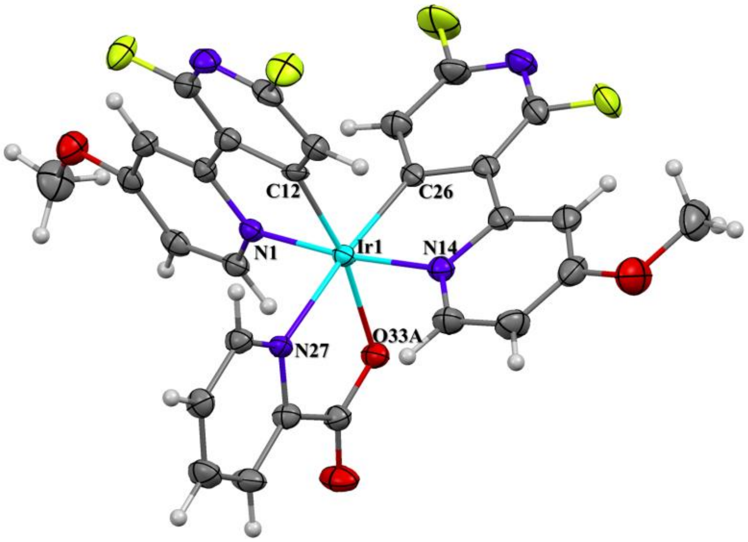

**Figure 2.2.** Crystal structure of complex **Ir4** with atom numbering scheme. Selected bond lengths (Å) and angles (˚): Ir(1)−C(12) 1.983(2), Ir(1)−C(26) 2.000(3), Ir(1)−O(33A) 2.158(2), Ir(1)−N(1) 2.048(2), Ir(1)−N(14) 2.050(2), Ir(1)−N(27) 2.154(5); N(1)−Ir(1)−N(14) 173.7(9), C(26)−Ir(1)−N(27) 174.7(9), C(12)−Ir(1)−O(33A) 169.2(9).

**Table 2.1.** Crystallographic and refinement data for complexes **Ir2** and **Ir4**

| | **Ir2** | **Ir4** |
|---|---|---|
| Formula | $C_{28} H_{18} F_4 Ir N_5 O_2$ | $C_{28} H_{18} F_4 Ir N_5 O_4$ |
| Formula weight | 724.67 | 841.60 |
| Temp (K) | 301(2) | 150(2) |
| Wavelength (Å) | 0.71073 | 0.71073 |
| Crystal system | Orthorhombic | monoclinic |
| Space group | *Pbca* | $P2_1/c$ |
| Crystal size ($mm^3$) | 0.20 × 0.20 × 0.20 | 0.50 × 0.40 × 0.30 |
| $a$ [Å] | 16.765(2) | 12.069(3) |
| $b$ [Å] | 15.096(8) | 12.029(3) |
| $c$ [Å] | 20.6420(10) | 19.562(5) |
| $\alpha$ [°] | 90.00 | 90.00 |
| $\beta$ [°] | 90.00 | 92.19 |
| $\gamma$ [°] | 90.00 | 90.00 |
| $V$ [$Å^3$] | 5224(3) | 2837.8(11) |
| $Z$ | 8 | 4 |
| $\rho_{\text{calc}}$[$g/cm^3$] | 1.843 | 1.970 |
| $\mu$ (Mo Kα) [$mm^{-1}$] | 5.176 | 4.967 |
| Total reflections | 31043 | 24916 |
| Unique reflections | 5260 | 6465 |
| $R_F$, $R_w(F^2)$ [$I > 2\sigma(I)$] | 0.0772, 0.1937 | 0.0250, .0530 |
| GOF on $F^2$ | 1.048 | 1.047 |
| CCDC | 973778 | 1005716 |

The bond lengths of Ir–C, Ir–N and Ir–O for **Ir2** and **Ir4** are within the range reported for those of related compounds $(dfpypy)_2$Irpic[7] and FIrpic (Table 2.2 and Figure 2.3).[6, 24] However, there is a significant effect on $C_1$–$C_2$ bond lengths in the cyclometalating ligand in the presence of electron-withdrawing and electron-donating substituents at the *C*4 position on the N-coordinating pyridine ring. Firstly, in the substitution of $–CF_3$ in the *C*4 position shortens the C1–C2 bond (1.443(2) Å) in **Ir2** that links both rings of the cyclometalating ligand as compared to unsubstituted parent compound $(dfpypy)_2$Irpic (1.470(1) Å), due to the strong electron-withdrawing effect (Hammett constant: $C\sigma_m = 0.43$) at the *meta*-C2 position.

**Table 2.2.** Average of selected bond lengths (Å) and angles (°) for complexes **Ir2**, **Ir4** and **Ir(dfpypy)$_2$pic**[a]

| **Bond length** | **Ir2** | **Ir4** | **Ir(dfpypy)$_2$ pic**[a] |
|---|---|---|---|
| Ir–N | 2.035(11) | 2.049(2) | 2.049(7) |
| Ir–C | 1.991(10) | 1.991(2) | 2.001(7) |
| Ir–O | 2.115(11) | 2.158(2) | 2.131(4) |
| Ir–N$_1$ | 2.150(11) | 2.125(2) | 2.115(7) |
| C$_1$–C$_2$ | 1.443(2) | 1.461(3) | 1.470(1) |
| **Bond angles** | | | |
| N–Ir–N | 172.5 | 173.8 | 175.6 |
| C–Ir–N$_1$ | 172.5 | 174.8 | 168.8 |
| C–Ir–O | 174.5 | 169.2 | 174.5 |
| C–Ir–C | 87.42 | 88.20 | 90.61 |
| O–Ir–N$_1$ | 77.09 | 77.24 | 77.24 |
| C–Ir–N | 80.47 | 80.57 | 80.67 |
| **Torsion angle** | | | |
| C$_2$–C$_3$–C$_4$–R | 176.56 | 178.05 | --- |

[a] The average bond length and bond angle values for Ir(dfpypy)$_2$pic were taken from ref 7.

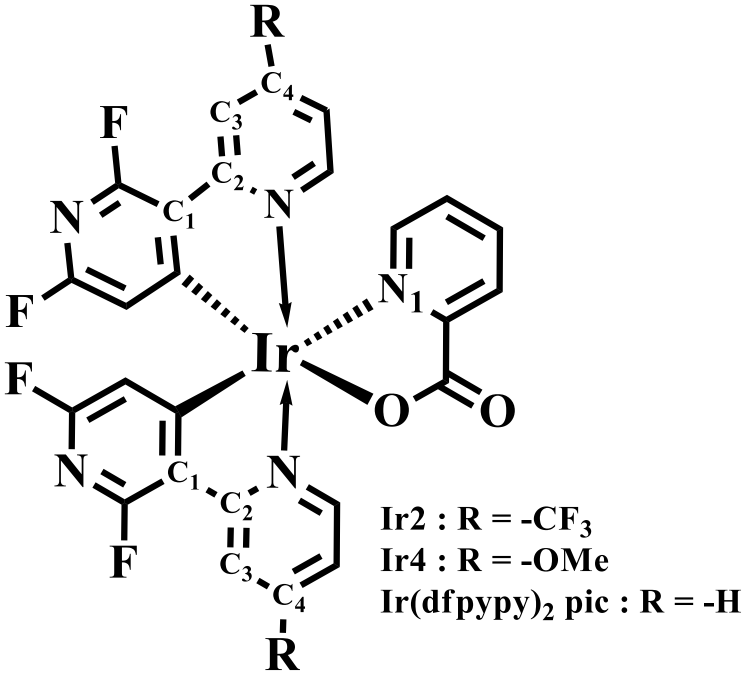

**Figure 2.3.** General structure of the complexes shows the label used for selected atoms as used in Table 2.2.

**Table 2.3.** Intermolecular hydrogen bond interactions for **Ir2**

| D-H···A | d(D-H) [Å] | d(H···A) [Å] | d(D···A) [Å] | <(DHA) [°] |
|---|---|---|---|---|
| C(42)-H(42A)···O(49)iv | 0.93 | 2.66 | 3.299(3) | 127 |
| C(3)-H(3A)···F(50)i | 0.93 | 3.06 | 3.821(5) | 140 |
| C(4)-H(4A)···F(51) ii | 0.93 | 3.06 | 3.953(2) | 161 |
| C(3)-H(3A)···N(16) i | 0.93 | 2.43 | 3.168(1) | 136 |
| C(17)-H(17A)···N(18)iii | 0.93 | 2.61 | 3.468(7) | 153 |

Symmetry transformations used to generate equivalent atoms: i) x, x-y,1/2+z; ii) y,-x+y,-z; iii) y, x,1/2-z; iv)1-x+y,1-x,z

**Table 2.4.** Intermolecular hydrogen bond interactions for **Ir4**

| D-H···A | d(D-H) [Å] | d(H···A) [Å] | d(D···A) [Å] | <(DHA) [°] |
|---|---|---|---|---|
| C(3)-H(3)···O(33A)i | 0.95 | 2.81 | 3.597(3) | 130 |
| C(13)-H(13B)···O(17)ii | 0.98 | 2.92 | 3.791(5) | 138 |
| C(90)-H(90B) ···O(17)vi | 0.99 | 2.83 | 3.869(4) | 161 |
| C(20)-H(20A)···O(33B)v | 0.98 | 2.61 | 3.514(4) | 141 |
| C(28)-H(28)···O(4)iv | 0.95 | 2.48 | 3.281(3) | 130 |
| C(13)-H(13C)···F(22)iii | 0.98 | 2.45 | 3.259(4) | 130 |
| C(13)-H(13C)···F(10)iv | 0.98 | 2.57 | 3.410(4) | 134 |
| C(20)-H(20B)···F(8)vi | 0.98 | 2.77 | 3.575(4) | 131 |
| C(20)-H(20B)···N(9)vi | 0.98 | 2.67 | 3.642(4) | 150 |
| C(90)-H(90A)···N(23)vii | 0.99 | 2.37 | 3.447(5) | 171 |

Symmetry transformations used to generate equivalent atoms: i)1-x,2-y,1-z,-1/2+z; ii)-1+x,3/2-y,1/2+z; iii)-1+x,y,z; iv)1-x,1-y,1-z; v)1+x,y,z; vi)2-x,1-y,1-z; vii)2-x,-1/2+y,3/2-z

However, in **Ir4**, the –OMe substitution moderately decreases the C1–C2 bond (1.461(3) Å). This can be explained on the basis of –OMe having a positive $C\sigma_m$ value (0.12). Secondly, *C*4′ substituents (–$CF_3$ and –OMe in complexes **Ir2** and **Ir4**, respectively) on the N-coordinating pyridine ring tend to deviate slightly from the plane of the cyclometalating ring, as exemplified by the C2–C3–C4–R torsion angles, due to the bulky nature of the substituents. The C(3A)–Ir(1)–N(6) bond angle [172.5(5)°] in **Ir2** and the C(26)–Ir(1)–N(27) bond angle [174.78(9)°] in **Ir4** are found to be moderately distorted from linearity, which may be caused by intermolecular interactions. Several strong intermolecular interactions such as edge-to-face C–H···π(py), and hydrogen bonding *via* C(π)–H···F or C(π)–H···O or C(π)–H···N are in fact observed in the crystal lattices of **Ir2** and **Ir4**. The details of the intermolecular interactions can be found from the Tables 2.3–2.4.

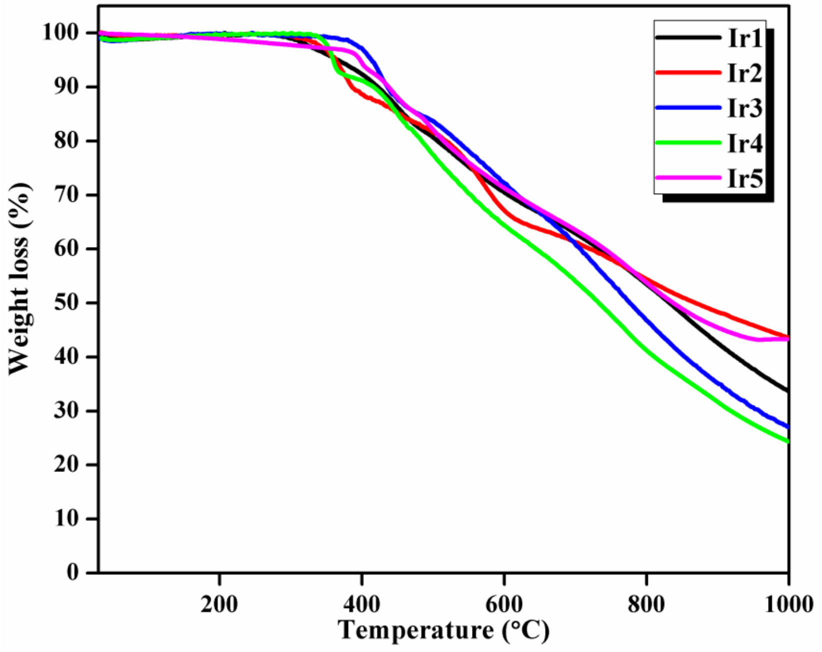

**Figure 2.4.** Thermogravimetric curves for complex **Ir1–Ir5** under $N_2$ atmosphere.

### 2.4.3. Thermal Properties

The thermal properties of the **Ir1–Ir5** were investigated by thermogravimetric analysis (TGA) and differential scanning calorimetry (DSC) at a scanning rate of 5 °C $\text{min}^{-1}$ under nitrogen atmosphere. As shown in Figure 2.4, **Ir3** and **Ir5** complexes are thermally stable with decomposition temperatures ($T_d$: at a 5% weight loss) higher than 415 °C. On the other hand, the thermal stability of the –CHO, $–CF_3$ and –OMe

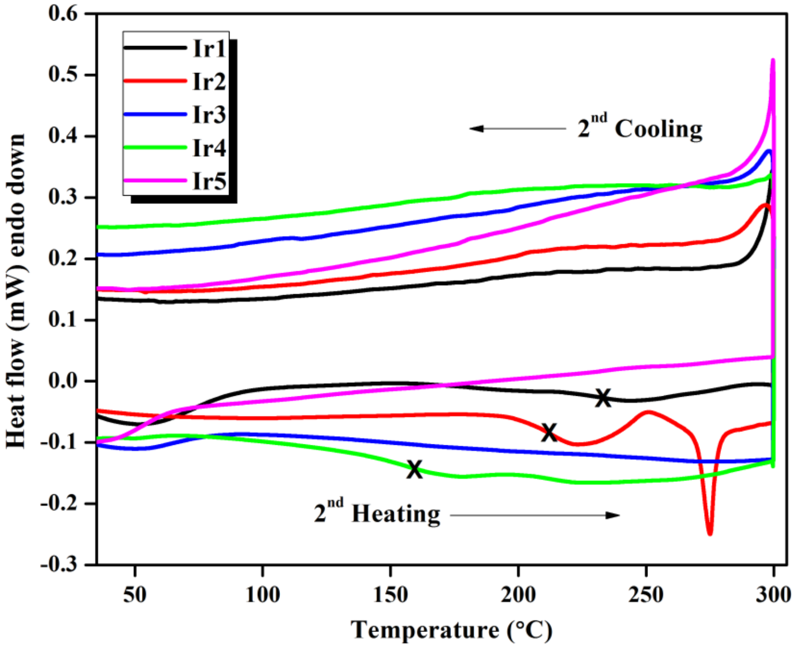

**Figure 2.5.** Differential scanning calorimetric curves for complex **Ir1–Ir5** under $N_2$ atmosphere.

**Table 2.5.** Electrochemical and thermal properties of Ir$^{3+}$ complexes **Ir1 – Ir5**

| Complex | $E_{ox}$$^{a}$ (V) | $E_{red}$$^{a}$ (V) | HOMO$^{b}$ (eV) | LUMO$^{c}$ (eV) | $E_{g(elec)}$$^{d}$ (eV) | $T_g$$^{e}$ (˚C) | $T_d$$^{f}$ (˚C) |
|---|---|---|---|---|---|---|---|
| **Ir1** | 1.75 | – 0.94 | – 6.07 | –3.42 | 2.65 | 231 | 367 |
| **Ir2** | 1.70 | – 1.43 | – 6.06 | –2.9 | 3.13 | 212 | 362 |
| **Ir3** | 1.78 | – 1.16 | – 6.13 | –3.21 | 2.92 | – | 415 |
| **Ir4** | 1.57 | – 1.77 | – 5.93 | –2.58 | 3.35 | 159 | 365 |
| **Ir5** | 1.21 | – 1.82 | – 5.57 | –2.54 | 3.03 | – | 397 |

[a] Electrochemical data *versus* ($FeCp_2^+/FeCp_2^0$) ($FeCp_2$ is ferrocene) were collected in $CH_3CN$/0.1 M TBAH (tetra-butylammoniumhexafluorophosphate). [b] HOMO = – [4.8 – (0.44) + $E_{oxd}$]. [c] LUMO = – [4.8 – (0.44) + $E_{red}$]. [d] Electrochemical band gap. [e] $T_g$ = glass transition temperature from DSC curve, Tg peak for **Ir3** and **Ir5** were not observed up to a temperature scan of 300˚C. [f] $T_d$ = decomposition temperature 5% weight loss from TG curve.

substituted iridium(III) complexes **Ir1**, **Ir2** and **Ir4** are found to be in the range 362–367 °C (Table 2.5). Further, these compounds show glass transition temperatures ($T_g$: from the second heating cycle of the DSC curve) in the range 159–231 °C, which guaranteed the morphological stability of the complexes (Figure 2.5).

### 2.4.4. Theoretical Calculations

The optimized structures of the iridium(III) complexes obtained by DFT method possess a distorted octahedral geometry around the iridium center, with C1 point group symmetry. The Ir–C (mean value: 2.005 Å) and Ir–N (mean value: 2.068 Å) bond lengths in the –OMe substituted iridium(III) complex (**Ir2**) obtained by structural optimization are in good agreement with the single crystal X-ray diffraction data Ir–C (mean value: 2.035 Å) [Table 2.6].

**Table 2.6.** Selected bond distances from the optimized ground (**$S_0$**) and triplet state (**$T_1$**) geometry for the complexes **Ir2** and **Ir4** together with the experimental values.

| Bond length (Å) | **Ir2** | | **Ir4** | | **Exp** | |
|---|---|---|---|---|---|---|
| | **$S_0$** | **$T_1$** | **$S_0$** | **$T_1$** | **Ir2** | **Ir4** |
| Ir-N1 | 2.208 | 2.209 | 2.204 | 2.215 | 2.150 | 2.125 |
| Ir-N2 | 2.062 | 2.086 | 2.081 | 2.023 | 2.046 | 2.050 |
| Ir-N3 | 2.075 | 2.021 | 2.067 | 2.087 | 2.025 | 2.048 |
| Ir-C1 | 2.006 | 2.002 | 2.003 | 2.005 | 1.965 | 1.983 |
| Ir-C2 | 2.005 | 2.008 | 2.005 | 2.004 | 1.987 | 2.000 |
| Ir-O1 | 2.165 | 2.158 | 2.173 | 2.167 | 2.115 | 2.157 |

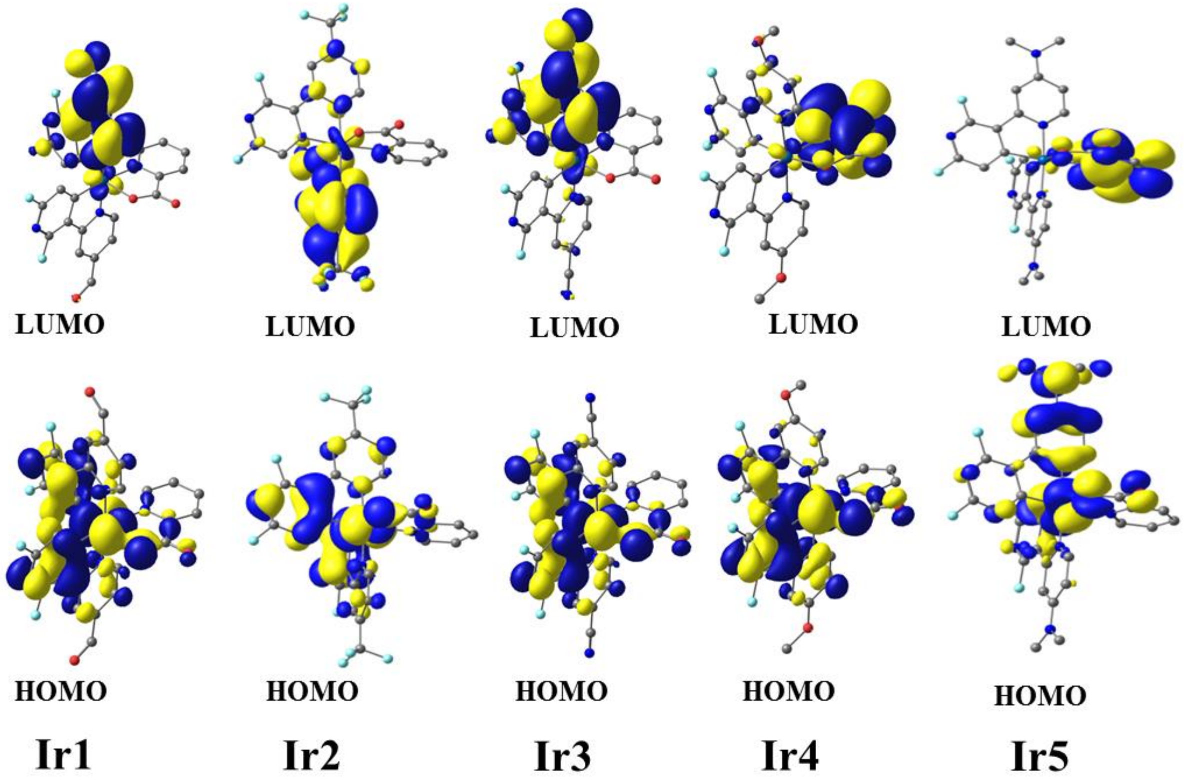

**Figure 2.6.** Selected molecular orbital diagram indicating isodensity HOMO and LUMO surfaces for complexes **Ir1−Ir5**. All of the molecular orbital surfaces correspond to an isocontour value of |Ψ| = 0.03.

Molecular orbital (MO) analysis indicated that the HOMO of electron-withdrawing group substituted iridium(III) complexes (**Ir1–Ir3**) is mainly localized on the 5d-orbitals of the iridium metal (51–52%), π-orbitals of the difluropyridyl moiety of the cyclometalated bypyridine ligand (28–29%) and a small contribution from the picolinate ancillary ligand (11–13%) (Figure 2.6 and 2.7 and Table 2.7). The present observation is similar to that of the HOMO orbital distribution of (dfpypy)Irpic reported elsewhere.[7] The LUMO is essentially localized on the substituted N-coordinated pyridyl moiety of the cyclometalated ligand (75–89%).

However, in the case of iridium(III) complex **Ir2**, the LUMO is not localized on the –$CF_3$ substituent. These results strongly indicate a HOMO−LUMO transition with the MLCT character in these complexes (**Ir1–Ir3**).

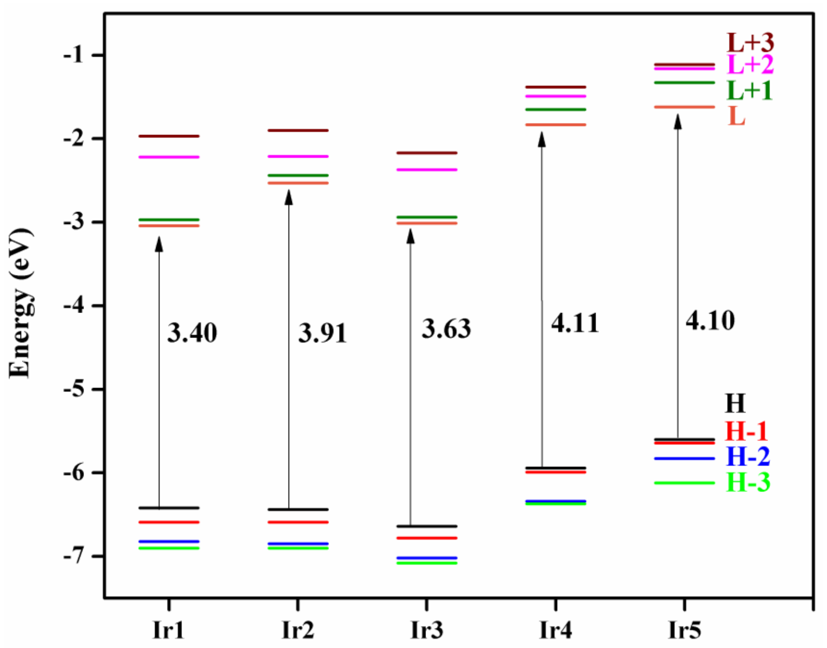

**Figure 2.7.** Partial molecular orbital diagram for complexes **Ir1−Ir5**. The arrows are intended to highlight the calculated HOMO−LUMO energy gaps (H = HOMO, L= LUMO).

In the case of the electron-donating group containing iridium(III) complexes, the HOMO is localized on the 5d-orbitals of the iridium atom (45–52%), π-orbitals of the substituted diflurobipyridine ligand (35–40%) and the picolinate ancillary ligand (12–14%). However, in the case of **Ir5** the HOMO contains major contribution from the N-coordinated pyridyl moiety of the cyclometalated ligand (30%). On the other hand, the LUMO is mainly localized on the picolinate ancillary ligand (90–93%) with minor contribution from the iridium metal center (2–3%) and the cyclometalated ligand

(4.3–7.1%). Thus the phosphorescence of electron-donating group substituted iridium(III) complexes may be described as mixed $^3$LC and $^3$MLCT transitions. These results are similar to that of unsubstituted (dfpypy)$_2$Ir(pic).[7]

**Table 2.7.** Calculated energy levels of the HOMO, HOMO-1, HOMO-2, LUMO, LUMO+1, and LUMO+2 and percentage of contribution of Iridium metal (Ir), 2',6'-difluoro-2,3'-bipyridine derivatives and picolinate (pic) ligands

| **Complex** | | **E (eV)** | **Ir$^{3+}$** | **Substituted pyridyl moiety** | **Difluoropyridyl moiety** | **pic** |
|---|---|---|---|---|---|---|
| **Ir1** | LUMO+3 | -1.969 | 1.71 | 57.94 | 30.83 | 13.16 |
| | LUMO+2 | -2.224 | 2.97 | 3.67 | 6.79 | 92.60 |
| | LUMO+1 | -2.974 | 4.7 | 88.90 | 10.11 | 1.01 |
| | LUMO | -3.038 | 4.89 | 88.42 | 9.77 | 1 52 |
| | HOMO | -6.422 | 51.20 | 7.77 | 29.44 | 11.59 |
| | HOMO-1 | -6.591 | 45.11 | 10.32 | 62.81 | 26.71 |
| | HOMO-2 | -6.823 | 6.54 | 16.57 | 53.50 | 30.18 |
| **Ir2** | LUMO+3 | -1.91 | 1.9 | 57.81 | 12.81 | 27.9 |
| | LUMO+2 | -2.25 | 3.3 | 4.14 | 2.45 | 92.2 |
| | LUMO+1 | -2.45 | 5.4 | 75.08 | 15.09 | 1.9 |
| | LUMO | -2.53 | 5.3 | 75.08 | 41.70 | 2.9 |
| | HOMO | -6.45 | 52.1 | 10.21 | 27.08 | 11.1 |
| | HOMO-1 | -6.63 | 47.1 | 13.82 | 13.96 | 25.2 |
| | HOMO-2 | -6.89 | 7.7 | 26.38 | 41.70 | 24.8 |
| **Ir3** | LUMO+3 | -2.174 | 1.55 | 64.81 | 21.81 | 11.83 |
| | LUMO+2 | -2.368 | 3.03 | 4.89 | 0.83 | 91.24 |
| | LUMO+1 | -2.942 | 5.32 | 84.19 | 9.22 | 1.27 |
| | LUMO | -3.015 | 5.53 | 82.61 | 9.82 | 2.04 |
| | HOMO | -6.645 | 51.75 | 6.79 | 28.31 | 13.14 |
| | HOMO-1 | -6.782 | 45.37 | 9.68 | 14.77 | 30.18 |
| | HOMO-2 | -7.019 | 1.53 | 4.62 | 15.43 | 78.42 |
| **Ir4** | LUMO+3 | -1.420 | 1.95 | 18.49 | 2.90 | 76.66 |
| | LUMO+2 | -1.506 | 5.11 | 65.34 | 26.99 | 2.56 |
| | LUMO+1 | -1.661 | 3.48 | 58.70 | 31.15 | 6.67 |
| | LUMO | -1.875 | 3.47 | 5.41 | 1.70 | 89.42 |
| | HOMO | -5.978 | 52.56 | 8.11 | 26.59 | 12.74 |
| | HOMO-1 | -6.040 | 50.11 | 14.73 | 13.60 | 21.55 |
| | HOMO-2 | -6.383 | 49.95 | 21.18 | 11.25 | 17.63 |
| **Ir5** | LUMO+3 | -1.05 | 2.6 | 14.60 | 2.37 | 80.4 |
| | LUMO+2 | -1.18 | 3.7 | 63.56 | 30.00 | 1.6 |
| | LUMO+1 | -1.32 | 3.5 | 55.83 | 27.81 | 6.6 |
| | LUMO | -1.55 | 2.8 | 3.34 | 0.87 | 93.0 |
| | HOMO | -5.62 | 45.0 | 30.43 | 9.86 | 14.6 |
| | HOMO-1 | -5.66 | 53.4 | 10.28 | 24.79 | 11.4 |
| | HOMO-2 | -5.86 | 40.8 | 52.16 | 3.85 | 3.0 |

## 2.4.5. Electrochemical Properties

To understand the electronic effects caused by the substituent on the *C*4′ position on the pyridyl moiety of the cyclometalated ligand, cyclic voltammetry experiments of the complexes **Ir1–Ir5** were carried out using ferrocene as the internal standard (Figures 2.8 and 2.9). The highest occupied molecular orbital (HOMO)/lowest unoccupied molecular orbital (LUMO) of complexes **Ir1–Ir5** are listed in Table 2.5. The $E_{\text{onset}}$ (oxd) value of the respective iridium(III) complex was determined using CV relative to a ferrocene/ferrocenium redox potential. All the iridium(III) complexes showed irreversible oxidation voltammograms. Kang and co-workers[7] also reported difficulties in observing the reversible oxidation potential for the parent compound $(\text{dfpypy})_2\text{Irpic}$. The investigations on DFT calculations indicate that the HOMO of electron-withdrawing group substituted iridium(III) complexes is localized at the iridium metal center and the difluropyridyl moiety. Thus the oxidation potentials are marginally influenced by the substitution of electron-withdrawing groups on the pyridyl moiety of the cyclometalated ligand. On the other hand, the substitution of the electron-donating group induces destabilization of the HOMO and hence a more negative shift of the oxidation peak potentials is noted (1.57 and 1.21 V for **Ir4** and **Ir5**). This can be due to more electron-donating features of the substituent groups in the pyridyl ring, which enhances the electron density at the metal center through an *ortho*-metalating nitrogen atom. Thus it becomes easier to remove the

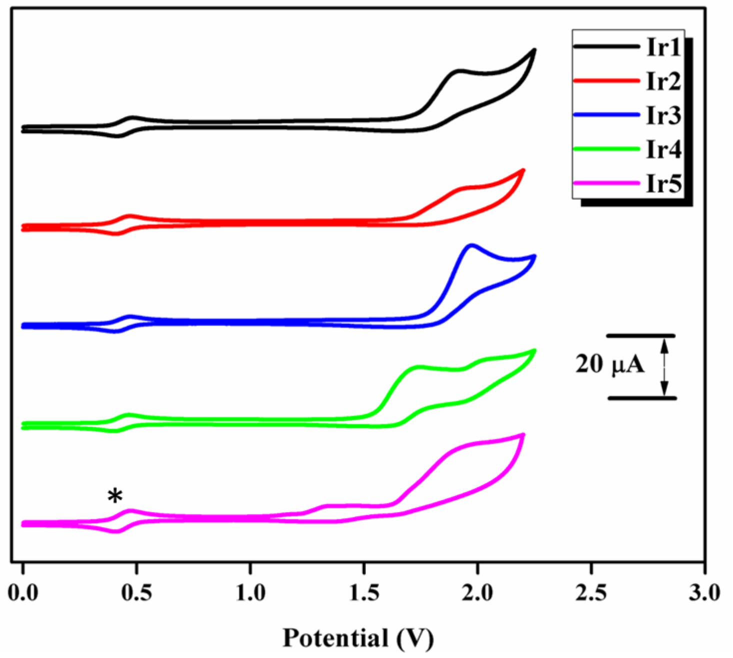

**Figure 2.8.** Comparison of oxidation potentials (vs Ag/AgCl in $CH_3CN$) of **Ir1**–**Ir5**, (oxidation potential $FeCp_2/FeCp_2^+$ =0.45 V, marked with asterisk).

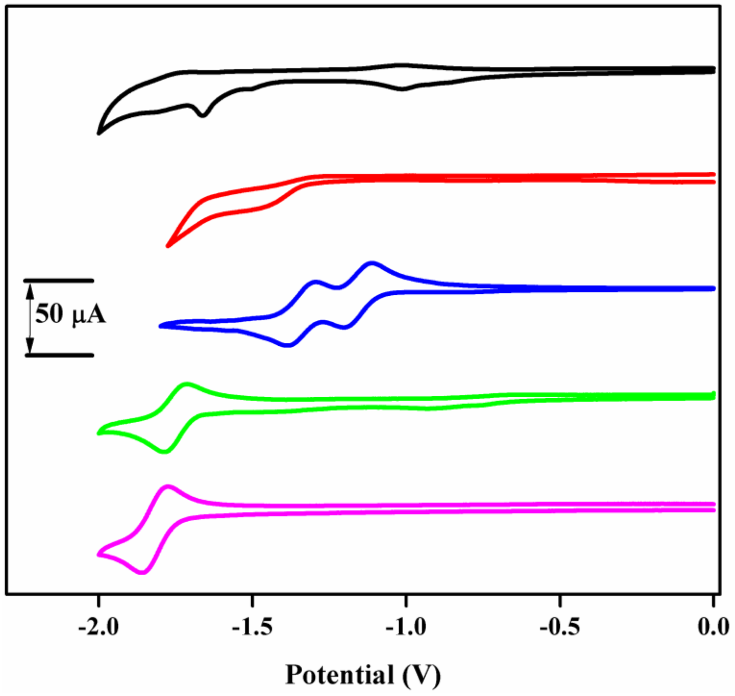

**Figure 2.9.** Comparison of reduction potentials (vs Ag/AgCl in $CH_3CN$) of **Ir1**–**Ir5**.

electrons from the HOMO. The –$NMe_2$ substituted **Ir5** shows the lowest oxidation potential among the series (1.21 V). As per the DFT calculations, the HOMO of **Ir5** is mainly localized on the iridium metal center, the N-coordinated pyridine ring and the electron-donating –$NMe_2$ substituent. Hence the first quasi reversible oxidation potential observed at 1.21 V in complex **Ir5** may be due to the oxidation of the –$NMe_2$ substituent in the pyridine ring.

All the iridium(III) complexes except **Ir1** and **Ir2** display reversible reduction potentials. The first reduction peak potential is observed at −0.94, −1.43, −1.16, −1.77 and −1.82 V, respectively, for **Ir1–Ir5**. The second reduction potential is detected at −1.66 and −1.31 V for **Ir1** and **Ir3**, respectively. However, the second reduction peak in the case of **Ir2**, **Ir4** and **Ir5** could not be obtained in the limit of the potential window of the experimental conditions. Since the LUMO orbitals are localized on the picolinate ancillary ligand in **Ir4** and **Ir5**, the substitution of electron-donating groups on the pyridyl moiety of the cyclometalated ligand shows a marginal effect on the reduction potentials of these complexes. However, the substitution of electron-withdrawing groups such as –$CF_3$ and –CN in **Ir2** and **Ir3** induces the stabilization of LUMO, which could be observed as a more positive shift of the reduction peak potential. The Swain–Lupton constant as a modification of the Hammett rule can be used as the electron accepting and donating parameter in explaining the observed reduction behaviour of these complexes. As shown in Table 2.8, a larger $F$ value is more σ-electron inductive (inductive effect), and a smaller $R$ is more π-electron donative (resonance effect). Among the electron-withdrawing substituted iridium(III) complexes, the –CN substituent has the highest *F* value of 0.51 and hence **Ir3** exhibits an oxidation potential of −1.16 V, which is 270 mV smaller than –$CF_3$ substituted iridium complex **Ir2** having a reduction potential of −1.43 V (*F* = 0.38). However, the reduction potential of **Ir1** is much lower than anticipated (−0.94 V *vs.* $Fc^+/Fc$) as per the Swain–Lupton constant. This can be attributed to the reduction of the –CHO group instead of the cyclometalated ligand as usually found in aromatic aldehydes.[25] This finding correlates well with the localization of mostly the –CHO group in the LUMO orbitals of **Ir1** (Figure 2.6).

**Table 2.8.** Swain−Lupton constants for the substituents[26]

| Substituent | *F* value | *R* value |
|---|---|---|
| **-H** | 0.03 | 0.00 |
| **-CHO** | 0.33 | 0.09 |
| **-$CF_3$** | 0.38 | 0.16 |
| **-CN** | 0.51 | 0.15 |
| **-OMe** | 0.29 | -0.56 |
| **-$NMe_2$** | 0.15 | -0.98 |

### 2.4.6. Electronic Spectroscopy

The UV-vis absorption spectra of iridium(III) compounds **Ir1–Ir5** recorded in degassed dichloromethane ($c = 5 \times 10^{-5}$ M) solution at room temperature are displayed in Figure 2.10, and the corresponding electronic absorption data are summarized in Table 2.9. The absorption of these complexes show intense bands with

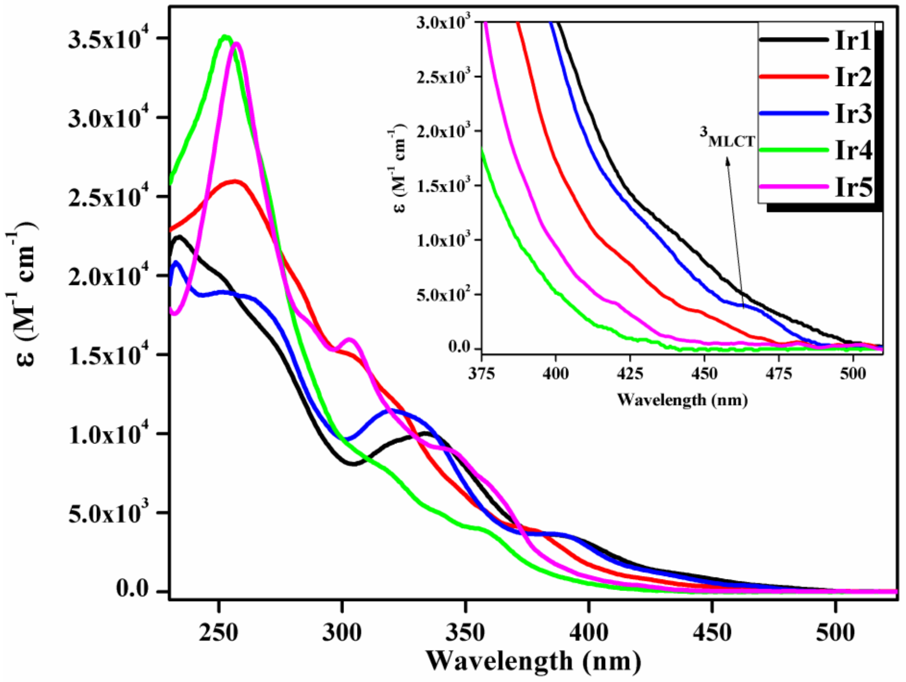

**Figure 2.10.** UV-vis absorption spectra of complexes **Ir1**–**Ir5** in dichloromethane ($c = 5 \times 10^{-5}$ M) at 298 K (inset: magnified absorption at 300- 500 nm region).

**Table 2.9.** Solution state photophysical properties of Ir$^{3+}$ complexes **Ir1**–**Ir5**

| Complex | Absorption$^a$ $\lambda_{max}$ (nm) ($\varepsilon \times 10^3$ M$^{-1}$ cm$^{-1}$) | Emission at 298 K in $CH_2Cl_2$ Solution | | | | | Emission 77 K$^f$ $\lambda_{max}$ (nm) |
|---|---|---|---|---|---|---|---|
| | | $\lambda_{max}{}^b$(nm) | $\Phi_{PL}{}^c$ | $\tau_{PL}$ (μs) | $k_r{}^d$ ($10^5$ S$^{-1}$) | $k_{nr}{}^e$ ($10^5$ S$^{-1}$) | |
| **Ir1** | 233 (20.0), 394 (3.0), 482 (0.2) | 540 | 0.79 | 1.94 | 4.07 | 1.08 | 511 |
| **Ir2** | 256 (26.0), 378 (4.0), 452 (0.4) | 468, 492 | 0.88 | 2.36 | 3.72 | 0.50 | 466 |
| **Ir3** | 233 (19.0), 391 (3.0), 464 (0.4) | 508 | 0.90 | 2.14 | 4.20 | 0.46 | 485 |
| **Ir4** | 252 (34.0), 356 (4.0), 430 (0.1) | 436, 464 | 0.58 | 1.13 | 5.13 | 3.71 | 434 |
| **Ir5** | 257 (35.0), 343 (9.0), 420 (0.6) | 520 | 0.14 | 0.31 | 4.51 | 27.74 | 476 |

[a] Absorption spectrum was measured in dichloromethane solution; [M] = 5.0 x $10^{-5}$. [b] Emission spectrum was measured in degassed dichloromethane; [M] = 5.0 × $10^{-5}$, $\lambda_{exc}$ = 360 nm. [c] Phosphorescence quantum efficiency measured in degassed $CH_2Cl_2$ by relative method by using Quinine sulphate monohydrate ($\Phi_{PL}$= 0.54) and Ir(ppy)$_3$ ($\Phi_{PL}$ = 0.98) as standards, respectively for blue and green emitting complexes. [d,e]Radiative as well as non-radiative rate constants were deduced by the $\Phi_{PL}$ of solution state and $\tau_{obs}$ according to two equations: $k_r = \Phi_{PL}/\tau_{obs}$, $k_{nr} = (1-\Phi_{PL})/\tau_{obs}$. [f]Emission spectrum was measured in freeze dichloromethane at 77K; [M] = 5.0 × $10^{-5}$, $\lambda_{exc}$= 360 nm.

extinction coefficients in the order of $10^4$ $M^{-1}$ $cm^{-1}$ in the 230–300 nm range, which were assigned to the spin-allowed intra-ligand $^1$LC ($^1\pi \rightarrow \pi^*$) transition of cyclometalated 2′,6′-difluoro-2,3′-bipyridine derivatives and picolinate ligands. The broad band at around 370–400 nm can be assigned to spin allowed metal-ligand charge-transfer ($^1$MLCT) bands with extinction coefficients in the order of $10^3$ $M^{-1}$ $cm^{-1}$. In addition, the spin-forbidden $^3$MLCT transition bands noted at around 420–464 nm indicate an efficient spin–orbit coupling, which is a prerequisite for phosphorescence emission (inset of Figure 2.10). The nature of substituents on the 4′ position at the pyridyl moiety of the cyclometalated ligand has significant effects on the extinction coefficient values of the intra-ligand ($\pi \rightarrow \pi^*$) transition band. However, no influence on the location of intra-ligand transition has been observed. The electron-donating group substituted iridium(III) complexes (**Ir4–Ir5**) exhibit extinction coefficients in the range 34 600–35 000 $M^{-1}$ $cm^{-1}$ for the $\pi \rightarrow \pi^*$ transition. On the other hand, low extinction coefficients 19 063–26 068 $M^{-1}$ $cm^{-1}$ are noted in the case of electron-withdrawing group containing complexes (**Ir1–Ir3**). Though the substituents have a small influence on the extinction coefficient at $^1$MLCT transition, there are significant differences in the location of these transitions. The substitution of electron-donating groups (–OMe and –$NMe_2$) in complexes **Ir4–Ir5** shows a blue shifted $^1$MLCT absorption bands around 356 and 343 nm, respectively, as compared to electron-withdrawing group substituted complexes **Ir1–Ir3** (381–394 nm).

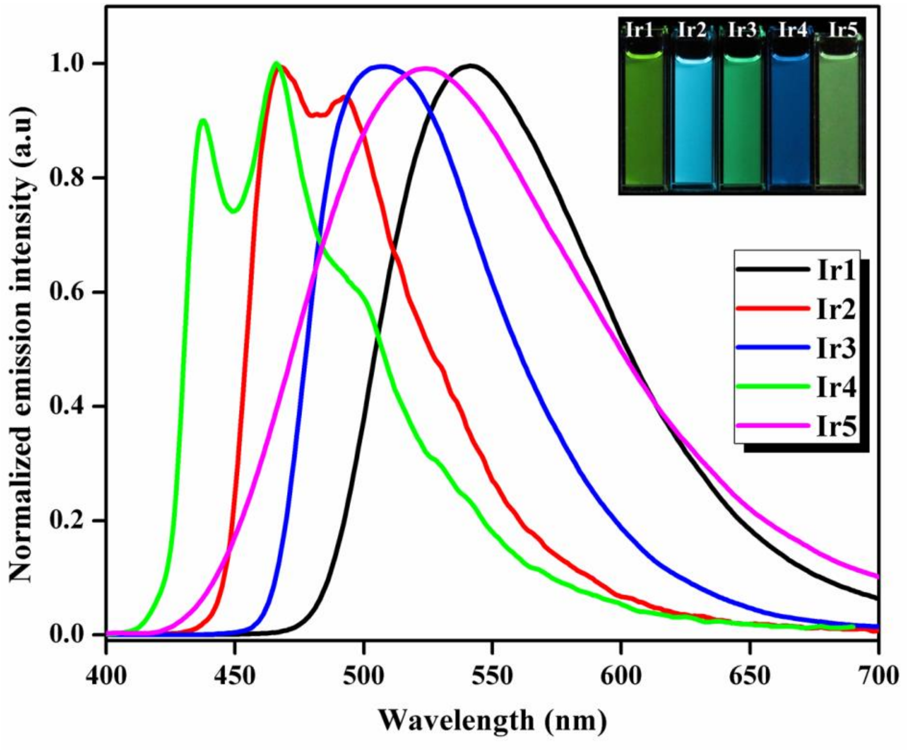

**Figure 2.11.** Emission spectra of complexes **Ir1−Ir5** in dichloromethane (c = 5 × $10^{-5}$M) at 298 K; inset: emission photographs of **Ir1–Ir5** in solution.

### 2.4.7. Solution State Emission Properties

Figure 2.11 shows normalized emission spectra of the investigated iridium(III) complexes **Ir1–Ir5** recorded in degassed dichloromethane solution ($c = 5.0 \times 10^{-5}$ M) at 298 K. The pertaining photophysical data are summarized in Table 2.9. The strong electron-withdrawing group substituted (–CN) iridium(III) complex (**Ir3**) displays a broad and bright green phosphorescence (450 to 700 nm; $\lambda_{\max} = 506$ nm) at room temperature in dichloromethane solution with an excellent quantum efficiency of 0.90, which is comparable to that of standard green emitter $Ir(ppy)_3$ ($\Phi_{PL}$ = 0.98).[27] The broad emission band exhibited by **Ir3** without the vibronic structure indicates that phosphorescence originates from the $^3$MLCT transition state. On the other hand, the iridium(III) complex (**Ir2**) containing less electron-withdrawing –$CF_3$ group ($C\sigma_p = 0.54$) exhibits intense sky-blue phosphorescence in the region 468–492 nm with a promising quantum efficiency ($\Phi_{PL} = 0.88$). It is interesting to note that the observed quantum efficiency of **Ir2** is very much comparable to that of commercial sky-blue emitter FIrpic ($\Phi_{PL} = 0.83$).[28] The vibronic structure of the emission bands in **Ir2** indicates a certain degree of mixing between the ligand centered $^3$LC and $^3$MLCT state. Surprisingly, a weak electron-withdrawing –CHO group ($C\sigma_p = 0.42$) substituted iridium(III) complex (**Ir1**) shows a broad emission profile in the range 470–700 nm ($\lambda_{max} = 540$ nm) with a quantum yield of 0.79. In general, the substitution of electron-withdrawing groups on the *C*4′ position at the pyridyl moiety red shifted the emission profiles of **Ir1–Ir3** as compared to unsubstituted iridium(III) complex $(dfpypy)_2$Irpic.[7] Our DFT studies (see section 2.4.4) indicate that the picolinate moiety essentially acts as an ancillary ligand in **Ir1–Ir3** and the emission properties are mainly of $^3$MLCT/$^3$LC nature, involving iridium d-orbitals and π–π* orbitals of the electron-withdrawing substituted 2′,6′-difluoro-2,3′-bipyridine cyclometalated units. It is well documented that acceptor groups are expected to stabilize the LUMO orbital that is involved by pulling out electron density.[29] This is in good agreement with the earlier investigations, which indicate that the triplet energy level of picolinate lies at the high energy level and is not involved in the electronic transition causing phosphorescence emission.[4f, 30] On the other hand, in the electron-donating substituted iridium(III) complexes **Ir4–Ir5**, the LUMO levels are found to be mainly located on the picolinate ligand. Therefore the substitution of the –OMe group in **Ir4** has induced marginal effects on the phosphorescence emission. However, the strong electron-donating $–NMe_2$ substituted iridium(III) complex (**Ir5**) shows a broad emission (420–700 nm; $\lambda_{max}$ = 520 nm) without vibrational features in the spectrum. The observed emission features can be attributed to the localization of the frontier molecular orbital on the $–NMe_2$ substituent, which inevitably leads to HOMO destabilization as evident from the theoretical calculations.

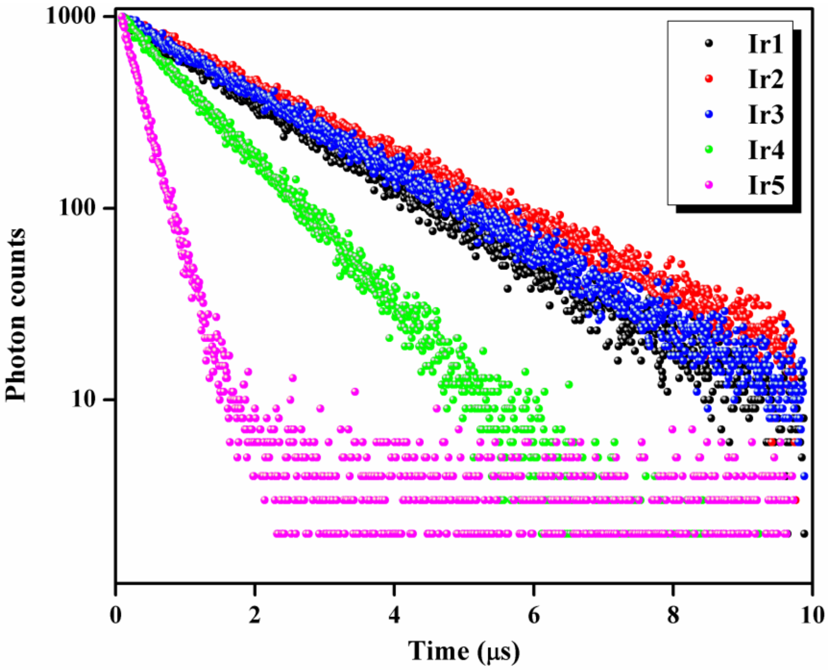

**Figure 2.12.** Lifetime decay profiles of complex **Ir1–Ir5** in degassed dichloromethane solution ($c = 5 \times 10^{-5}$ M, $\lambda_{exc}$ = 375 nm) at 298 K.

To gain insights into the relaxation dynamics of the investigated iridium(III) complexes **Ir1–Ir5**, the phosphorescence lifetimes ($\tau$) in dichloromethane solutions were measured at 298 K (Figure 2.12). All the complexes showed single exponential decay profiles with lifetimes in the range of 0.31–2.36 μs, which are indicative of the phosphorescence origin. The excited state lifetime values, radiative and non-radiative decay rates of the iridium(III) complexes are depicted in Table 2.9. It is noteworthy to mention that the electron-donating group (–OMe) substituted iridium(III) complex **Ir4** exhibits a moderately lower quantum efficiency ($\Phi_{PL}$ = 0.58) when compared to (dfpypy)$_2$Irpic [$\Phi_{PL}$ = 0.90]. This can be explained on the basis of destabilization of the LUMO, which will probably decrease the separation of the $^3$MC d–d* state and the designated $^3$MLCT or $^3$LC emissive states, and consequently intensifies the deactivation pathways. Conversely, poor quantum efficiency is observed in the case of iridium(III) complex **Ir5** due to large vibrational decay pathways ($k_{nr}$ = 27.7 × 10$^5$ s$^{-1}$) associated with the –NMe$_2$ group. At the same time high quantum yields have been noted for complexes **Ir1–Ir3** which are substituted with electron-withdrawing groups. This can be related to the stabilization of LUMO orbitals substituted with electron-withdrawing groups leading to increase the separation of the $^3$MC d–d* state and the designated $^3$MLCT or $^3$LC emissive states, and which in turn reduces the deactivation pathways.[5c] This is also in good agreement with the observed low non-radiative decay rates in these complexes ($k_{nr}$ = 0.46–1.08 × 10$^5$ s$^{-1}$).

**Table 2.10.** Calculated singlet-triplet splitting energy at the B3LYP/6-31G* level

| Complexes | $\mathbf{S_1}$ | $\mathbf{T_1}$ | $\mathbf{\Delta E_{S1\text{-}T1}}$ |
|---|---|---|---|
| **Ir1** | 2.561 | 2.054 | 0.507 |
| **Ir2** | 2.914 | 2.232 | 0.682 |
| **Ir3** | 2.706 | 2.112 | 0.594 |
| **Ir4** | 3.103 | 2.339 | 0.764 |
| **Ir5** | 3.050 | 2.329 | 0.721 |

It is well known that a minimal difference between the singlet ($S_1$) and triplet ($T_1$) splitting energy ($\Delta E_{S1-T1}$) is favorable for enhancing the intersystem crossing (ISC) efficiency, which in turn leading to an increased radiative rate constant ($k_r$).[31] Therefore, it would be informative to obtain further insights into the evolution of $k_r$ by concentrating on singlet–triplet energy differences for these complexes. Thus, a small $\Delta E_{S1-T1}$ (Table 2.10) and high $k_r$ values (Table 2.9) noted for **Ir1–Ir3** clearly supports the observed high quantum efficiencies and lifetime values in these compounds. On the other hand, the high $\Delta E_{S1-T1}$ values diminish the ISC efficiency in **Ir4** and **Ir5**, which in turn responsible for exhibiting the poor quantum efficiencies and lifetime values in these complexes.

In order to understand the changes in the geometry structures of these complexes upon excitation, the geometry parameters of the complexes in the lowest-lying triplet states ($T_1$) are calculated (Table 2.11). The Ir–N1 (N1: picolinate ligand) bonds are elongated in **Ir4** and **Ir5**, which suggests the larger involvement of the ancillary ligand in the $T_1$ state rather than from the cyclometalated ligand. Moreover, the elongated distances are responsible for the increase of metal-centered ($^3$MC) non-radiative decay rates that accounts for the less quantum efficiency observed in these complexes. In contrast, the Ir–N1 bonds are not elongated in **Ir1–Ir3**, which indicates that the ancillary ligand participation in the emissive excited state is minimal. Further the shortening of bond distances (Ir–N2 and Ir–N3) are noted in **Ir1–Ir3**, which suggests that larger involvement of the cyclometalating ligand in the $T_1$ state rather than from the ancillary ligand. Moreover, the shortened distances are helpful to decrease the metal-centered (MC) non-radiative decay that accounts for the higher efficiency in these complexes.

**Table 2.11.** Selected bond distances and bond angles from the optimized ground (**$S_0$**) and triplet state (**$T_1$**) geometry for the complexes **Ir1-Ir5**

| **Bond length (Å)** | **Ir1** | | **Ir2** | | **Ir3** | | **Ir4** | | **Ir5** | |
|---|---|---|---|---|---|---|---|---|---|---|
| | **$S_0$** | **$T_1$** | **$S_0$** | **$T_1$** | **$S_0$** | **$T_1$** | **$S_0$** | **$T_1$** | **$S_0$** | **$T_1$** |
| Ir-N1 | 2.207 | 2.207 | 2.208 | 2.209 | 2.207 | 2.209 | 2.204 | 2.215 | 2.204 | 2.222 |
| Ir-N2 | 2.073 | 2.010 | 2.062 | 2.086 | 2.073 | 2.001 | 2.081 | 2.023 | 2.067 | 2.099 |
| Ir-N3 | 2.060 | 2.093 | 2.075 | 2.021 | 2.060 | 2.098 | 2.067 | 2.087 | 2.081 | 1.992 |
| Ir-C1 | 2.006 | 2.011 | 2.006 | 2.002 | 2.006 | 2.011 | 2.003 | 2.005 | 2.005 | 2.016 |
| Ir-C2 | 2.007 | 2.004 | 2.005 | 2.008 | 2.007 | 2.009 | 2.005 | 2.004 | 2.001 | 2.007 |
| Ir-O1 | 2.167 | 2.148 | 2.165 | 2.158 | 2.163 | 2.143 | 2.173 | 2.167 | 2.177 | 2.162 |

## 2.4.8. Emission Properties in the Freeze Solvent Matrix

It is clear from the emission spectra at 77 K depicted in Figure 2.13 that all the complexes display vibrational progressions. The peak emissions ($E_{\mathrm{em(0-0)}}$) are blue shifted by 44, 29 and 23 nm for **Ir5**, **Ir1** and **Ir3**, respectively, compared to their room temperature peak emissions. This can be attributed to the rigidochromic effect[32] associated with the complexes having a greater MLCT character of the emitting state.

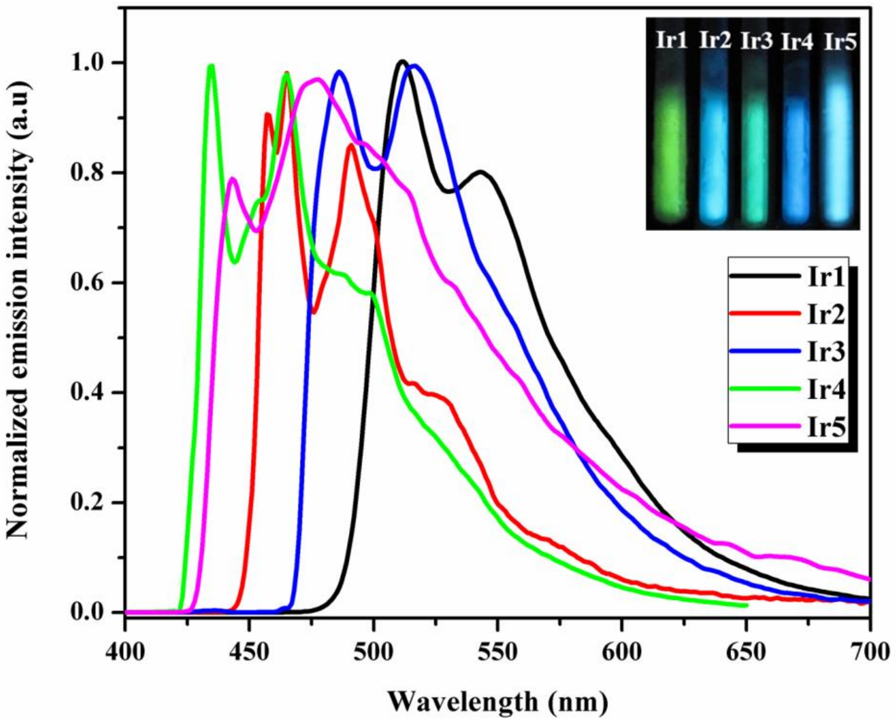

**Figure 2.13.** Emission spectra of complexes **Ir1−Ir5** in freeze dichloromethane ($c = 5 \times 10^{-5}$ M) at 77 K.; inset: emission photographs of **Ir1–Ir5** in freeze dichloromethane.

**Table 2.12.** Excited state properties of $Ir^{3+}$ complexes **Ir1–Ir5**

| Complex | $^{a}E_{em}(0\text{-}0)$ (nm) | $^{b}\Delta\upsilon_{1/2}$ ($cm^{-1}$) | $^{c}\hbar\omega_M$ ($cm^{-1}$) | $^{d}S_M$ |
|---|---|---|---|---|
| **Ir1** | 511 | 2487 | 1153 | 0.85 |
| **Ir2** | 457 | 2326 | 1562 | 0.99 |
| **Ir3** | 486 | 3208 | 1197 | 1.08 |
| **Ir4** | 435 | 3454 | 1437 | 1.03 |
| **Ir5** | 443 | 4672 | 1609 | 1.36 |

[a]Obtained from the peak emission wavelength in dichloromethane at 77K. [b]Full width half maximum for the (0-0) band obtained from the emission spectra at 77K. [c]From the energy difference of first two emission peaks at 77K. [d]The Huang–Rhys factor, $S_M$ was estimated from the peak heights and energies of the first two peaks of the emission spectra at 77 K [$S_M = (I_{0,1}/I_{0,0})\,(\bar{\upsilon}_{0,0}/\bar{\upsilon}_{0,1})$].

However, a moderate blue shift (1−4 nm) has been noted in complexes **Ir2** and **Ir4**, indicating the domination of the LC character in the excited state.[33] The Full Width Half Maximum (FWHM, $\Delta\upsilon_{1/2}$) values (Table 2.12) of the resolved highest energy vibronic bands of **Ir1–Ir5** are 2487, 2326, 3208, 3454 and 4672 cm$^{-1}$, respectively. The large FWHM value of **Ir5** indicates the highest reorganizational energy in the corresponding excited state. The energy difference of first two emission peaks ($\hbar\omega_M$ value) of these complexes lie in the range of 1457–1609 cm$^{-1}$ indicating that the dominant vibrational mode associated with the excited distortion can be ascribed to the aromatic in-plane and out-of-plane ring stretching and bending vibrations (ring breathing modes).[34] The degree of the vibrational non-radiative decay can be estimated by the Huang–Rhys factor ($S_M$). The $S_M$ values of complexes **Ir1–Ir5** are found to be 0.85, 0.99, 1.08, 1.03 and 1.36, respectively (Table 2.12). The larger the $S_M$ value, the stronger the coupling between the dominant ligand-localized vibrations in the excited and ground states.[35] Thus a large Huang–Rhys factor leads to increased vibrational non-radiative decay and as a result small $\Phi_{PL}$ in **Ir5**.

### 2.4.9. Emission Properties in the PMMA Polymer Matrix

Figure 2.14 shows the normalized emission spectra of 5 wt% of **Ir1–Ir5** doped in a poly(methyl methacrylate) (PMMA) polymer film at ambient temperature. In the spin coated thin films, complexes **Ir2**, **Ir3** and **Ir4** exhibited virtually identical emission profiles similar to those observed in the corresponding fluid state, which indicate that there is little intermolecular interaction in the amorphous state.[7] However, **Ir1** and **Ir5** exhibited strong emissions with a blue shift (10 nm for **Ir1** and

50 nm for **Ir5**) with less resolved emission compared to those observed in the corresponding fluid state. The photoluminescence quantum efficiencies are found to be 0.67, 0.84, 0.98, 0.94 and 0.40 for complexes **Ir1–Ir5**, respectively, for the doped PMMA films (Table 2.13).

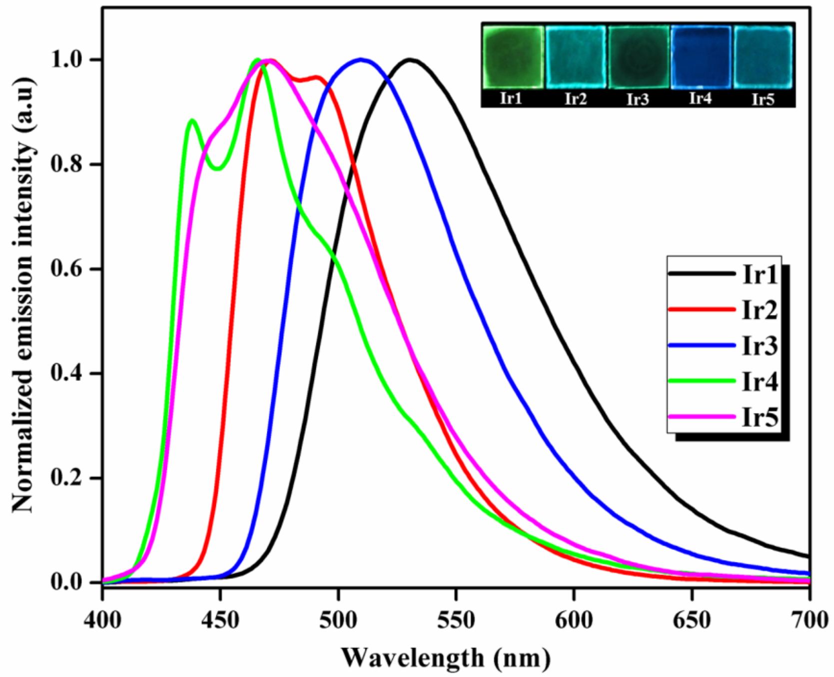

**Figure 2.14.** Emission spectra of complexes **Ir1–Ir5** in 5 wt % doped PMMA film; inset: emission photographs of **Ir1–Ir5** in spin coated PMMA film.

**Table 2.13.** Photophysical properties of $Ir^{3+}$ complexes **Ir1–Ir5** in PMMA polymer film

| Complex | Emission at 298 K in 5 wt% doped PMMA film | | | | |
|---|---|---|---|---|---|
| | $\lambda_{max}$[a] (nm) | $\Phi_{PL}$[b] | $\tau_{PL}$ (μs) | $k_r$[c] ($10^5 S^{-1}$) | $k_{nr}$[d] ($10^5 S^{-1}$) |
| **Ir1** | 530 | 0.67 | 2.14 | 3.13 | 1.54 |
| **Ir2** | 470, 491 | 0.84 | 1.91 | 4.39 | 0.83 |
| **Ir3** | 508 | 0.98 | 2.15 | 4.55 | 0.09 |
| **Ir4** | 437, 465 | 0.92 | 1.85 | 4.97 | 0.43 |
| **Ir5** | 470 | 0.40 | 1.11 | 3.60 | 5.40 |

[a] Emission spectrum was measured in 5wt% doped PMMA film, $\lambda_{exc}$ = 360 nm. [b] Quantum efficiency measured by absolute method using integrating sphere. [c,d] Radiative as well as non-radiative rate constants were deduced by the $\Phi_{PL}$ of solid state and $\tau_{obs}$ according to two equations: $k_r = \Phi_{PL}/\tau_{obs}$, $k_{nr} = (1 - \Phi_{PL})/\tau_{obs}$.

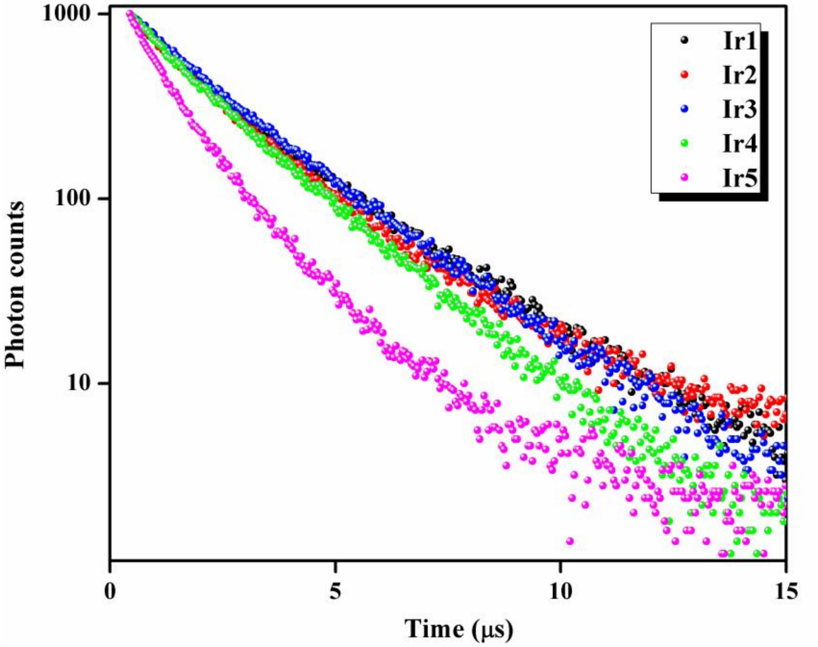

**Figure 2.15** Lifetime decay profiles of complex **Ir1–Ir5** in 5 wt% doped PMMA film ($\lambda_{exc}$ = 375 nm) at 298 K.

In general, all the compounds exhibited higher quantum efficiencies in PMMA thin films as compared to the solution state due to the suppression of non-radiative pathways in the rigid polymer. The transient phosphorescence lifetimes for complex **Ir1–Ir5** are in the range 1.11–2.15 μs (Table 2.13 and Figure 2.15). The observed $k_{nr}$ values of the iridium(III) complexes in the current study can be correlated with the nature of the substituent on the cyclometalated ligands. Among the substituents investigated, in general the electron-withdrawing substituted iridium(III) complexes have low $k_{nr}$ values and hence exhibit high quantum efficiency. Conversely, electron-donating group (–$NMe_2$) substituted iridium(III) complex (**Ir5**) has the highest $k_{nr}$ value, which displays the lowest quantum efficiency due to the distortional vibrations of the dimethyl amino group causing a great deal of non-radiative depopulation of the excited state.[36] However, the –OMe substituted **Ir4** shows a promising quantum efficiency which is having a low $k_{nr}$ and the highest $k_r$ among the series.

### 2.4.10. Electroluminescence Properties

To evaluate the performance of the new Ir(III) compounds in PhOLEDs, a series of OLED devices were prepared by following a multi-layered structure with CBP (4,4′-bis(*N*-carbazolyl)-1,1′-biphenyl) as the host. The typical structure of the multi-layered devices is ITO (120 nm)/$F_4$-TCNQ (2.5 nm)/α-NPD (45 nm)/emissive layer (30 nm)/BCP (6 nm)/$Alq_3$ (30 nm)/LiF (1 nm)/Al (150 nm), as shown in Figure 2.16. Figure 2.17 depicts the EL spectra of OLEDs fabricated using 5 wt% **Ir2**, **Ir3** and **Ir4** doped CBP. 5 wt% **Ir2** doped in CBP showed the EL spectrum with a dominant peak at 480 nm and a shoulder peak at 520 nm owing to triplet exciton relaxation. EL spectra of **Ir2** is found to differ from its PL spectra; mainly the peak observed nearly at 500 nm has reduced in intensity in the EL spectra and both peaks has been red shifted in EL. A device with 5 wt% **Ir3** doped CBP as an emissive layer has a peak at 530 nm and the shape of EL spectra nearly resembles the PL spectra. The EL spectrum of 5 wt% **Ir4** doped CBP is constituted of three peaks at 460, 490 and 540 nm, respectively. CIE colour co-ordinates measured for these devices are listed in Table 2.14 and also depicted inside the CIE diagram in Figure

2.17. It is evident from the figure that **Ir2** emits in the bluish region, Ir3 in the green while **Ir4** in the blue region of the visible spectrum as also observed from the PL results. It is interesting note that there is no residual emission from the host CBP for each device, which means that the energy and/or charge transfer from the host exciton to the phosphor is complete upon electrical excitation.

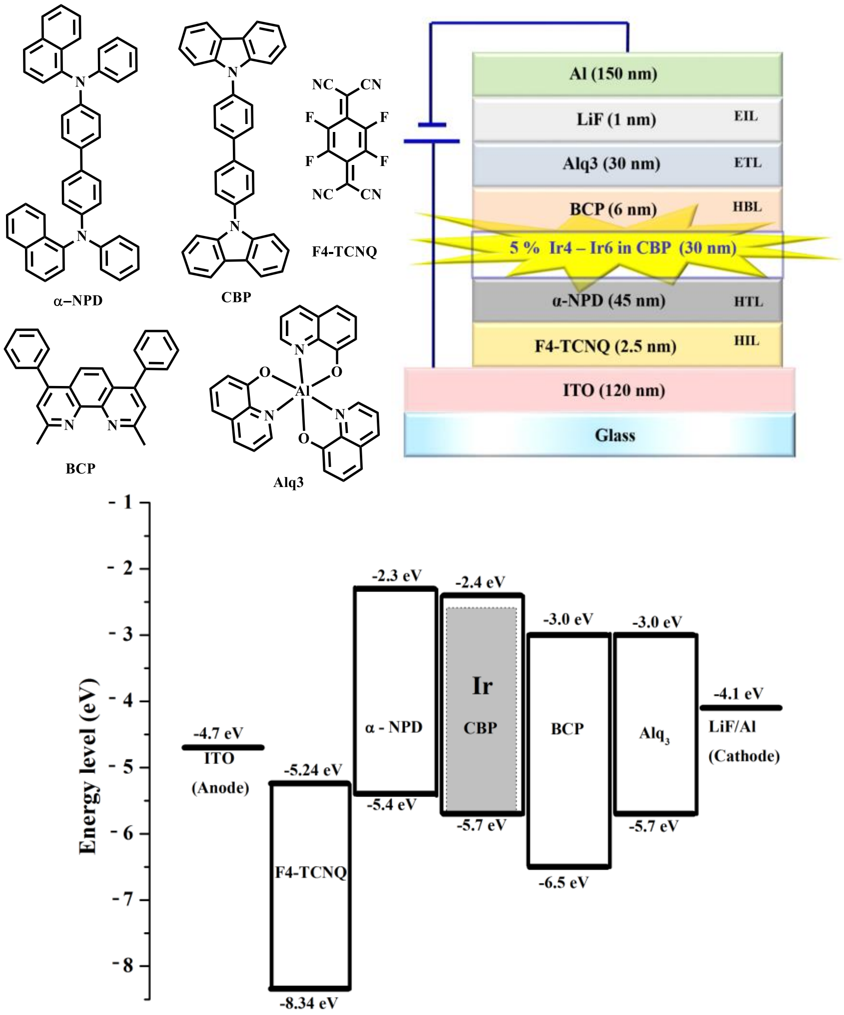

**Figure 2.16.** Schematic EL device structure (right top), the chemical formulas of materials used for the device preparation (left top) and energy level diagram of the device with Ir(III) compounds (**Ir2–Ir4**) as dopants (bottom).

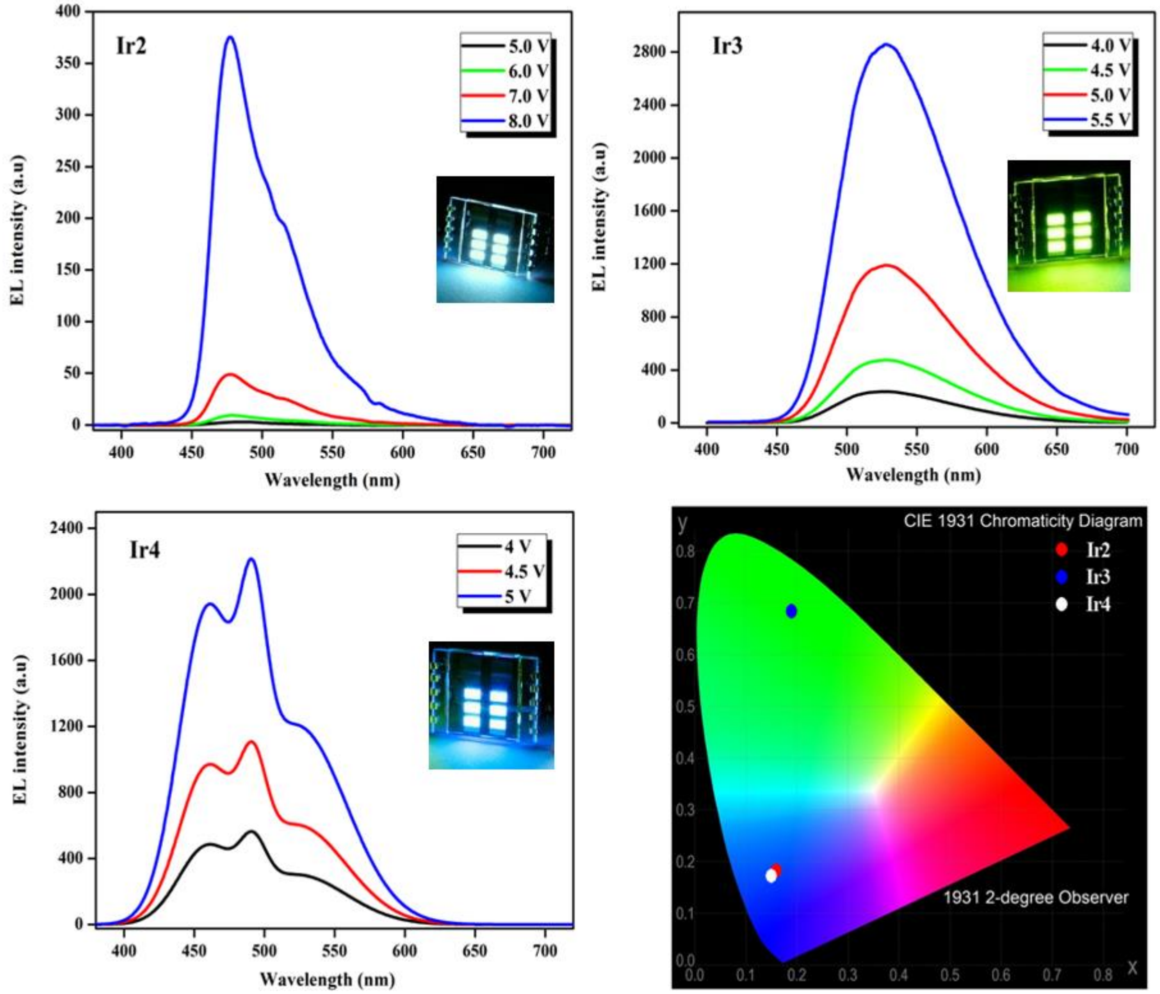

**Figure 2.17.** Electroluminescence (EL) plots for compounds **Ir2–Ir4** and CIE 1931 chromaticity diagram for the device with Ir(III) compounds (**Ir2–Ir4**) as dopants (right bottom).

**Table 2.14.** EL performance data of the **Ir2**, **Ir3 and Ir4** as phosphorescent dopant in CBP

| Device | $V_{on}$ (V) | $L_{max}$ (cd/m$^2$) | $\eta_c$ (Cd/A) | $\eta_p$ (lm/W) | EQE (max) | CIE$_{(x,y)}$ |
|---|---|---|---|---|---|---|
| **Ir2** | 3.5 | 13,400 | 12.6 | 5.3 | 3.2 % | (0.16, 0.18) |
| **Ir3** | 3.5 | 28,200 | 14.7 | 7.6 | 2.1 % | (0.19, 0.68) |
| **Ir4** | 3.5 | 33,180 | 11.6 | 5.8 | 4.7 % | (0.15, 0.17) |

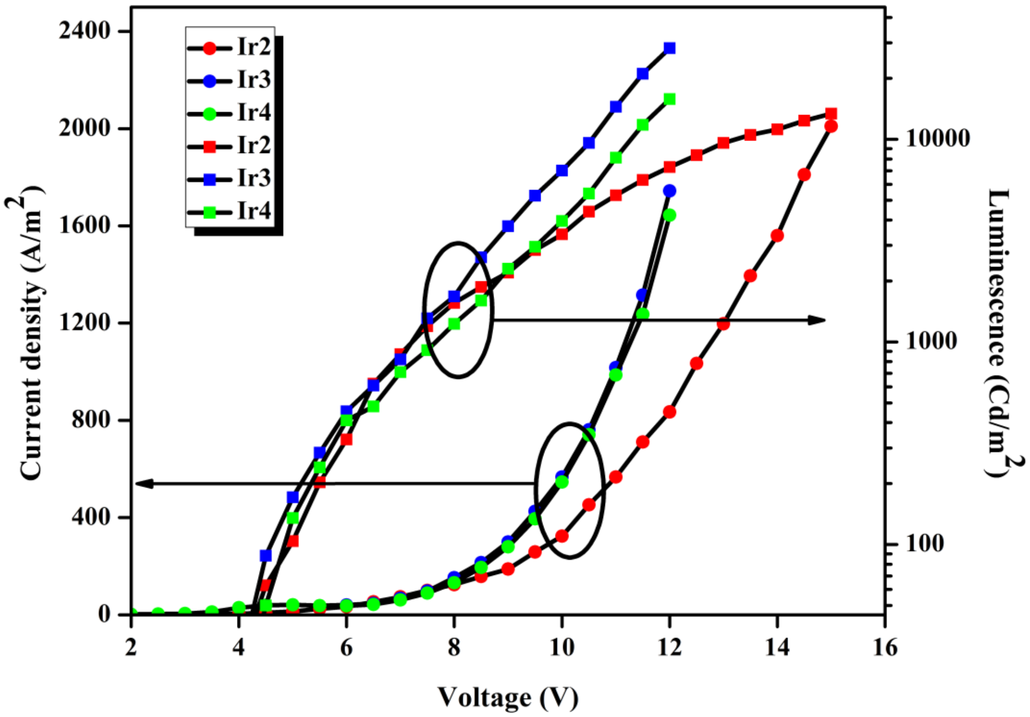

**Figure 2.18.** Current density–voltage–luminescence (J–V–L) characteristics of **Ir2**–**Ir4** as phosphorescent dopants.

Figure 2.18 shows the *J–V–L* characteristics of these devices and the efficiency parameters are listed in Table 2.14. All devices were found to possess a low turn-on voltage (3.5 V) corresponding to a luminous intensity of 10 cd $m^{-2}$. OLEDs with 5 wt% **Ir2** doped CBP as an emissive layer showed a maximum luminescence of about 15 000 cd $m^{-2}$ with a peak current and a power efficiency of 12.6 cd $A^{-1}$ and 5.3 lm $W^{-1}$, respectively. The peak efficiency for OLEDs with 5 wt% **Ir3** doped CBP and 5 wt% **Ir4** doped CBP were found to be 14.5 cd $A^{-1}$, 7.6 lm $W^{-1}$ and 11.6 cd $A^{-1}$, 5.76 lm $W^{-1}$, respectively. EL results indicate that the synthesized materials can be used as efficient phosphorescent dopants.

## 2.5. Conclusions

- In conclusion, a series of bis(2′,6′-difluoro-2,3′-bipyridinato-*N*,*C*4′)iridium (picolinate) complexes [(dfpypy)$_2$Ir(pic): **Ir1–Ir5**] with different electron-withdrawing (–CHO, –CF$_3$ and –CN) and electron-donating substituents (–OMe and –NMe$_2$) on the 4′ position at the pyridyl moiety of the 2′,6′-difluoro-2,3′-bipyridine ligands has been synthesized, well characterized and investigated their photophysical properties.
- The results demonstrated that the phosphorescence emission colour of the iridium complexes and quantum efficiencies are influenced by the electron–withdrawing or electron-donating feature of the substituent.
- The electron-withdrawing group (–CHO, –CF$_3$, and –CN) substituted iridium(III) complexes **Ir1–Ir3** display intense yellowish green, sky-blue and green emissions, respectively, at room temperature in both solution and in thin-film with excellent quantum efficiencies ($\Phi_{\mathrm{PL}}$ = 0.79–0.90 in solution and 0.67 to 0.98 in thin film).
- The iridium(III) complex bearing the electron-donating group (–OMe) shows pure and intense blue emission with a promising quantum efficiency in solution ($\Phi_{\mathrm{PL}}$ = 0.58) and in thin-film ($\Phi_{\mathrm{PL}}$ = 0.92). Conversely, the –NMe$_2$ substituted iridium(III) complex (**Ir5**) exhibits a broad emission in the

green region with a poor quantum efficiency ($\Phi_{PL}$ = 0.14 in solution; 0.40 in thin-film).

- DFT calculations disclose that the picolinate moiety essentially acts as an ancillary ligand in **Ir1–Ir3** and the emission properties are mainly manifested by $^3$MLCT/$^3$LC, involving iridium d-orbitals and π–π* orbitals of the electron-withdrawing substituted 2′,6′-difluoro-2,3′-bipyridine cyclometalated units.
- On the other hand, in the electron-donating substituted iridium(III) complexes **Ir4–Ir5**, the LUMO levels are found to be mainly localized on the picolinate ligand. Thus the phosphorescence of **Ir4–Ir5** may be resulted from mixed $^3$LC and $^3$MLCT transitions.
- Most importantly, the –OMe, –CF$_3$ and –CN substituted iridium(III) complexes display excellent emissions in the blue and green regions with high quantum efficiencies.
- The combination of smaller $\Delta E_{S1-T1}$ and higher contribution of MLCT in the emission process result in the higher quantum yields and excited state lifetimes in **Ir1–Ir3** compounds.
- Finally, fabrication of complex **Ir4** successfully achieves nearly deep-blue OLEDs, showing a bright blue emission with CIEs of (0.15, 0.17), a power efficiency of 5.76 lm W$^{-1}$, and an EQE as high as 4.7% with the maximum luminance of 33 180 cd m$^{-2}$.

- The results clearly demonstrate that the newly designed iridium(III) complexes exhibit excellent thermal and morphological stabilities and electroluminescence properties. Hence these complexes may find potential applications in PhOLEDS.

## 2.6. References

(1) (a) Yersin, H., *Highly Efficient OLEDs with Phosphorescent Materials*. Wiley-VCH: Weinheim, Germany 2008. (b) Chen, S. M.; Tan, G. P.; Wong, W. Y.; Kwok, H. S., *Adv. Funct. Mater.* **2011,** *21*, 3785-3793. (c) Lo, S. C.; Bera, R. N.; Harding, R. E.; Burn, P. L.; Samuel, I. D. W., *Adv. Funct. Mater.* **2008,** *18*, 3080-3090. (d) Chen, Z. Q.; Bian, Z. Q.; Huang, C. H., *Adv. Mater.* **2010,** *22*, 1534-1539. (e) Holder, E.; Langeveld, B. M. W.; Schubert, U. S., *Adv. Mater.* **2005,** *17*, 1109-1121. (f) Kang, D. M.; Kang, J. W.; Park, J. W.; Jung, S. O.; Lee, S. H.; Park, H. D.; Kim, Y. H.; Shin, S. C.; Kim, J. J.; Kwon, S. K., *Adv. Mater.* **2008,** *20*, 2003-2008. (g) Xiao, L. X.; Chen, Z. J.; Qu, B.; Luo, J. X.; Kong, S.; Gong, Q. H.; Kido, J. J., *Adv. Mater.* **2011,** *23*, 926-952. (h) Adachi, C.; Kwong, R. C.; Djurovich, P.; Adamovich, V.; Baldo, M. A.; Thompson, M. E.; Forrest, S. R., *Appl. Phys. Lett.* **2001,** *79*, 2082-2084. (i) Chou, P. T.; Chi, Y., *Chem. Eur. J.* **2007,** *13*, 380-395. (j) Hsieh, C. H.; Wu, F. I.; Fan, C. H.; Huang, M. J.; Lu, K. Y.; Chou, P. Y.; Yang, Y. H. O.; Wu, S. H.; Chen, I. C.; Chou, S. H.; Wong, K. T.; Cheng, C. H., *Chem. Eur. J.* **2011,** *17*, 9180-9187. (k) Chi, Y.; Chou, P. T., *Chem. Soc. Rev.* **2007,** *36*, 1421-1431. (l) Hong, Y. N.; Lam, J. W. Y.; Tang, B. Z., *Chem. Soc. Rev.* **2011,** *40*, 5361-5388. (m) Williams, J. A. G.; Wilkinson, A. J.; Whittle, V. L., *Dalton Trans.* **2008**, 2081-2099. (n) Chang, Y. Y.; Hung, J. Y.; Chi, Y.; Chyn, J. P.; Chung, M. W.; Lin, C. L.; Chou, P. T.; Lee, G. H.; Chang, C. H.; Lin, W. C., *Inorg. Chem.* **2011,** *50*, 5075-5084. (o) Du, B. S.; Lin, C. H.; Chi, Y.; Hung, J. Y.; Chung, M. W.; Lin, T. Y.; Lee, G. H.; Wong, K. T.; Chou, P. T.; Hung, W. Y.; Chiu, H. C., *Inorg. Chem.* **2010,** *49*, 8713-8723. (p) Rai, V. K.; Nishiura, M.; Takimoto, M.; Zhao, S. S.; Liu, Y.; Hou, Z. M., *Inorg. Chem.* **2012,** *51*,

822-835. (q) Ren, X. F.; Kondakova, M. E.; Giesen, D. J.; Rajeswaran, M.; Madaras, M.; Lenhart, W. C., *Inorg. Chem.* **2010,** *49*, 1301-1303. (r) Schneidenbach, D.; Ammermann, S.; Debeaux, M.; Freund, A.; Zollner, M.; Daniliuc, C.; Jones, P. G.; Kowalsky, W.; Johannes, H. H., *Inorg. Chem.* **2010,** *49*, 397-406. (s) Adachi, C.; Baldo, M. A.; Thompson, M. E.; Forrest, S. R., *J. Appl. Phys.* **2001,** *90*, 5048-5051. (t) Wong, W. Y.; Ho, C. L., *J. Mater. Chem.* **2009,** *19*, 4457-4482. (u) Fernandez-Hernandez, J. M.; Yang, C. H.; Beltran, J. I.; Lemaur, V.; Polo, F.; Frohlich, R.; Cornil, J.; De Cola, L., *J. Am. Chem. Soc.* **2011,** *133*, 10543-10558. (v) Nazeeruddin, M. K.; Humphry-Baker, R.; Berner, D.; Rivier, S.; Zuppiroli, L.; Graetzel, M., *J. Am. Chem. Soc.* **2003,** *125*, 8790-8797. (w) Baldo, M. A.; O'Brien, D. F.; You, Y.; Shoustikov, A.; Sibley, S.; Thompson, M. E.; Forrest, S. R., *Nature* **1998,** *395*, 151-154. (x) Ho, C. L.; Wong, W. Y., *New J. Chem.* **2013,** *37*, 1665-1683. (y) Pu, Y. J.; Iguchi, N.; Aizawa, N.; Sasabe, H.; Nakayama, K.; Kido, J., *Org. Electron.* **2011,** *12*, 2103-2110. (z) Baldo, M. A.; Adachi, C.; Forrest, S. R., *Phys. Rev. B.* **2000,** *62*, 10967-10977.

(2) (a) Baldo, M. A.; Lamansky, S.; Burrows, P. E.; Thompson, M. E.; Forrest, S. R., *Appl. Phys. Lett.* **1999,** *75*, 4-6. (b) Chi, Y.; Chou, P. T., *Chem. Soc. Rev.* **2010,** *39*, 638-655. (c) Lamansky, S.; Djurovich, P.; Murphy, D.; Abdel-Razzaq, F.; Lee, H. E.; Adachi, C.; Burrows, P. E.; Forrest, S. R.; Thompson, M. E., *J. Am. Chem. Soc.* **2001,** *123*, 4304-4312. (d) Liu, Z. W.; Guan, M.; Bian, Z. Q.; Nie, D. B.; Gong, Z. L.; Li, Z. B.; Huang, C. H., *Adv. Funct. Mater.* **2006,** *16*, 1441-1448. (e) Wagenknecht, P. S.; Ford, P. C., *Coord. Chem. Rev.* **2011,** *255*, 591-616. (f) Wong, W. Y.; Zhou, G. J.; Yu, X. M.; Kwok, H. S.; Lin, Z. Y., *Adv. Funct. Mater.* **2007,** *17*, 315-323. (g) Wong, W. Y.; Zhou, G. J.; Yu, X. M.; Kwok, H. S.; Tang, B. Z., *Adv. Funct. Mater.* **2006,** *16*, 838-846. (h) Yang, C. H.; Su, W. L.; Fang, K. H.; Wang, S. P.; Sun, I. W., *Organometallics* **2006,** *25*, 4514-4519. (i) Zhou, G. J.; Wong, W. Y.; Yao, B.; Xie, Z. Y.; Wang, L. X., *Angew. Chem. Int. Ed.* **2007,** *46*, 1149-1151. (j) Helander, M. G.; Wang, Z. B.; Qiu, J.; Greiner, M. T.; Puzzo, D. P.; Liu, Z. W.; Lu, Z. H., *Science* **2011,** *332*, 944-947. (k) Kim, S. Y.; Jeong, W. I.; Mayr, C.; Park, Y. S.; Kim, K. H.;

Lee, J. H.; Moon, C. K.; Brutting, W.; Kim, J. J., *Adv. Funct. Mater.* **2013,** *23*, 3896-3900. (l) Lee, S.; Kim, K. H.; Limbach, D.; Park, Y. S.; Kim, J. J., *Adv. Funct. Mater.* **2013,** *23*, 4105-4110. (m) Lee, S.; Limbach, D.; Kim, K. H.; Yoo, S. J.; Park, Y. S.; Kim, J. J., *Org. Electron.* **2013,** *14*, 1856-1860. (n) Leem, D. S.; Jung, S. O.; Kim, S. O.; Park, J. W.; Kim, J. W.; Park, Y. S.; Kim, Y. H.; Kwon, S. K.; Kim, J. J., *J. Mater. Chem.* **2009,** *19*, 8824-8828. (o) Park, Y. S.; Kang, J. W.; Kang, D. M.; Park, J. W.; Kim, Y. H.; Kwon, S. K.; Kim, J. J., *Adv. Mater.* **2008,** *20*, 1957-+. (p) Park, Y. S.; Lee, S.; Kim, K. H.; Kim, S. Y.; Lee, J. H.; Kim, J. J., *Adv. Funct. Mater.* **2013,** *23*, 4914-4920. (q) Tanaka, D.; Sasabe, H.; Li, Y. J.; Su, S. J.; Takeda, T.; Kido, J., *Japanese. J. Appl. Phy. Part 2* **2007,** *46*, L10-L12. (r) Yang, C. H.; Cheng, Y. M.; Chi, Y.; Hsu, C. J.; Fang, F. C.; Wong, K. T.; Chou, P. T.; Chang, C. H.; Tsai, M. H.; Wu, C. C., *Angew. Chem. Int. Ed.* **2007,** *46*, 2418-2421.

(3) (a) Tao, Y. T.; Wang, Q. A.; Yang, C. L.; Zhong, C.; Qin, J. G.; Ma, D. G., *Adv. Funct. Mater.* **2010,** *20*, 2923-2929. (b) Chou, H. H.; Cheng, C. H., *Adv. Mater.* **2010,** *22*, 2468-2477. (c) Tsuzuki, T.; Shirasawa, N.; Suzuki, T.; Tokito, S., *Adv. Mater.* **2003,** *15*, 1455-1458. (d) Wong, W. Y.; Ho, C. L.; Gao, Z. Q.; Mi, B. X.; Chen, C. H.; Cheah, K. W.; Lin, Z. Y., *Angew. Chem. Int. Ed.* **2006,** *45*, 7800-7803. (e) Park, N. G.; Kwak, M. Y.; Kim, B. O.; Kwon, O. K.; Kim, Y. K.; You, B.; Kim, T. W.; Kim, Y. S., *Jpn. J. Appl. Phys. Part1* **2002,** *41*, 1523-1526. (f) Tanaka, D.; Agata, Y.; Takeda, T.; Watanabe, S.; Kido, J., *Jpn. J. App.l Phys. Part 2* **2007,** *46*, L117-L119. (g) Tamayo, A. B.; Alleyne, B. D.; Djurovich, P. I.; Lamansky, S.; Tsyba, I.; Ho, N. N.; Bau, R.; Thompson, M. E., *J. Am. Chem. Soc.* **2003,** *125*, 7377-7387.

(4) (a) Coppo, P.; Plummer, E. A.; De Cola, L., *Chem. Commun.* **2004**, 1774-1775. (b) Grushin, V. V.; Herron, N.; LeCloux, D. D.; Marshall, W. J.; Petrov, V. A.; Wang, Y., *Chem. Commun.* **2001**, 1494-1495. (c) Shi, C.; Sun, H. B.; Jiang, Q. B.; Zhao, Q.; Wang, J. X.; Huang, W.; Yan, H., *Chem. Commun.* **2013,** *49*, 4746-4748. (d) Fan, C.; Li, Y. H.; Yang, C. L.; Wu, H. B.; Qin, J. G.; Cao, Y., *Chem. Mater.* **2012,** *24*, 4581-4587. (e) Aoki, S.; Matsuo, Y.; Ogura, S.; Ohwada, H.; Hisamatsu, Y.; Moromizato, S.; Shiro, M.; Kitamura, M., *Inorg. Chem.* **2011,** *50*, 806-818. (f) Baranoff, E.;

Curchod, B. F. E.; Monti, F.; Steimer, F.; Accorsi, G.; Tavernelli, I.; Rothlisberger, U.; Scopelliti, R.; Gratzel, M.; Nazeeruddin, M. K., *Inorg. Chem.* **2012,** *51*, 799-811. (g) Xu, Q. L.; Wang, C. C.; Li, T. Y.; Teng, M. Y.; Zhang, S.; Jing, Y. M.; Yang, X.; Li, W. N.; Lin, C.; Zheng, Y. X.; Zuo, J. L.; You, X. Z., *Inorg. Chem.* **2013,** *52*, 4916-4925. (h) Xu, M. L.; Zhou, R.; Che, G. B.; Wang, G. Y.; Wang, Z. J.; Xiao, Q., *J. Lumin.* **2011,** *131*, 909-914. (i) Ragni, R.; Plummer, E. A.; Brunner, K.; Hofstraat, J. W.; Babudri, F.; Farinola, G. M.; Naso, F.; De Cola, L., *J. Mater. Chem.* **2006,** *16*, 1161-1170. (j) Kozhevnikov, V. N.; Dahms, K.; Bryce, M. R., *J. Org. Chem.* **2011,** *76*, 5143-5148. (k) Park, H. J.; Kim, J. N.; Yoo, H. J.; Wee, K. R.; Kang, S. O.; Cho, D. W.; Yoon, U. C., *J. Org. Chem.* **2013,** *78*, 8054-8064. (l) Avilov, I.; Minoofar, P.; Cornil, J.; De Cola, L., *J. Am. Chem. Soc.* **2007,** *129*, 8247-8258. (m) Lee, S.; Kim, S. O.; Shin, H.; Yun, H. J.; Yang, K.; Kwon, S. K.; Kim, J. J.; Kim, Y. H., *J. Am. Chem. Soc.* **2013,** *135*, 14321-14328. (n) Seo, H. J.; Yoo, K. M.; Song, M.; Park, J. S.; Jin, S. H.; Kim, Y. I.; Kim, J. J., *Org. Electron.* **2010,** *11*, 564-572. (o) Oh, H.; Park, K. M.; Hwang, H.; Oh, S.; Lee, J. H.; Lu, J. S.; Wang, S. N.; Kang, Y., *Organometallics* **2013,** *32*, 6427-6436. (p) Wu, L. L.; Yang, C. H.; Sun, I. W.; Chu, S. Y.; Kao, P. C.; Huang, H. H., *Organometallics* **2007,** *26*, 2017-2023.

(5) (a) Haneder, S.; Da Como, E.; Feldmann, J.; Lupton, J. M.; Lennartz, C.; Erk, P.; Fuchs, E.; Molt, O.; Munster, I.; Schildknecht, C.; Wagenblast, G., *Adv. Mater.* **2008,** *20*, 3325-3328. (b) Sasabe, H.; Chiba, T.; Su, S. J.; Pu, Y. J.; Nakayama, K. I.; Kido, J., *Chem. Commun.* **2008**, 5821-5823. (c) Chou, P. T.; Chi, Y.; Chung, M. W.; Lin, C. C., *Coord. Chem. Rev.* **2011,** *255*, 2653-2665. (d) Karatsu, T.; Takahashi, M.; Yagai, S.; Kitamura, A., *Inorg. Chem.* **2013,** *52*, 12338-12350. (e) Meerheim, R.; Scholz, S.; Olthof, S.; Schwartz, G.; Reineke, S.; Walzer, K.; Leo, K., *J. Appl. Phys.* **2008,** *104*, 014510-014515. (f) Lee, S.; Kim, S.-O.; Shin, H.; Yun, H.-J.; Yang, K.; Kwon, S.-K.; Kim, J.-J.; Kim, Y.-H., *J. Am. Chem. Soc.* **2013,** *135*, 14321-14328. (g) Fu, H. S.; Cheng, Y. M.; Chou, P. T.; Chi, Y., *Mater. Today* **2011,** *14*, 472-479.

(6) Lee, S. J.; Park, K. M.; Yang, K.; Kang, Y., *Inorg. Chem.* **2009,** *48*, 1030-1037.

(7) Kang, Y.; Chang, Y. L.; Lu, J. S.; Ko, S. B.; Rao, Y. L.; Varlan, M.; Lu, Z. H.; Wang, S. N., *J. Mater. Chem. C* **2013,** *1*, 441-450.

(8) Yang, C. H.; Mauro, M.; Polo, F.; Watanabe, S.; Muenster, I.; Frohlich, R.; De Cola, L., *Chem. Mater.* **2012,** *24*, 3684-3695.

(9) Park, H. R.; Lim, D. H.; Kim, Y. K.; Ha, Y., *J. Nanosci. Nanotechno.* **2012,** *12*, 668-673.

(10) Kessler, F.; Watanabe, Y.; Sasabe, H.; Katagiri, H.; Nazeeruddin, M. K.; Gratzel, M.; Kido, J., *J. Mater. Chem. C* **2013,** *1*, 1070-1075.

(11) (a) Lee, S.-J.; Yang, S.-G.; Kim, H.-Y.; Kim, Y.-K.; Hwang, S.-H.; Shin, D.-Y.; Do, Y.-R.; Jung, D.-H.; Suwon-si, *U.S. Patent 2005/0170209 Al* **2005**. (b) Mingjie, Z.; Ping, W.; , *WIPO Patent WO/2013/000166* **2013**.

(12) (a) Bejoymohandas, K. S.; George, T. M.; Bhattacharya, S.; Natarajan, S.; Reddy, M. L. P., *J. Mater. Chem. C* **2014,** *2*, 515-523. (b) Garces, F. O.; King, K. A.; Watts, R. J., *Inorg. Chem.* **1988,** *27*, 3464-3471. (c) Nonoyama, M., *Bull. Chem. Soc. Jpn.* **1974,** *47*, 767-769.

(13) (a) CrystalClear 2.1, Rigaku Corporation: Tokyo, Japan. (b) Pflugrath, J. W., *Acta. Crystallogr. D* **1999,** *55*, 1718-1725.

(14) Sheldrick, G. M., *SADABS Siemens Area Detector Absorption Correction Program* University of Göttingen, Göttingen, Germany, 1994.

(15) Brouwer, A. M., *Pure Appl. Chem.* **2011,** *83*, 2213-2228.

(16) King, K. A.; Spellane, P. J.; Watts, R. J., *J. Am. Chem. Soc.* **1985,** *107*, 1431−1432.

(17) J. C. de Mello; H. F. Wittmann; Friend, R. H., *Adv. Mater.* **1997,** *9*, 230-232.

(18) Liu, Y.; Liu, M. S.; Jen, A. K. Y., *Acta Polym.* **1999,** *50*, 105-108.

(19) (a) Becke, A. D., *J. Chem. Phys.* **1993,** *98*, 5648-5652. (b) Lee, C. T.; Yang, W. T.; Parr, R. G., *Phys. Rev. B* **1988,** *37*, 785-789.

(20) Gorelsky, S. I., *SWizard program (version 4.6)* **2007**.

(21) Frisch, M. J.; Trucks, G. W.; Schlegel, H. B.; Scuseria, G. E.; Robb, M. A.; Cheeseman, J. R.; Scalmani, G.; Barone, V.; Mennucci, B.; Petersson, G. A., *et al. GAUSSIAN 09, Revision A.02* **2009.**

(22) Tyagi, P.; Kumar, A.; Giri, L. I.; Dalai, M. K.; Tuli, S.; Kamalasanan, M. N.; Srivastava, R., *Opt. Lett.* **2013,** *38*, 3854-3857.

(23) Baranoff, E.; Curchod, B. F. E.; Frey, J.; Scopelliti, R.; Kessler, F.; Tavernelli, I.; Rothlisberger, U.; Gratzel, M.; Nazeeruddin, M. K., *Inorg. Chem.* **2012,** *51*, 215-224.

(24) Xu, M. L.; Che, G. B.; Li, X. Y.; Xiao, Q., *Acta. Crystallogr. E.* **2009,** *65*, M28-U379.

(25) Udhayan, R.; Basheerahmed, K.; Srinivasan, K., *Bull. Electrochem.* **1988,** *4*, 163-165.

(26) Hansch, C.; Leo, A.; Taft, R. W., *Chem. Rev.* **1991,** *91*, 165-195.

(27) Hofbeck, T.; Yersin, H., *Inorg. Chem.* **2010,** *49*, 9290-9299.

(28) (a) You, Y.; Kim, K. S.; Ahn, T. K.; Kim, D.; Park, S. Y., *J Phys Chem C* **2007,** *111*, 4052-4060. (b) You, Y. M.; Park, S. Y., *J. Am. Chem. Soc.* **2005,** *127*, 12438-12439.

(29) Frey, J.; Curchod, B. F. E.; Scopelliti, R.; Tavernelli, I.; Rothlisberger, U.; Nazeeruddin, M. K.; Baranoff, E., *Dalton Trans.* **2014,** *43*, 5667–5679.

(30) Lamansky, S.; Djurovich, P.; Murphy, D.; Abdel-Razzaq, F.; Kwong, R.; Tsyba, I.; Bortz, M.; Mui, B.; Bau, R.; Thompson, M. E., *Inorg. Chem.* **2001,** *40*, 1704-1711.

(31) Li, J.; Zhang, Q.; He, H.; Wang, L.; Zhang, J., *Dalton Trans* **2015,** *44*, 8577-8589.

(32) Zanoni, K. P. S.; Kariyazaki, B. K.; Ito, A.; Brennaman, M. K.; Meyer, T. J.; Iha, N. Y. M., *Inorg. Chem.* **2014,** *53*, 4089-4099.

(33) Han, L. L.; Yang, D. F.; Li, W. L.; Chu, B.; Chen, Y. R.; Su, Z. S.; Zhang, D. Y.; Yan, F.; Wu, S. H.; Wang, J. B.; Hu, Z. Z.; Zhang, Z. Q., *Appl. Phys. Lett.* **2009,** *94*, 3303-3308.

(34) (a) Damrauer, N. H.; Boussie, T. R.; Devenney, M.; McCusker, J. K., *J. Am. Chem. Soc.* **1997,** *119*, 8253-8268. (b) Han, L. L.; Yang, D. F.; Li, W. L.; Chu, B.; Chen, Y. R.; Su, Z. S.; Zhang, D. Y.; Yan, F.; Wu, S. H.; Wang, J. B.; Hu, Z. Z.; Zhang, Z. Q., *Appl. Phys. Lett.* **2009,** *94*. (c) Humbs, W.; Yersin, H., *Inorg. Chim. Acta* **1997,** *265*, 139-147. (d) Kober, E. M.; Caspar, J. V.; Lumpkin, R. S.; Meyer, T. J., *J. Phys. Chem.* **1986,** *90*, 3722-3729. (e) Nakamato, N., *Infrared and Raman Spectra of Inorganic and Coordination Compounds*. 3rd edn ed.; Wiley: New York, 1977. (f) Rillema, D. P.; Blanton, C. B.; Shaver, R. J.; Jackman, D. C.; Boldaji, M.; Bundy, S.; Worl, L. A.; Meyer, T. J., *Inorg. Chem.* **1992,** *31*, 1600-1606. (g) Yersin, H., *Proc. SPIE–Int. Soc. Opt. Eng.* **2004,** *5214*, 124-140. (h) Yersin, H.; Schutzenmeier, S.; Wiedenhofer, H.; Vonzelewsky, A., *J. Phys. Chem.* **1993,** *97*, 13496-13499.

(35) (a) Caspar, J. V.; T.D.Westmoreland; Allen, G. H.; Bradley, P. G.; Meyer, T. J.; Woodruff, W. H., *J. Am. Chem. Soc* **1984,** *106*, 3492-3501. (b) Watts, R. J., *Comments Inorg. Chem.* **1991,** *11*, 303-308.

(36) Lyu, Y. Y.; Byun, Y.; Kwon, O.; Han, E.; Jeon, W. S.; Das, R. R.; Char, K., *J. Phys. Chem. B* **2006,** *110*, 10303-10314.

# Chapter 3

## A Highly Selective Chemosensor for Cyanide Derived from a Formyl-Functionalized Phosphorescent Iridium(III) Complex

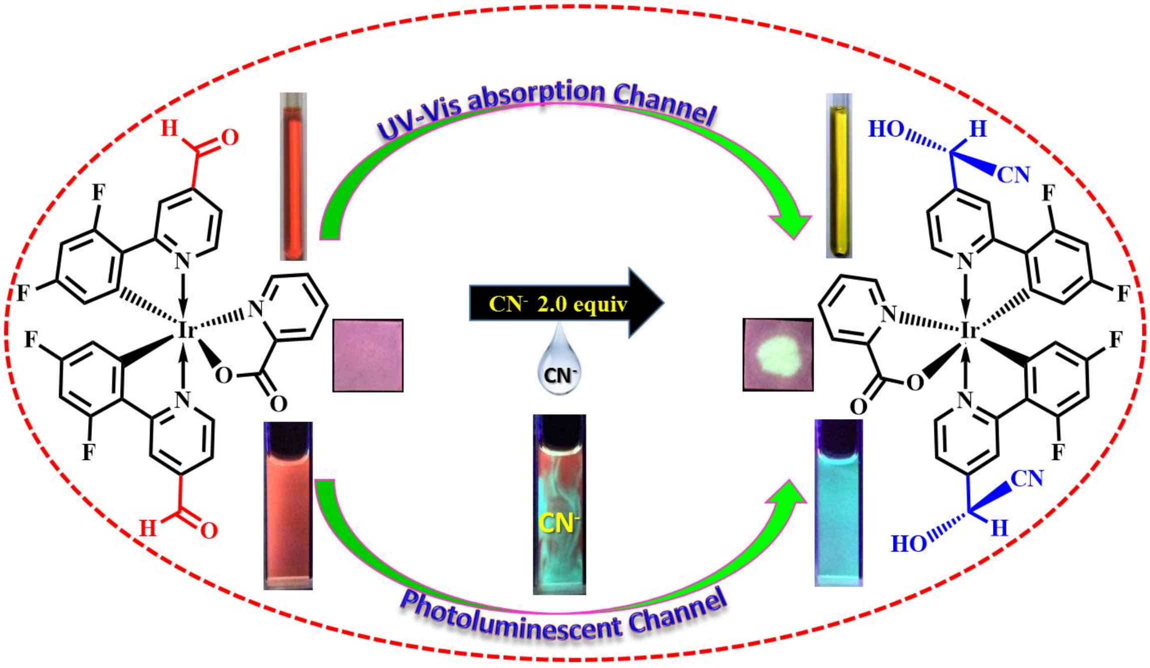

### 3.1. Abstract

*A new phosphorescent iridium(III) complex, bis[2′,6′-difluorophenyl-4-formyl-pyridinato-N,C4′]iridium(III) (picolinate) (**IrC**), was synthesized, fully characterized by various spectroscopic techniques, and utilized for the detection of $CN^-$ on the basis of the widely known hypothesis of the formation of cyanohydrins. The solid-state structure of the developed **IrC** was authenticated by single-crystal X-ray diffraction. Notably, the iridium(III) complex exhibits intense red phosphorescence in the solid state at 298 K (photoluminescence quantum efficiency, $\Phi_{PL}$ = 0.16) and faint emission in acetonitrile solution ($\Phi_{PL}$ = 0.02). The cyanide anion binding properties with **IrC***

*in pure and aqueous acetonitrile solutions were systematically investigated using two different channels: i.e., by means of UV–vis absorption and photoluminescence. The addition of 2.0 equiv of cyanide to a solution of the iridium(III) complex in acetonitrile (c = 20 μM) visibly changes the color from orange to yellow. On the other hand, the PL intensity of* ***IrC*** *at 480 nm was dramatically enhanced ~$5.36 \times 10^2$-fold within 100 s along with a strong signature of a blue shift of the emission by ~155 nm with a detection limit of $2.16 \times 10^{-8}$ M. The cyanohydrin formation mechanism is further supported by results of a $^1$H NMR titration of* ***IrC*** *with $CN^-$. As an integral part of this work, phosphorescent test strips have been constructed by impregnating Whatman filter paper with* ***IrC*** *for the trace detection of $CN^-$ in the contact mode, exhibiting a detection limit at the nanogram level (~265 ng/mL). Finally, density functional theory (DFT) and time-dependent density functional theory (TD-DFT) calculations were performed to understand the electronic structure and the corresponding transitions involved in the designed phosphorescent iridium(III) complex probe and its cyanide adduct.*

---

**K. S. Bejoymohandas**; Ajay Kumar; S. Sreenadh; E. Varathan; S. Varughese; V. Subramanian; and M. L. P. Reddy, *ACS Inorganic Chemistry*, 55, **2016**, 3448−3461.

## 3.2. Introduction

Cyanide is a strikingly toxic inorganic anion that adversely affects human health and the environment.[1] The maximum acceptable level of cyanide in drinking water is 1.9 μM, as per the requirements of the World Health Organization.[2] In spite of their extreme toxicity, various cyanide-containing compounds are still widely used in different industrial processes such as in gold mining, electroplating, and various metallurgical industries, causing their leakage into the aquatic environment.[3] Consequently, there is considerable interest in the selective detection of aqueous cyanide at submicromolar levels by using simple and visual methods.[4] As of today, various colorimetric and fluorometric receptors are known for the sensing of cyanide ions, in which many transition-metal complexes have been utilized.[5] Nevertheless, fluorescent chemodosimeters based on specific chemical reactions always show better selectivity, and some of them display a detection limit at the submicromolar level for cyanide in organic solvents.[6]

It is well documented that phosphorescent iridium(III) complexes have attractive features such as long lifetime, large Stokes shift, high stability, excellent color tuning, and lower self-quenching in comparison to conventional organic fluorophores.[7] Due to these unique photophysical properties, iridium(III) complexes have been recognized as potential luminescent materials for applications in light-emitting devices and chemosensors.[8] Li and co-workers have reported a ratiometric upconversion luminescence (UCL) probe for the selective detection of cyanide anion in aqueous solution with a detection limit of 0.18 μM based on a chromophoric iridium(III) complex coated nanosystem ($NaYF_4$: 20% Yb, 1.6% Er, 0.4% Tm nanocrystals).[9] Silica nanoparticles doped with an iridium(III) compound for rapid and fluorometric detection of cyanide anion have also been reported.[10] However, the detection of cyanide using a simple phosphorescent iridium(III) complex in a pure organic solvent or in aqueous solution is not yet known.

It is well-known that cyanide has a strong affinity for an electron-deficient carbonyl unit (C═O), which is known to form cyanohydrin, and thus interferences from acetate and fluoride ions can be minimized by designing a novel chemosensor particularly for cyanide.[11] Our recent results demonstrated that the functionalization of an aldehyde group on the 4′-position of the N-coordinating pyridyl moiety in the cyclometalated ligand of an iridium(III) complex induces localization of the LUMO on the substituent.[12] Thus, disturbing the LUMO levels associated with the −CHO substituent may produce significant changes in the emission profiles of the iridium(III) complexes. These factors have inspired us to develop a new phosphorescent iridium(III) complex, functionalized with electron-deficient carbonyl units (Chart 3.1), that can be employed for the sensing of $CN^-$. The interaction of the designed iridium(III) complex with $CN^-$ was investigated by UV–vis absorption, photoluminescence (PL), FT-IR, and $^1H$ NMR spectroscopy and ESI-mass spectrometry. Theoretical studies also have been performed to generate more insights into the electronic structure and transitions involved in the phosphorescent iridium(III) probe and its corresponding cyanide adduct.

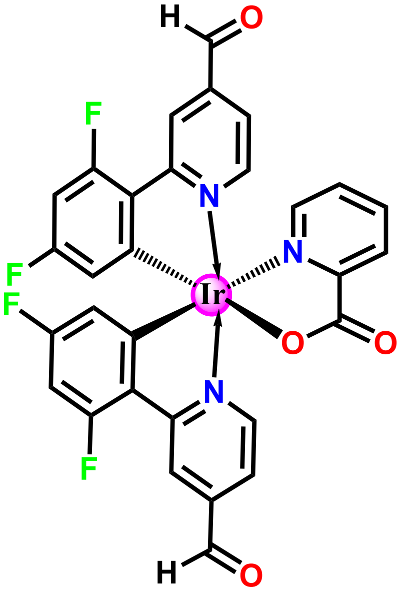

**Chart 3.1.** Chemical structure of the iridium(III) complex **IrC**.

## 3.3. Experimental Section

### 3.3.1. Materials and Physical Measurements

A 500 MHz Bruker NMR spectrometer was used to record the $^{1}H$, $^{19}F$, and $^{13}C$ NMR spectra of the iridium(III) complex in $CDCl_3$ solution. In the $^{1}H$ NMR titration experiments with $CN^{-}$, $CD_3CN$ has been used. The chemical shifts ($\delta$) of the signals are given in ppm and referenced to the internal standard tetramethylsilane ($Si(CH_3)_4$). The signal splittings are abbreviated as follows: s = singlet; d = doublet; t = triplet; dd = doublet of doublets; td = triplet of doublets; m = multiplet. Coupling constants ($J$)

are given in hertz (Hz). Electrospray ionization (ESI) mass spectra were recorded on a Thermo Scientific Exactive Benchtop LC/MS Orbitrap mass spectrometer. Elemental analysis (C, H, and N) measurements were performed using an Elementar-Vario MICRO Cube elemental analyzer. A PerkinElmer Spectrum Two FT-IR spectrometer using KBr was employed to obtain the FT-IR spectral data. Sodium sulfate (anhydrous), sodium carbonate, potassium carbonate, tetrakis(triphenylphosphine) palladium(0), (2,6-difluorophenyl)boronic acid, 2-bromopyridine-4-carboxaldehyde, $IrCl_3 \cdot xH_2O$, and picolinic acid were employed in the synthesis of the iridium(III) complex **IrC**. These chemicals were purchased from Alfa Aesar and were used without any further purification. The precursor salts of all the anions used in this work such as tetra-n-butylammonium cyanide ($[CH_3(CH_2)_3]_4N^+CN^-$), tetra-n-butylammonium fluoride ($[CH_3(CH_2)_3]_4N^+F^-$), tetra-n-butylammonium chloride ($[CH_3(CH_2)_3]_4N^+Cl^-$), tetra-n-butylammonium bromide ($[CH_3(CH_2)_3]_4N^+Br^-$), tetra-n-butylammonium iodide ($[CH_3(CH_2)_3]_4N^+I^-$), tetra-n-butylammonium acetate ($[CH_3(CH_2)_3]_4N^+AcO^-$), tetra-n-butylammonium benzoate ($[CH_3(CH_2)_3]_4N^+BzO^-$), tetra-n-butylammonium perchlorate ($[CH_3(CH_2)_3]_4N^+ClO_4^-$), tetra-n-butylammonium dihydrogen phosphate ($[CH_3(CH_2)_3]_4N^+H_2PO_4^-$), tetra-n-butylammonium bisulfate ($[CH_3(CH_2)_3]_4N^+HSO_4^-$), tetra-n-butylammonium azide ($[CH_3(CH_2)_3]_4N^+N_3^-$), tetra-n-butylammonium nitrate ($[CH_3(CH_2)_3]_4N^+NO_3^-$), tetra-n-butylammonium hydroxide ($[CH_3(CH_2)_3]_4N^+OH^-$), tetra-n-butylammonium hexafluorophosphate ($[CH_3(CH_2)_3]_4N^+PF_6^-$), and sodium bisulfite were purchased from Sigma-Aldrich. The cyclometalated ligand, namely 2-(2,4-difluorophenyl)-4-formylpyridine, was synthesized for the first time and fully characterized. The synthesis of the iridium dimer complex $[(C^\wedge N)_2Ir(\mu\text{-}Cl)]_2$ was carried out by a standard procedure proposed by Watts and co-workers,[13] using $IrCl_3 \cdot xH_2O$ and 2-(2,4-difluorophenyl)-4-formylpyridine in a mixture of 2-ethoxyethanol and water. Thin-layer chromatography (TLC) was used to monitor the reaction progress (silica gel 60 F254, Merck Co.), and the spots were observed under UV light at 254 and 365 nm. Silica column chromatography was performed using silica gel (230–400 mesh, Merck Co.). The dry solvents were used as received from Merck Millipore. All other reagents are of analytical grade and were used as received from Alfa Aesar unless otherwise specified.

### 3.3.2. Synthesis of 2-(2,4-Difluorophenyl)-4-formylpyridine

To a mixture of 2-bromopyridine-4-carboxaldehyde (1.0 equiv), 2,6-(difluorophenyl)boronic acid (1.2 equiv), and tetrakis(triphenylphosphine) palladium(0) (0.06 equiv) in 25 mL of dry tetrahydrofuran (THF) was added $Na_2CO_3$ (10 mL, 5% in water) at room temperature. The resulting reaction mixture was refluxed for 24 h under a nitrogen atmosphere. The reaction was monitored by TLC. After completion of the reaction, the crude mixture was cooled to room temperature and THF was removed under vacuum distillation. Then the residue obtained was extracted with dichloromethane and water. The organic layer was collected, and the solvent was removed to give the crude product. The crude product was then purified by silica column chromatography (1/9 ethyl acetate/n-hexane). Yield: 80%. $^1$H NMR ($CDCl_3$, 500 MHz): *δ* 10.13 (s, 1H); 8.96 (d, *J* = 4.5 Hz, 1H); 8.18–8.17 (m, 1H); 8.10–8.06 (m, 1H); 7.68 (dd, *J* = 5 and 1.5 Hz, 1H); 7.06–7.02 (m, 1H); 6.98–6.94 (m, 1H). $^{13}$C NMR ($CDCl_3$, 126 MHz): *δ* 191.43, 164.74, 154.27, 151.06, 142.42, 132.24, 132.21, 132.16, 132.13, 123.22, 123.14, 120.45, 112.30, 112.27, 112.13, 112.10, 104.82, 104.61, 104.41, 99.98. $^{19}$F NMR ($CDCl_3$, 470 MHz): *δ* −107.72, −112.31. (ESI-MS): *m/z* 220.05 [M + 1].

### 3.3.3. Synthesis of the Iridium(III) Dimer Complex $[(CHOdfppy)_2Ir(\mu\text{-}Cl)]_2$

$IrCl_3{\cdot}xH_2O$ (270 mg, 0.89 mmol) and 2-(2,4-difluorophenyl)-4-formylpyridine (390 mg, 1.78 mmol) were dissolved in 20 mL of a 2-ethoxyethanol and water (3/1) mixture and refluxed at 140 °C for 24 h. After the reaction mixture was cooled, the addition of 20 mL of $H_2O$ gave an orange precipitate that was filtered and washed with diethyl ether. The crude product was used for the next reaction without further purification (yield: 74%).

### 3.3.4. Synthesis of Bis[2′,6′-difluorophenyl-4-formylpyridinato-N,C4′]iridium(III) Picolinate (IrC)

The μ-chloro-bridged iridium(III) dimer $[(CHOdfppy)_2Ir(\mu\text{-}Cl)]_2$ (1.0 equiv), picolinic acid (2.6 equiv), and sodium carbonate (11.0 equiv) were stirred overnight in a mixture (3/1) of dichloromethane and ethanol (40 mL) at 60 °C under an argon atmosphere. The solvent was removed by evaporation under reduced pressure. The crude product obtained was poured into water and extracted with dichloromethane (3 × 50 mL). The combined organic layers were dried over $Na_2SO_4$. A crude residue was obtained after removal of the solvent. The desired complex was obtained as an orange powder after the purification of crude product by silica column chromatography using $CH_2Cl_2$/methanol in a 9/1 ratio as an eluent. The purified sample was recrystallized (from dichloromethane/hexane; 50/50 v/v) and vacuum-dried. Yield: 41%. Anal. Calcd for $C_{30}H_{16}F_4IrN_3O_4$: C, 48.00; H, 2.15; N, 5.60. Found: C, 48.10; H, 2.30; N, 5.73. $^1H$ NMR ($CDCl_3$, 500 MHz): $\delta$ 10.16 (s, 2H); 9.03 (d, $J$ = 6 Hz, 1H); 8.68 (s, 1H); 8.63 (s, 1H); 8.37 (d, $J$ = 7.5 Hz, 1H); 8.01 (td, $J$ = 7.12 and 1.5 Hz, 1H); 7.77 (d, $J$ = 5 Hz, 1H); 7.64 (d, $J$ = 6 Hz, 1H); 7.59 (dd, $J$ = 6 and 1.5 Hz, 1H); 7.50–7.48 (m, 1H); 7.39 (dd, $J$ = 6 and 1.5 Hz, 1H); 6.59–6.54 (m, 1H); 6.51–6.47 (m, 1H); 5.81 (dd, $J$ = 8.5 and 2 Hz, 1H); 5.54 (dd, $J$ = 8.5 and 2 Hz, 1H). $^{19}F$ NMR ($CDCl_3$, 470 MHz): $\delta$ −104.51, −105.32, −108.12, −108.91. ESI-MS: [$C_{30}H_{16}F_4IrN_3O_4 \cdot Na$], calcd m/z 773.01, found m/z 774.06 [M + 1]; [$C_{30}H_{16}F_4IrN_3O_4 \cdot 2CH_3OH \cdot Na$], calcd *m/z* 837.13, found *m/z* 838.11 [M + 1].

### 3.3.5. X-ray Crystallographic Analysis

Single-crystal XRD data for **IrC** were collected with a Rigaku Saturn 724+ diffractometer using graphite-monochromated Mo K$\alpha$ radiation, and the data were processed using Rigaku Crystal Clear software.[14] The molecular structure of the

**Table 3.1.** Crystallographic and refinement data for **IrC**

| | **IrC** |
|---|---|
| Formula | $C_{32} H_{16} Cl_4 F_4 Ir N_3 O_4$ |
| Formula weight | 916.48 |
| Temp (K) | 298 (2) |
| Wavelength (Å) | 0.71073 |
| Crystal system | triclinic |
| Space group | $\bar{P}1$ |
| Crystal size (mm$^3$) | 0.20 × 0.20 × 0.20 |
| a [Å] | 10.6113 (6) |
| b [Å] | 11.9461 (7) |
| c [Å] | 14.5644 (8) |
| α [°] | 81.002 (3) |
| β [°] | 70.850 (2) |
| γ [°] | 68.847 (2) |
| V [Å$^3$] | 1625.04 (16) |
| Z | 2 |
| Density, $\rho_{calc}$ [g/cm$^3$] | 1.873 |
| F(000) | 884 |
| Theta range | 1.48-26.37° |
| μ (Mo Kα) [mm$^{-1}$] | 4.503 |
| reflns collected | 26216 |
| independent reflns | 6641 [R(int) = 0.0903] |
| abs corr | empirical |
| $T_{max}$ and $T_{min}$ | 0.435 and 0.400 |
| data/restraints/parameters | 6641/0/438 |
| final R indices [I >2σ(I)] | R1 = 0.0511, wR1 = 0.1359 |
| R indices (all data) | R1 = 0.0591, wR1 = 0.1459 |
| largest diff. peak and hole, e·Å$^{-3}$ | 1.991 and -2.427 |
| goodness-of-fit on F$^2$ | 1.015 |
| CCDC | 1435265 |

complex was solved and refined by the SHELXTL suite of programs.[15] The disordered solvent molecules could not be adequately modeled. The bypass procedure in Platon[16] was used to remove the electronic contribution from these solvents. Selected crystallographic data and the structure refinement parameters are summarized in Table 3.1. Selected bond lengths and angles are given in Table 3.2.

Crystallographic data have been deposited with the Cambridge Crystallographic Data Centre, and the following code was allocated: CCDC-1435265. These data can be obtained free of charge via the Internet: www.ccdc.cam.ac.uk/data_request/cif.

**Table 3.2.** Selected bond lengths [Å] and bond angles [°], torsion angles [°] for **IrC** around the Ir(III) octahedra

| **IrC** | | | | | |
|---|---|---|---|---|---|
| **Bonds** | | | 14 | N1A—Ir1A—N2A | 174.2(2) |
| 1 | Ir1A—O1A | 2.155(7) | 15 | N1A—Ir1A—N3A | 89.6(2) |
| 2 | Ir1A—N1A | 2.017(5) | 16 | N1A—Ir1A—C8A | 80.6(3) |
| 3 | Ir1A—N2A | 2.037(6) | 17 | N1A—Ir1A—C13A | 94.8(3) |
| 4 | Ir1A—N3A | 2.141(6) | 18 | N2A—Ir1A—N3A | 95.5(3) |
| 5 | Ir1A—C8A | 1.997(9) | 19 | N2A—Ir1A—C8A | 95.9(3) |
| 6 | Ir1A—C13A | 2.009(6) | 20 | N2A—Ir1A—C13A | 80.5(3) |
| 7 | C1A—C7A | 1.46(1) | 21 | N3A—Ir1A—C8A | 100.2(3) |
| 8 | C18A—C19A | 1.453(7) | 22 | N3A—Ir1A—C13A | 171.3(3) |
| **Bond Angles** | | | 23 | C8A—Ir1A—C13A | 88.0(3) |
| 9 | O1A—Ir1A—N1A | 95.0(2) | **Torsion Angles** | | |
| 10 | O1A—Ir1A—N2A | 88.8(2) | 24 | N1A—C1A—C7A—C8A | -3.8(9) |
| 11 | O1A—Ir1A—N3A | 76.8(2) | 25 | C2A—C1A—C7A—C8A | 175.1(7) |
| 12 | O1A—Ir1A—C8A | 174.7(3) | 26 | C17A—C18A—C19A—N2A | 178.1(7) |
| 13 | O1A—Ir1A—C13A | 95.4(3) | 27 | C17A—C18A—C19A—C20A | -2(1) |

### 3.3.6. Photophysical Characterization

The procedures and the instrumental techniques used for the characterization of photophysical properties of the developed iridium(III) complex were the same as those described in Chapter 2.

### 3.3.7. Quantum Yield Measurements

Photoluminescence quantum yields of the powder sample as well as the sample in the solution state were measured by using a calibrated integrating sphere in a SPEX Fluorolog spectrofluorimeter. A Xe arc lamp was used to excite the sample placed in the sphere, with 375 nm as the excitation wavelength. The integrating sphere was calibrated using tris(8-hydroxyquinolinato)aluminum ($Alq_3$) and quinine sulfate before solid- and solution-state measurements, respectively. The absolute quantum yield was calculated by the method described by de Mello et al.[17]

### 3.3.8. Cyclic Voltammetry

The instruments and the methodologies utilized for obtaining the cyclic voltammetry data for **IrC** and **IrC+(CN)$_2$** were the same as those described in Chapter 2. Concentrations of the iridium(III) complex and supporting electrolyte were $5 \times 10^{-3}$ and 0.1 M, respectively. The ferrocenium/ferrocene couple ($FeCp_2^+/FeCp_2^0$) was used as an internal reference. The energy level of $FeCp_2^+/FeCp_2^0$ was assumed at −4.8 eV under vacuum.[18] All solutions for the electrochemical studies were deaerated with prepurified argon gas before measurements.

### 3.3.9. Computational Methods

The ground-state geometries of all metal complexes in the $S_0$ state were optimized by using a density functional theory (DFT) based method with B3LYP hybrid functional and a LANL2DZ basis set for the iridium (Ir) atom and a 6-31G* basis set for the rest of the atoms. Frequency calculations were also performed at the same level of theory. The optimizations and vibrational data confirmed that the structures were minima on the corresponding potential energy surface. Using the optimized geometries, the absorption spectra in acetonitrile media were calculated by employing a time-dependent density functional theory (TD-DFT) approach with the B3LYP/6-31G* method using the PCM approach. The Swizard program was employed to evaluate the contribution of singly excited state configurations to each electronic transition.[19] All calculations were carried out with the Gaussian 09 package.[20]

### 3.3.10. Determination of Association Constant

The association constant ($K_a$) of **IrC** with $CN^-$ was determined on the basis of the absorbance titration curve using the Benesi–Hildebrand[21] equation (eq 1)

$$1/(A_{max}-A_0) = 1/(A_1-A_0)[1/K_a[G]^2 + 1] \qquad (1)$$

where $A_1$ and $A_0$ represent the absorbance of the host in the presence and absence of ions, respectively, $A_{max}$ is the saturated absorbance of the host in the presence of an excess amount of ions, and [G] is the concentration of $CN^-$ added.

### 3.3.11. Determination of Detection Limit of $CN^-$ in the Solution State

The detection limit was calculated from the emission titration. The phosphorescence emission spectrum of the chemodosimeter **IrC** was measured eight times, and the corresponding standard deviation of the blank measurement was calculated. To find the slope, the ratio of the phosphorescence intensities at 480 and 635 nm ($I_{480}/I_{635}$) was plotted as a concentration of $CN^-$. Finally the detection limit was calculated as $3\sigma/k$, where $\sigma$ is the standard deviation of blank measurement and $k$ is the slope of the plot of the fluorescence intensity ratio versus $CN^-$ concentration.[22]

### 3.3.12. Preparation of Filter Paper Test Strips

Filter paper (2 cm × 2 cm) test strips were prepared by dip-coating the **IrC** solution in dichloromethane ($1 \times 10^{-4}$ M) followed by the removal of solvent under vacuum at room temperature. The dip-coating of the solution allowed the adsorption of **IrC** on the filter paper and shows reddish emission under UV illumination (365 nm). These paper strips were used for the detection of cyanide anion.

### 3.3.13. Detection of Cyanide Anion in Drinking Water

A stock solution of tetra-n-butylammonium cyanide ($[CH_3(CH_2)_3]_4N^+CN^-$) ($1 \times 10^{-3}$ M) was prepared by dissolving it in drinking water by stirring at room temperature (0.228 mg/mL). This solution was diluted to different concentrations and used for the test samples.

### 3.3.14. Contact Mode Visual Detection of Cyanide Anion

Tetra-n-butylammonium cyanide solutions of various concentrations in drinking water ($1 \times 10^{-7}$ to $1 \times 10^{-3}$ M) were spotted onto the complex-impregnated luminescent test strips at the desired concentration level using a glass microsyringe. A solvent blank was spotted close to the spot of each cyanide ion. To ensure consistent analysis, all depositions were performed from a 10 μL volume, producing a spot of ~1.0 cm in diameter. After solvent evaporation, the filter paper was illuminated with 365 nm UV light. An independent observer identified the color change from red to green at the spotted area. Each set of experiments was repeated three times for consistency. The test strip was placed in such a way that the excitation beam fell on the spot where the anions were added. Emission was collected by a front-face mode using a sample holder used to record film emissions. Emission of a blank sample was monitored by the addition of solvent alone. The detection limit was calculated from the lowest concentration of the $CN^-$ that enabled an independent observer to detect the quenching visually.

### 3.3.15. Contact Mode Selectivity Experiments for Cyanide Anion

Tetra-n-butylammonium salt solution of various anions in drinking water with a concentration of $1 \times 10^{-3}$ M were prepared and spotted onto the test strips using a glass microsyringe. Consistent analysis was ensured by making all depositions from a

10 μL volume, which eventually produced a spot of ∼1.0 cm in diameter. After solvent evaporation, the filter paper was illuminated with 365 nm UV light. A color change from red to green at the spotted area was identified only in the case of cyanide addition. Emission from the spotted area was collected by the front face mode using a film sample holder. Solvent alone was added in the case of blank measurements.

### 3.3.16. Isolation of Cyanide Adduct for ESI-MS and FT-IR Measurements

The addition of 2.0 equiv of $CN^-$ was carried out in a 2.0 μM solution of **IrC** in acetonitrile. Then, the solution was concentrated, and the excess tetra-n-butylammonium cations and cyanide anions present in the crude mixture were removed through water workup with dichloromethane. The organic layer was concentrated and dried, and the yellow powder obtained was utilized for the ESI-MS and FT-IR measurements.

## 3.4. Results and Discussion

### 3.4.1. Synthesis and Characterization

The cyclometalating ligand 2-(2,4-difluorophenyl)-4-formylpyridine used in the current study was synthesized by a conventional Suzuki coupling reaction of 2-bromopyridine-4-carboxaldehyde with 2,6-(difluorophenyl)boronic acid in the presence of sodium carbonate and tetrakis(triphenylphosphine)palladium(0) as a catalyst (Scheme 3.1).

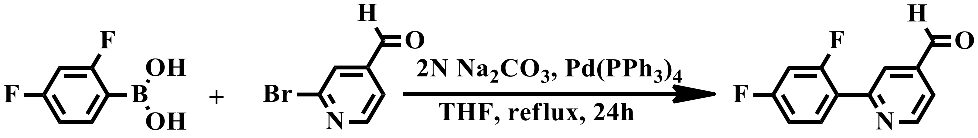

**Scheme 3.1.** Synthetic Route of 2-(2,4-difluorophenyl)-4-formylpyridine

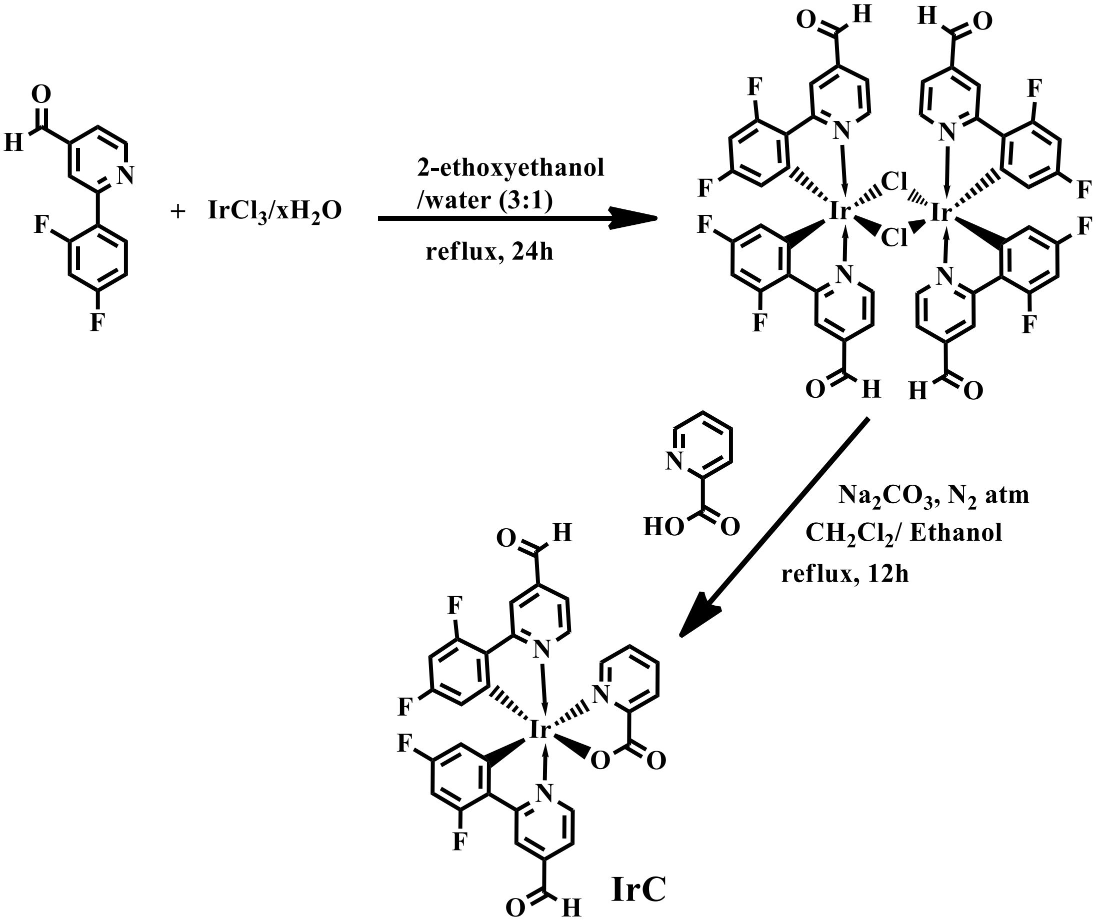

**Scheme 3.2.** Synthetic Routes of Heteroleptic Ir$^{3+}$ Complex **IrC**

It is important to mention that the pure ligand could only be obtained after column chromatographic separation using 10% ethyl acetate in hexane in a yield of

80%. The newly synthesized ligand has been fully characterized by $^{1}H$, $^{19}F$, and $^{13}C$ NMR and FT-IR spectroscopy and ESI mass spectrometry. The dimer precursor employed in the synthesis of the iridium(III) complex was prepared by a standard procedure proposed by Watts and co-workers.[13] The μ-chloro-bridged dimer was formed through the reaction of the cyclometalated ligand with $IrCl_3 \cdot xH_2O$ in a mixture of 2-ethoxyethanol and water. The new iridium complex **IrC** was obtained in the presence of $Na_2CO_3$ via the reaction of the μ-chloro-bridged dimer and an ancillary ligand, picolinic acid. A pictorial synthetic pathway leading to the desired iridium(III) complex (**IrC**) is depicted in Scheme 3.2. After column chromatographic purification and recrystallization from a dichloromethane/hexane solvent mixture, a pure complex was obtained with a moderate yield of 41%. Detailed characterizations such as $^{1}H$ and $^{19}F$ NMR, FT-IR spectroscopy, and ESI mass spectrometry and elemental analyses were performed on the newly synthesized complex for the structural confirmation.

### 3.4.2. Crystal Structure

Slow diffusion of hexane into a solution of the iridium(III) complex in dichloromethane resulted in the growth of single crystals of **IrC**. The molecular structure of the iridium(III) complex obtained by X-ray single-crystal diffraction techniques is shown in Figure 3.1. Selected crystallographic data and the structure refinement parameters are summarized in Table 3.1. Selected bond lengths and angles are given in Table 3.2. The iridium complex was found to crystallize in the triclinic crystal system with a $P\bar{1}$ space group. The structure reveals that the iridium center adopts a distorted-octahedral coordination geometry, comprising two chelating cyclometalated 2′,6′-bis(difluorophenyl)-4-formylpyridinato ligands with *cis* C,C and *trans* N,N inclinations and one picolinate ancillary ligand with narrow ligand bite angles ranging from 76.8(2) to 100.2(3)°. These results are in good agreement with the crystal structure of the parent iridium(III) complex, bis[3,5-difluoro-2-(2-pyridyl)phenyl](picolinato)iridium(III) (FIrpic).[23]

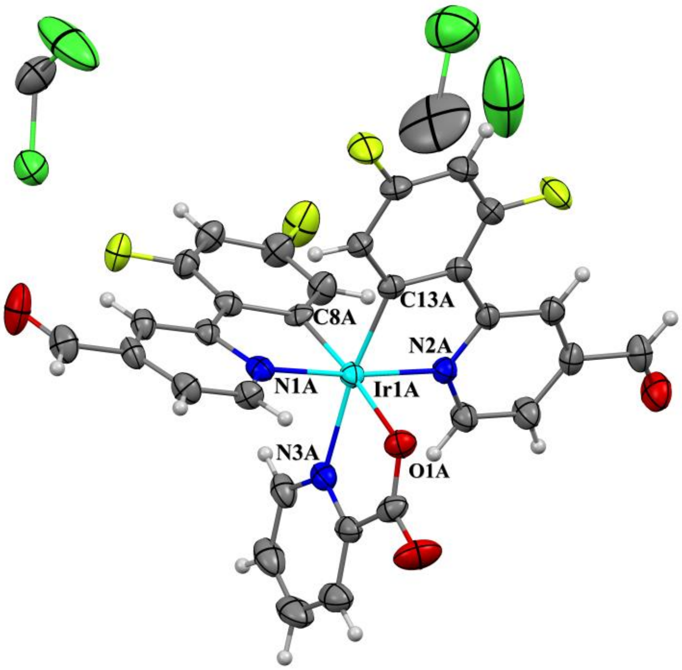

**Figure 3.1.** Crystal structure of complex **IrC** with the atom numbering scheme. Thermal ellipsoid drawing is presented at the 30% probability level. Selected bond lengths (Å) and angles (1): Ir(1A)–C(13A) 2.009(6), Ir(1A)–C(8A) 1.997(9), Ir(1A)–O(1A) 2.155(7), Ir(1A)–N(1A) 2.017(5), Ir(1A)–N(2A) 2.037(6), Ir(1A)–N(3A) 2.141(6); N(1A)–Ir(1A)–N(2A) 174.2(2), C(13A)–Ir(1A)–N(3A) 171.3(3), C(8A)–Ir(1A)–O(1A) 174.7(3).

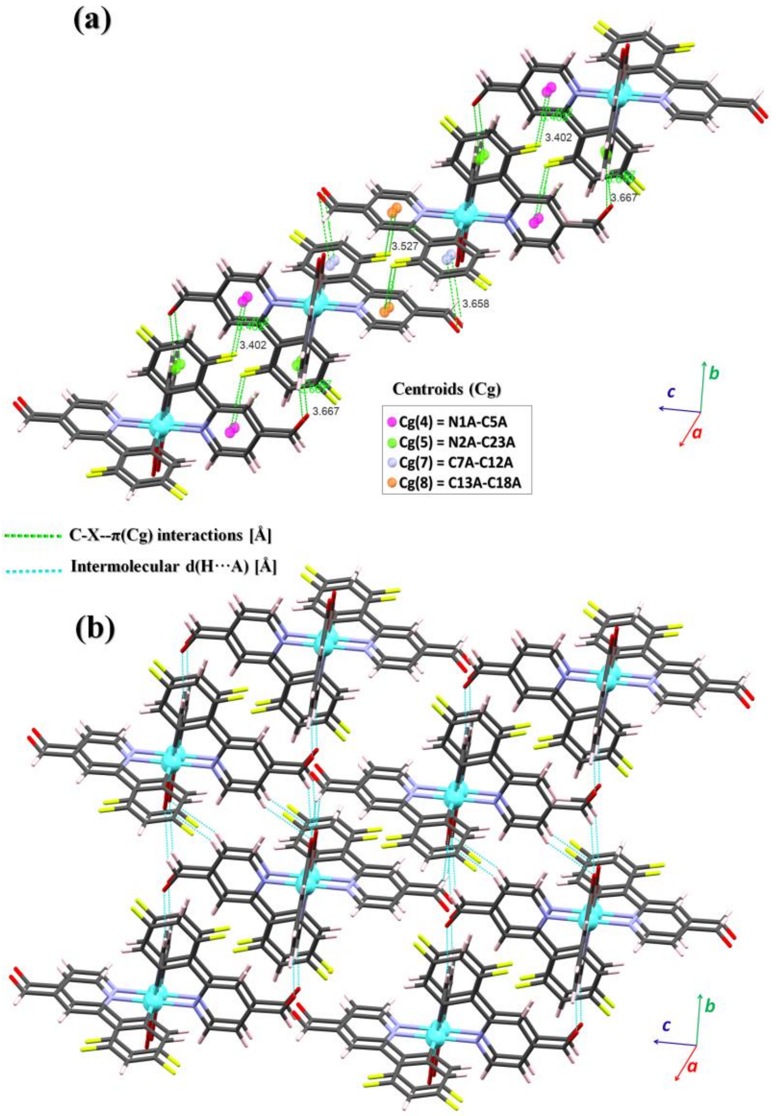

**Figure 3.2.** A crystal packing structure of the complexes **IrC** with intermolecular (a) C–F···π (formylpyridyl), C=O···π (diflurophenyl) (green) and (b) C–H···O (blue) interactions shown as dashed lines. The solvent molecules not involved in intermolecular interactions have been omitted for clarity.

The Ir–N bond lengths, ranging from 2.017(5) to 2.037(6) Å, and Ir–C bond lengths, ranging from 1.997(9) to 2.009(6) Å, are found to be similar to those of the parent complex, FIrpic (1.995 and 2.045 Å; averages of Ir–C and Ir–N bonds, respectively). On the other hand, the ancillary picolinate ligand bond distances are slightly elongated to 2.155(7) Å for Ir1A–O1A and 2.141(6) Å for Ir1A–N3A in comparison to those of iridium bonds with cyclometalated ligands. This trend is in good agreement with the strong *trans* effect exercised by the Ir–C bonds.[24] Within the complex, the difluorophenyl and substituted pyridine rings of both cyclometalated ligands are approximately coplanar with maximum dihedral angle ranges from 2.0(1) to 3.8(2)°. The selected bond lengths, torsion angles, and ligand bite angles for **IrC** are given in Table 3.2. It can be inferred from the above observations that the overall geometry around the metal center is not significantly influenced by the presence of a formyl group at the 4′-position of the N-coordinated pyridyl moiety of the cyclometalated ligand.

The crystal packing structure of **IrC** is displayed in Figure 3.2. The scrutiny of the X-ray single-crystal structure of **IrC** helps disclose distances in support of weak intermolecular interactions, such as the C–H···O (average H···O distance 2.67 Å with an average bond angle ∠C–H···O = 141°), C–H···F hydrogen bonds (average H···F distance 2.26 Å with average bond angle ∠C–H···F = 123°), and C–H···N hydrogen bonds (H···N distance 2.58 Å with ∠C–H···N = 121°). Further, there are a few stacking interactions of the type C–X···$\pi$ (edge-to-face phenyl C–F···$\pi$ (4-formylpyridyl centroid, Cg4), average F···Cg distance 3.46 Å, and formyl C═O···$\pi$ (2,6-difluorophenyl Cg7) interactions, average O···Cg distance 3.66 Å) existing in the system. A logical analysis of the structure reveals that the lone pair of the carbonyl group could be pointing toward the electron-deficient ring on the adjacent molecular entity. However, the C–F···*π* interaction could be an aftermath effect of the aforesaid stacking interactions. Their exact contribution toward the structure stabilization can only be evaluated through a charge-density study. A summation of the structural parameters for the intermolecular interactions can be found in Tables 3.3 and 3.4.

**Table 3.3.** Intermolecular hydrogen bond interactions for **IrC**

| D-H···A | d(D-H) [Å] | d(H···A) [Å] | d(D···A) [Å] | <(DHA) [°] |
|---|---|---|---|---|
| C(2A)--H(2A)···F(1A) | 0.93 | 2.24 | 2.853(9) | 123 |
| C(20A)--H(20A)···F(3A) | 0.93 | 2.28 | 2.881(10) | 122 |
| C(4A)--H(4A)···O(2A) i | 0.93 | 2.78 | 3.548(11) | 141 |
| C(5A)--H(5A)···O(1A) | 0.93 | 2.57 | 3.148(9) | 121 |
| C(6A)--H(6A)···O(2A) i | 0.93 | 2.48 | 3.286(12) | 145 |
| C(11A)--H(11A)···O(4A) ii | 0.93 | 2.87 | 3.629(12) | 140 |
| C(20A)--H(20A)···O(1A) iii | 0.93 | 2.87 | 3.601(9) | 136 |
| C(24A)--H(24A)···O(1A) iii | 0.93 | 2.52 | 3.340(11) | 147 |
| C(25A)--H(25A)···O(3A) iv | 0.93 | 2.41 | 3.211(13) | 145 |
| C(26A)--H(26A)···O(4A) v | 0.93 | 2.89 | 3.753(15) | 155 |
| C(23A)--H(23A)···N(3A) | 0.93 | 2.58 | 3.160(9) | 121 |

Symmetry transformations used to generate equivalent atoms: i) 1-x,2-y,1-z; ii) 1-x,1-y,-z; iii)1-x,2-y,-z; iv) 1-x,1-y,1-z; v) 2-x,1-y,-z;

**Table 3.4.** Intermolecular C-X--π(Cg) interactions for **IrC**

| C-X··· π(Cg) | d(X··· π(Cg) [Å] | <(CXCg) [°] |
|---|---|---|
| C(12A) -F(1A)···Cg(4) i | 3.402(6) | 100.2 |
| C(17A) -F(3A)···Cg(5) ii | 3.526(7) | 88.6 |
| C(6A) -O(3A)···Cg(7) i | 3.667(11) | 85.5 |
| C(24A) -O(4A)···Cg(8) ii | 3.657(8) | 71.8 |

Cg: centroid of the π ring system; Cg(4) = N1A-C1A-C2A-C3A-C4A-C5A; Cg(5) = N2A-C19A-C20A-C21A-C22A-C23A; Cg(7) = C7A-C8A-C9A-C10A-C11A-C12A; Cg(8) = C13A-C14A-C15A-C16A-C17A-C18A. Symmetry transformations used to generate equivalent atoms: i) 1-x,1-y,1-z; ii) 1-x,2-y,-z.

### 3.4.3. Electronic Spectrum of IrC

The UV–vis absorption spectrum of **IrC** recorded in acetonitrile solution ($c = 2 \times 10^{-5}$ M) at room temperature is depicted in Figure 3.3, and the pertinent electronic absorption data are summarized in Table 3.5. The spin-allowed intraligand $^1$LC ($^1\pi \rightarrow \pi^*$) transition originating from the cyclometalated 2′,6′-difluoro-4-formylpyridine and picolinate ancillary ligands can be seen in the 220–260 nm region as intense bands with large molar extinction coefficients on the order of ~49000 M$^{-1}$ cm$^{-1}$. Another strong absorption peak centered at 340 nm can be assigned to a spin-allowed ligand–ligand charge transfer ($^1$LLCT) or intraligand charge transfer ($^1$ILCT) band, indicating a greater contribution from the formyl substituent in the pyridyl moiety with an extinction coefficient on the order of ~27000 M$^{-1}$ cm$^{-1}$. The spin-allowed metal to ligand charge transfer ($^1$MLCT) transition can be seen as a broad absorption spanning the 400–500 nm region with a low molar extinction coefficient on the order of ~3020 M$^{-1}$ cm$^{-1}$. In addition, the spin-forbidden $^3$MLCT transition band noted in the 500–550 nm region with the very low extinction coefficient of ~230 M$^{-1}$ cm$^{-1}$ indicates efficient spin–orbit coupling, which is a prerequisite for phosphorescent emission. The theoretical predictions of the absorption profile of **IrC** are in good agreement with the experimental data (see section 3.4.10).

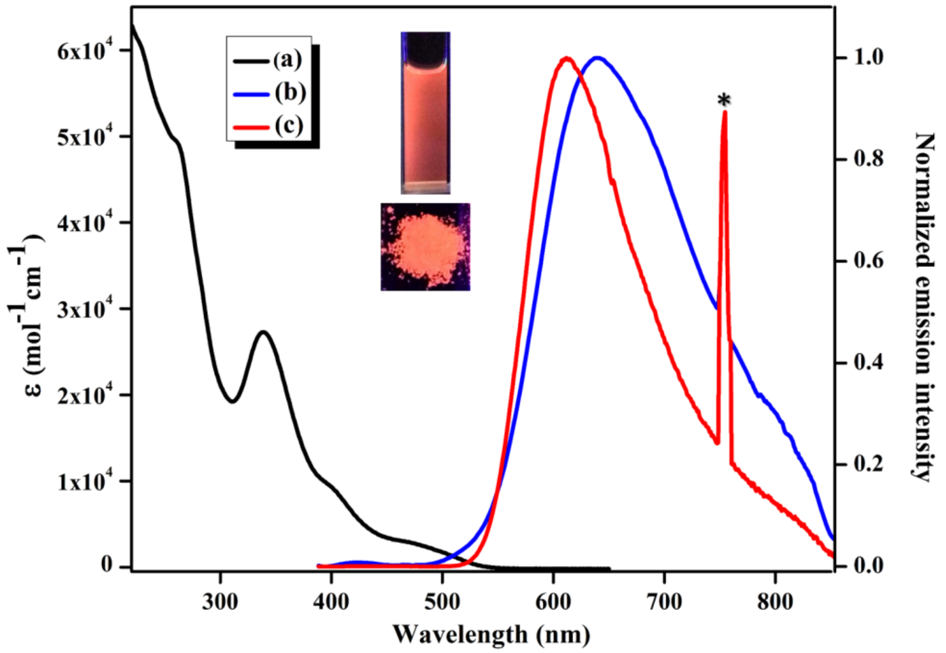

**Figure 3.3.** Absorption (a) and emission (b) spectra of **IrC** in acetonitrile solution ($c$ = 2 ×10$^{-5}$ M) and solid state emission (c) profile ($\lambda_{exc}$ =375 nm) of **IrC** at room temperature. At 750 nm (*) indicates the second harmonic peak of the excitation wavelength.

### 3.4.4. Solution and Solid-State Emission Properties of IrC

Figure 3.3 illustrates the ambient-temperature normalized emission spectrum of **IrC** in acetonitrile solution ($c$ = 2.0 × 10$^{-5}$ M) excited at 375 nm. The corresponding photophysical data of **IrC** are given in Table 3.5. **IrC** exhibits a faint and broad phosphorescence in the region 500–850 nm ($\lambda_{max}$ 635 nm) with a quantum yield of 0.02 (in deaerated acetonitrile solution). The room-temperature emission profile of **IrC** is featureless and broad with a full-width at half-maximum (fwhm) value of ~166 nm (~3489 cm$^{-1}$). This indicates the dominance of a $^3$MLCT excited-state emission rather than a ligand-centered (LC) $^3\pi$–$\pi$* excited-state emission.

**Table 3.5.** Photophysical properties of **IrC** and cyanide adduct

| **Complex** | **Absorption**$^{a}$ **$\lambda_{max}$ (nm) ($\varepsilon \times 10^{-3}$ /M$^{-1}$ cm$^{-1}$)** | **Emission at 298 K in $CH_3CN$ Solution** | | | | | **Solid-state emission** | |
|---|---|---|---|---|---|---|---|---|
| | | **$\lambda_{max}^{a}$ (nm)** | **$\Phi_{PL}^{b}$** | **$\tau_{PL}$ (μs)** | **$k_r^{d}$ ($10^5$ S$^{-1}$)** | **$k_{nr}^{e}$ ($10^5$ S$^{-1}$)** | **$\lambda_{max}^{b}$ (nm)** | **$\Phi_{PL}^{c}$** |
| **IrC** | 260 (49.04)<br>340 (27.3)<br>475 (3.02)<br>533 (0.23) | 635 | 0.02 | 0.05 | 0.4 | 19.6 | 611 | 0.16 |
| **IrC+(CN)$_2$** | 253 (65.00)<br>312 (25.20)<br>375 (9.38)<br>456 (0.96) | 480<br>498 | 0.11 | 0.75 | 0.14 | 1.18 | - | - |

[a] Absorption and emission spectra were measured in acetonitrile solution; $c = 2.0 \times 10^{-5}$ M , $\lambda_{exc} = 375$ nm. [b,c]Quantum efficiency measured by absolute method using integrating sphere. [d,e]Radiative as well as non-radiative rate constants were deduced by the $\Phi_{PL}$ of solution state and $\tau_{obs}$ according to two equations: $k_r = \Phi_{PL}/\tau_{obs}$, $k_{nr} = (1-\Phi_{PL})/\tau_{obs}$.

Notably, the introduction of an electron-withdrawing −CHO group (Hammett constant, $C_{\sigma p} = 0.42$) on the C4′ position of the pyridyl moiety of the cyclometalated ligand has significantly red shifted the emission profile at about 165 nm (~5528 cm$^{-1}$) in comparison to the unsubstituted iridium(III) complex FIrpic ($\lambda_{max}$ at 470 nm).[25] It is well documented that the substitution of an electron-withdrawing group at the C4′ position on the pyridyl moiety is expected to register a bathochromic shift in the emission profile of the iridium(III) complex due to the stabilization of the LUMO. Further, a large red shift indicates the greater delocalization of charge in the excited $^3$MLCT state. As evidenced from our DFT studies (see below), the picolinate moiety merely acts as an ancillary ligand in **IrC** and the emission properties are mainly of $^3$MLCT/$^3$LC nature, involving iridium d orbitals and $\pi$–$\pi$* orbitals of the formyl-substituted 2′,6′-difluorophenylpyridine cyclometalated units. The LUMO is heavily oriented on the electron-deficient formyl moiety, which stabilizes the negative charge on the cyclometalated ligand upon excitation. Further, the highly polar nature of the acetonitrile solvent will also contribute to the stabilization of LUMO levels, which results in the large bathochromic shift. In our recent study, a similar behavior has been observed with a large bathochromic emission shift of about 100 nm (~4209 $cm^{-1}$) in a −CHO substituted cyclometalated iridium(III) complex.[12] On the other hand, notably broad and more intense red phosphorescence ($\lambda_{max}$ at 611 nm) was noticed for **IrC** in the solid state with a quantum yield of 0.16 (Figure 3.3). The difference in the solution as well as solid-state quantum yields indicates the presence of aggregation-induced phosphorescent emission (AIPE), an uncommon phenomenon among luminescent iridium(III) complexes.[26] A transition from the less emissive $^3$LC or $^3$MLCT excited state to the emissive metal to ligand to ligand charge transfer ($^3$MLLCT) transition as a result of the excimeric interactions between the cyclometalating ligands of neighboring complexes or the restriction of intramolecular rotation (RIR) in the solid state could be the reason for AIPE.[26c, 26h, 27] Scrutiny of the single-crystal structure indicates the existence of several C–F···$\pi$ interactions between difluorophenyl and formylpyridine units and C═O···$\pi$ interactions between formyl-substituted N-coordinating pyridine and the $\pi$ ring of the difluorophenyl moiety of the cyclometalated ligands with interplanar separations of 3.4 and 3.6 Å, respectively. Solution-state emission properties were dominated by a −CHO connected pyridyl moiety centered $^3$MLCT state leading to a weak emission in solution due to strong nonradiative decay pathways ($k_{nr}$ = 19.6 × $10^5$ $s^{-1}$) involving contributions from the −CHO substituent. Meantime in the solid state, the existing C–F···$\pi$ and C═O···$\pi$ interactions of cyclometalated ligands extend the overall degree of $\pi$ conjugation. This can be seen from the 10 nm red shift (~273 $cm^{-1}$) in the solid state emission profile in comparison to less polar dichloromethane solvent ($\lambda_{max}$ at 601 nm, Figure 3.4) which, in turn, generates a more emissive excited state based on $^3$MLLCT.

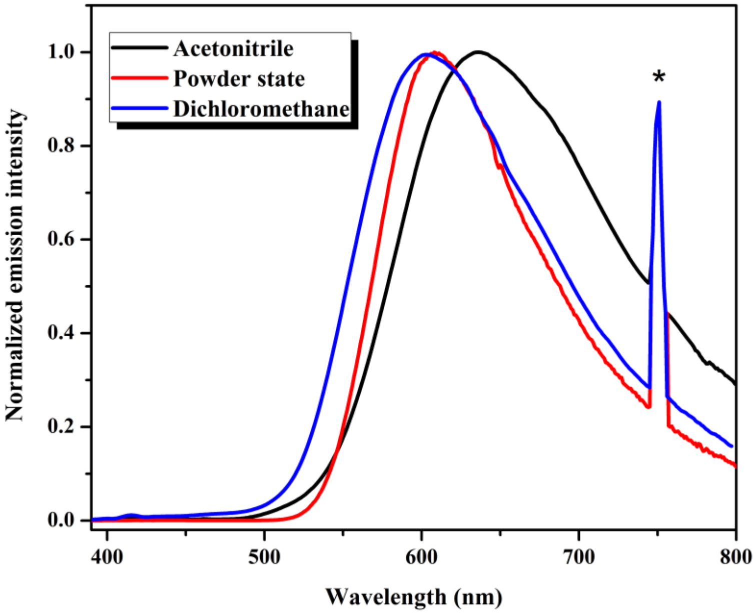

**Figure 3.4.** Comparison of normalized emission profiles of **IrC** recorded in acetonitrile, dichloromethane and powder state at 298 K ($\lambda_{exc}$ = 375 nm).

### 3.4.5. Detection of Cyanide in UV–Vis and Photoluminescence Channels

The ability of the newly developed **IrC** to act as a chemosensor for different anions (2.0 equiv) has been examined by UV–vis absorption and PL spectroscopy in $CH_3CN$

solution at room temperature. **IrC** displays remarkable absorption changes exclusively in the presence of $CN^-$ in the UV–vis channel (Figure 3.5). Upon addition of 2.0 equiv of $CN^-$ to an acetonitrile solution of **IrC** the absorption maximum dramatically blue shifted from 475 to 375 nm ($\Delta\lambda$ = 100 nm, 5614 $cm^{-1}$). As a consequence, a prominent orange to yellow color change was observed (Figure 3.5, inset). In contrast to the above, no significant color change has been noted in the presence of other competing anions, such as $AcO^-$, $BzO^-$, $ClO_4^-$, $H_2PO_4^-$, $HSO_4^-$, $N_3^-$, $NO_3^-$, $OH^-$, $PF_6^-$, $F^-$, $Cl^-$, $Br^-$, $HSO_3^-$, and $I^-$ (Figure 3.5). These observations clearly highlight a selective reaction of $CN^-$ with the −CHO group attached to the 4′-position of the N-coordinating pyridyl moiety of the cyclometalated ligand. To understand more about the reasons for the color change, herein, UV–vis titration experiments have been performed (Figure 3.6). The incremental addition of $CN^-$ (0.0–2.0 equiv) to a $CH_3CN$ solution of **IrC** ($c = 2 \times 10^{-5}$ M) at room temperature reveals a gradual decrease of the broad $^1$MLCT absorbance at 475 nm and $^1$LLCT peak at 340 nm. At the same time, a new sharp band appeared at 253 nm ($\varepsilon = 6.5 \times 10^4$ $M^{-1}$ $cm^{-1}$). In addition, two new broad bands at 310 nm ($\varepsilon = 2.6 \times 10^4$ $M^{-1}$ $cm^{-1}$) and 380 nm ($\varepsilon = 0.9 \times 10^4$ $M^{-1}$ $cm^{-1}$) are also noted. However, no further change is observed in the absorption profile beyond the addition of 2.0 equiv of $CN^-$ ions.

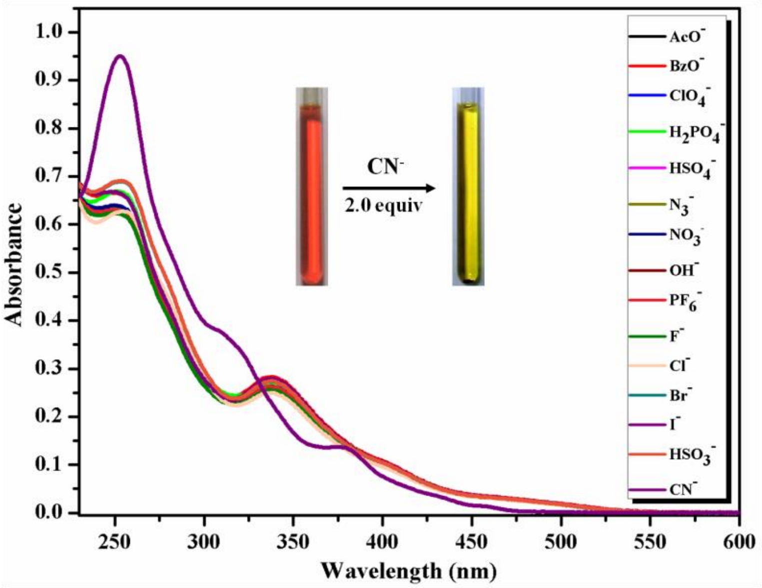

**Figure 3.5.** UV−vis absorption spectra of **IrC** (20 μM) with different anions (2.0 equiv) in $CH_3CN$. Photograph showing the color change from reddish orange to yellow under day light upon addition of $CN^-$ at 2.0 mM concentration.

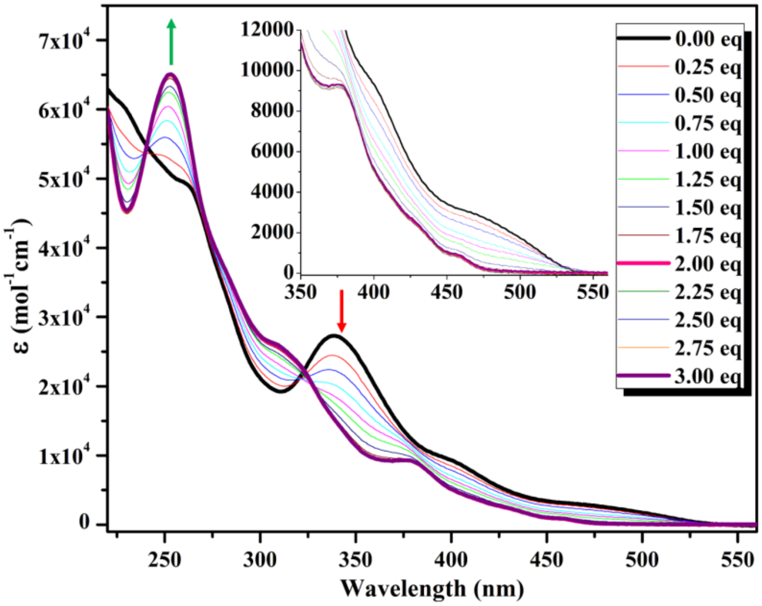

**Figure 3.6.** UV−vis absorption titration of **IrC** (20 μM) with $CN^-$ (0 to 2.0 equiv) in $CH_3CN$ at 298K. Inset: magnified absorption in the 350-500 nm regions.

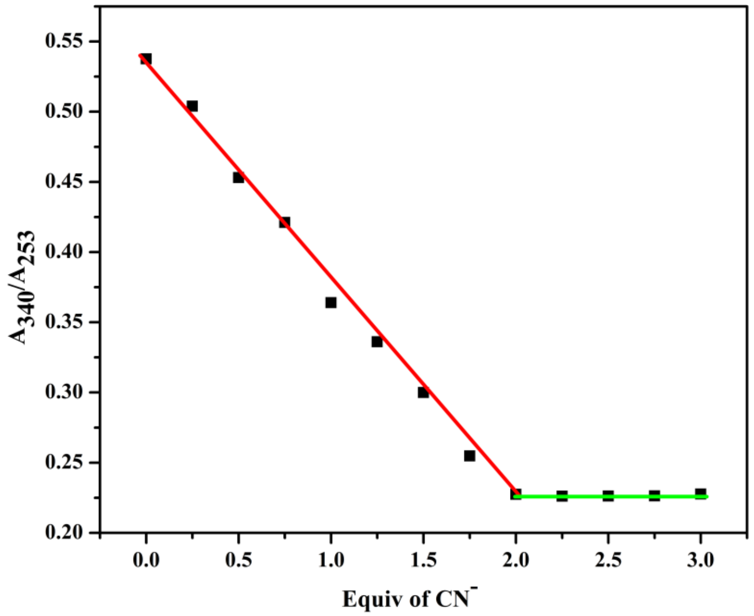

**Figure 3.7.** Plot of $A_{340}/A_{253}$ (ratio of absorbance at 340 and 253 nm) against the amount of added $CN^-$ to 20 μM solution of **IrC**. (Red as well as green lines serve to indicate the completion of 1:2 adduct formation).

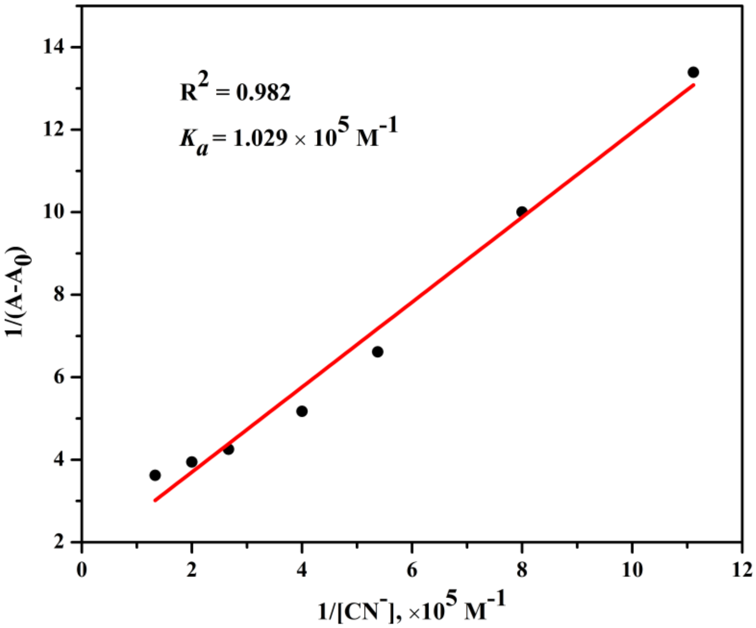

**Figure 3.8.** Benesi-Hildebrand plot of **IrC** with $CN^-$.

A plot of the absorbance ratio at 340 and 253 nm ($A_{340}/A_{253}$) as a function of the amount of cyanide clearly indicated that $A_{340}/A_{253}$ decreases linearly up to 2.0 equiv of $CN^{-}$ addition (Figure 3.7). After that, the ratio becomes constant, disclosing a 1:2 binding stoichiometry of **IrC** and $CN^{-}$. The association constant ($K_a$) of **IrC** with $CN^{-}$ was determined using the Benesi–Hildebrand equation.[21] The measured absorbance ($1/(A - A_0)$) varied as a function of $1/[CN^{-}]$ in a linear relationship ($R^2 = 0.9820$), indicating the formation of 1:2 stoichiometry between $CN^{-}$ and **IrC**. The association constant of **IrC** with $CN^{-}$ in $CH_3CN$ solution was calculated to be $1.029 \times 10^5$ $M^{-1}$ (Figure 3.8). Thus, the above results clearly demonstrate that $CN^{-}$ can be quantitatively determined in the UV–vis channel by interaction with the −CHO group of the iridium(III) complex **IrC**.

The lower energy of $^1$MLCT at ~475 nm is due to the iridium(III) (d orbital) to −CHO substituted pyridyl moiety ($\pi^*$ orbital) charge transfer transition. The electron-deficient character of the −CHO group and its $\pi$ conjugation with the N-coordinating pyridyl ring are expected to decrease the LUMO energy level in **IrC**. Upon addition of $CN^{-}$ to the **IrC**, the $^1$MLCT absorption band was blue-shifted to ~380 nm, which can be attributed to an iridium (d orbital) to pyridyl moiety of the cyclometalated ligand ($\pi^*$ orbital) charge transfer transition. A significant enhancement in the LUMO energy is expected after cyanide addition to the −CHO group due to the much less electron withdrawing character of the cyanohydrin group and concomitant loss of extended $\pi$ conjugation. To get more insights into the changes in the transition occurring after the addition of $CN^-$ ion to **IrC**, time-dependent DFT (TD-DFT) calculations were conducted, showing partial MLCT switching indeed from iridium(III) → CHOdfppy($\pi^*$) to iridium(III) → dfppy($\pi^*$).

As stated earlier, **IrC** exhibits a rather weak and broad emission profile with a maximum at 635 nm in acetonitrile. The addition of 2.0 equiv of various anions to the acetonitrile solution of **IrC** ($c = 2 \times 10^{-5}$ M) shows notable changes only with $CN^-$, which results in a ∼155 nm (∼5085 $cm^{-1}$) blue shift of the emission maximum (Figure 3.9). As a consequence, the emission color changed from red to sky blue in the presence of $CN^-$ (inset of Figure 3.9). The emission intensity has been greatly enhanced (∼536-fold at 480 nm) with a quantum yield of 0.11.

The $CN^-$ detection ability was examined through PL titration studies in detail. The plot of the PL intensity change ($I - I_0$, where $I$ = intensity after $CN^-$ addition and $I_0$ = intensity before $CN^-$ addition) at 480 nm for **IrC** as a function of the $CN^-$ concentration shows a good linear relationship in the range of 0.0–2.0 equiv of $CN^-$ (Figure 3.10). Thereafter no change in the emission intensity was noted beyond 2.0 equiv of $CN^-$, confirming the formation of the 1:2 adduct [**IrC+(CN)$_2$**]. In order to further understand the binding stoichiometry of **IrC** with $CN^-$, Job plot experiments were also carried out by means of a continuous-variation method.[28]

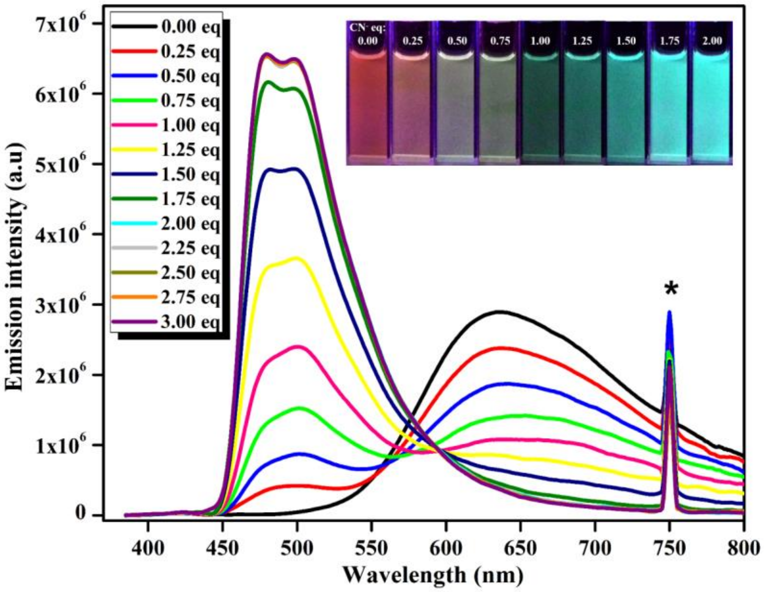

**Figure 3.9.** Photoluminescence titration of **IrC** (*c* = 20 μM) with $CN^-$ solution (0.0 to 3.0 equiv) in $CH_3CN$ at 298K ($\lambda_{exc}$= 375 nm). (Inset) Photograph showing the transition of reddish orange to sky-blue phosphorescence upon addition of 0.0 to 2.0 equiv of $CN^-$, under 365 nm hand held UV excitation. At 750 nm (*) indicates the second harmonic peak of the excitation wavelength.

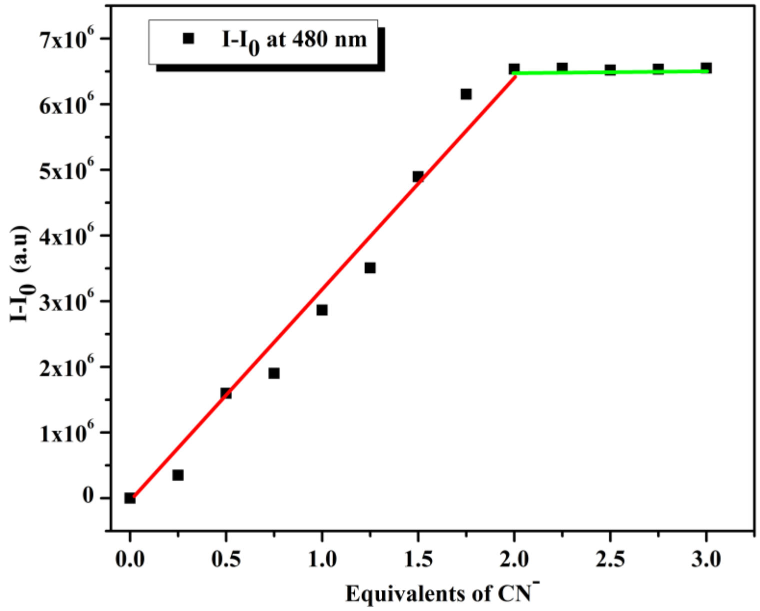

**Figure 3.10.** Plot of the PL intensity change 480 nm upon addition of 0.0 to 3.0 equiv of $CN^-$ (Red as well as green lines serve to indicate the completion of 1:2 adduct formation).

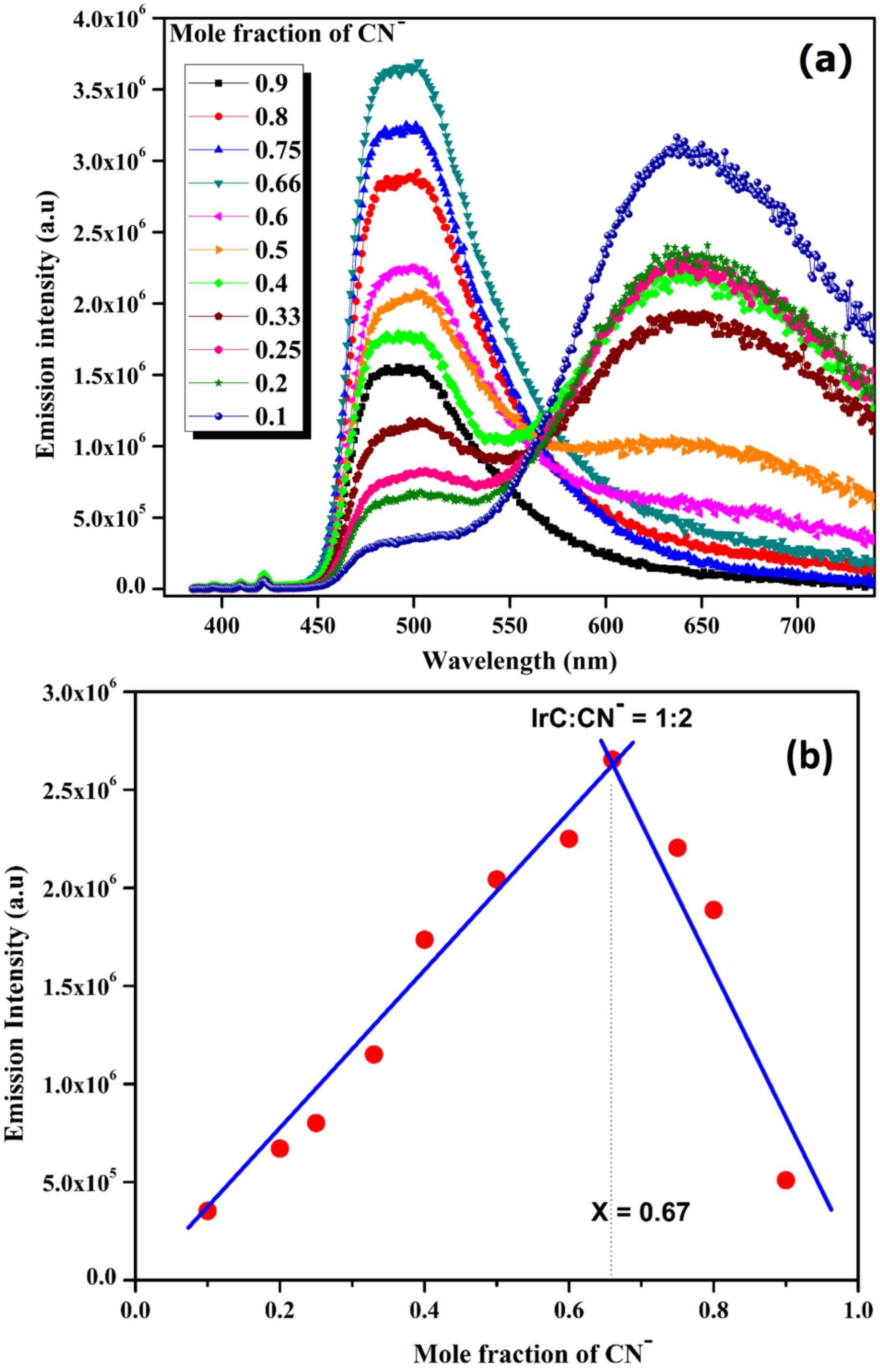

**Figure 3.11. (a)** Phosphorescence emission spectra of **IrC+(CN⁻)** adduct complexes at different mole fractions of $CN^-$ in $CH_3CN$ at 298K ($\lambda_{exc}$= 375 nm) **(b)** Job plot of **IrC+(CN⁻)** adduct complexes, where the phosphorescence emission intensity at 480 nm is plotted against mole fraction of $CN^-$, at a constant total concentration of 2.0 × $10^{-5}$ M in acetonitrile solutions.

In Figure 3.11, the phosphorescence emission intensity of the **IrC+(CN$^-$)** adduct at 480 nm is plotted against the mole fraction of CN$^-$ at a constant total concentration (20 µM). The maximum emission intensity was reached when the mole fraction of CN$^-$ was 0.67. These results clearly indicate a 1:2 binding stoichiometry of **IrC** with CN$^-$. **IrC** contains two reactive −CHO groups connected to the 4′-position of the N-coordinating pyridyl moiety of both cyclometalating ligands. Thus, −CHO groups of **IrC** may interact with CN$^-$ simultaneously at the same rate. This is in good agreement with the earlier report that CN$^-$ may interact with both carbonyl groups of a similar fluorescent organic probe.[29] The CN$^-$ detection limit is found to be 2.16 × $10^{-8}$ M (Figures 3.12–3.14), which is lower than that for many of the reported CN$^-$ sensors based on luminescent metal complexes, as can be seen from Table 3.6.

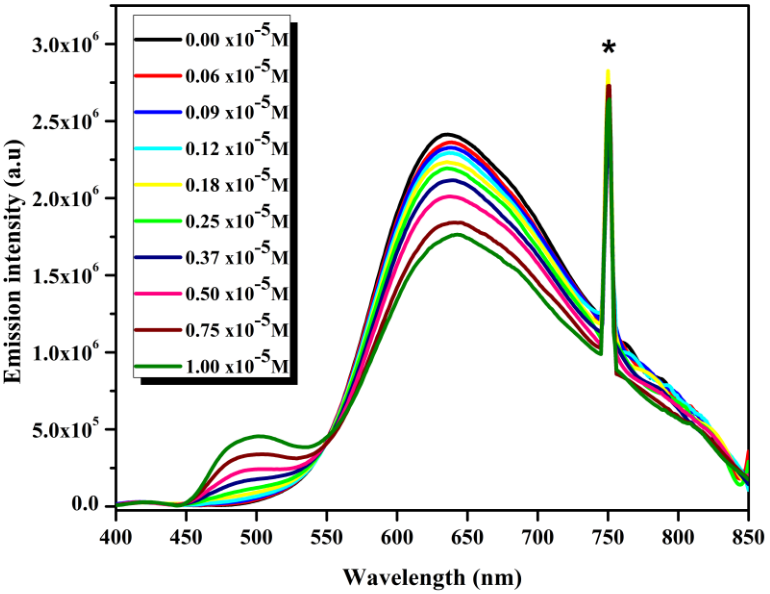

**Figure 3.12.** Photoluminescence titration of **IrC** with low concentration levels of CN$^-$**)** (0.0-10.0 µM) ($\lambda_{exc}$ = 375 nm). At 750 nm (*) indicates the second harmonic peak of the excitation wavelength.

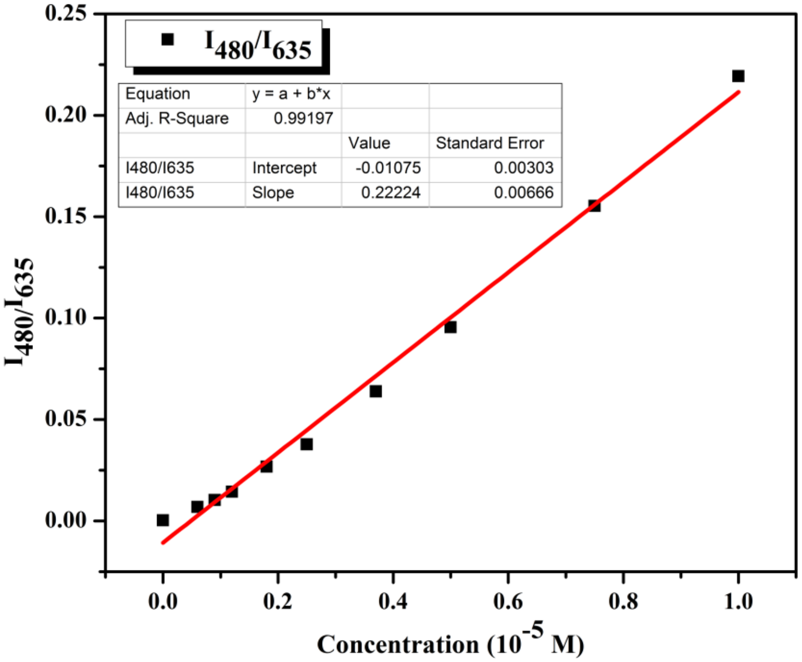

**Figure 3.13.** Plot of $I_{480}/I_{635}$ *vs* $CN^-$ (0.0-10.0 μM ) shows a good linear relationship.

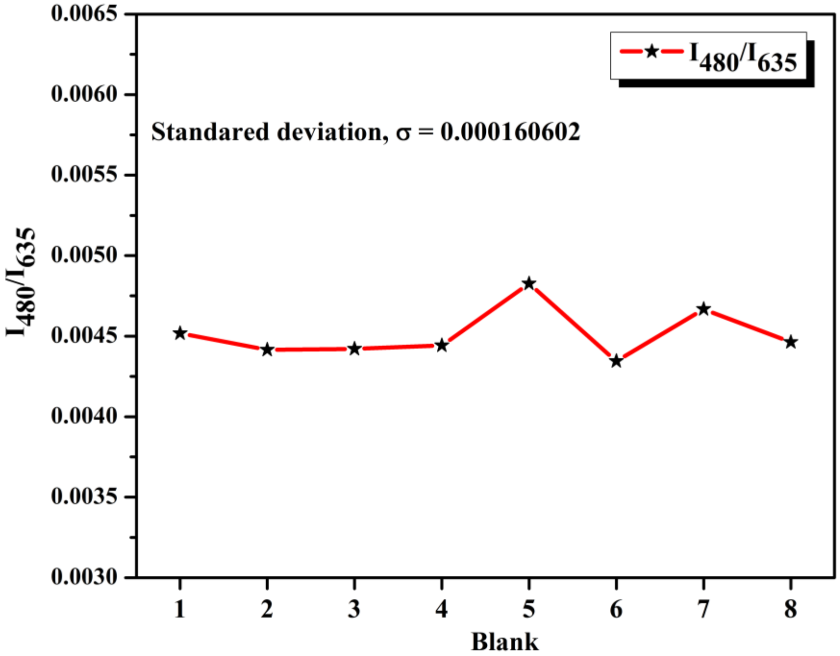

**Figure 3.14.** Plot of $I_{480}/I_{635}$ *vs* blank solutions for the calculation of standard deviation.

**Table 3.6.** Comparison of present manuscript with previous reports with respect to type of heavy metal complexes used for the detection of cyanide.

| **S. No.** | **Publication** | **System** | **Detection limit** |
|---|---|---|---|
| **1** | Current work | Highly sensitive dual-channel chemosensor for cyanide based on formyl functionalized phosphorescent iridium(III) complex | 2.16 × $10^{-8}$ M (in acetonitrile) and ~264.8 ng/mL (in drinking water) |
| **2** | *New J. Chem. 2010, 34, 132–136* | Multisignaling detection of cyanide anions based on an iridium(III) complex: remarkable enhancement of sensitivity by coordination effect | 40 × $10^{-6}$ (in drinking water) |
| **3** | *J. Am. Chem. Soc. 2011, 133, 15276–15279* | Iridium(III) complex-coated nanosystem for ratiometric upconversion luminescence bioimaging of cyanide anions | 0.18 × $10^{-6}$ M |
| **4** | *Adv. Funct. Mater*. 2012, *22*, 2667–2672 | Iridium-complex-modified upconversion nanophosphors for effective lret detection of cyanide anions in pure water | 62.6 × $10^{-6}$ M |
| **5** | *Chem. Commun.*, 2013, 49, 255-257 | A $CN^-$ specific turn-on phosphorescent probe with probable application for enzymatic assay and as an imaging reagent | 0.38 × $10^{-6}$ M (in buffer medium of pH 7.6.) |
| **6** | *Chem. Commun.*, 2012, 48, 2707–2709 | A lab-on-a-molecule for anions in aqueous solution: using Kolbe electrolysis and radical methylation at iridium for sensing | - |
| **7** | *Microchim Acta, 2015 182, 2561–2566* | Silica nanoparticles doped with an iridium(III) complex for rapid and fluorometric detection of cyanide | 1.66 × $10^{-6}$ M |
| **8** | *Inorg. Chem. 2013, 52, 4890−4897* | Switching of reverse charge transfers for a rational design of an OFF−ON phosphorescent chemodosimeter of cyanide anions | 6 × $10^{-6}$ M |
| **9** | *Inorg. Chem. 2012, 51, 7075−7086* | Rapid and highly sensitive dual-channel detection of cyanide by bis-heteroleptic ruthenium(II) complexes | 0.18 × $10^{-6}$ M |
| **10** | *Dalton Trans., 2015, 44, 18607-18623* | Pyrene and imidazole functionalized luminescent bimetallic Ru(II) terpyridine complexes as efficient optical chemosensors for cyanide in aqueous, organic and solid media | 9.79 × $10^{-8}$ M |

To gain more insight into the relaxation dynamics of the **IrC** excited state, phosphorescence lifetimes ($\tau$) in deaerated acetonitrile solution were measured at 298 K before and after adding 2.0 equiv of $CN^-$ by monitoring the peak at 635 nm for **IrC** and 480 nm for **IrC+(CN)$_2$** (Figure 3.15). Both of the excited state species showed single-exponential decay profiles with a lifetime of 0.06 μs for **IrC** and 0.75 μs for **IrC+(CN)$_2$**, which is indicative of the phosphorescence origin for the excited states in each case. The excited state lifetime value and radiative and nonradiative decay rates of the iridium(III) complex and corresponding $CN^-$ adduct are depicted in Table 3. The poor quantum efficiency ($\Phi_{PL} = 0.02$) associated with **IrC** could be due to the involvement of the −CHO group in the MLCT transition, leading to a partial weakening of the $\pi$(C═O) bond due to the negative charge in the pyridyl moiety of the cyclometalated ligand upon photoexcitation,[30] which will eventually induce large vibrational decay pathways ($k_{nr} = 19.6 \times 10^5$ s$^{-1}$). Meanwhile, a more pronounced quantum yield ($\Phi_{PL} = 0.11$) has been noticed with the newly formed **IrC+(CN)$_2$**. The enhanced luminescence could be due to the confinement of the MLCT transition between the iridium(III) center and $\pi$ rings of the cyclometalated ligands in a manner identical with that for FIrpic, which in turn reduces the deactivation pathways.[25] This is also in good agreement with the observed low nonradiative decay rates associated with the excited **IrC+(CN)$_2$** at 480 nm ($k_{nr} = 1.18 \times 10^5$ s$^{-1}$).

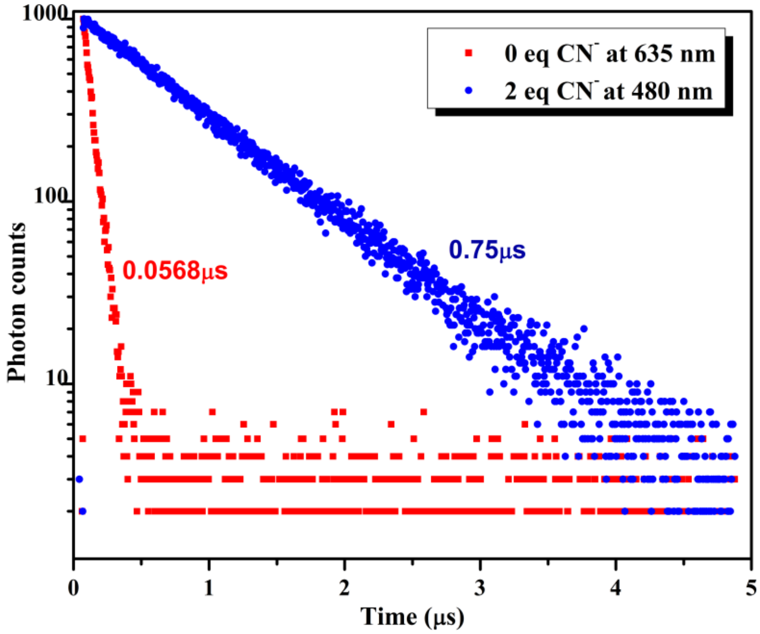

**Figure 3.15.** Lifetime decay profiles of **IrC** (*c* = 20 μM) in acetonitrile at 635 nm before adding CN$^-$ and at 480 nm after adding 2.0 equiv of CN$^-$ ($\lambda_{exc}$= 375 nm).

A competition study has been performed with a view to confirm the selectivity of **IrC** toward CN$^-$. No remarkable PL intensity enhancement was observed upon addition of other potentially competing anions (2.0 equiv of AcO$^-$, BzO$^-$, $ClO_4^-$, $H_2PO_4^-$, $HSO_4^-$, $N_3^-$, $NO_3^-$, OH$^-$, $PF_6^-$, F$^-$, Cl$^-$, Br$^-$, $HSO_3^-$, and I$^-$) to a 20 μM solution of **IrC** in $CH_3CN$ in the absence of cyanide (Figure 3.16). The addition of 2.0 equiv of CN$^-$ to **IrC** in the presence of an excess of other anions (10.0 equiv) evokes a PL enhancement which is reproducible (inset of Figure 3.16). It is noteworthy to mention that anions such as bisulfite and perchlorate that are well-known to compete in the detection of CN$^-$ are found to not interfere in the developed chemosensor system.

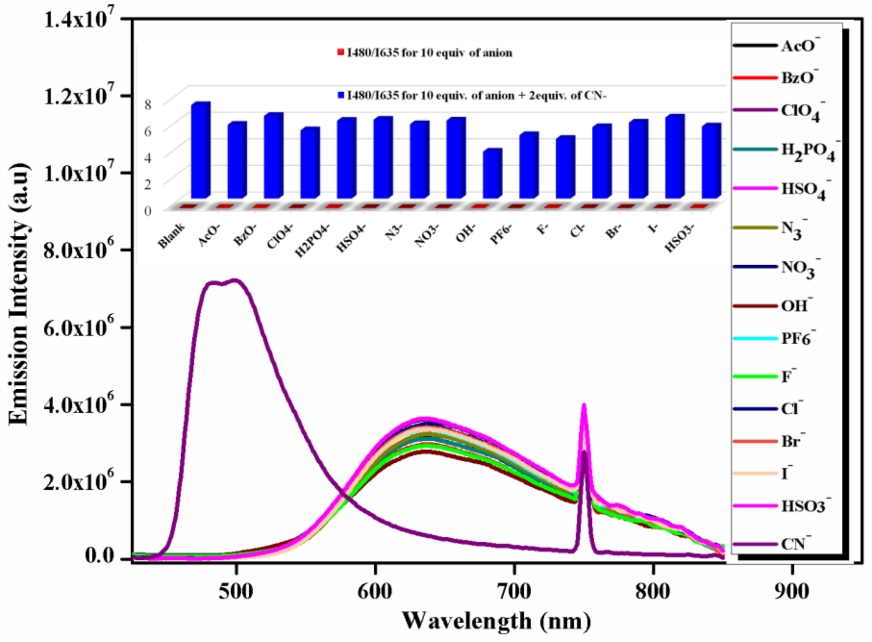

**Figure 3.16.** PL spectra of **IrC** (20 μM) with different anions (2.0 equiv). (Inset) Behavior of **IrC** toward $CN^-$ (2.0 equiv) under the competitive presence of other anions (10.0 equiv) as measured by emission spectra in $CH_3CN$. At 750 nm (*) indicates the second harmonic peak of the excitation wavelength.

### 3.4.6. Detection of $CN^-$ in Aqueous Acetonitrile Solution

For practical use of the **IrC** probe, PL titrations were carried out in $CH_3CN/H_2O$ solutions (99/1, 97/3 and 95/5 v/v) and compared with the emission properties in pure acetonitrile solution (Figure 3.17). However, unlike the titration process in pure $CH_3CN$ solution, here a maximum of ~5.0 equiv of $CN^-$ is required to complete the reaction in 5% aqueous acetonitrile ($CH_3CN/H_2O$; 95/5 v/v). On the other hand, in 3% aqueous acetonitrile ($CH_3CN/H_2O$; 97/3 v/v), the reaction requires a minimum of 3.0 equiv of $CN^-$. In the case of 1% aqueous acetonitrile ($CH_3CN/H_2O$; 99/1 v/v) a minimum of 2.0 equiv of $CN^-$ is required for completing the reaction, which is similar

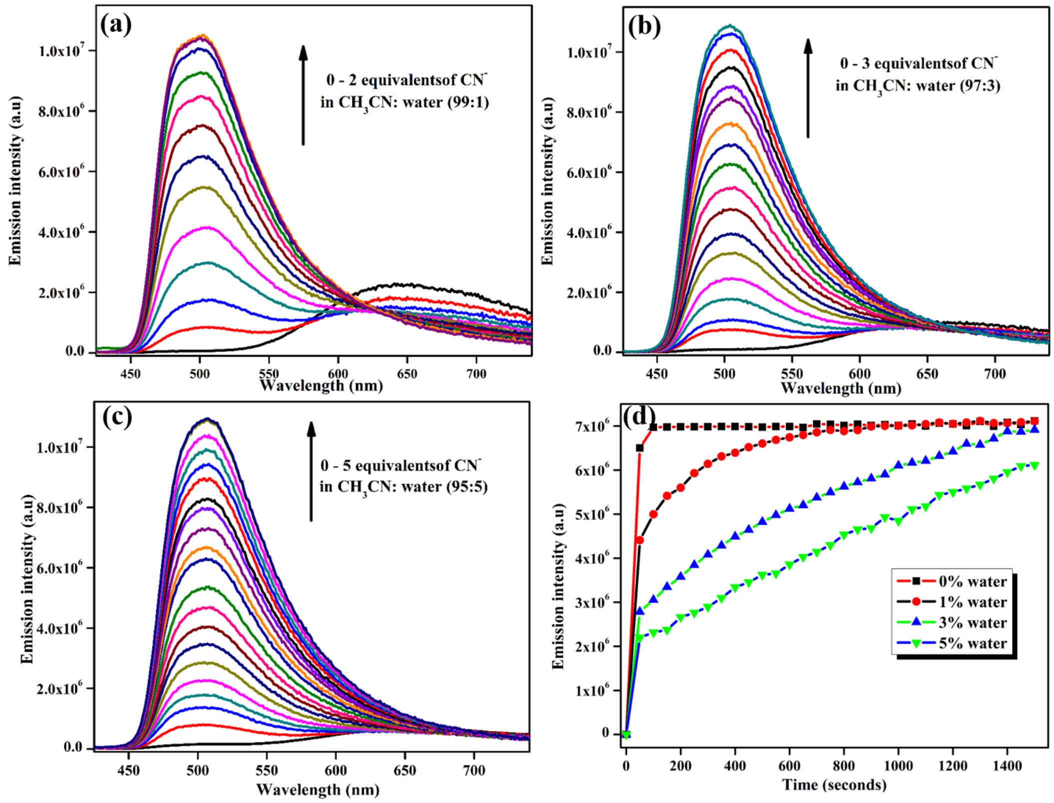

**Figure 3.17.** Photoluminescence titration of **IrC** with CN⁻ in (a) 1%, (b) 3% and (c) 5% aqueous acetonitrile. (d) Kinetics of the photoluminescence response of **IrC** upon addition of 2.0 equiv of CN⁻ in pure acetonitrile and in 1%, 3% and 5% aqueous acetonitrile at room temperature ($\lambda_{exc}$= 375 nm).

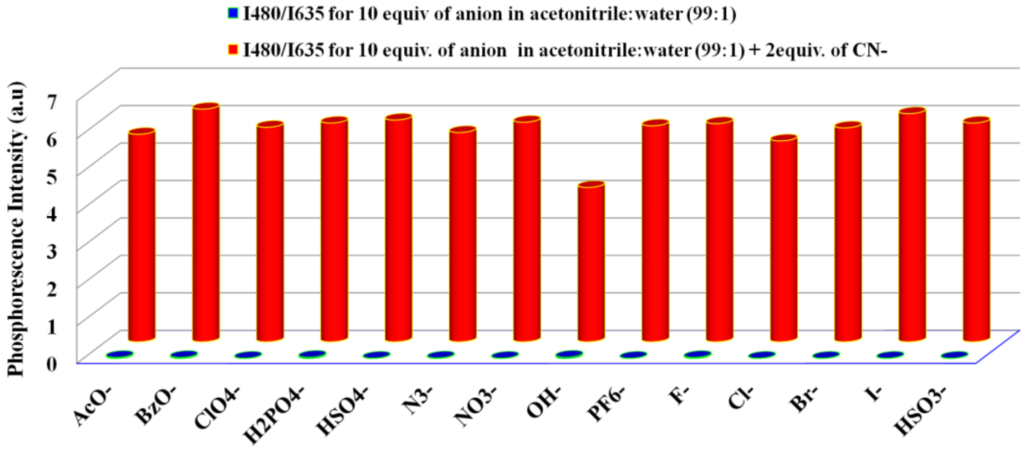

**Figure 3.18.** Phosphorescence response of **IrC** toward CN⁻ and other anions as measured in 1% aqueous acetonitrile solution ($\lambda_{exc}$= 375 nm).

to that of pure $CH_3CN$. This study clearly demonstrates that the reactivity of cyanide with **IrC** in aqueous solution is very critical to the presence of water content. These results are in good agreement with those for the earlier reported cyanide sensors, where the strong hydration of $CN^-$ in aqueous solution reduces its nucleophilicity.[11h] Further, a study of the time dependence (Figure 3.17d) shows that the PL intensity continues to increase beyond 25 min in 5% aqueous acetonitrile solution ($CH_3CN/H_2O$; 95/5 v/v), implying that a much slower reaction in comparison to pure $CH_3CN$ solution (100 s). In 3% aqueous solution ($CH_3CN/H_2O$; 97/3 v/v), the reaction requires 22 min for completion. On the other hand, 10 min is required to complete the reaction in the case of 1% aqueous solution ($CH_3CN/H_2O$; 99/1 v/v). A good selectivity has also been noted toward cyanide under these conditions (Figure 3.18). Thus, it can be concluded from these investigations that **IrC** is more selective and sensitive toward $CN^-$ in pure acetonitrile as well as in solutions containing 1% of water, which qualifies it for real-world applications.

### 3.4.7. Contact Mode Detection of $CN^-$ by Luminescent Test Strips

Motivated by the favorable features of **IrC** as a potential sensor for $CN^-$ in solution, we have prepared red luminescent test strips using **IrC** for the detection of $CN^-$ anions by contact mode. As discussed earlier, **IrC** shows excellent luminescent properties in the solid state in comparison to the solution state (see section 3.4.4). This observation has prompted us to develop luminescent Whatman filter paper test strips

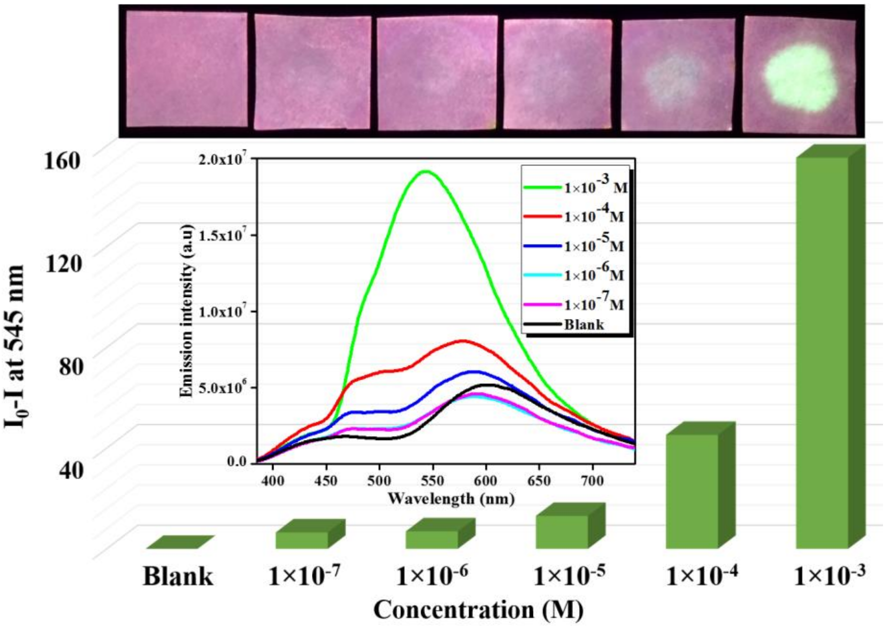

**Figure 3.19.** Plot of the emission intensity at 545 nm of the test strips against concentration of added $CN^-$ anions in drinking water (10 μL, $1{\times}10^{-7}$ to $1{\times}10^{-3}$ M). Inset figure shows the corresponding emission spectra ($\lambda_{exc}$= 375 nm) and images were taken under 365 nm UV excitation.

(2.0 cm × 2.0 cm) by impregnation with **IrC** ($1 \times 10^{-4}$ M in dichloromethane), and they exhibit red phosphorescence when excited with 375 nm (preparation methods of test strips can be found in the Experimental Section). Different concentrations of $CN^-$ solution ($c = 1 \times 10^{-7}$ to $1 \times 10^{-3}$ M) have been prepared in drinking water. Small spots (10 μL) of different concentrations of $CN^-$ solution in water were created on **IrC**-impregnated test strips. The emission from the applied area on the test strips has transformed from red to greenish spots of different strengths (Figure 3.19). The emission spectrum illustrates a peak at 600 nm for blank test strips, and it blue-shifts 55 nm (1682 $cm^{-1}$) to 545 nm upon addition of a $1 \times 10^{-3}$ M $CN^-$ solution.

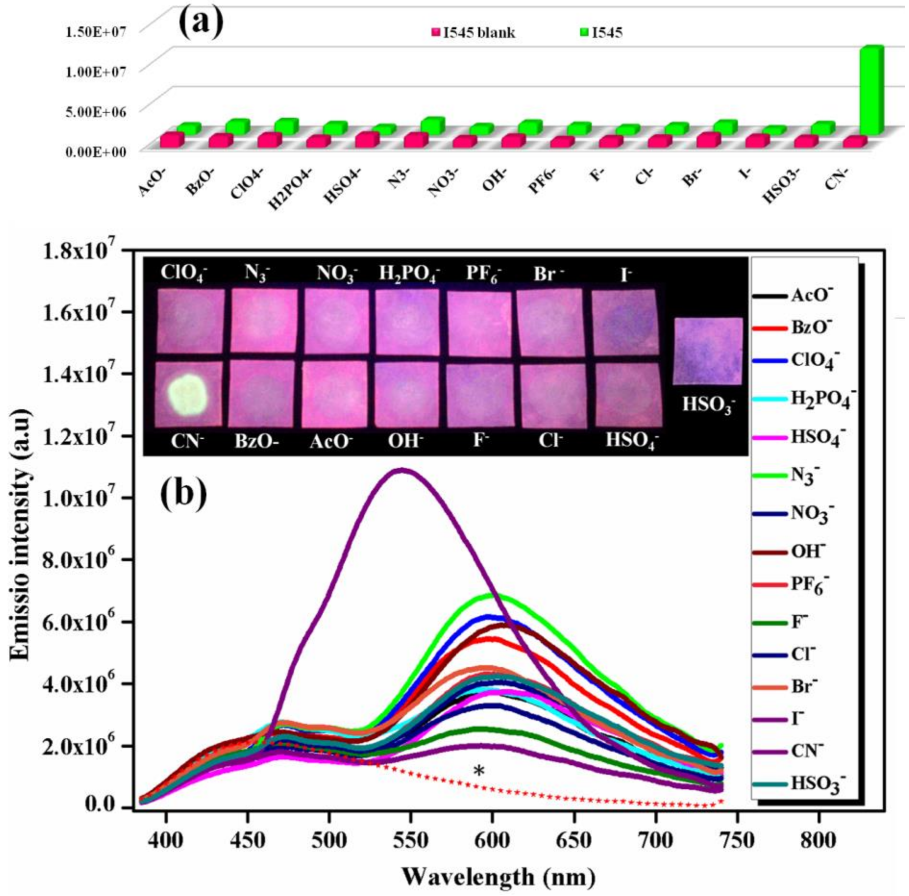

**Figure 3.20.** (a) Selectivity response and (b) Emission spectra of **IrC** impregnated test strips toward $CN^-$ and other anions (10 μL of 10 μM solution) at $\lambda_{exc}$= 375 nm. Inset figure shows photographs of test strips under 365 nm UV excitation. Blue emission from blank filter paper has been indexed with an asterisk (*).

The plot of the emission intensity at 545 nm from the test strips against the concentration of added $CN^-$ anion in drinking water (10 μL, $1 \times 10^{-7}$ to $1 \times 10^{-3}$ M) shows the regulation of the sensing behavior of **IrC** practically applicable by varying the concentration of $CN^-$ even up to $10^{-5}$ M (~264.8 ng/mL). The phosphorescence response of **IrC** impregnated test strips toward competitive anions was also investigated to confirm the selectivity of the developed luminescent test strips toward cyanide ions. As displayed in Figure 3.20, the addition of 10 μL of $CN^-$ solution ($c$ = 10 μM) to the test strips created a noticeable change in the emission color from red to green. In contrast to the above, no emission color change has been noticed with the addition of 10 μL of potentially competing anions ($AcO^-$, $BzO^-$, $ClO_4^-$, $H_2PO_4^-$, $HSO_4^-$, $N_3^-$, $NO_3^-$, $OH^-$, $PF_6^-$, $F^-$, $Cl^-$, $Br^-$, $HSO_3^-$, and $I^-$) to the test strips. The selectivity plot of emission intensity at 545 nm *vs* various anions (Figure 3.20a) demonstrates the practical utility of the **IrC** impregnated test strips for the instant on-site visualization of trace amounts of cyanide ions present in drinking water.

### 3.4.8. Confirmation of the Interaction of IrC with $CN^-$ by $^1H$ NMR, ESI-MS, and FT-IR Studies

The confirmation of the nature of the interaction of **IrC** with $CN^-$ has been ascertained by $^1H$ NMR spectroscopic titration. Figure 3.21 shows the $^1H$ NMR spectra of **IrC** upon addition of (stepwise) 0.0–2.0 equiv of tetrabutylammonium cyanide in $CD_3CN$ solution. The addition of cyanide resulted in a disappearance of the aldehyde proton (H*) signal (at $\delta$ 10.17 ppm) and the simultaneous appearance of a new peak corresponding to the cyanohydrin proton, −CH(CN)OH (H*) at $\delta$ 7.57 ppm. The disappearance of the aldehyde proton (H*) signal upon addition of 0.2 equiv of $CN^-$ may be due to the hydration of the unreacted formyl group by the water molecule present in the added analyte solution. This hydration phenomenon induces the formation of a highly reversible gem-diol, which exists in a rapid equilibrium with the aldehyde.[31] The stepwise appearance of the proton signal at 7.57 ppm clearly indicates the formation of cyanohydrin. Upon addition of 2.0 equiv of $CN^-$, upfield shifts are noted for the formylated pyridyl ring protons of the cyclometalated ligand. The signals for $H_a$ (8.92 ppm), $H_b$ (8.64 ppm), and $H_c$ (8.20 ppm) were shifted upfield to 8.75, 8.55, and 8.16 ppm, respectively. These spectral shifts are virtually stopped after adding 2.0 equiv of cyanide. On the other hand, the $H_d$ signal (8.72 ppm) from the ancillary picolinate ligand and other aromatic signals (8.10–7.55 ppm) corresponding to the phenyl ring protons of the cyclometalated ligands did not change.

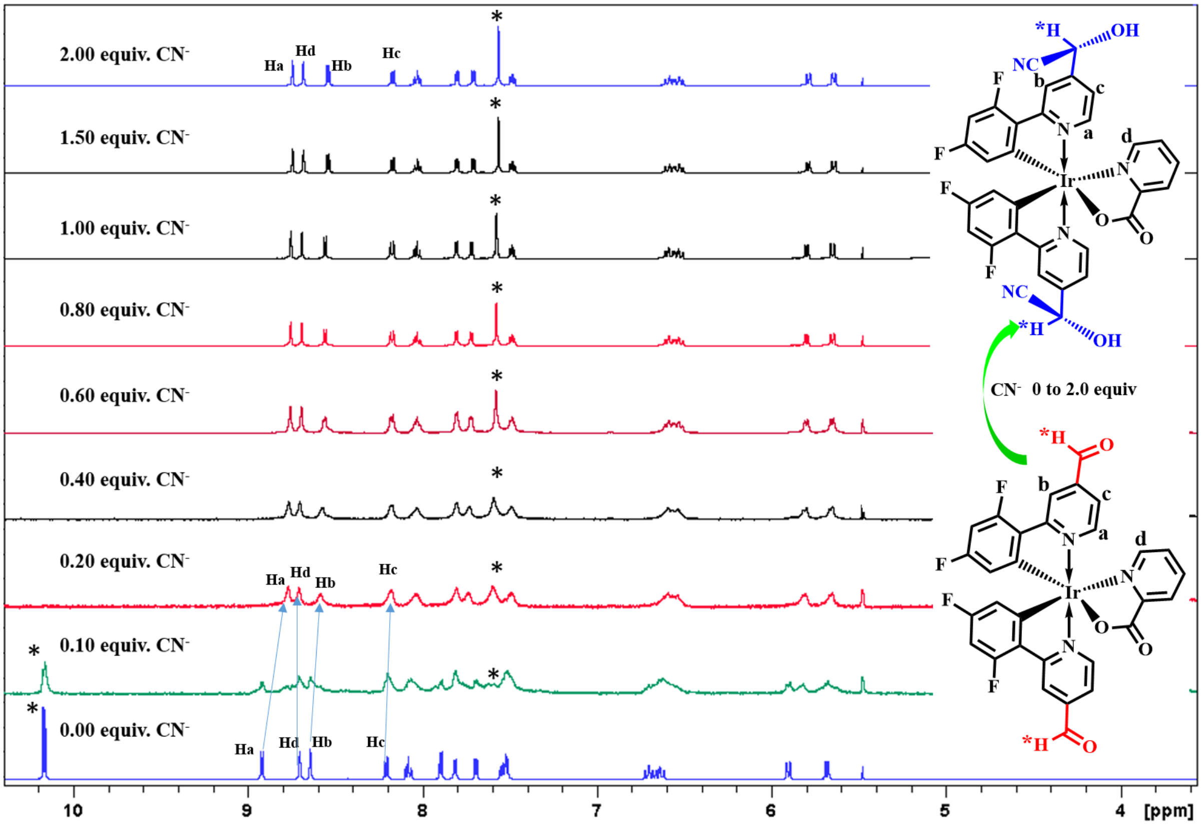

**Figure 3.21.** $^1H$ NMR titration spectra indicating the reaction of **IrC** with $CN^-$ in $CD_3CN$ at room temperature. The asterisks (*) and letters (a, b and c) signs are used to index specific proton signals.

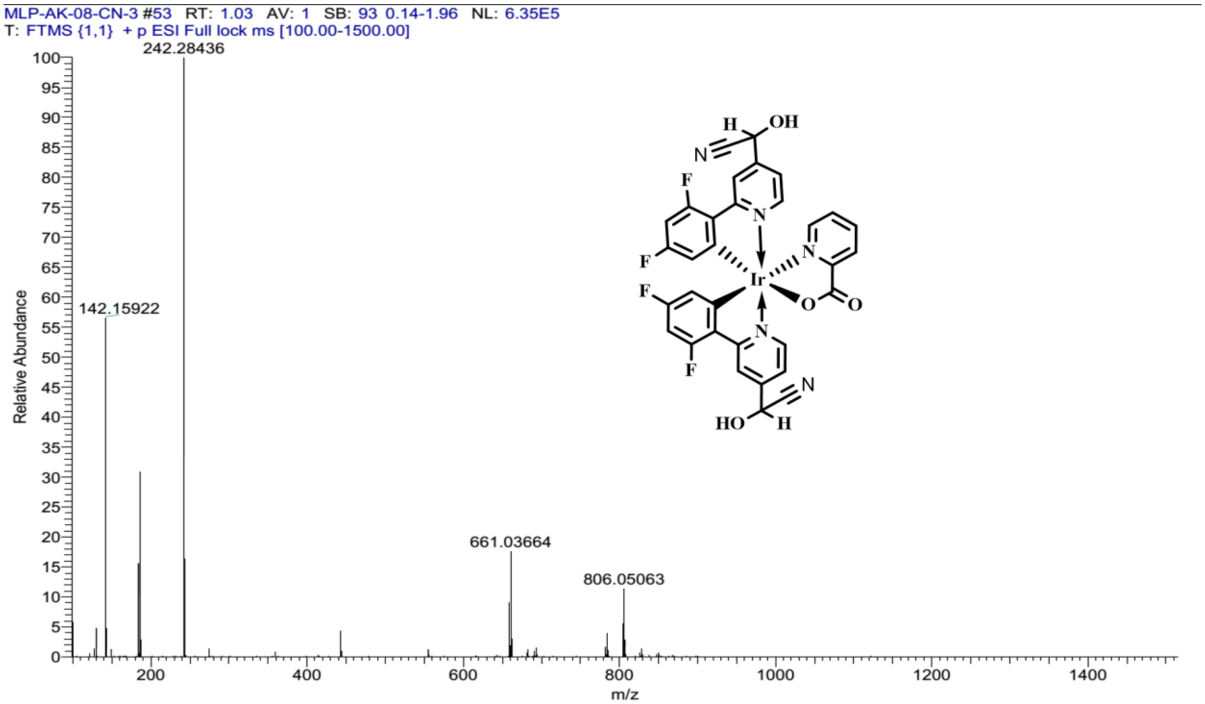

**Figure 3.22.** ESI-MS spectrum of (2',6'-difluoro-4-(formyl)-2,3'-bipyridinato-N,C4') Iridium(III) (picolinate), [**IrC**] after addition of 2.0 equivalents of CN⁻ anions. **IrC+(CN)₂**: m/z = 806.05 [$M^{+1}$].

The formation of cyanohydrin was further confirmed by ESI mass spectrometry and FT-IR spectroscopy. The electospray ionization mass spectrum of the isolated yellow solid (see the Experimental Section 3.3.16 for the isolation of the cyanide adduct) showed a molecular mass of 806.05 (Figure 3.22), which corresponds to the formula of [**IrC+(CN)₂** + 1] (calculated m/z 806.09). On the other hand, the FT-IR spectrum clearly indicates the appearance of the −C≡N stretching frequency at 2248 $cm^{-1}$ and disappearance of the −C═O stretching frequency (1706 $cm^{-1}$) of the aldehyde group in **IrC** (Figure 3.23).

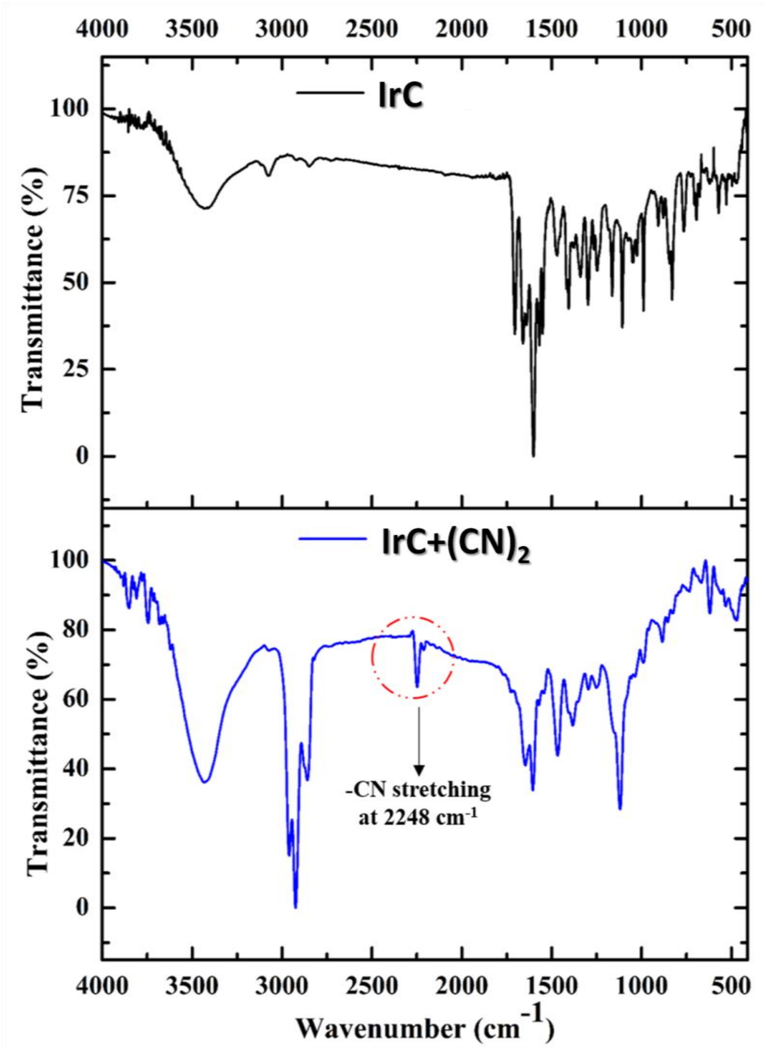

**Figure 3.23.** Comparison of FT-IR spectrum of **IrC** before and after the addition of 2.0 equiv of CN$^-$ anion.

On the basis of the results from NMR chemical shifts, FT-IR spectroscopy, and ESI mass spectrometry, the most plausible mechanism for the formation of the cyanide adduct (cyanohydrin) is proposed (Scheme 3.3). The strongly electron deficient nature of the −CHO groups from **IrC** make it susceptible to the nucleophilic attack of CN$^-$ to the carbonyl groups through the formation of a cyanohydrin, which is a very stable adduct, thus making the reaction completely irreversible.[11k]

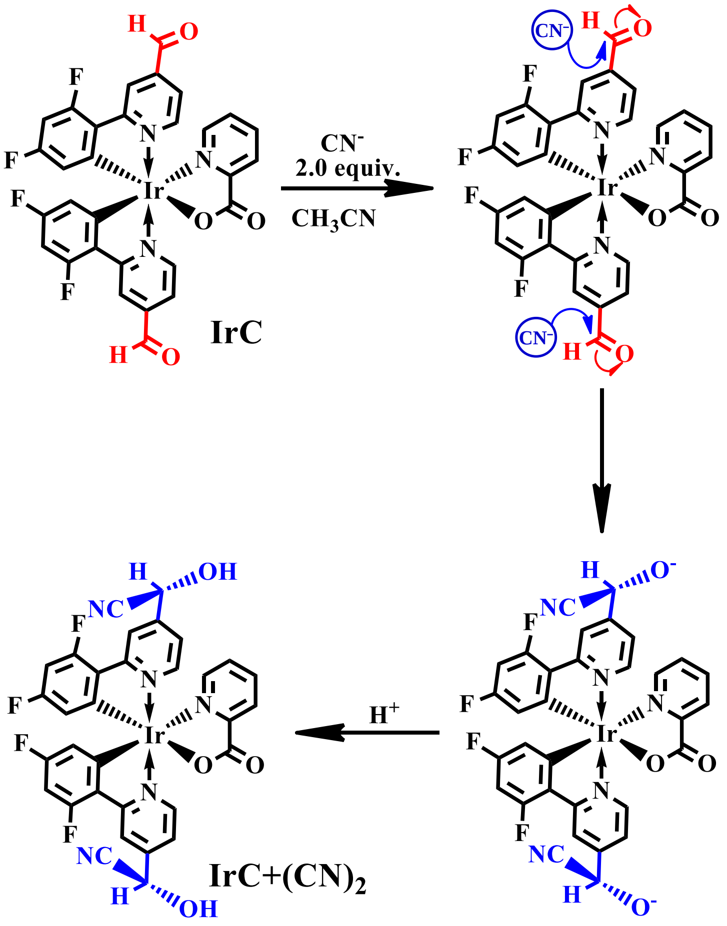

**Scheme 3.3.** Cyanohydrin Formation Mechanism for the Detection of Cyanide by **IrC**

### 3.4.9. Electrochemistry on the Interaction of IrC with CN⁻

To realize the electronic effects caused by the change of substituents on the C4′ position on the pyridyl moiety of the cyclometalated ligand in **IrC**, the electrochemical behaviour of **IrC** has been studied before and after the addition of 2.0 equivalents of $CN^-$ anions by cyclic voltammetry experiments in deaerated $CH_3CN$ solution using ferrocene as the internal standard and the results are depicted in Figure 3.24. The calculated HOMO and LUMO for **IrC** and its cyanide adduct are listed in

Table 3.7. Quasi-reversible oxidation voltammograms were observed at identical potentials (~1.46 to 1.47 V) for both experiments (before and after the addition of $CN^-$ anions), indicating the oxidation potential originated from the iridium metal center ($Ir^{3+}/Ir^{4+}$) has been least affected by the change of substituent from –CHO to −CH(CN)OH (cyanohydrin). Correspondingly, the calculated energy levels of highest occupied molecular orbitals (HOMO) stands almost same (–5.82 eV) in both cases. While scanning to the negative potential range, **IrC** exhibits two irreversible reduction potentials. First reduction potential occurs at −0.94 V can be attributed to the reduction of the –CHO group as usually found in formyl group substituted iridium(III) complexes and aromatic aldehydes. Second reduction potential occurs at −1.70 V could be due to the reduction of N-coordinating pyridyl moiety of the cyclometalated ligand. Upon addition of 2.0 equiv of the $CN^-$ ions to the experimental solution, the reduction potential correspond to –CHO substituent observed at −0.94 has been completely vanished and the cyclometalated ligand based reduction peak at −1.63 V dominates. The calculated LUMO experienced a more negative shift (~0.71 eV) from −3.43 to −2.72 eV. This observation clearly points out the change in the localization of LUMO from –CHO group to cyclometalated ligand upon conversion of –CHO substituent to –CH(CN)OH (cyanohydrin). These assumptions were strongly supported by the density functional theory (DFT) calculations

**Table 3.7.** Electochemical properties of **IrC** and **IrC+(CN)$_2$**

| Complex | $E_{oxd}$ $^a$(V) | $E_{red}$$^a$ (V) | HOMO$^b$ (eV) | LUMO$^c$ (eV) | $E_{g(elec)}$$^d$ (eV) | $E_{g(calc)}$$^e$ (eV) |
|---|---|---|---|---|---|---|
| **IrC** | 1.46 | -0.94<br>-1.70 | -5.82 | -3.43 | 2.39 | 3.01 |
| **IrC+(CN)$_2$** | 1.47 | -1.63 | -5.83 | -2.72 | 3.11 | 3.62 |

$^a$Electrochemical data versus ($FeCp_2^+/FeCp_2^0$) ($FeCp_2$ is ferrocene) were collected in $CH_3CN$/0.1 M TBAH (tetra-butylammoniumhexafluorophosphate). $^b$HOMO = -[4.8-(0.44) + $E_{oxd}$]. $^c$LUMO = -[4.8 -(0.44) + $E_{red}$]. $^d$Electrochemical band gap experimental. $^e$Electrochemical band gap theoretical.

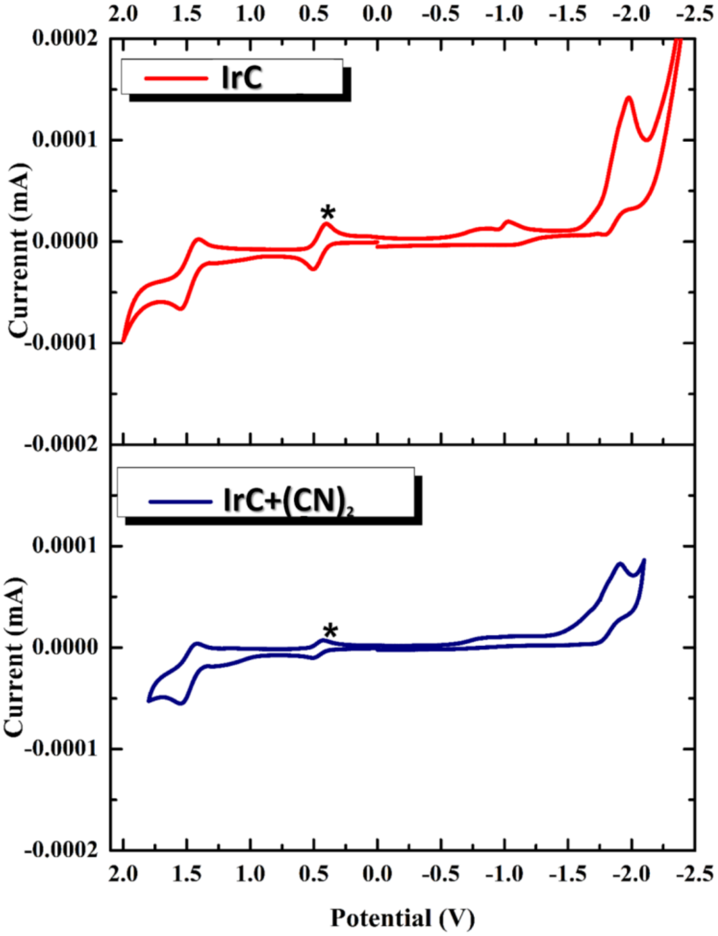

**Figure 3.24.** Comparison of redox potentials (vs Ag/AgCl in $CH_3CN$) of **IrC** before and after the addition of 2.0 equiv of $CN^-$, (oxidation potential $FeCp_2/FeCp_2^+$ =0.44 V, marked with asterisk).

### 3.4.10. Theoretical Studies

The ground-state ($S_0$) geometrical structures of iridium complex with −CHO as well as −CH(CN)OH (cyanohydrin) substituents were optimized using density functional theory (DFT) based on the B3LYP method. Further, the excited-state vertical transitions of the model compounds were also predicted by using the time-dependent density functional theory (TD-DFT) approach. The optimized structures possess a distorted-octahedral geometry around the iridium center, with C1 point group symmetry. There exists a good correlation with the observed absorption spectrum of **IrC** before and after the addition of $CN^-$. Molecular orbital (MO) analysis has been carried out on the optimized structures to get more insights regarding the localization of molecular orbital at each energy level. Figure 3.25 gives a molecular orbital diagram indicating isodensity HOMO and LUMO energy surfaces and calculated energy levels for **IrC** and its $CN^-$ adduct. As can be seen from Figure 3.25, HOMO surfaces for both complexes are similar to the electron density, and this density is distributed through the 5d orbitals of iridium metal and the 2,6-difluorophenyl moiety of the cyclometalated ligand. This accounts for the identical HOMO energy levels experimentally revealed for both complexes from the electrochemical studies (see Figure 3.24). The calculated HOMO energy levels are −5.81 and −5.61 eV for **IrC** and **IrC+(CN)$_2$**, respectively. Furthermore, the calculated HOMO values are akin to that of the experimentally determined first oxidation potential (Table 3.7). The present observation is similar to the HOMO orbital distribution of FIrpic reported elsewhere.[25]

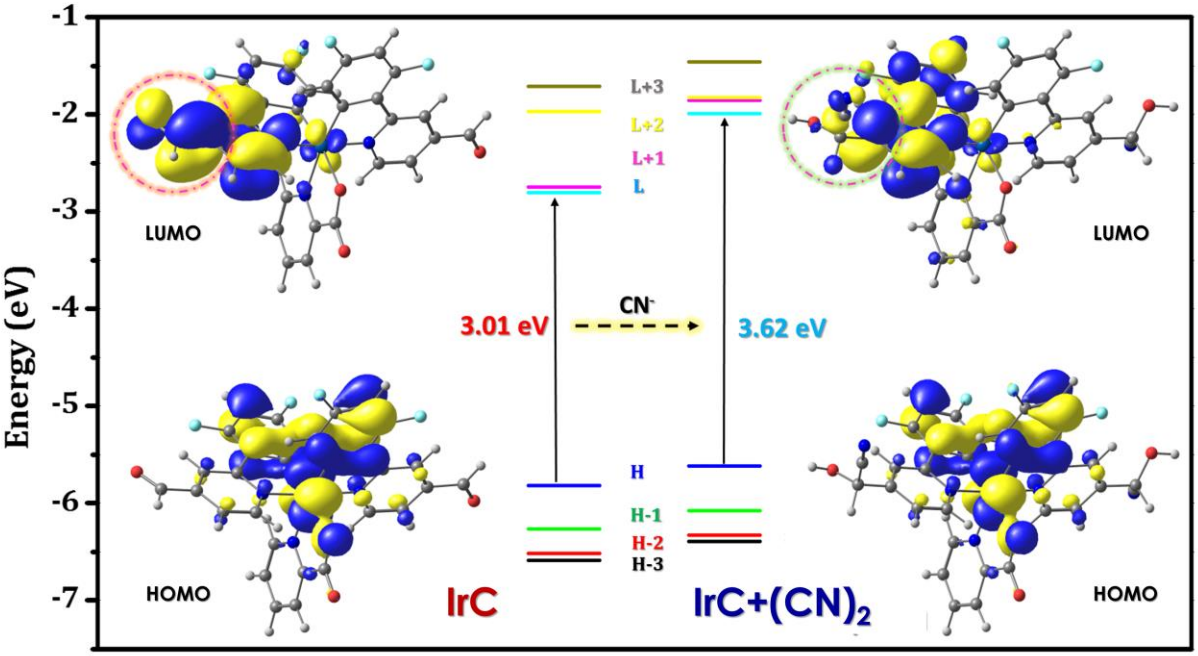

**Figure 3.25.** Selected molecular orbital diagram indicating isodensity HOMO and LUMO surfaces for **IrC** before and after the addition of 2.0 equiv of CN$^-$. All of the molecular orbital surfaces correspond to an isocontour value of |ψ| = 0.03. The arrows are intended to highlight the calculated HOMO-LUMO energy gaps (H = HOMO and L = LUMO).

The LUMO of **IrC** is essentially localized on the −CHO substituent and the attached N-coordinated pyridyl moiety of the cyclometalated ligand due to the electron-accepting nature of the −CHO substituent and predominant conjugation of −C═O group with the connected pyridyl moiety. The same can be illustrated further from the rich electron density observed at the −C–C– bond connecting the carbonyl group of −CHO and the pyridyl ring. As a result, the LUMO energy levels are more stabilized (−2.80 eV), and we observed a first reduction potential based on the −CHO group in the electrochemical studies (Figure 3.24). This observation clearly accounts for the noticed red shift of 165 nm (∼5528 cm$^{-1}$) from 635 to 470 nm in the emission profile of **IrC** in comparison to FIrpic as well as $^1$MLCT absorption bands appearing in the visible region (400–500 nm) as per our previous discussions. However, after the addition of CN$^-$, −CHO has been converted to −CH(CN)OH (cyanohydrin) in **IrC+(CN)$_2$** and the LUMO is strictly localized within the N-pyridyl moiety of the cyclometalated ligand due to the lack of any conjugation between the pyridyl moiety and cyanohydrin substituent. As a result, the LUMO energy levels are more destabilized (from −2.80 to −1.98 eV) in **IrC+(CN)$_2$** in comparison to **IrC**. Thus, the LUMO destabilization has induced a widening of the energy band gap from 3.01 to 3.62 eV. These observations are in agreement with the blue shift of ∼155 nm (∼5085 cm$^{-1}$) observed in the emission spectrum as well as the hypsochromic shift noticed from 475 to 375 nm in the $^1$MLCT absorption bands of **IrC** upon addition of 2.0 equiv of CN$^-$.

## 3.5. Conclusions

- In summary, herein a highly selective probe for the sensing of CN$^-$ in a semiaqueous environment has been developed for the first time on the basis of a simple phosphorescent iridium(III) complex with a detection limit of $2.16 \times 10^{-8}$ M.

- A unique colorimetric and ratiometric phosphorescence response to the cyanide is realized through interaction of the electron-deficient formyl moiety of the cyclometalated iridium(III) complex with $CN^-$ through the formation of cyanohydrin.
- The formation of cyanohydrin has been further corroborated by $^1$H NMR, ESI-MS, and FT-IR spectral studies.
- In addition, phosphorescent test strips have been fabricated and utilized for the detection of nanogram levels of cyanide in drinking water.
- Finally, theoretical calculations furnished detailed insights into the electronic structure and transitions involved in the iridium(III) compound and its corresponding cyanide adduct.

## 3.6. References

(1) (a) Baskin, S. I.; Brewer, T. G.; Sidell, F.; Takafuji, E. T.; Franz, D. R., *Medical Aspects of Chemical and Biological Warfare*, Eds.; TMM Publication: Washington, 1997, pp 1271-1286. (b) Kulig, K. W., *Cyanide Toxicity*, U.S. Department of Health and Human Services, Atlanta,1991. (c) Takano, R., *J. Exp. Med.* **1916,** *24*, 207–211.

(2) (a) *Guidelines for Drinking-Water Quality*, World Health Organization, Geneva, 1996. (b) Shan, D.; Mousty, C.; Cosnier, S., *Anal. Chem.* **2004,** *76*, 178-183.

(3) (a) Hathaway, G. J.; Proctor, N. H., *Chemical Hazards of the Workplace, 5th ed*, John Wiley & Sons, Inc.: Hoboken, 2004; pp 2190−2191. (b) Koenig, R., *Science* **2000,** *287*, 1737–1738. (c) Patnaik, P. A., *Comprehensive Guide to the Hazardous Properties of Chemical Substance*, van Nostrand Reinhold: New York, 1992; pp

1229−1244. (d) Taylor, J.; Roney, N.; Fransen, M. E.; Swarts, S., *Toxicological Profile for Cyanide*, DIANE Publishing, Atlanta, 2006. (e) Vennesland, B.; Comm, E. E.; Knownles, C. J.; Westly, J.; Wissing, F., *Cyanide in Biology*, Academic Press, London,1981.

(4) (a) Kaur, K.; Saini, R.; Kumar, A.; Luxami, V.; Kaur, N.; Singh, P.; Kumar, S., *Coord. Chem. Rev.* **2012,** *256*, 1992-2028. (b) Kubik, S., *Chem. Soc. Rev.* **2010,** *39*, 3648-3663. (c) Lebeda, F. J.; Deshpande, S. S., *Anal. Biochem.* **1990,** *187*, 302-309. (d) Ma, J. A.; Dasgupta, P. K., *Anal. Chim. Acta* **2010,** *673*, 117-125. (e) Wang, F.; Wang, L.; Chen, X. Q.; Yoon, J. Y., *Chem. Soc. Rev.* **2014,** *43*, 4312-4324.

(5) (a) Aebli, B.; Mannel-Croise, C.; Zelder, F., *Inorg. Chem.* **2014,** *53*, 2516-2520. (b) Anzenbacher, P.; Tyson, D. S.; Jursikova, K.; Castellano, F. N., *J. Am. Chem. Soc.* **2002,** *124*, 6232-6233. (c) Biradar, A. A.; Biradar, A. V.; Sun, T.; Chan, Y.; Huang, X. X.; Asefa, T., *Sens. Actuators, B* **2016,** *222*, 112-119. (d) Fillaut, J. L.; Akdas-Kilig, H.; Dean, E.; Latouche, C.; Boucekkine, A., *Inorg. Chem.* **2013,** *52*, 4890-4897. (e) Holaday, M. G. D.; Tarafdar, G.; Adinarayana, B.; Reddy, M. L. P.; Srinivasan, A., *Chem. Commun.* **2014,** *50*, 10834-10836. (f) Jung, H. S.; Han, J. H.; Kim, Z. H.; Kang, C.; Kim, J. S., *Org. Lett.* **2011,** *13*, 5056-5059. (g) Jung, K. H.; Lee, K. H., *Anal. Chem.* **2015,** *87*, 9308-9314. (h) Karmakar, S.; Maity, D.; Mardanya, S.; Baitalik, S., *Dalton Trans.* **2015,** *44*, 18607-18623. (i) Kim, Y. H.; Hong, J. I., *Chem. Commun.* **2002**, 512-513. (j) Kumar, R.; Chaudhri, N.; Sankar, M., *Dalton Trans.* **2015,** *44*, 9149-9157. (k) Lee, J. H.; Jeong, A. R.; Shin, I. S.; Kim, H. J.; Hong, J. I., *Org. Lett.* **2010,** *12*, 764-767. (l) Li, M. J.; Lin, Z. H.; Chen, X. D.; Chen, G. N., *Dalton Trans.* **2014,** *43*, 11745-11751. (m) Lou, B.; Chen, Z. Q.; Bian, Z. Q.; Huang, C. H., *New J. Chem.* **2010,** *34*, 132-136. (n) Maldonado, C. R.; Touceda-Varela, A.; Jones, A. C.; Mareque-Rivas, J. C., *Chem. Commun.* **2011,** *47*, 11700-11702. (o) Mannel-Croise, C.; Zelder, F., *Inorg. Chem.* **2009,** *48*, 1272-1274. (p) Panda, C.; Dhar, B. B.; Malvi, B.; Bhattacharjee, Y.; Sen Gupta, S., *Chem. Commun.* **2013,** *49*, 2216-2218. (q) Reddy, G. U.; Das, P.; Saha, S.; Baidya, M.; Ghosh, S. K.; Das, A., *Chem. Commun.* **2013,** *49*, 255-257. (r) Rhaman, M. M.;

Alamgir, A.; Wong, B. M.; Powell, D. R.; Hossain, M. A., *RSC Advances* **2014,** *4*, 54263-54267. (s) Schmittel, M.; Shu, Q. H., *Chem. Commun.* **2012,** *48*, 2707-2709. (t) Wade, C. R.; Gabbai, F. P., *Inorg. Chem.* **2010,** *49*, 714-720. (u) Xie, Y. S.; Ding, Y. B.; Li, X.; Wang, C.; Hill, J. P.; Ariga, K.; Zhang, W. B.; Zhu, W. H., *Chem. Commun.* **2012,** *48*, 11513-11515. (v) Zou, Q.; Li, X.; Zhang, J. J.; Zhou, J.; Sun, B. B.; Tian, H., *Chem. Commun.* **2012,** *48*, 2095-2097.

(6) (a) Kang, N. Y.; Ha, H. H.; Yun, S. W.; Yu, Y. H.; Chang, Y. T., *Chem. Soc. Rev.* **2011,** *40*, 3613-3626. (b) Martinez-Manez, R.; Sancenon, F., *Coord. Chem. Rev.* **2006,** *250*, 3081-3093. (c) Xu, Z.; Chen, X.; Kim, H. N.; Yoon, J., *Chem. Soc. Rev.* **2010,** *39*, 127-137.

(7) (a) Baldo, M. A.; Lamansky, S.; Burrows, P. E.; Thompson, M. E.; Forrest, S. R., *Appl. Phys. Lett.* **1999,** *75*, 4-6. (b) Chi, Y.; Chou, P. T., *Chem. Soc. Rev.* **2010,** *39*, 638-655. (c) Fan, C.; Yang, C. L., *Chem. Soc. Rev.* **2014,** *43*, 6439-6469. (d) Lamansky, S.; Djurovich, P.; Murphy, D.; Abdel-Razzaq, F.; Lee, H. E.; Adachi, C.; Burrows, P. E.; Forrest, S. R.; Thompson, M. E., *J. Am. Chem. Soc.* **2001,** *123*, 4304-4312. (e) Liu, Z. W.; Guan, M.; Bian, Z. Q.; Nie, D. B.; Gong, Z. L.; Li, Z. B.; Huang, C. H., *Adv. Funct. Mater.* **2006,** *16*, 1441-1448. (f) Wagenknecht, P. S.; Ford, P. C., *Coord. Chem. Rev.* **2011,** *255*, 591-616. (g) Wong, W. Y.; Zhou, G. J.; Yu, X. M.; Kwok, H. S.; Lin, Z. Y., *Adv. Funct. Mater.* **2007,** *17*, 315-323. (h) Wong, W. Y.; Zhou, G. J.; Yu, X. M.; Kwok, H. S.; Tang, B. Z., *Adv. Funct. Mater.* **2006,** *16*, 838-846. (i) Yang, C. H.; Su, W. L.; Fang, K. H.; Wang, S. P.; Sun, I. W., *Organometallics* **2006,** *25*, 4514-4519. (j) Zanoni, K. P. S.; Coppo, R. L.; Amaral, R. C.; Iha, N. Y. M., *Dalton Trans.* **2015,** *44*, 14559-14573. (k) Zhou, G. J.; Wong, W. Y.; Yao, B.; Xie, Z. Y.; Wang, L. X., *Angew. Chem. Int. Ed.* **2007,** *46*, 1149-1151.

(8) (a) Chen, Z. Q.; Bian, Z. Q.; Huang, C. H., *Adv. Mater.* **2010,** *22*, 1534-1539. (b) Cheng, S.; Liu, S. J.; Zhou, L. X.; Xu, W. J.; Zhao, Q.; Huang, W., *Progress in Chemistry* **2011,** *23*, 679-686. (c) Guerchais, V.; Fillaut, J. L., *Coord. Chem. Rev.*

**2011,** *255*, 2448-2457. (d) Guo, Y. H.; Mei, Q. B.; Yan, F.; Wang, L. X.; Weng, J. N.; Zhang, B.; Huang, W., *Acta Physico-Chimica Sinica* **2012,** *28*, 739-750. (e) Minaev, B.; Baryshnikov, G.; Agren, H., *Phys. Chem. Chem. Phys.* **2014,** *16*, 1719-1758. (f) Wong, W. Y.; Ho, C. L., *Coord. Chem. Rev.* **2009,** *253*, 1709-1758. (g) You, Y.; Nam, W., *Chem. Soc. Rev.* **2012,** *41*, 7061-7084. (h) Zhao, Q. A.; Li, F. Y.; Huang, C. H., *Chem. Soc. Rev.* **2010,** *39*, 3007-3030. (i) Zhao, Q. A.; Liu, S. J.; Huang, W., *Macromol. Rapid Commun.* **2010,** *31*, 794-807.

(9) (a) Liu, J. L.; Liu, Y.; Liu, Q.; Li, C. Y.; Sun, L. N.; Li, F. Y., *J. Am. Chem. Soc.* **2011,** *133*, 15276-15279. (b) Yao, L. M.; Zhou, J.; Liu, J. L.; Feng, W.; Li, F. Y., *Adv. Funct. Mater.* **2012,** *22*, 2667-2672.

(10) Mu, J. J.; Feng, Q. Y.; Chen, X. D.; Li, J.; Wang, H. L.; Li, M. J., *Microchim. Acta* **2015,** *182*, 2561-2566.

(11) (a) Cho, D. G.; Kim, J. H.; Sessler, J. L., *J. Am. Chem. Soc.* **2008,** *130*, 12163-12167. (b) Cho, D. G.; Sessler, J. L., *Chem. Soc. Rev.* **2009,** *38*, 1647-1662. (c) Goswami, S.; Manna, A.; Paul, S.; Das, A. K.; Aich, K.; Nandi, P. K., *Chem. Commun.* **2013,** *49*, 2912-2914. (d) Hong, S. J.; Yoo, J.; Kim, S. H.; Kim, J. S.; Yoon, J.; Lee, C. H., *Chem. Commun.* **2009**, 189-191. (e) Lv, X.; Liu, J.; Liu, Y. L.; Zhao, Y.; Chen, M. L.; Wang, P.; Guo, W., *Sens. Actuators, B* **2011,** *158*, 405-410. (f) Madhu, S.; Basu, S. K.; Jadhav, S.; Ravikanth, M., *Analyst* **2013,** *138*, 299-306. (g) Sessler, J. L.; Cho, D. G., *Org. Lett.* **2008,** *10*, 73-75. (h) Kim, D. S.; Chung, Y. M.; Jun, M.; Ahn, K. H., *J. Org. Chem.* **2009,** *74*, 4849-4854. (i) Kim, Y. K.; Lee, Y. H.; Lee, H. Y.; Kim, M. K.; Cha, G. S.; Ahn, K. H., *Org. Lett.* **2003,** *5*, 4003-4006. (j) Lee, K. S.; Kim, H. J.; Kim, G. H.; Shin, I.; Hong, J. I., *Org. Lett.* **2008,** *10*, 49-51. (k) Khatua, S.; Samanta, D.; Bats, J. W.; Schmittel, M., *Inorg. Chem.* **2012,** *51*, 7075-7086.

(12) Bejoymohandas, K. S.; Kumar, A.; Varughese, S.; Varathan, E.; Subramanian, V.; Reddy, M. L. P., *J. Mater. Chem. C* **2015,** *3*, 7405-7420.

(13) Garces, F. O.; King, K. A.; Watts, R. J., *Inorg. Chem.* **1988,** *27*, 3464-3471.

(14) (a) *CrystalClear 2.1*, , Rigaku Corporation: Tokyo, Japan. (b) Pflugrath, J. W., *Acta Crystallogr., Sect. D: Biol. Crystallogr.* **1999,** *55*, 1718-1725.

(15) Sheldrick, G. M., *SADABS Siemens Area Detector Absorption Correction Program*, University of Göttingen, Göttingen, Germany, 1994.

(16) (a) Spek, A. L.; Vandersluis, P., *Acta Crystallogr., Sect. C: Cryst. Struct. Commun.* **1990,** *46*, 1357-1358. (b) Vandersluis, P.; Spek, A. L., *Acta Crystallogr., Sect. C: Cryst. Struct. Commun.* **1990,** *46*, 883-886. (c) Vandersluis, P.; Spek, A. L., *Acta Crystallogr., Sect. A: Found. Crystallogr.* **1990,** *46*, 194-201.

(17) deMello, J. C.; Wittmann, H. F.; Friend, R. H., *Adv. Mater.* **1997,** *9*, 230-&.

(18) Liu, Y.; Liu, M. S.; Jen, A. K. Y., *Acta Polym.* **1999,** *50*, 105-108.

(19) Gorelsky, S. I., *SWizard program (version 4.6)*, University of Ottawa, Canada, 2007.

(20) Frisch, M. J.; Trucks, G. W.; Schlegel, H. B.; Scuseria, G. E.; Robb, M. A.; Cheeseman, J. R.; Scalmani, G.; Barone, V.; Mennucci, B.; Petersson, G. A., *GAUSSIAN 09, Revision A.02*, Gaussian, Inc.: Wallingford, CT, 2009.

(21) (a) Chen, B.; Ding, Y.; Li, X.; Zhu, W.; Hill, J. P.; Ariga, K.; Xie, Y., *Chem. Commun.* **2013,** *49*, 10136-10138. (b) Ding, Y.; Li, X.; Li, T.; Zhu, W.; Xie, Y., *J. Org. Chem.* **2013,** *78*, 5328-5338. (c) Xie, Y.; Ding, Y.; Li, X.; Wang, C.; Hill, J. P.; Ariga, K.; Zhang, W.; Zhu, W., *Chem. Commun.* **2012,** *48*, 11513-11515.

(22) (a) AnalyticalMethodsCommittee, *Analyst* **1987,** *112*, 199-204. (b) Lin, Q.; Liu, X.; Wei, T. B.; Zhang, Y. M., *Chem.-Asian J.* **2013,** *8*, 3015-3021. (c) Zhu, B. C.; Gao, C. C.; Zhao, Y. Z.; Liu, C. Y.; Li, Y. M.; Wei, Q.; Ma, Z. M.; Du, B.; Zhang, X. L., *Chem. Commun.* **2011,** *47*, 8656-8658.

(23) Xu, M. L.; Che, G. B.; Li, X. Y.; Xiao, Q., *Acta Crystallogr., Sect. E: Struct. Rep. Online* **2009,** *65*, M28-U379.

(24) (a) Lee, J.; Oh, H.; Kim, J.; Park, K. M.; Yook, K. S.; Lee, J. Y.; Kang, Y., *J. Mater. Chem. C* **2014,** *2*, 6040-6047. (b) Orselli, E.; Albuquerque, R. Q.; Fransen, P. M.; Frohlich, R.; Janssen, H. M.; De Cola, L., *J. Mater. Chem.* **2008,** *18*, 4579-4590. (c) Orselli, E.; Kottas, G. S.; Konradsson, A. E.; Coppo, P.; Frohlich, R.; Frtshlich, R.; De Cola, L.; van Dijken, A.; Buchel, M.; Borner, H., *Inorg. Chem.* **2007,** *46*, 11082-11093. (d) Song, Y. H.; Yeh, S. J.; Chen, C. T.; Chi, Y.; Liu, C. S.; Yu, J. K.; Hu, Y. H.; Chou, P. T.; Peng, S. M.; Lee, G. H., *Adv. Funct. Mater.* **2004,** *14*, 1221-1226.

(25) Baranoff, E.; Curchod, B. F. E., *Dalton Trans.* **2015,** *44*, 8318-8329.

(26) (a) Hong, Y. N.; Lam, J. W. Y.; Tang, B. Z., *Chem. Commun.* **2009**, 4332-4353. (b) Hong, Y. N.; Lam, J. W. Y.; Tang, B. Z., *Chem. Soc. Rev.* **2011,** *40*, 5361-5388. (c) Huang, K. W.; Wu, H. Z.; Shi, M.; Li, F. Y.; Yi, T.; Huang, C. H., *Chem. Commun.* **2009**, 1243-1245. (d) Liu, S. J.; Sun, H. B.; Ma, Y.; Ye, S. H.; Liu, X. M.; Zhou, X. H.; Mou, X.; Wang, L. H.; Zhao, Q.; Huang, W., *J. Mater. Chem.* **2012,** *22*, 22167-22173. (e) Wu, H. Z.; Yang, T. S.; Zhao, Q. A.; Zhou, J.; Li, C. Y.; Li, F. Y., *Dalton Trans.* **2011,** *40*, 1969-1976. (f) You, Y.; Huh, H. S.; Kim, K. S.; Lee, S. W.; Kim, D.; Park, S. Y., *Chem. Commun.* **2008**, 3998-4000. (g) Zhao, N.; Wu, Y. H.; Luo, J.; Shi, L. X.; Chen, Z. N., *Analyst* **2013,** *138*, 894-900. (h) Zhao, Q.; Li, L.; Li, F. Y.; Yu, M. X.; Liu, Z. P.; Yi, T.; Huang, C. H., *Chem. Commun.* **2008**, 685-687. (i) Zhao, Z. J.; Chang, Z. F.; He, B. R.; Chen, B.; Deng, C. M.; Lu, P.; Qiu, H. Y.; Tang, B. Z., *Chem. Eur. J* **2013,** *19*, 11512-11517. (j) Zhou, J.; Chang, Z. F.; Jiang, Y. B.; He, B. R.; Du, M.; Lu, P.; Hong, Y. N.; Kwok, H. S.; Qin, A. J.; Qiu, H. Y.; Zhao, Z. J.; Tang, B. Z., *Chem. Commun.* **2013,** *49*, 2491-2493. (k) Zhou, J.; He, B. R.; Chen, B.; Lu, P.; Sung, H. H. Y.; Williams, I. D.; Qin, A. J.; Qiu, H. Y.; Zhao, Z. J.; Tang, B. Z., *Dyes. Pigm.* **2013,** *99*, 520-525.

(27) (a) Bejoymohandas, K. S.; George, T. M.; Bhattacharya, S.; Natarajan, S.; Reddy, M. L. P., *J. Mater. Chem. C* **2014,** *2*, 515-523. (b) Mei, J.; Hong, Y. N.; Lam, J. W. Y.; Qin, A. J.; Tang, Y. H.; Tang, B. Z., *Adv. Mater.* **2014,** *26*, 5429-5479. (c) Mei, J.; Leung, N. L. C.; Kwok, R. T. K.; Lam, J. W. Y.; Tang, B. Z., *Chem. Rev.* **2015,**

*115*, 11718-11940. (d) Sathish, V.; Ramdass, A.; Thanasekaran, P.; Lu, K. L.; Rajagopal, S., *J. Photochem. Photobiol., C* **2015,** *23*, 25-44. (e) Zhu, Y. C.; Zhou, L.; Li, H. Y.; Xu, Q. L.; Teng, M. Y.; Zheng, Y. X.; Zuo, J. L.; Zhang, H. J.; You, X. Z., *Adv. Mater.* **2011,** *23*, 4041-4046.

(28) Renny, J. S.; Tomasevich, L. L.; Tallmadge, E. H.; Collum, D. B., *Angew. Chem. Int. Ed.* **2013,** *52*, 11998-12013.

(29) Chen, C. L.; Chen, Y. H.; Chen, C. Y.; Sun, S. S., *Org. Lett.* **2006,** *8*, 5053-5056.

(30) (a) Beeby, A.; Bettington, S.; Samuel, I. D. W.; Wang, Z. J., *J. Mater. Chem.* **2003,** *13*, 80-83. (b) Welby, C. E.; Gilmartin, L.; Marriott, R. R.; Zahid, A.; Rice, C. R.; Gibson, E. A.; Elliott, P. I. P., *Dalton Trans.* **2013,** *42*, 13527-13536.

(31) (a) Buschmann, H.-J.; Dutkiewicz, E.; Knoche, W., *Berichte der Bunsengesellschaft für physikalische Chemie* **1982,** *86*, 129-134. (b) Cabani, S.; Gianni, P.; Matteoli, E., *J. Phys. Chem.* **1972,** *76*, 2959-2966. (c) Greenzaid, P.; Luz, Z.; Samuel, D., *J. Am. Chem. Soc.* **1967,** *89*, 749-756. (d) McDonald, R. S.; Martin, E. V., *Can. J. Chem.* **1979,** *57*, 506-516.

# Chapter 4

## AIPE-Active Green Phosphorescent Iridium(III) Complex Impregnated Test Strips for the Vapor-Phase Detection of 2,4,6-Trinitrotoluene (TNT)

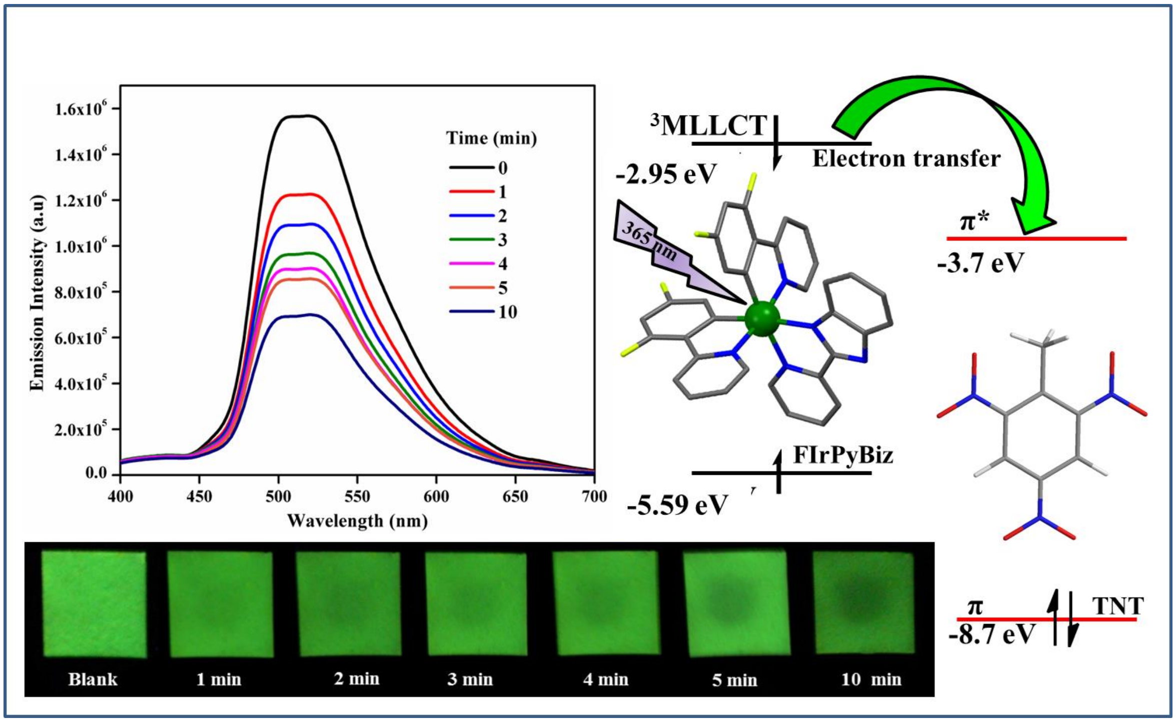

### 4.1. Abstract

*Detection of explosives, especially trinitrotoluene (TNT), is of utmost importance due to its highly explosive nature and environmental hazard. Therefore, detection of TNT has been a matter of great concern to the scientific community worldwide. Herein, a new aggregation-induced phosphorescent emission (AIPE)-active bis(2-(2,4-difluorophenyl)pyridinato-N,C2')iridium(III) (2-(2-pyridyl)benzimidazolato-N,N') complex [**FIrPyBiz**] has been developed and serves as a molecular probe for the detection of TNT in the vapor phase, solid phase, and aqueous media. In addition,*

*phosphorescent test strips have been constructed by impregnating Whatman filter paper with aggregates of* ***FIrPyBiz*** *for trace detection of TNT in contact mode, with detection limits in nanograms, by taking advantage of the excited state interaction of AIPE-active phosphorescent iridium(III) complex with that of TNT and the associated photophysical properties.*

**K. S. Bejoymohandas**; T. M. George; S. Bhattacharya; S. Natarajan; and M. L. P. Reddy, *Journal of Materials Chemistry C*, 2, **2014**, 515–523.

## 4.2. Introduction

The development of cyclometalated iridium(III) complexes as efficient luminescent materials has received tremendous attention due to their potential applications in OLEDs,[1] organic photovoltaics,[2] luminescence sensing,[3] and biomedical imaging.[4] The design of solid state emitting materials, with high quantum yield based on iridium(III) complexes, is important in the development of efficient electroluminescent devices. However, the emissive triplet excited state of some of the iridium(III) complexes is often quenched in the aggregation state, which limits their applications. Li and co-workers[5] discovered the aggregation-induced phosphorescent emission (AIPE) phenomenon for the first time in iridium(III) complexes by carrying out X-ray diffraction studies as well as DFT calculations, and explained it on the basis of the formation of excimers *via* π–π stacking of adjacent pyridyl rings of 2-phenylpyridine ligands. Later, through intensive theoretical calculations and by using photophysical data, Park *et al.*[6] concluded that the restriction of intramolecular rotation was the main cause of the AIPE. Recently many AIPE-active cyclometalated iridium(III) complexes have been utilized for the sensing of metal ions and bioprobes for cellular imaging.[7] Tang and coworkers[8] have made pioneering contributions to understanding the AIPE in many luminogenic materials and explained the AIPE phenomenon on the basis of restriction of intramolecular rotations (RIR) in aggregated states, which blocks the non-radiative pathway and opens up the radiative channel. As a result, the molecules become emissive in the aggregate state.[9]

As a result of illegal transport and terrorist activities, the detection of chemical explosives is of prime importance for military operations, homeland security, environmental cleaning and human security. TNT is a commonly used explosive in landmines and military operations that contaminates the environment and ground water, posing a threat to human health.[10] Therefore, the development of cost-efficient, selective, sensitive and portable detection methods for TNT is highly desirable. The detection of low quantities of TNT is particularly challenging, due its relatively low vapor pressure compared to other explosive chemicals.[11] Consequently, several approaches using quantum dots,[12] gold nanoparticles,[13] silver–gold alloy nanostructures,[14] conjugated polymers,[15] self-assembled ultrathin films[16] and fluorescent molecular assemblies and gels[10a, 17] have been reported for the detection of TNT. However, to the best of our knowledge, AIPE materials based on iridium(III) complexes for the detection of explosives have not been identified until now. In order to develop efficient luminescent materials based on iridium(III) complexes, an attempt has been made in our laboratory to design a new class of iridium(III) complex featuring 2,6-difluorophenylpyridine as a cyclometalating ligand and a series of ancillary ligands consisting of 2-(pyridyl)-1*H*-benzimidazole, 2-(2′-hydroxyphenyl)benzimidazole, 2-(2′-hydroxyphenyl)benzothiazole. The photophysical studies demonstrated that the bis(2-(2,4-difluorophenyl)pyridinato-*N*,*C*2′)iridium(III) (2-(2-pyridyl)benzimidazolato-*N*,*N*′) complex [**FIrPyBiz**] (Chart 4.1) exhibits a superior aggregation induced phenomenon in an acetone–water mixture compared to other iridium(III) complexes. Hence **FIrPyBiz** has been chosen to further investigate the sensing behaviour of nitro explosives. Herein, we have demonstrated the first example of the detection of TNT by a AIPE-active iridium(III) complex in vapor, solid and aqueous phases.

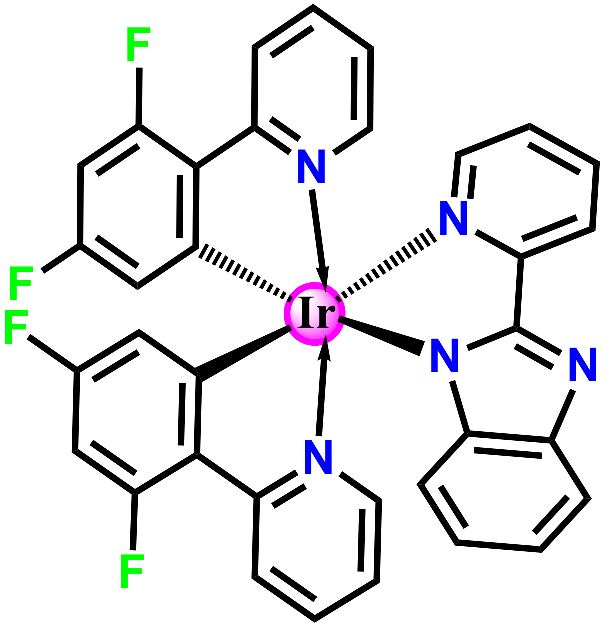

**Chart 4.1.** Chemical structure of the iridium(III) complex **FIrPyBiz**.

## 4.3. Experimental Section

### 4.3.1. Materials

Sodium carbonate, tetrakis(triphenylphosphine)palladium(0), 2-bromopyridine, 2,4-difluorophenylboronic acid, 2-pyridyl benzimidazole **(PyBiz)** and $IrCl_3 \cdot x(H_2O)$ were purchased from Sigma Aldrich and were used without any further purification. The cyclometalated chelating ligand 2-(2,4-difluorophenyl) pyridine (**dfppy**) and the corresponding chloride-bridged dimer $[(dfppy)_2Ir(\mu\text{-}Cl)]_2$ were synthesized according to previously reported procedures.[18] All the nitroaromatics used in this work, such as picric acid (PA), 2,4-dinitrotoluene (DNT), *o*-nitrotoluene (*o*NT), *p*-nitrotoluene (*p*NT) and nitrobenzene (NB), and other organic compounds such as benzoquinone (BQ), benzoic acid (BA) and nitromethane (NM) of analytical grade, were also obtained from Sigma Aldrich and used directly without any further purification. 2,4,6-Trinitrotoluene (TNT) was prepared according to the synthesis procedure reported elsewhere.[19] (Caution: since the TNT used in the present study is a highly explosive chemical, it should only be handled in small quantities). All other reagents were of an analytical grade and were used as received. Reactions were monitored by thin layer chromatography (TLC). Commercial TLC plates (silica gel 60 F254, Merck Co.) were used and the spots were observed under UV light at 254 and 365 nm. Silica column chromatography was performed using silica gel (100–200 mesh, Merck Co.).

### 4.3.2. Synthesis of FIrPyBiz

The iridium dimer $[(\text{dfppy})_2\text{Ir}(\mu\text{-Cl})]_2$ (0.300 g, 0.246 mmol), sodium carbonate (0.287 g, 2.71 mmol) and 2.6 equivalent ancillary ligand (2-pyridyl benzimidazole) were dissolved in 30 mL of 2-ethoxy ethanol. The reaction vessel was degassed and maintained under a nitrogen atmosphere. The reaction mixture was stirred for 15 h at 140 °C. The cooled crude mixture was then poured into ethyl acetate (100 mL) and extracted with water (75 mL × 3 times) to remove the 2-ethoxy ethanol. The organic layer was dried over anhydrous sodium sulfate and was vacuum dried. The crude product obtained was purified using silica column chromatography with ethyl acetate: *n*-hexane (5 : 1) to give a yellow solid, which was further recrystallized from a dichloromethane–hexane mixture, vacuum dried at 80 °C and subjected to additional characterization techniques. Yield 70% (0.273 g); $^1$H NMR (500 MHz, $CDCl_3$): $\delta$ 8.62 (d, $J$ = 8.0 Hz, 1H), 8.25 (t, $J$ = 9.7 Hz, 2H), 7.90 (t, $J$ = 7.7 Hz, 1H), 7.79 (d, $J$ = 7.9 Hz, 2H), 7.68 (dt, $J$ = 15.9, 8.6 Hz, 3H), 7.55 (d, $J$ = 5.7 Hz, 1H), 7.20 (t, $J$ = 6.4 Hz, 1H), 7.14 (t, $J$ = 7.5 Hz, 1H), 6.87 (q, $J$ = 6.7 Hz, 3H), 6.56 (dt, $J$ = 27.9, 10.8 Hz, 2H), 6.28 (d, $J$ = 8.2 Hz, 1H), 5.84 (dd, $J$ = 19.4, 9.2 Hz, 2H). $^{13}$C NMR (126 MHz, $CDCl_3$) $\delta$ 165.39, 154.09, 153.29, 149.90, 149.32, 148.39, 143.71, 138.50, 137.98, 137.77, 128.52, 124.77, 123.05, 122.36, 121.82, 118.79, 115.27, 114.38, 98.77. MS (FAB): $m/z$ $[M + 1]^+$ calcd: 768.13, found: 768.39. Elemental analysis calcd (%) for $C_{34}H_{20}F_4IrN_5$: C 53.26, H 2.63, N 9.13; found: C 53.26, H 2.58, N 9.13.

### 4.3.3. Physical Measurements

A Bruker 500 MHz NMR spectrometer was used to record the $^1$H and $^{13}$C NMR spectra of the complex in $CDCl_3$ solution. The mass spectrum was recorded on a JEOL JSM 600 fast atom bombardment (FAB) high resolution mass spectrometer (FAB-MS). Elemental analysis was performed with a Perkin-Elmer Series 2 Elemental Analyzer 2400. The absorbance spectrum of the complex was measured with a UV-vis spectrophotometer (Shimadzu, UV-2450). Neat films of the complexes on quartz plates were used for the diffuse reflectance spectra on a Shimadzu, UV-2450 UV-vis-NIR spectrophotometer, using $BaSO_4$ as a reference. The reflectance data were converted into absorption using the Kubelka–Munk function. The photoluminescence (PL) spectrum of the iridium(III) complex was recorded on a Spex-Fluorolog FL22 spectrofluorimeter equipped with a double grating 0.22 m Spex 1680 monochromator and a 450 W Xe lamp as the excitation source. Transmission electron microscopy (TEM) and electron diffraction (ED) pattern analysis were performed on a JEOL 2010 (200 kV) in an AIPE complex solution (70% $H_2O$ + 30% acetone) and placed on a carbon-coated grid and allowed to dry at room temperature.

### 4.3.4. Quantum Yield Measurements

Photoluminescence quantum yield of the powder sample and the solution state were measured using a calibrated integrating sphere in a SPEX Fluorolog Spectrofluorimeter. A Xe-arc lamp was used to excite the sample placed in the sphere, with 365 nm as the excitation wavelength. Absolute quantum yield was calculated on the basis of the de Mello method[20] using the equation

$$\Phi_{\mathrm{PL}} = [E_{\mathrm{i}}(\lambda) - (1 - A)E_0(\lambda)]/L_{\mathrm{e}}(\lambda)A \qquad (1)$$

In eqn (2)

$$A = [L_0(\lambda) - L_{\mathrm{i}}(\lambda)]/L_0(\lambda) \qquad (2)$$

where $E_{\mathrm{i}}(\lambda)$ and $E_0(\lambda)$ are the integrated luminescence as a result of direct excitation of sample and secondary excitation, respectively. $A$ is the absorbance of the sample calculated using eqn (1). $L_{\mathrm{i}}(\lambda)$ is the integrated excitation when the sample is directly excited, $L_0(\lambda)$ is the integrated excitation when the excitation light first hits the sphere and reflects to the sample, and $L_{\mathrm{e}}(\lambda)$ is the integrated excitation profile for an empty sphere.

### 4.3.5. Electrochemical Measurements

Cyclic voltammetry experiments were carried out with a BAS 50W voltammetric analyzer using three electrode cell assemblies. Pt wires were used for counter electrodes, a quasi Ag/Ag$^+$ wire was used for a reference electrode and a platinum electrode was used as a working electrode. Measurements were carried out in acetonitrile solution, with tetrabutylammonium hexafluorophosphate as a supporting electrolyte, at a scan rate of 100 mV $s^{-1}$. Concentrations of the iridium(III) complex and supporting electrolyte were $5 \times 10^{-3}$ and 0.1 M, respectively. The ferrocenium/ferrocene couple ($FeCp_2^+/FeCp_2^0$) was used as an internal reference. The energy level of $Fc/Fc^+$ was assumed to be −4.8 eV in a vacuum.[21] All solutions for the electrochemical studies were deaerated with pre-purified Ar gas prior to the measurements.

### 4.3.6. Lifetime Measurements

Phosphorescence lifetimes were measured using an IBH (FluoroCube) time-correlated picosecond single photon counting (TCSPC) system. A pulsed diode laser (<100 ps pulse duration) at a wavelength of 375 nm (NanoLED-10) was used to excite the MLCT states of the complexes with a repetition rate of 50 kHz. The detection system consists of a microchannel plate photomultiplier (5000U-09B, Hamamatsu) with a 38.6 ps response time, coupled to a monochromator (5000 M) and TCSPC electronics (Data Station Hub included Hub-NL, a NanoLED controller and preinstalled Fluorescence Measurement and Analysis Studio (FMAS) software). The phosphorescence lifetime values were determined by deconvolution of the instrument response function with biexponential decay using DAS6 decay analysis software. The quality of the fit has been judged by the fitting parameters, such as $\chi^2$ (<1.2), as well as the visual inspection of the residuals.

### 4.3.7. X-ray Crystal Structure Determination

Single crystals of **FIrPyBiz** suitable for X-ray diffraction studies were grown from a concentrated solution of the complex in a mixture of dichloromethane and hexane. The single-crystal XRD data were collected with a Bruker AXS Smart Apex CCD diffractometer at 293 K. The X-ray generator was operated at 50 kV and 35 mA using Mo Kα ($\lambda$ = 0.71073 Å) radiation. The data were reduced using SAINT+,[22] and an empirical absorption correction was applied using the SADABS program.[23] The structure was solved and refined by using SHELXL-97 in the WINGX suite of programs (v.1.63.04a).[24] The highly disordered solvent molecules in the compound **FIrPyBiz** were accounted for by using the SQUEEZE program present in the WinGX platon program.[25] All of the hydrogen positions were initially located in the difference Fourier maps, and for the final refinement, the hydrogen atoms were placed in geometrically ideal positions and refined in the riding mode. Final refinement included the atomic positions of all of the atoms, anisotropic thermal parameters for all of the non-hydrogen atoms, and isotropic thermal parameters for all of the hydrogen atoms. Full-matrix least-squares refinement against $F^2$ was carried out using the WINGX package of programs.[26] The solvents, like dichloromethane and hexane, present in the compound (a total of 92 electrons) were removed from the single crystal structure using the SQUEEZE program. Selected crystal data and data collection and refinement parameters are listed in Table 4.1.

**Table 4.1.** Crystallographic and refinement data for **FIrPyBiz**

| | **FIrPyBiz** |
|---|---|
| Formula | $C_{34}H_{20}F_4IrN_5$ |
| Molecular weight | 766.75 |
| Crystal system | Triclinic |
| Space group | $P\bar{1}$ |
| Crystal size (mm$^3$) | 0.20 × 0.14 × 0.11 |
| $a$ [Å] | 12.5196(3) |
| $b$ [Å] | 16.0199(5) |
| $c$ [Å] | 17.2926(4) |
| $\alpha$ [°] | 99.607(2) |
| $\beta$ [°] | 101.025(2) |
| $\gamma$ [°] | 106.326(2) |
| $V$ [Å$^3$] | 3176.08(14) |
| $Z$ | 4 |
| $\rho_{\text{calc}}$[g cm$^{-1}$] | 1.604 |
| Temp (K) | 293 |
| $\mu$ (Mo K$_\alpha$) (mm$^{-1}$) | 4.258 |
| Reflections collected | 24 642 |
| Independent reflections | 12 493 |
| $R_F$, $R_w(F^2)$ (all data) | 0.0524, 0.0871 |
| $R_F$, $R_w(F^2)$ [$I > 2\sigma(I)$] | 0.0361, 0.0790 |
| GOF | 1.000 |
| CCDC | 1435265 |

## 4.3.8. Experimental Methods for the Detection of TNT

**Preparation of filter paper test strips:** Filter paper (2 cm × 2 cm) test strips were prepared by dip-coating the **FIrPyBiz** solution in dichloromethane ($1 \times 10^{-4}$ M) followed by removal of solvent under a vacuum at room temperature. The dip-coating of the solution allowed the adsorption of **FIrPyBiz** on the filter paper and shows a greenish emission under UV-illumination (365 nm). These paper strips were used for the detection of TNT.

**Detection of TNT in drinking water:** A stock solution of TNT ($1 \times 10^{-3}$ M) was prepared by dissolving the TNT in drinking water while stirring overnight at room temperature (0.228 mg $mL^{-1}$). This solution was diluted to different concentrations and used as the test samples.

**Contact mode visual detection of TNT:** The TNT solution of various concentrations in drinking water ($1 \times 10^{-15}$ to $1 \times 10^{-3}$ M) were spotted onto the test strips at the desired concentration level using a glass micro-syringe. A solvent blank was spotted near the spot of each explosive. In order to ensure consistent analysis, all depositions were prepared from a 10 μL volume, thereby producing a spot of ∼0.5 cm in diameter. After solvent evaporation, the filter paper was illuminated with a 365 nm UV light. The dark spots were identified by an independent observer, and each set of experiments was repeated three times for consistency. The test strip was placed in such a way that the excitation beam fell on the spot where TNT was added. Emission was collected by a front face mode using a film sample holder. Emission of a blank sample was monitored by the addition of a solvent alone. The detection limit was calculated from the lowest concentration of TNT that enabled an independent observer to visually detect the quenching.

**Vapor phase detection of TNT:** The saturated vapors of TNT were created by keeping solid TNT (100 mg) in a sealed vial for 24 h at room temperature. The test strips were placed on top of the glass vial containing saturated TNT vapors for definite time intervals at room temperature. The circular area that was exposed to the

TNT vapors was quenched. The emission intensity was measured before and after exposure of the sample. All the measurements were carried out in a front face mode.

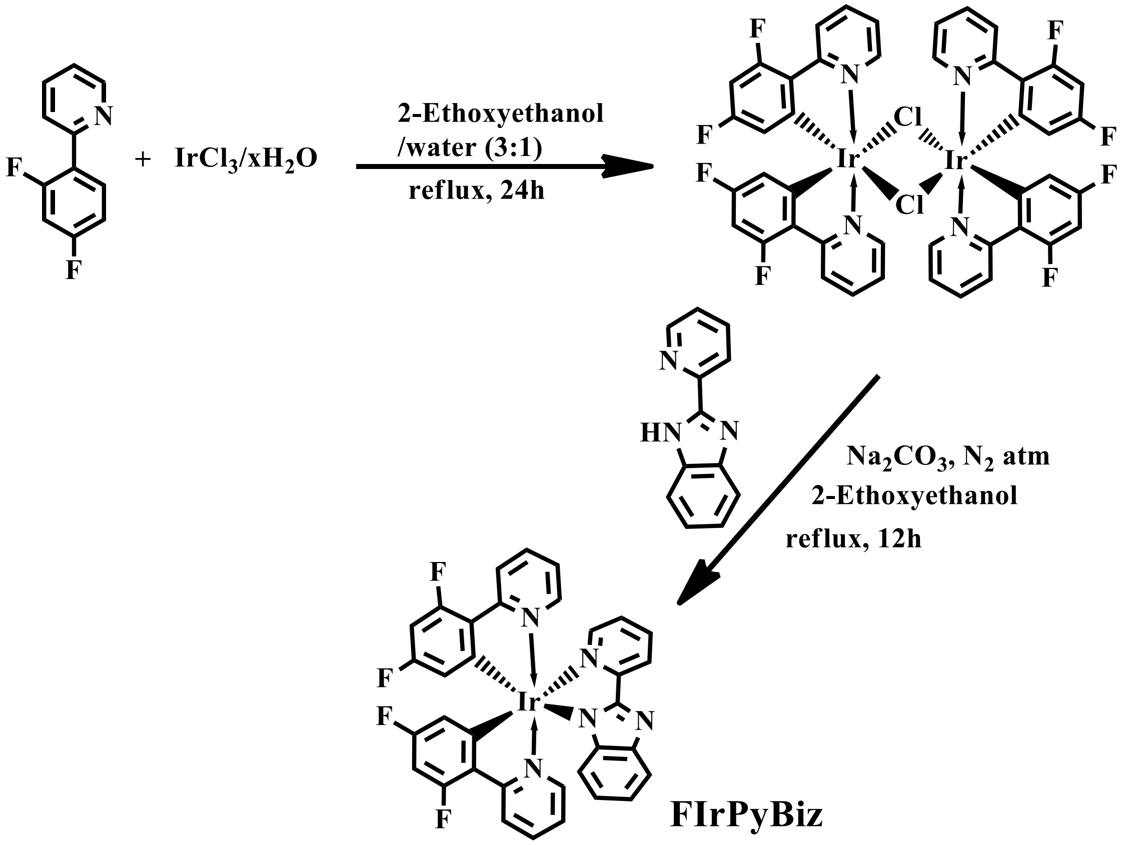

**Scheme 4.1.** Synthetic Routes of Heteroleptic Ir$^{3+}$ Complex **FIrPyBiz**

## 4.4. Results and Discussion

### 4.4.1. Synthesis and Characterization

The synthetic route of **FIrPyBiz** is shown in Scheme 4.1. Treatment of the iridium dimer of 2-(2,4-difluorophenyl)pyridine $[(dfppy)_2Ir(\mu\text{-}Cl)]_2$ with a corresponding ancillary ligand 2-pyridyl benzimidazole by a bridge-splitting reaction in 2-ethoxyethanol, readily produces the iridium(III) bis(2-(2,4-difluorophenyl)pyridinato-

*N*,*C*2′)(2-(2-pyridyl)benzimidazolato-*N*,*N*′) complex (**FIrPyBiz**) in a good yield (70%). The final product was obtained after chromatographic purification. The synthesized iridium complex (**FIrPyBiz**) has been fully characterized by $^1$H, $^{13}$C NMR spectroscopy, FAB-Mass spectrometry and elemental analysis.

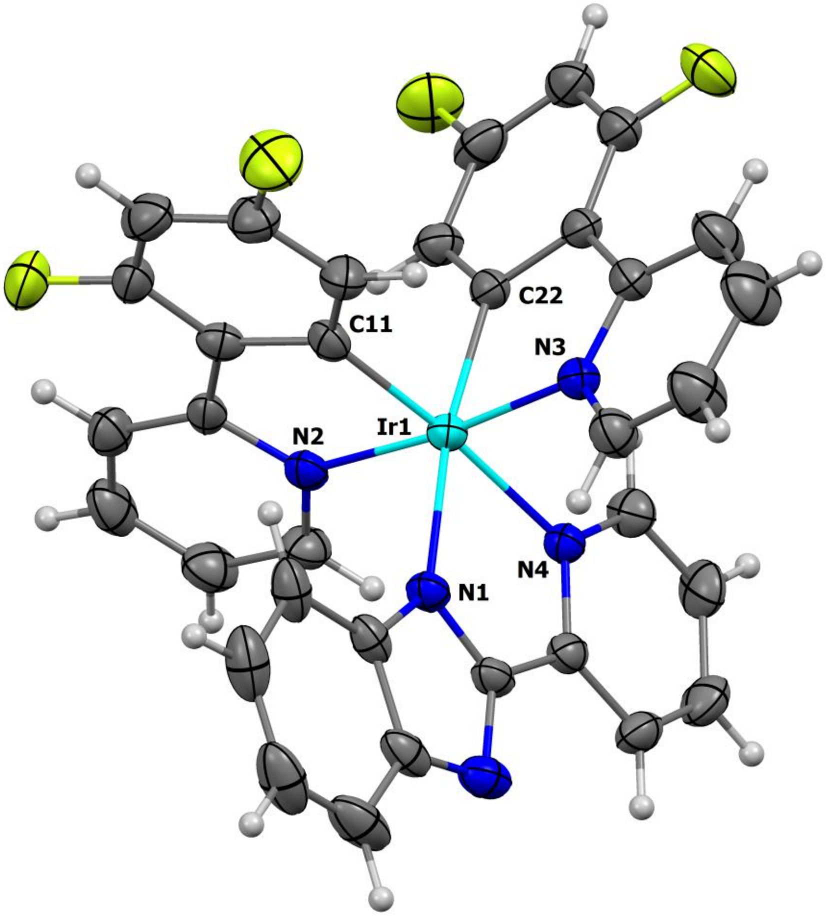

**Figure 4.1.** Crystal structure of complex **FIrPyBiz** with the atom numbering scheme. Thermal ellipsoid drawing is presented at the 30% probability level. Selected bond lengths (Å) and angles (°): Ir1–C11 2.000(5), Ir1–C22 2.014(5), Ir1–N4 2.147(4), Ir1–N1 2.125(5), Ir1–N3 2.057(4), Ir1–N2 2.054(4); N3–Ir1–N2 171.7(2), C11–Ir1–N4 174.5(2)s, C22–Ir1–N1 173.2(2).

**FIrPyBiz** was structurally authenticated by single-crystal X-ray diffraction analysis. The compound crystallizes in the triclinic space group $P\bar{1}$. The central Ir$^{3+}$ion is surrounded by two nitrogen and two carbon atoms from two cyclometalated 2-(2,4-diflurophenyl) pyridine ligands, and two nitrogen atoms from an ancillary ligand 2-pyridylbenzimidazole, as shown in Figure 4.1. The coordination polyhedra can be best described as distorted octahedral geometry. The dfppy ligands adopt a mutually eclipsed configuration with the nitrogen atoms N(2) and N(3) residing at the *trans* locations while the Ir–N distances lie between 2.053(4) and 2.056(4) Å. The cyclometalated carbon atoms C(11) and C(22) are mutually *cis* on the iridium and show similar distances of 2.000(5) and 2.014(5) Å. The PyBiz ligand displays slightly elongated Ir–N distances of 2.125(4) and 2.147(4) Å *vs.* those of the *trans*-orientated Ir–N distances of the dfppy ligands. The overall molecular structure is similar to the earlier reported iridium(III) complexes.[27]

The electrochemical properties of **FIrPyBiz** were investigated by cyclic voltammetry (Figure 4.2 and Table 4.2). The HOMO levels of the complex were calculated from the oxidation potentials and the LUMO levels were calculated from the reduction potential. As summarized in Table 4.2, the HOMO/LUMO levels of **FIrPyBiz** are −5.59/−2.95 eV.

**Table 4.2.** Electrochemical data of **FIrPyBiz**

| | $E_{\text{oxd}}$ (V) | $E_{\text{red}}$ (V) | HOMO[a] (eV) | LUMO[b] (eV) | $E_{\text{g, ec}}$[c] (V) | $E_{\text{g,opt}}$[d] (V) |
|---|---|---|---|---|---|---|
| **FIrPyBiz** | 1.25 | −1.38 | −5.59 | −2.95 | 2.64 | 2.60 |

[a] HOMO = $-(4.8 - 0.46 + E_{\text{oxd}})$ eV. [b] LUMO = $-(4.8 - 0.46 + E_{\text{red}})$ eV. [c] Electrochemical band gap, estimated from $E_{\text{g, ec}} = E_{\text{LUMO}} - E_{\text{HOMO}}$. [d] Optical band gap, estimated from the absorption edge.

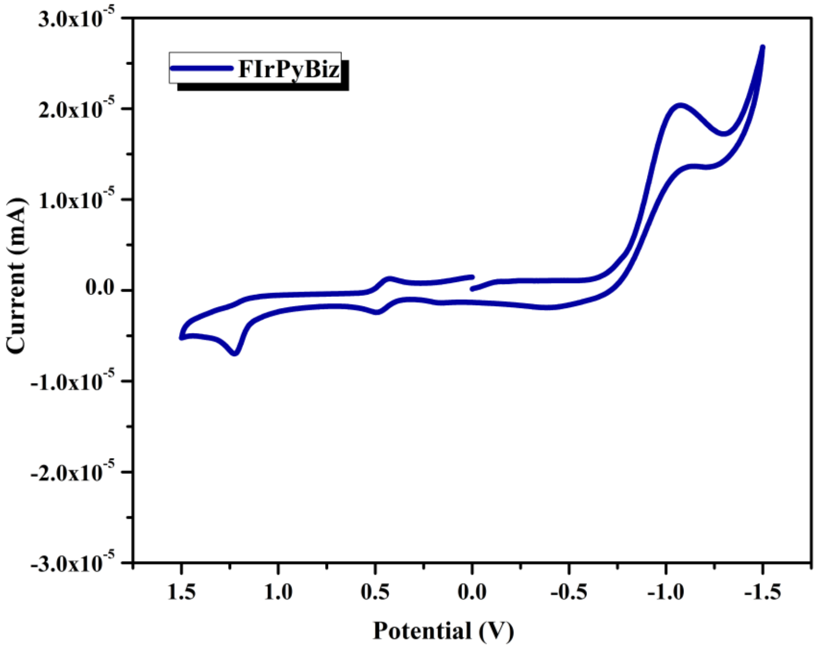

**Figure 4.2.** Cyclic voltammograms of **FIrPyBiz** at a scan rate of 100 mVs$^{-1}$.

### 4.4.2. Photophysical Properties

The UV-vis absorption spectra of the dfppy ligand, PyBiz and the new complex **FIrPyBiz** in dichloromethane at $c = 1 \times 10^{-5}$ M are displayed in Figure 4.3 and the pertinent data are summarized in Table 4.3. The major absorption bands of the ligands are in the region 235–320 nm. For the complex **FIrPyBiz**, the absorption peaks appearing before 300 nm are assigned to spin-allowed ligand-centered ($\pi \rightarrow \pi^*$) transitions. However after coordinating with the Ir$^{3+}$atom, this band becomes broader than that of the free ligands. On the other hand, somewhat weaker bands are observed at lower energy after 320 nm, which correspond to electronic excitations to the allowed and spin-forbidden metal-to-ligand charge-transfer states ($^1$MLCT and $^3$MLCT, respectively) and LLCT transition. **FIrPyBiz** exhibits weak emission in soluble organic solvents such as acetone, with low quantum yield in air-equilibrated acetone solution ($\Phi_{\text{solution}} < 0.01\%$) (Table 4.3). On the other hand, bright greenish yellow emission is observed in the solid state (Figure 4.4) with a quantum yield of 7.4% in air at an ambient temperature. Thus, **FIrPyBiz** exhibits remarkable AIPE with $\Phi_{\text{solid}}/\Phi_{\text{solution}} = 7.4 \times 10^2$.

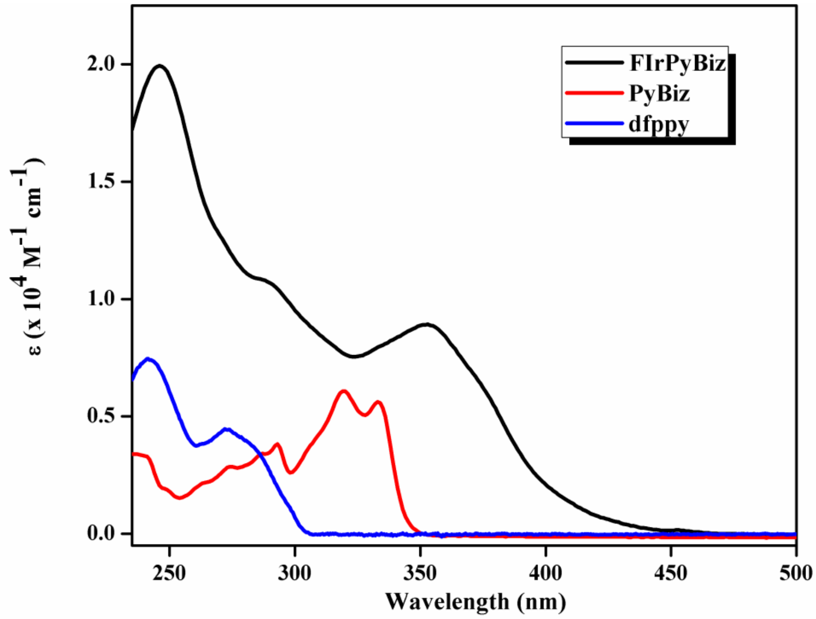

**Figure 4.3.** Absorption spectra of **dfppy**, **FIrPyBiz** and **PyBiz** in $CH_2Cl_2$ solution ($c = 1\times10^{-5}$ M).

**Table 4.3.** Photophysical data of **FIrPyBiz**

| | Absorption[a] | Emission, 298 K | | | |
|---|---|---|---|---|---|
| | $\lambda_{max}$, (nm) ($\varepsilon$, $10^4$ $M^{-1}$ $cm^{-1}$) | $\lambda_{max}$ (nm)[b] | $\lambda_{max}$ (nm)[c] | $\Phi_{PL}$[d] | $\Phi_{PL}$[e] |
| **FIrPyBiz** | 245 (1.98), 351 (0.80) | 508 | 550 | 0.01% | 7.4% |

[a]Absorption spectrum were measured in dichloromethane solution; [M] = 1.0 x $10^{-5}$. [b]Emission spectrum was measured in acetone; [M] = 5.0 x $10^{-5}$, $\lambda_{exc}$= 365 nm. [c]Emission spectrum in solid state, $\lambda_{exc}$= 365 nm. [d]Solution state phosphorescence quantum efficiency. [e]Solid state phosphorescence quantum efficiency.

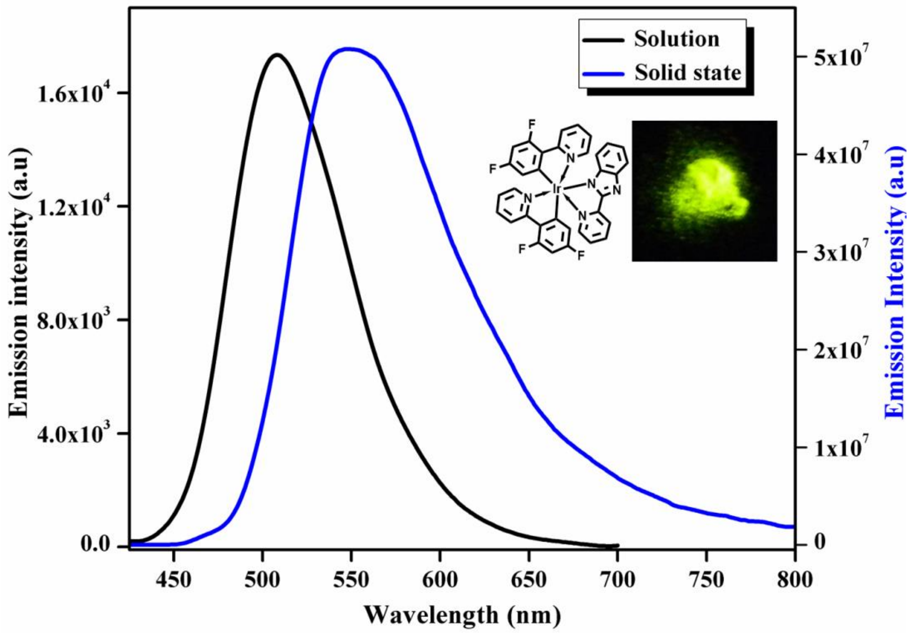

**Figure 4.4.** Room temperature emission spectrum of **FIrPyBiz** in acetone solution (*c* = 5μM) and in solid state ($\lambda_{exc}$ = 365 nm).

To investigate the AIPE properties of **FIrPyBiz**, the photoluminescent (PL) spectrum of the iridium(III) complex in different ratios of water–acetone mixtures has been studied and the results are depicted in Figure 4.5. Since water is a non-solvent of **FIrPyBiz**, the complex aggregates in mixtures at high water ratios. The results demonstrated that the complex in pure acetone solvent exhibits a faint emission. However, it is interesting to note that the emission intensity of the complex is remarkably enhanced ($1.28 \times 10^2$ fold) when the water fraction exceeds 70%, indicating that **FIrPyBiz** has a significant AIPE effect. The AIPE phenomenon may be further attributed to the excimeric interactions between the cyclometalating ligands of adjacent complexes, resulting in a switch from the non-emissive $^3$LX excited state to the emissive $^3$MLLCT transition.[5, 28]

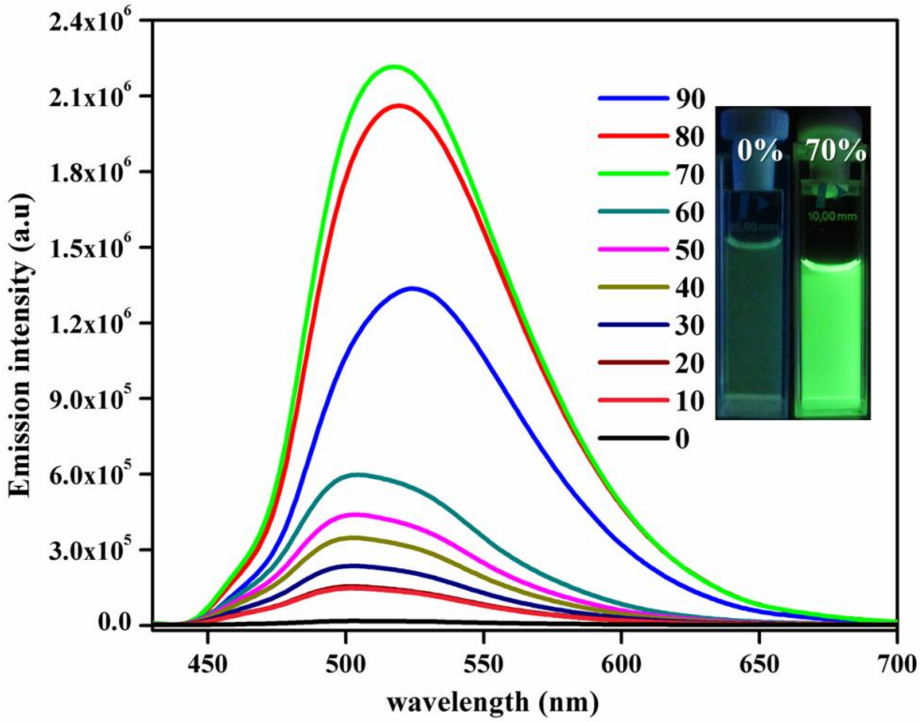

**Figure 4.5.** Emission spectrum of **FIrPyBiz** (*c* = 5μM) in acetone–water mixtures with different water fractions (0–90%) at room temperature ($\lambda_{exc}$ = 365 nm).

A critical account on π–π stacking in metal complexes with aromatic nitrogen-containing ligands revealed that a near face-to-face π-stacking interaction is a rare phenomenon.[29] Usually the π-ring planes overlap in an offset or displaced geometry. A similar phenomenon has been noticed in the present study after the scrutiny of the crystal structure of **FIrPyBiz**, as depicted in Figure 4.6. The π-ring planes of the pyridyl moiety of dfppy and diflurophenyl unit of the adjacent dfppy ligand are overlapped in an offset or displaced geometry, with a plane to plane distance of 3.35 Å. Similar interactions have also been reported elsewhere in blue-green phosphorescent iridium(III) complexes.[28] Furthermore, the CF···π interactions between pyridine and difluorophenyl units of dfppy ligands with an interplanar separation of 3.38 Å are also observed. In solution, the ancillary ligand PyBiz dominates the excited state properties, which switches the photoluminescent decay of the dfppy-centered $^3$MLCT state, leading to a very weak emission in solution. On the other hand, in the solid state strong π–π and CF···π interactions of dfppy ligands elongate the overall π-conjugation degree and reduce the energy level of π* of dfppy. As a result, the triplet energy level of the charge transfer state from iridium to the interacting dfppy is reduced and the dfppy ligands are involved in the excited state of **FIrPyBiz** in the solid state. Hence, the emission of $^3$MLLCT based on the interaction of dfppy is observed and red shifted significantly (~40 nm = 1437 cm$^{-1}$).

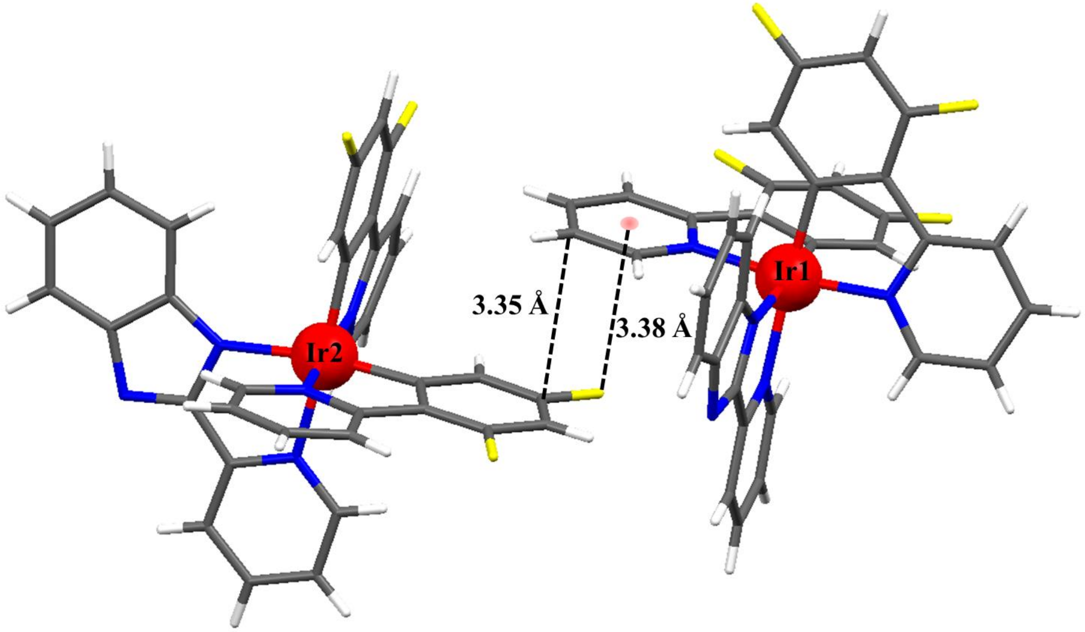

**Figure 4.6.** Crystal structure shows the molecular packing in **FIrPyBiz**.

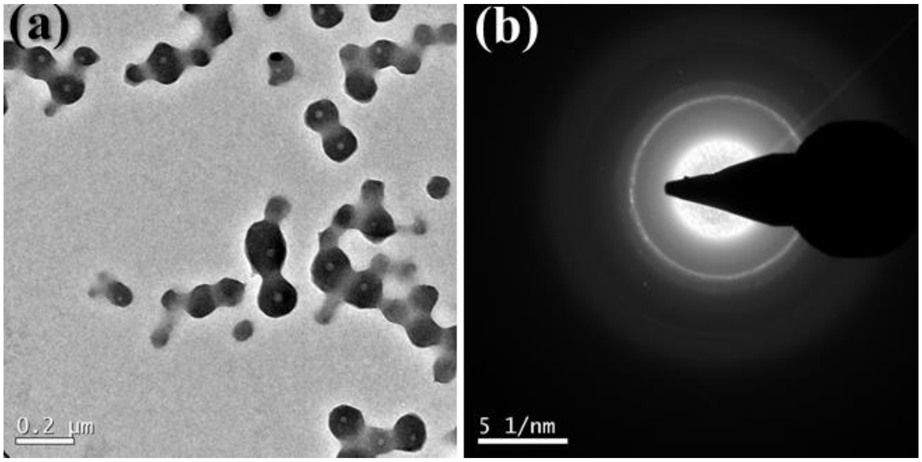

**Figure 4.7.** TEM image (a) of aggregates of **FIrPyBiz** and ED pattern (b) formed in water/acetone mixtures with water content of 70%, respectively.

In order to know more about the morphology of the AIPE sample, the TEM and ED measurements have been performed for an aggregated sample (70% $H_2O$ + 30% acetone containing **FIrPyBiz**; $c$ = 5 µM) and the results are displayed in Figure 4.7. The presence of nano-aggregates in the TEM picture clearly suggests that the enhanced emission of **FIrPyBiz** is due to the formation of aggregates. Moreover, these aggregates show only a ring type diffuse halo as observed from the ED pattern, indicating the polycrystalline nature of the AIPE sample.

### 4.4.3. TNT Detection: Solution State

The phosphorescent emission response of the nano-aggregates of **FIrPyBiz**, in an acetone–water mixture with 70% water content, against TNT is shown in Figure 4.8.

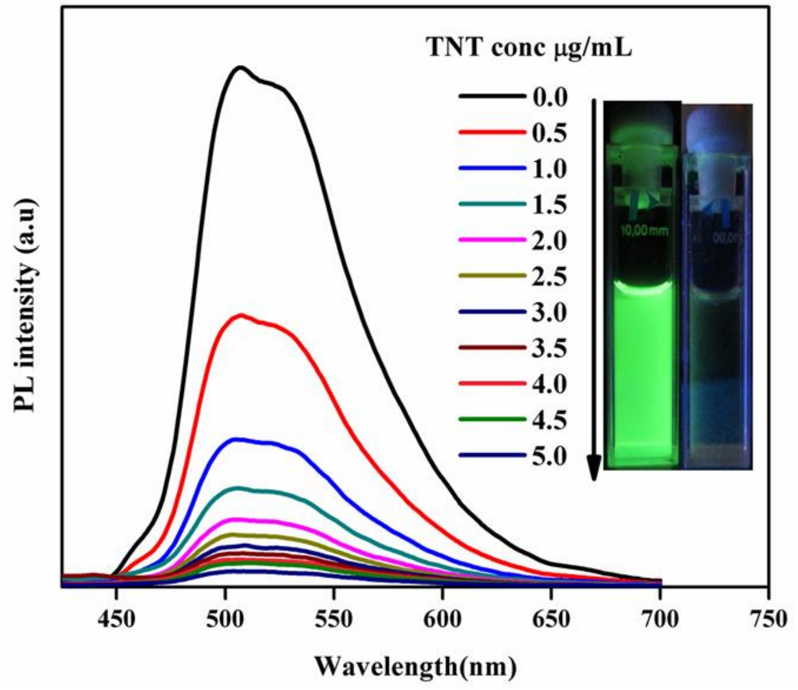

**Figure 4.8.** Phosphorescence spectra of **FIrPyBiz** (c = 5μM) in acetone–water (30: 70%) containing different amounts of TNT ($\lambda_{exc}$ = 365 nm).

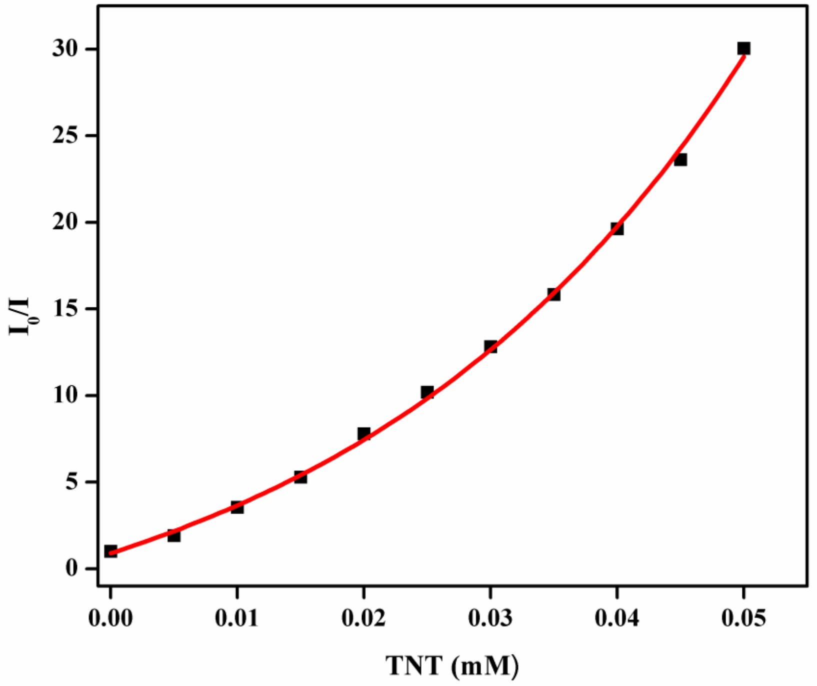

**Figure 4.9.** Stern – Volmer plots of relative PL intensities ($I_0/I$) versus TNT concentrations. Herein, $I_0$ = PL intensity at TNT = 0 μg $mL^{-1}$ ($K_{sv}$ = 74,160 L $mol^{-1}$).

It was observed that an addition of 5 μg $mL^{-1}$ TNT to the solution of **FIrPyBiz**, resulted in 98% quenching of emission. The quenching of emission in **FIrPyBiz** (70 : 30% $H_2O$–acetone) upon the addition of TNT can also be observed by the naked eye (inset of Figure 4.8). The detection limit of **FIrPyBiz** as a phosphorescent sensor for TNT is found to be 9.08 μg $mL^{-1}$ (Figure 4.9), which is low enough for the detection of micromolar concentrations of TNT. This finding demonstrates the utility of aggregates of **FIrPyBiz** in the detection of TNT. In order to understand the excited-state behaviour of **FIrPyBiz** in 70% $H_2O$ : 30% acetone mixtures, the phosphorescence lifetime decay profiles before and after addition of TNT were recorded (Figure 4.10). These data of **FIrPyBiz** ($\lambda_{exc}$ = 375 nm) exhibited a single exponential character with a lifetime of 0.62 μs when monitored at 520 nm. Upon the addition of TNT, a fast single exponential decay with a time constant of 0.22 μs was observed. The decrease in the lifetime can be attributed to the interaction of TNT with the **FIrPyBiz** in the excited state.

The Stern–Volmer plot (Figure 4.9) for TNT exhibits a nonlinear dependence when its concentration is higher than 0.03 mM. A linear Stern–Volmer relationship may be observed if either a static or dynamic quenching process is dominant. Thus, in the case of higher concentrations of TNT, the two processes may be competitive, which results in a nonlinear Stern–Volmer relationship. This could also arise from aggregation of the analyte with a chromophore. Trogler and co-workers[30] noted similar behaviour in the case of sensors for picric acid. The quenching constant is evaluated to be 74 160 L mol$^{-1}$ for **FIrPyBiz**, which is higher than many of the reported fluorescent sensors (Table 4.4).

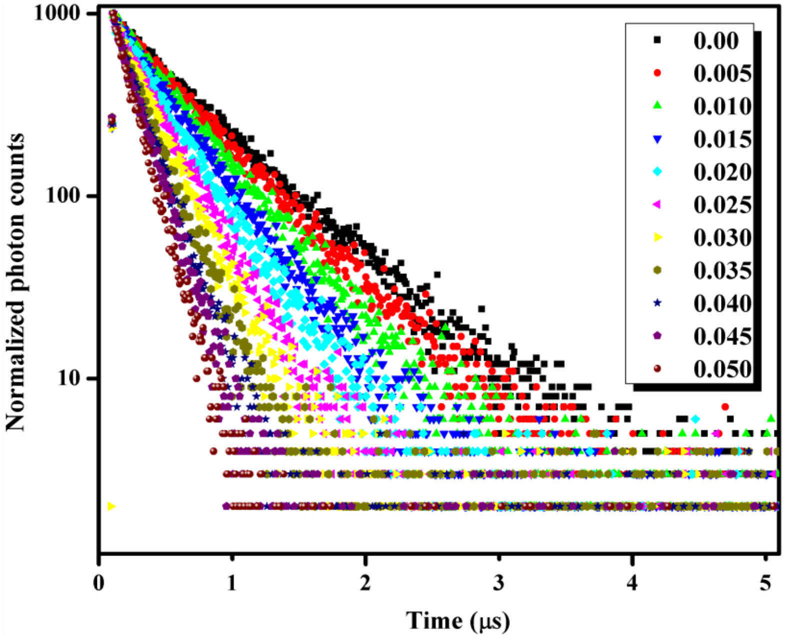

**Figure 4.10.** Lifetime decay profiles of **FIrPyBiz** (c = 5μM) in acetone–water (30: 70%) containing different amounts of TNT (0 to 0.05mM) ($\lambda_{exc}$ = 365 nm).

**Table 4.4.** Comparison of present work with previous reports with respect to type of system used, stern-volmer constant and phase of experimentation

| Sl. No. | Publication | System | $K_{SV}$ ($M^{-1}$) | Phase |
|---|---|---|---|---|
| 1 | Present work | AIPE active phosphorescent Iridium(III) complex | $7.4 \times 10^4$ | Vapor, Solid and solution |
| 2 | *J. Mater. Chem.* 2011, 21, 9130 | π-Electron rich fluorescent aromatic compounds | $1.97 \times 10^4$ | Solution |
| 3 | *J. Mater. Chem.* 2012, 22, 11574 | Fluorescent self-assembled monolayer film | $1.47 \times 10^4$ | Solution |
| 4 | *J. Mater. Chem.* 2012, 22, 2908 | Silica anchored fluorescent organosilicon polymers | $10 \times 10^3$ | Solid state |
| 5 | *Chem. Commun.* 2012, *48*, 4633 | Conjugated polymer encapsulated in mesoporous silica nanoparticles | $3.73\times 10^3$ | Solution |

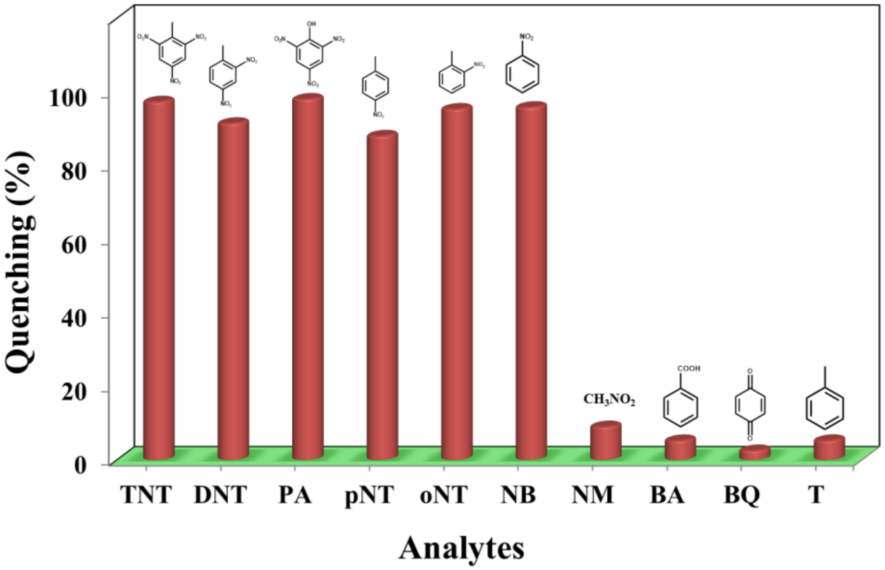

**Figure 4.11.** Selectivity graph of **FIrPyBiz** towards nitroaromatics for 5 μg/mL analyte.

The quenching of phosphorescent emission with the different compounds examined follows the order: TNT ~ picric acid (PA) > *o*-nitrotoluene (*o*NT) ~ nitrobenzene (NB) > 2,4-dinitrotoluene (DNT) > *p*-nitrotoluene (*p*NT) > nitromethane (NM) > benzoic acid (BA) ~ toluene (T) > benzoquinone (BQ) (Figure 4.11). Negligible change in the emission was observed on addition of NM, BA, T and BQ. It is evident from the result that the most electron-deficient aromatic substrates generated the greatest quenching. This is consistent with the proposed mechanism in which a nitro aromatic analyte acts as a PL quencher as a result of an electron transfer event (Figure 4.12). Thus, the higher energy of the LUMO (lowest unoccupied molecular orbitals) [−2.95 eV] of **FIrPyBiz** allows electrons to jump to the lower energy of the LUMO of nitroaromatics (TNT = −3.70 eV; DNT = −3.30 eV; NB = −3.35 eV).[30]

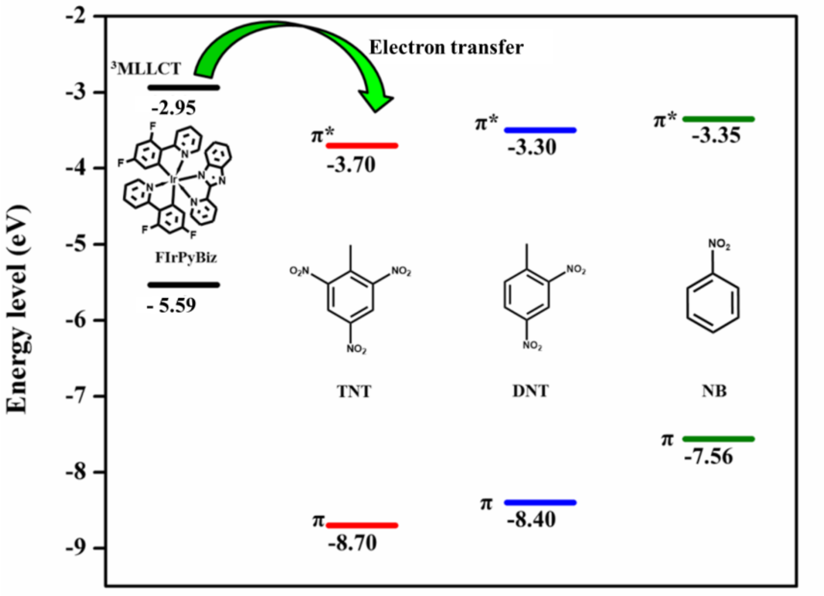

**Figure 4.12.** HOMO and LUMO energy levels of **FIrPyBiz**, TNT, DNT and NB.

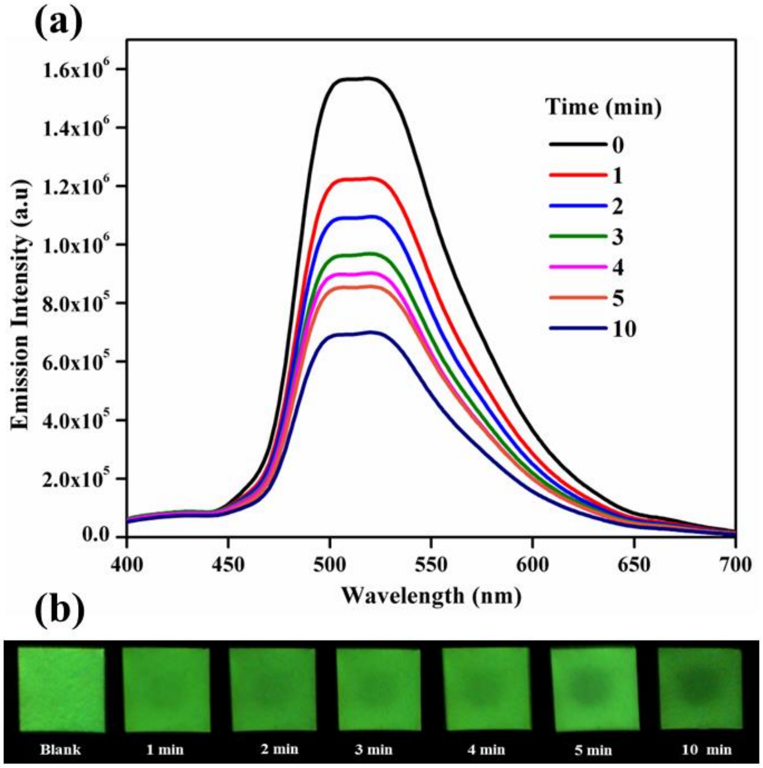

**Figure 4.13.** Change in emission intensity (a) and photographs (b) of **FIrPyBiz** impregnated paper strips on exposing to the vapours of solid TNT ($\lambda_{exc}$ = 365 nm).

### 4.4.4. TNT Detection: Vapor Phase

The use of **FIrPyBiz** for the detection of TNT vapors was also studied. A Whatman filter paper strips (2.0 cm × 2.0 cm) impregnated with **FIrPyBiz** ($1 \times 10^{-4}$ M in dichloromethane) showed efficient quenching of phosphorescence when exposed to saturated TNT vapors. Following exposure for 60 s, 22% quenching was observed in the presence of TNT (Figure 4.13), which demonstrates the practical sensitivity and applicability of **FIrPyBiz** for vapors of TNT. A comparison of the response times of **FIrPyBiz** impregnated test strips with vapors of various nitroaromatics have also been investigated after exposure for 60 s and the results are depicted in Figure 4.14. The percentage of quenching of the various nitroaromatics is found to be in the order of their respective vapor pressures at 20 °C.

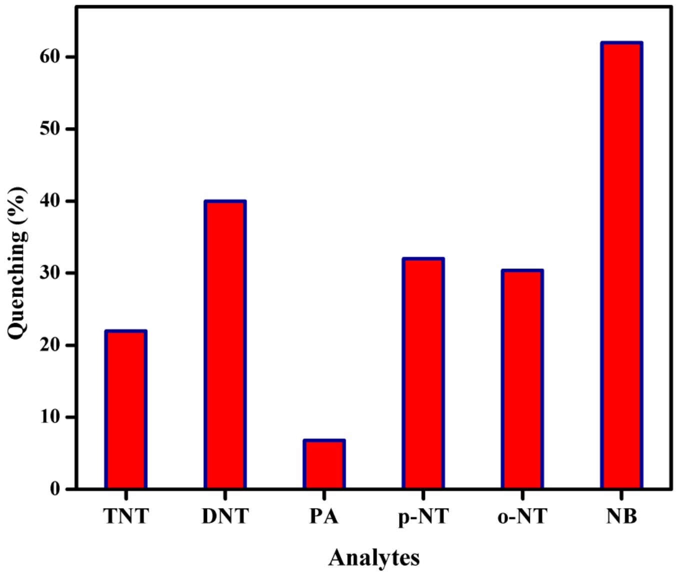

**Figure 4.14.** Comparison of the phosphorescence quenching efficiency of **FIrPyBiz** impregnated test strips upon exposure to saturated vapors of different nitro aromatic analyte for 60 s ($\lambda_{exc}$ = 365 nm).

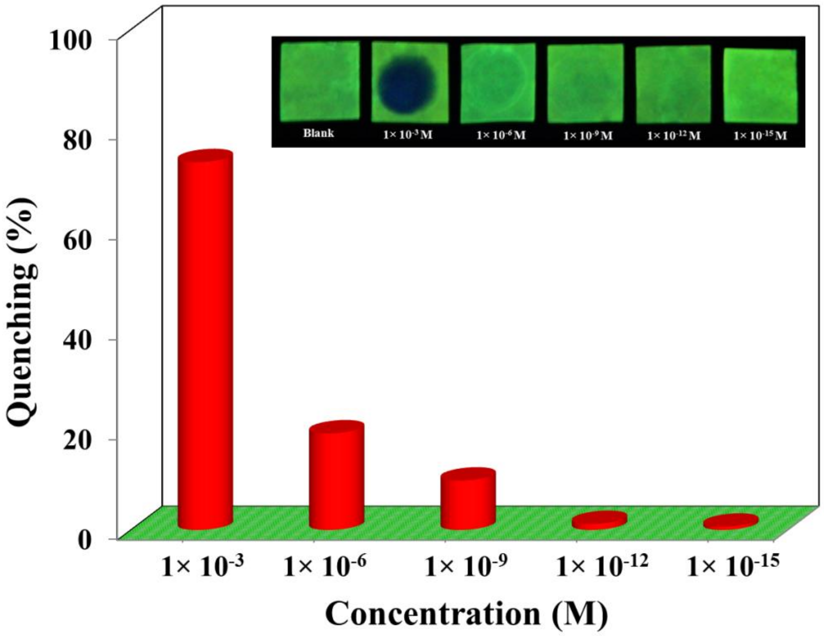

**Figure 4.15.** Plot of the emission at 510 nm (% of quenching) of the test strips against concentration of added TNT in drinking water (10 μL, 1 × $10^{-15}$ – 1 × $10^{-3}$ M).

### 4.4.5. TNT Detection: Contact Mode

Efforts have been made to detect the TNT in contact mode by applying small spots (10 μL) of different concentrations of TNT solution on to **FIrPyBiz** impregnated test strips. Dark spots of different strengths were formed (Figure 4.15), which shows that the regulation of the quenching behaviour of TNT is also practically applicable by varying the concentration of TNT, even up to $10^{-9}$ M (~22.7 ng $\mathrm{mL}^{-1}$). The contact-mode response to TNT by the filter paper strips was also tested by placing TNT crystals over the test strips for 10 s, resulting in black spots upon illumination with a UV lamp (Figure 4.16). In another experiment, a human thumb (gloved) was rubbed with TNT and then all visible TNT particles were brushed off, followed by pressing the thumb against a test strip. The fingerprint of the thumb could be seen as quenched luminescence when illuminated with UV light. These images illustrate the utility of the **FIrPyBiz** impregnated test strips for the on-site instant visualization of trace residues of TNT present on a specimen.

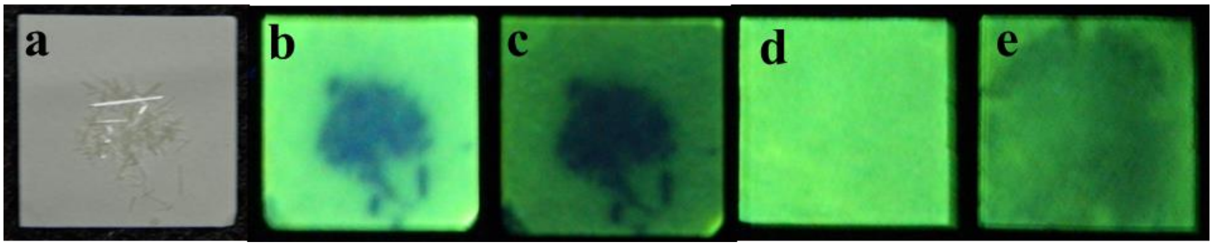

**Figure 4.16.** Photographs of **FIrPyBiz** impregnated test strips under different experimental conditions. (a) TNT crystal on top under day light (b) TNT crystal on top under UV light. (c) Upon removal of the crystals after 10 seconds. (d, e) Thumb impression before after rubbing with TNT crystals, respectively. All photographs were taken under 365 nm UV illumination.

## 4.5. Conclusions

- For the first time we have demonstrated a new AIPE-active iridium(III) complex as a phosphorescent emission probe for the detection of TNT at a nanogram level.
- Most importantly, by analyzing the influence of molecular packing on the photophysical properties of **FIrPyBiz**, it can be concluded that the formation of excimers by π–π stacking of adjacent difluorophenyl and pyridyl rings of dfppy ligands plays a key role in the AIPE phenomenon.

- However, the detection limit and sensitivity for the detection of TNT using AIPE active iridium(III) complex is not attractive compared to the existing literature. Better selectivity and lower detection limits can be obtained by tuning the LUMO levels of AIPE-active iridium(III) complexes appropriately to match the LUMO level of TNT for effective electron transfer to occur.

## 4.6. References

(1) (a) Chiu, Y. C.; Hung, J. Y.; Chi, Y.; Chen, C. C.; Chang, C. H.; Wu, C. C.; Cheng, Y. M.; Yu, Y. C.; Lee, G. H.; Chou, P. T., *Adv. Mater.* **2009,** *21*, 2221-2226. (b) Xiao, L. X.; Chen, Z. J.; Qu, B.; Luo, J. X.; Kong, S.; Gong, Q. H.; Kido, J. J., *Adv. Mater.* **2011,** *23*, 926-952. (c) Adachi, C.; Baldo, M. A.; Thompson, M. E.; Forrest, S. R., *J. Appl. Phys.* **2001,** *90*, 5048-5051. (d) Lamansky, S.; Djurovich, P.; Murphy, D.; Abdel-Razzaq, F.; Lee, H. E.; Adachi, C.; Burrows, P. E.; Forrest, S. R.; Thompson, M. E., *J. Am. Chem. Soc.* **2001,** *123*, 4304-4312. (e) Nazeeruddin, M. K.; Humphry-Baker, R.; Berner, D.; Rivier, S.; Zuppiroli, L.; Graetzel, M., *J. Am. Chem. Soc.* **2003,** *125*, 8790-8797. (f) Baldo, M. A.; Thompson, M. E.; Forrest, S. R., *Nature* **2000,** *403*, 750-753. (g) Reineke, S.; Lindner, F.; Schwartz, G.; Seidler, N.; Walzer, K.; Lussem, B.; Leo, K., *Nature* **2009,** *459*, 234-236. (h) Kido, J.; Kimura, M.; Nagai, K., *Science* **1995,** *267*, 1332-1334.

(2) (a) Yang, C. M.; Wu, C. H.; Liao, H. H.; Lai, K. Y.; Cheng, H. P.; Horng, S. F.; Meng, H. F.; Shy, J. T., *Appl. Phys. Lett.* **2007,** *90*, 133509-133511. (b) Schulz, G. L.; Holdcroft, S., *Chem. Mater.* **2008,** *20*, 5351-5355. (c) Nazeeruddin, M. K.; Gratzel, M., *Photofunctional Transition Metals Complexes* **2007,** *123*, 113-175.

(3) (a) Chen, Z. Q.; Bian, Z. Q.; Huang, C. H., *Adv. Mater.* **2010,** *22*, 1534-1539. (b) You, Y.; Nam, W., *Chem. Soc. Rev.* **2012,** *41*, 7061-7084. (c) Zhao, Q. A.; Li, F. Y.; Huang, C. H., *Chem. Soc. Rev.* **2010,** *39*, 3007-3030. (d) Guerchais, V.; Fillaut, J.

L., *Coord. Chem. Rev.* **2011,** *255*, 2448-2457. (e) Shan, G. G.; Li, H. B.; Sun, H. Z.; Zhu, D. X.; Cao, H. T.; Su, Z. M., *J.Mater.Chem.C.* **2013,** *1*, 1440-1449. (f) Lou, B.; Chen, Z. Q.; Bian, Z. Q.; Huang, C. H., *New J. Chem.* **2010,** *34*, 132-136.

(4) (a) Zhao, Q.; Huang, C. H.; Li, F. Y., *Chem. Soc. Rev.* **2011,** *40*, 2508-2524. (b) Jiang, W. L.; Gao, Y.; Sun, Y.; Ding, F.; Xu, Y.; Bian, Z. Q.; Li, F. Y.; Bian, J.; Huang, C. H., *Inorg. Chem.* **2010,** *49*, 3252-3260. (c) Lo, K. K. W.; Li, S. P. Y.; Zhang, K. Y., *New J. Chem.* **2011,** *35*, 265-287. (d) Zhao, Q.; Yu, M. X.; Shi, L. X.; Liu, S. J.; Li, C. Y.; Shi, M.; Zhou, Z. G.; Huang, C. H.; Li, F. Y., *Organometallics* **2010,** *29*, 1085-1091. (e) Lo, K. K. W., *Photophysics of Organometallics* **2010,** *29*, 115-158.

(5) (a) Huang, K. W.; Wu, H. Z.; Shi, M.; Li, F. Y.; Yi, T.; Huang, C. H., *Chem. Commun.* **2009**, 1243-1245. (b) Zhao, Q.; Li, L.; Li, F. Y.; Yu, M. X.; Liu, Z. P.; Yi, T.; Huang, C. H., *Chem. Commun.* **2008**, 685-687.

(6) You, Y.; Huh, H. S.; Kim, K. S.; Lee, S. W.; Kim, D.; Park, S. Y., *Chem. Commun.* **2008**, 3998-4000.

(7) (a) Zhao, N.; Wu, Y. H.; Luo, J.; Shi, L. X.; Chen, Z. N., *Analyst* **2013,** *138*, 894-900. (b) Wu, H. Z.; Yang, T. S.; Zhao, Q. A.; Zhou, J.; Li, C. Y.; Li, F. Y., *Dalton Trans.* **2011,** *40*, 1969-1976. (c) Liu, S. J.; Sun, H. B.; Ma, Y.; Ye, S. H.; Liu, X. M.; Zhou, X. H.; Mou, X.; Wang, L. H.; Zhao, Q.; Huang, W., *J. Mater. Chem.* **2012,** *22*, 22167-22173.

(8) (a) Zhao, Z. J.; Chang, Z. F.; He, B. R.; Chen, B.; Deng, C. M.; Lu, P.; Qiu, H. Y.; Tang, B. Z., *Chem. Eur. J* **2013,** *19*, 11512-11517. (b) Hong, Y. N.; Lam, J. W. Y.; Tang, B. Z., *Chem. Commun.* **2009**, 4332-4353. (c) Zhou, J.; Chang, Z. F.; Jiang, Y. B.; He, B. R.; Du, M.; Lu, P.; Hong, Y. N.; Kwok, H. S.; Qin, A. J.; Qiu, H. Y.; Zhao, Z. J.; Tang, B. Z., *Chem. Commun.* **2013,** *49*, 2491-2493. (d) Hong, Y. N.; Lam, J. W. Y.; Tang, B. Z., *Chem. Soc. Rev.* **2011,** *40*, 5361-5388. (e) Zhou, J.; He, B. R.; Chen, B.; Lu, P.; Sung, H. H. Y.; Williams, I. D.; Qin, A. J.; Qiu, H. Y.; Zhao, Z. J.; Tang, B. Z., *Dyes. Pigm.* **2013,** *99*, 520-525.

(9) (a) Luo, X. L.; Li, J. N.; Li, C. H.; Heng, L. P.; Dong, Y. Q.; Liu, Z. P.; Bo, Z. S.; Tang, B. Z., *Adv. Mater.* **2011,** *23*, 3261-+. (b) Zhao, Z. J.; Lam, J. W. Y.; Chan, C. Y. K.; Chen, S. M.; Liu, J. Z.; Lu, P.; Rodriguez, M.; Maldonado, J. L.; Ramos-Ortiz, G.; Sung, H. H. Y.; Williams, I. D.; Su, H. M.; Wong, K. S.; Ma, Y. G.; Kwok, H. S.; Qiu, H. Y.; Tang, B. Z., *Adv. Mater.* **2011,** *23*, 5430-+. (c) Liu, J. Z.; Su, H. M.; Meng, L. M.; Zhao, Y. H.; Deng, C. M.; Ng, J. C. Y.; Lu, P.; Faisal, M.; Lam, J. W. Y.; Huang, X. H.; Wu, H. K.; Wong, K. S.; Tang, B. Z., *Chem. Sci.* **2012,** *3*, 2737-2747. (d) Shi, J. Q.; Chang, N.; Li, C. H.; Mei, J.; Deng, C. M.; Luo, X. L.; Liu, Z. P.; Bo, Z. S.; Dong, Y. Q.; Tang, B. Z., *Chem. Commun.* **2012,** *48*, 10675-10677. (e) Zhao, Z. J.; Lam, J. W. Y.; Tang, B. Z., *Curr. Org. Chem.* **2010,** *14*, 2109-2132. (f) Li, Z.; Dong, Y.; Mi, B. X.; Tang, Y. H.; Haussler, M.; Tong, H.; Dong, Y. P.; Lam, J. W. Y.; Ren, Y.; Sung, H. H. Y.; Wong, K. S.; Gao, P.; Williams, I. D.; Kwok, H. S.; Tang, B. Z., *J. Phys. Chem. B* **2005,** *109*, 10061-10066. (g) Gao, X.; Peng, Q.; Niu, Y. L.; Wang, D.; Shuai, Z. G., *Phys. Chem. Chem. Phys.* **2012,** *14*, 14207-14216.

(10) (a) Kartha, K. K.; Babu, S. S.; Srinivasan, S.; Ajayaghosh, A., *J. Am. Chem. Soc.* **2012,** *134*, 4834-4841. (b) Kumar, M.; Vij, V.; Bhalla, V., *Langmuir* **2012,** *28*, 12417-12421. (c) Fainberg, A., *Science* **1992,** *255*, 1531-1537.

(11) Pushkarsky, M. B.; Dunayevskiy, I. G.; Prasanna, M.; Tsekoun, A. G.; Go, R.; Patel, C. K. N., *Proc. Nat. Acd. Sci. USA* **2006,** *103*, 19630-19634.

(12) (a) Goldman, E. R.; Medintz, I. L.; Whitley, J. L.; Hayhurst, A.; Clapp, A. R.; Uyeda, H. T.; Deschamps, J. R.; Lassman, M. E.; Mattoussi, H., *J. Am. Chem. Soc.* **2005,** *127*, 6744-6751. (b) Zhang, K.; Zhou, H. B.; Mei, Q. S.; Wang, S. H.; Guan, G. J.; Liu, R. Y.; Zhang, J.; Zhang, Z. P., *J. Am. Chem. Soc.* **2011,** *133*, 8424-8427.

(13) Qu, W. G.; Deng, B.; Zhong, S. L.; Shi, H. Y.; Wang, S. S.; Xu, A. W., *Chem. Commun.* **2011,** *47*, 1237-1239.

(14) (a) Mathew, A.; Sajanlal, P. R.; Pradeep, T., *Angew. Chem. Int. Ed.* **2012,** *51*, 9596-9600. (b) Yang, L. B.; Chen, G. Y.; Wang, J.; Wang, T. T.; Li, M. Q.; Liu, J. H., *J. Mater. Chem.* **2009,** *19*, 6849-6856.

(15) (a) Wang, X. H.; Guo, Y. Z.; Li, D.; Chen, H.; Sun, R. C., *Chem. Commun.* **2012,** *48*, 5569-5571. (b) Sanchez, J. C.; Trogler, W. C., *J. Mater. Chem.* **2008,** *18*, 3143-3156. (c) Shanmugaraju, S.; Joshi, S. A.; Mukherjee, P. S., *J. Mater. Chem.* **2011,** *21*, 9130-9138. (d) Yang, J. S.; Swager, T. M., *J. Am. Chem. Soc.* **1998,** *120*, 11864-11873.

(16) Zhang, Y. L.; Xia, J.; Feng, X.; Tong, B.; Shi, J. B.; Zhi, J. G.; Dong, Y. P.; Wei, Y., *Sens. Actuators, B* **2012,** *161*, 587-593.

(17) Vijayakumar, C.; Tobin, G.; Schmitt, W.; Kim, M. J.; Takeuchi, M., *Chem. Commun.* **2010,** *46*, 874-876.

(18) You, Y. M.; Park, S. Y., *J. Am. Chem. Soc.* **2005,** *127*, 12438-12439.

(19) Dorey, R. C.; Carper, W. R., *J. Chem. Eng. Data* **1984,** *29*, 93-97.

(20) J. C. de Mello; H. F. Wittmann; Friend, R. H., *Adv. Mater.* **1997,** *9*, 230-232.

(21) Liu, Y.; Liu, M. S.; Jen, A. K. Y., *Acta Polym.* **1999,** *50*, 105-108.

(22) *SMART* (version 5.628); *SAINT* (version 6.45a); *XPREP*; *SHELXTL, Madison, WI,* . Bruker AXS Inc.: 2004.

(23) Sheldrick, G. M., *Siemens Area Correction Absorption Correction Program*. University of Gottingen: Gottingen, Germany, 1994.

(24) Sheldrick, G. M., *SHELXL-97 Program for Crystal Structure Solution and Refinement*. University of Gottingen:: Gottingen, Germany, 1997.

(25) Vandersluis, P.; Spek, A. L., *Acta Crystallogr. Sect. A* **1990,** *46*, 194-201.

(26) Farrugia, J. L., *J. App. Crystallogr* **1999,** *32*, 837−838.

(27) (a) Song, Y. H.; Yeh, S. J.; Chen, C. T.; Chi, Y.; Liu, C. S.; Yu, J. K.; Hu, Y. H.; Chou, P. T.; Peng, S. M.; Lee, G. H., *Adv. Funct. Mater.* **2004,** *14*, 1221-1226. (b) Orselli, E.; Kottas, G. S.; Konradsson, A. E.; Coppo, P.; Frohlich, R.; Frtshlich, R.; De Cola, L.; van Dijken, A.; Buchel, M.; Borner, H., *Inorg. Chem.* **2007,** *46*, 11082-11093. (c) Orselli, E.; Albuquerque, R. Q.; Fransen, P. M.; Frohlich, R.; Janssen, H. M.; De Cola, L., *J. Mater. Chem.* **2008,** *18*, 4579-4590.

(28) Zhu, Y. C.; Zhou, L.; Li, H. Y.; Xu, Q. L.; Teng, M. Y.; Zheng, Y. X.; Zuo, J. L.; Zhang, H. J.; You, X. Z., *Adv. Mater.* **2011,** *23,* 4041-4046.

(29) Janiak, C., *J. Chem. Soc., Dalton Trans.* **2000**, 3885–3896.

(30) Sohn, H.; Sailor, M. J.; Magde, D.; Trogler, W. C., *J. Am. Chem. Soc.* **2003,** *125*, 3821-3830.

# Papers Presented at Conferences

1. AIPE-Active Green Phosphorescent Iridium(III) Complex Impregnated Test Strips for the Vapor-Phase Detection of 2,4,6-Trinitrotoluene (TNT). **K. S. Bejoymohandas**, M. V. Lucky, P. K Thejus, Alikunhi, T. M. George, S. Bhattacharya, S. Natarajan & M. L. P. Reddy.

   Presented a poster at the *International Conference on Advanced Functional Material (ICAFM)* organized by CSIR-NIIST, Thiruvananthapuram, India during February 19-21, **2014**.

2. AIPE-Active Green Phosphorescent Iridium(III) Complex Impregnated Test Strips for the Vapor-Phase Detection of 2,4,6-Trinitrotoluene (TNT). **K. S. Bejoymohandas**, T. M. George, & M. L. P. Reddy.

   Presented a poster in the *Indian Society of Analytical Scientists conference (ISAS 2014; Theme - Advanced Technologies for Material Processing and Diagnostics)* held at Kochi. Kerala during September 18-21, **2014**. (***Best poster award***).

3. Photophysical Properties of Bis(2′,6′-difluoro-2,3′-bipyridinato-N,C4′) iridium(picolinate) Complexes: Effect of Electron-withdrawing and Electron-donating group Substituent at the 4′ Position on the Pyridyl moiety of the Cyclometalated Ligand. **K. S. Bejoymohandas,** M. V. Lucky, P. K. Thejus, M. Alikunhi, S. Varughese, E. Varathan, V. Subramanian & M. L. P. Reddy.

   Presented a poster at the *8th Asian Photochemistry Conference (APC-2014)* organized jointly by IISER and CSIR-NIIST, held from November 10-13, **2014** at Thiruvananthapuram.

4. Inorganic Oxides Displaying Intense Orange Color with Impressive Solar Reflectance Based on $Mn^{4+}$ in Octahedral Geometry in $Y_2Ti_2O_7$. **K. S. Bejoymohandas**, Sheethu Jose & M. L. P. Reddy.

   Presented a poster at the *International Conference on Science, Technology and Applications of Rare earths (ICSTAR 2015)* organized by Rare Earths Association of India (REAI) held at Thiruvananthapuram during April 23-25, **2015**.

5. Photophysical and Electroluminescent Properties of Bis(2′,6′-difluoro-2,3′-bipyridinato-N,C4′)iridium(picolinate) Complexes: Effect Of Electron-Withdrawing and Electron-Donating Group Substituent at the 4′ Position on the Pyridyl Moiety of the

Cyclometalated Ligand. **K. S. Bejoymohandas**, Arunandan Kumar, S. Varughese, E. Varathan, V. Subramanian & M. L. P. Reddy.

Presented a poster at the *National Conference on Analytical Science for Technological Excellence and Environmental Sustainability* organized by the Indian Society of Analytical Scientists, held in Munnar, Kerala, India during September 24-26, **2015**.

6. Photophysical and Electroluminescent Properties of Bis(2′,6′-difluoro-2,3′-bipyridinato-N,C4′)iridium(picolinate) Complexes: Effect Of Electron-Withdrawing and Electron-Donating Group Substituent at the 4′ Position on the Pyridyl Moiety of the Cyclometalated Ligand. **K. S. Bejoymohandas**, Ajay Kumar, S. Sreenadh, S. Varughese & M. L. P. Reddy.

   Presented a paper at the poster session in the *International Symposium on Photonic Applications and Nanomaterials (ISPAN-2015)* during 28-30 October **2015** organized by Sree Chitra Tirunal Institute for Medical Sciences and Technology, Thiruvananthapuram.

# List of Publications

## From the thesis

1. AIPE-active green phosphorescent iridium(III) complex impregnated test strips for the vapor phase detection of 2,4,6-trinitrotoluene (TNT); **K. S. Bejoymohandas**, T. M. George, S. Bhattacharya, S. Natarajan and M. L. P. Reddy.

   *Journal of Materials Chemistry C*, **2014**, 2, 515–523.

2. Photophysical and electroluminescence properties of bis(2',6'-difluoro-2,3'-bipyridinato-,C4')iridium-(picolinate) complexes: effect of electron-withdrawing and electron-donating group substituents at the 4' position of the pyridyl moiety of the cyclometalated ligand; **K. S. Bejoymohandas**, Arunandan Kumar, S. Varughese, E. Varathan, V. Subramanian and M. L. P. Reddy.

   *Journal of Materials Chemistry C*, **2015**, 3, 7405–7420.

3. Highly Selective Chemosensor for Cyanide Derived from Formyl Functionalized Phosphorescent Iridium(III) Complex; **K. S. Bejoymohandas**, Ajay Kumar, S. Sreenadh, E. Varathan, S. Varughese, V. Subramanian, and M. L. P. Reddy.

   *ACS Inorganic Chemistry*, **2016,** 55, 3448−3461.

4. Evolution of 2, 3′−bipyridine class of cyclometalating ligands as efficient phosphorescent iridium(III) emitters for applications in organic light emitting diodes; M. L. P. Reddy, **K. S. Bejoymohandas**.

   *Journal of Photochemistry and Photobiology, C: Photochemistry Reviews*, **2016**, 29, 29−47.

## Out of the thesis

5. Amending the anisotropy barrier and luminescence behavior of heterometallic trinuclear linear [$M^{II}$-$Ln^{III}$-$M^{II]}$ ($Ln^{III}$=Gd, Tb, Dy; $M^{II}$=Mg/Zn) complexes by change from divalent paramagnetic to diamagnetic metal ions; Sourav Das, **K. S. Bejoymohandas**, Atanu Dey, Sourav Biswas, M. L. P. Reddy, Roser Morales, Eliseo Ruiz, Silvia Titos-Padilla, Enrique Colacio, and Vadapalli Chandrasekhar.

   *Chemistry A European Journa*l. **2015**, 21, 1 – 17.